Polymer-surfactant stabilised drug nanoparticles

Tirop, Lucy

Awarding institution:
King's College London

Title: Polymer-surfactant stabilised drug nanoparticles

Author: Lucy Tirop

Polymer-surfactant stabilised drug nanoparticles

Lucy Jemutai Tirop

B.Pharm

A Thesis submitted for the degree of

Doctor of Philosophy

King's College London

2012

Institute of Pharmaceutical Science
School of Biomedical Sciences
King's College London
January 2012

Abstract

Wet bead milling, in which the drug is milled in presence of stabilisers such as polymers and surfactants, has enabled the formulation of poorly water-soluble drugs as nanoparticles, with five products having reached the market. During the milling process, the polymer and/or surfactant adsorbs onto the freshly cleaved drug surfaces to provide ionic or steric stabilisation. Despite the success of wet bead milling, mastery of the mechanism behind nanoparticle stabilization is still lacking. To investigate whether any relationship exists between drug, stabiliser and stabilisation, eight structurally different poorly water-soluble drugs were milled in presence of thirteen different pharmaceutically acceptable stabilisers and the resultant particle size determined by photon correlation spectroscopy. Nanoparticles of the BCS class II drug, griseofulvin, could only be produced in presence of anionic stabilisers namely sodium dodecyl sulphate, aerosol-OT or hydroxypropylmethylcellulose acetate succinate. Surfactant adsorption isotherms obtained indirectly by measuring their depletion from solution revealed a maximum surfactant adsorption of ~ 2.2 mg/m^2 on the griseofulvin nanoparticle surfaces. The use of ionic surfactants/polymers in oral formulations is however sub-optimal. Consequently, polymer-surfactant co-stabilisation, used to take advantage of the synergy between ionic and non-ionic stabilisers, was investigated by the inclusion of the non-ionic polymer hydroxypropylmethylcellulose (HPMC) into the anionic surfactant-drug slurry prior to milling. The effect of varying HPMC molecular weight and concentration on griseofulvin nanoparticle production was established. Polymer adsorption isotherms were obtained directly via small angle neutron scattering. Inclusion of HPMC in the milling slurry resulted in its co-adsorption with anionic surfactant on the griseofulvin nanoparticle surfaces and a corresponding reduction in the amount of anionic surfactant adsorbed. Notably HPMC on its own could not adsorb onto the griseofulvin nanoparticles.

Acknowledgements

My sincere gratitude goes to my supervisor Prof. Jayne Lawrence for her invaluable guidance, support and encouragement throughout the research. Without her this journey would not have been possible. I would also like to acknowledge my co-supervisor Dr. Dave Barlow for providing direction for the computational modelling. I am grateful to Dr. Jerry Heng and Umang Shah (Imperial College London) for their help with the growth and characterisation of macroscopic drug crystals, Dr. Stephen King (ISIS, Rutherford Appleton Labs) for his help with SANS data analysis, Dr. Anthony Brian (King's College London), Dr. Kenneth Shankland (University of Reading), and Dr. Steve Hinder (University of Surrey) for performing the scanning electron microscopy, X-ray diffraction and X-ray photoelectron spectroscopy experiments respectively.

The financial support for this research was provided by the Commonwealth Scholarship Commission (UK) and is gratefully acknowledged. I am indebted to the University of Nairobi for nominating me for the Commonwealth doctoral scholarship and for granting me study leave to undertake my research.

I thank all my friends and members of the Molecular Biophysics group who made my time in London both interesting and fulfilling. In particular, I acknowledge Tawi, Jane and Noma for their kindness and emotional support.

My deepest gratitude goes to my family for their constant love and encouragement; this thesis is a testament to their support. Special thanks go to my father, David, and my siblings Elsie, Susan and Collins. My mother, Hellen, though no longer with us, remains an inspiration in my life.

Finally, I thank God for keeping me in good health and enabling me complete this thesis.

Table of Contents

List of Figures

Chapter 1 Introduction

Chapter 2 Wet bead milling

Chapter 4 Small angle neutron scattering

Chapter 6 General discussion

List of Tables

List of Appendices

Abbreviations and Symbols

Å	angstrom
ANOVA	analysis of variance
AOT	aerosol-OT
A_{SL}	area per surfactant molecule at solid-liquid interface
BCS	biopharmaceutics classification system
cac	critical aggregation concentration
CCD	charge coupled device
CCDC	Cambridge crystallographic data centre
CD	circular dichroism
CIF	crystallographic information file
cmc	critical micellar concentration
CO_2	carbon dioxide
d(H)	hydrodynamic diameter
D_2O	deuterium oxide
DCS	developability classification system
DDAPS	dimethyl dodecyl amino propane sulphate
DLVO	Derjaguin, Landau, Verweey and Overbeek
dQ/dt	dissolution rate
d-SDS	deuterated sodium dodecyl sulphate
DTAB	dodecyl trimethyl ammonium bromide
F 127	Pluronic F 127
FASSIF	fasted state stimulated intestinal fluid
FDA	Food and Drug Administration
GIT	gastrointestinal tract
gm	gram
GSK	GlaxoSmithKline
H_2O	water
He	helium
HEC	hydroxyethylcellulose
HLB	hydrophilic lipophilic balance
HPC	hydroxypropylcellulose

HPLC	high performance liquid chromatography
HPMC	hydroxypropylmethylcellulose
HPMCAS	hypromellose acetate succinate
hr	hour
h-SDS	hydrogenated sodium dodecyl sulphate
Hz	hertz
I(Q)	neutron flux
ILL	Institut Laue Langevin
K_b	boltzman constant
K_H	huggins constant
K_K	kraemer constant
log P	partition coefficient
m	meter
min	minute
M_n	nominal molecular weight
mV	millivolts
M_v	viscosity averaged molecular weight
N_A	avogardos number
ND	not determined
NF	not formed
NIST	National Institute of Standards and Technology
nm	nanometre
NMR	nuclear magnetic resonance
ORD	optical rotatory dispersion
P_{eff}	permeability coefficient
P(Q)	form factor
PCS	photon correlation spectroscopy
PDB	program database
PEO	polyethylene oxide
PI	polydispersity index
pK_a	acid dissociation constant
PSD	particle size distribution
PSI	Paul Scherrer Institut
PVP	polyvinylpyrrolidone

Q	neutron scattering vector
RESS	rapid expansion of supercritical solutions
rpm	rotations per minute
S(Q)	structure factor
s.d.	standard deviation
SA	surface area
SANS	small angle neutron scattering
SAS	supercritical anti-solvent
SCF	super critical fluids
SDS	sodium dodecyl sulphate
SEM	scanning electron microscopy
SLAD	solubility limited absorbable dose
SLD	scattering length density
T	temperature
TOF	time of flight
UPW	ultra pure water
USP	United States Pharmacopeia
UV/Vis	ultraviolet/visible
V	volt
V_A	attractive forces acting on a particle
V_R	repulsive forces acting on a particle
V_S	steric forces acting on a particle
V_T	total force acting on a particle
WBM	wet bead milling
XPS	X-ray photoelectron spectroscopy
XRD	X-ray diffraction
x_s	polymer adsorption energy parameter
YTZ	yttrium zirconium
Γ	adsorption density
γ	interfacial tension
γ_L^d	dispersive component of liquid surface energy
γ_L^p	polar component of liquid surface energy
γ_{LV}	liquid-vapour interfacial energy
γ_S^d	dispersive component of solid surface energy

γ_{SL}	solid-liquid interfacial energy
γ_S^p	polar component of solid surface energy
γ_{SV}	solid-vapour interfacial energy
η	intrincic viscosity
λ	wavelength
$\rho_l - \rho_m$	contrast point
ρ_l	scattering length density of adsorbed layer
ρ_m	scattering length density of media
ρ_p	scattering length density of scattering particles
σ	second moment of thickness of the adsorbed layer
Φz	volume fraction profile
χ^2	chi-square statistic

Chapter 1
Introduction

1.1 Drug bioavailability from oral dosage forms

Bioavailability is a measure of the rate and extent at which a drug reaches the systemic circulation, and thereby accesses its site(s) of action. The vast majority of drugs marketed worldwide are orally administered and as a consequence their efficacy is dependent on their relative bioavailability (Custodio et al, 2008). The relative bioavailability of an orally administered compound is obtained by comparing the compound's oral bioavailability to that of an equal amount of the intravenously

delivered compound. Unlike the intravenous route in which drugs are injected directly into the systemic circulation, oral dosage forms must first undergo, depending upon the formulation in which they are contained, disintegration/disaggregation, followed by dissolution and absorption across the gastrointestinal membrane prior to entry into the systemic circulation. In addition, orally administered drugs may undergo metabolism in the liver, the so called 'first pass effect'. The bioavailability of orally administered drugs therefore is the superposition of two processes, namely absorption across the gastrointestinal membrane and first pass metabolism as illustrated in Figure 1.1.

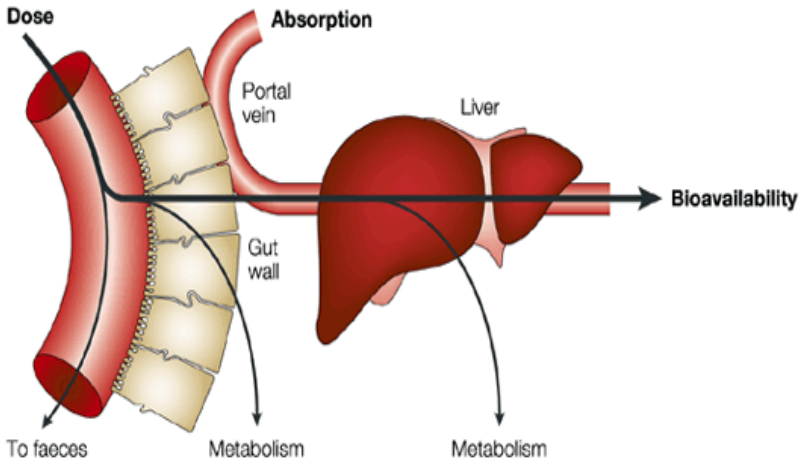

Figure 1.1: Diagrammatic representation of the steps that may influence the bioavailability of an orally administered drug (van de Waterbreemd et al, 2003).

The amount of drug absorbed across the gastrointestinal membrane is determined by its solubility and permeability. Prior to absorption, orally administered drug must generally first undergo dissolution. The only exception to this requirement is when a drug is administered in the form of a solution. Dissolution rate is dependent on the particle size of a drug, with smaller particles exhibiting a higher dissolution rate. However, prior to dissolution some formulations must undergo additional steps. For example, a tablet must first undergo disintegration into granules, followed by deaggregation of the granules to primary drug particles prior to dissolution occurring (Figure 1.2).

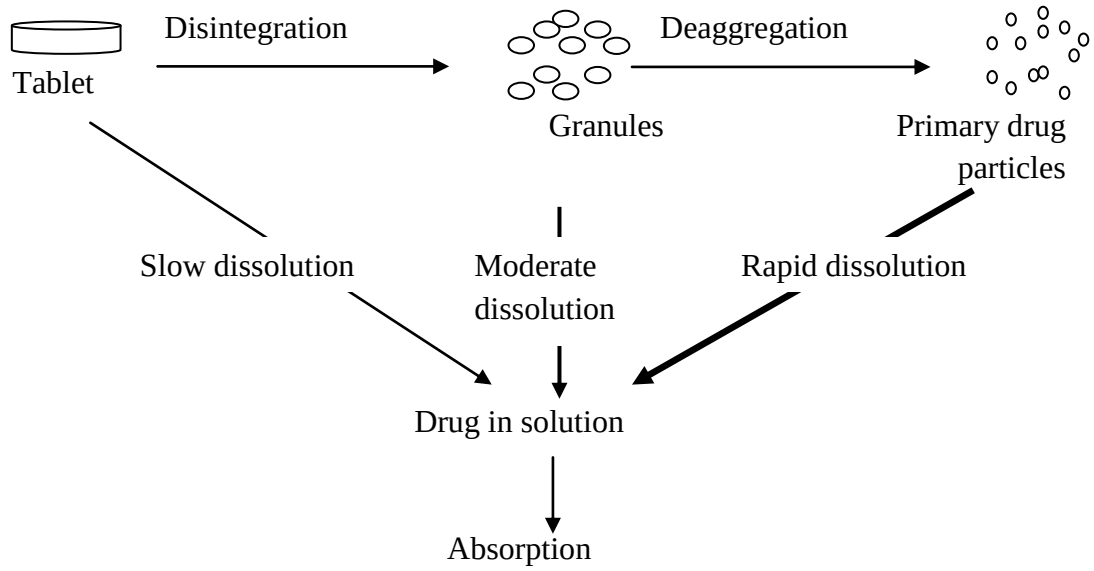

Figure 1.2: Major steps following the oral administration of a tablet (Rubinstein et al, 1977).

Other factors that affect the dissolution of a drug include its pKa, log P and the pH and volume of the intestinal contents. Log P is defined as the ratio of distribution of the unionized form of a drug between octanol and water at equilibrium. A high log P value is therefore usually taken to indicate a high lipophilicity (Lindenberg et al, 2004), although it is important to note that because log P is a distribution ratio, a high log P does not necessarily mean that the drug has a high solubility in organic/lipophilic phases. Slow dissolution of a drug invariably leads to poor bioavailability, thus necessitating formulation attempts to increase the apparent water-solubility of such drugs. The drug may also undergo complexation with formulation excipients, ingested food or other drugs within the gastrointestinal tract, thereby reducing the fraction of the drug available for dissolution.

Subsequent to dissolution, the drug will undergo diffusion through the intestinal media followed by permeation through the intestinal wall. The main site of absorption is the small intestine due to its rich blood supply which corresponds to about 25% of cardiac output, and its high surface area due to the presence of a brush border consisting of villi and microvilli (Ganong 2005). Absorption of drugs from the gastrointestinal tract is mainly via transcellular pathways such as passive or facilitated diffusion, active transport or endocytosis, although transport may also occur via paracellular pathways through tight junctions (Figure 1.3). Only unionized

drug can be absorbed passively through the lipophilic intestinal membranes (Hogben et al, 1959).

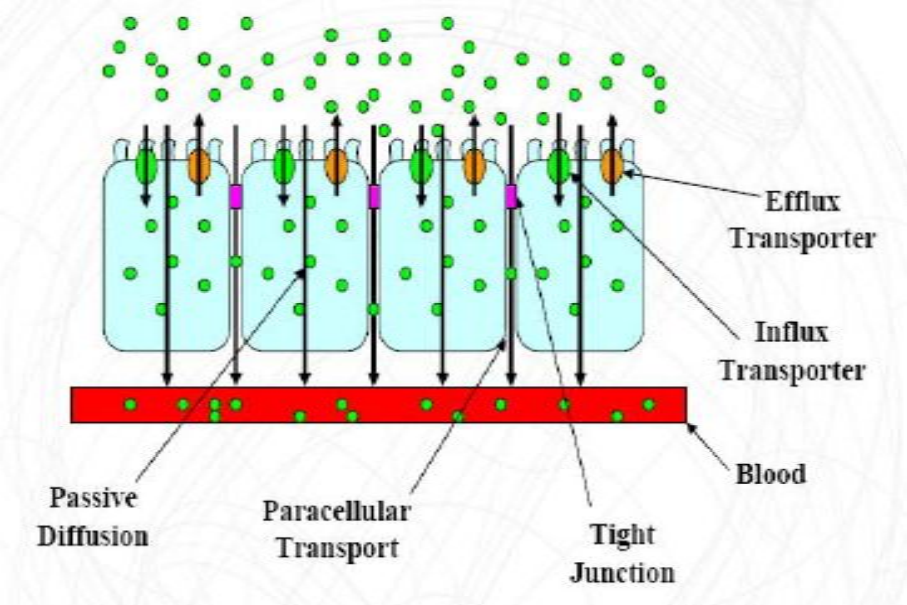

Figure 1.3: Mechanisms of intestinal drug absorption (adapted from Ganong 2005).

Drug absorption in the gastrointestinal tract is affected by physiological factors such as gastrointestinal pH, motility, blood flow, tract length and surface area as well as by physiochemical drug factors e.g. log P, molecular size, pKa, and the presence of other drugs or food in the gut (Orme 1984).

Transport can also occur in the other direction, for example intestinal efflux transporters reduce net drug absorption by pumping drug back into intestinal lumen. P-glycoprotein (p-gp), an efflux transporter, has been shown to reduce the absorption of cyclosporine (Lown et al, 1997) amongst other drugs. In addition, drug may be metabolized during its transit through the gut wall. Finally, the first pass effect reduces the amount of drug reaching the systemic circulation unaltered as drug reaching the liver may be altered by way of enzymatic biotransformation. As a consequence, the bioavailability of an orally administered drug is the fraction that survives the various barriers it encounters during its passage from the gut lumen to the systemic circulation (Kwan 1997).

1.2 Poorly water-soluble drugs and their classification

The poor water solubility of many drugs poses a significant challenge to the pharmaceutical industry entailing significant resources in time and money. An

estimated 40% of newly discovered active pharmaceutical compounds are poorly water-soluble (Lipinski, 2002). As drug discovery screening does not generally discriminate against solubility but rather on lipophilicity, highly lipophilic but poorly water-soluble drugs frequently end up in the drug development pipeline (Chaubal, 2004). However, many of these poorly water-soluble compounds have promising therapeutic potential thereby warranting further research into their formulation.

Poor water solubility, in practical terms refers to the scenario in which the dissolution of a dose of drug takes longer than its transit through the absorptive sites in the gastrointestinal solubility resulting in its poor bioavailability. Dissolution rate, defined as amount of solid that goes into solution per unit time under standardized conditions of liquid/solid interface, temperature and solvent composition, is a function of the drug's aqueous solubility and it's dose:solubility ratio. The dose:solubility ratio is defined as the volume of liquid required to completely dissolve a particular dose of drug. An aqueous solubility of below 100 µg/mL and a dose:solubility ratio of greater than one litre is often linked with poor-water solubility (Dressman et al, 2001).

Poorly water-soluble drugs often exhibit inadequate clinical performance due to their poor, erratic dissolution and bioavailability profiles, high fed-fasted ratio, and high inter-patient variability. Table 1.1 gives the USP definition of solubility. Many drug classification systems incorporate the drug's aqueous solubility as a critical defining parameter.

Table 1.1: Solubility definition in the USP (USP 26, NF 21, 2003).

Description forms (solubility definition)	**Parts of solvent required to dissolve one part of solute**	**Solubility range (mg/mL)**
Very soluble (VS)	<1	>1000
Freely soluble (FS)	From 1 to 10	100–1000
Soluble (S)	From 10 to 30	33–100
Sparingly soluble (SPS)	From 30 to 100	10–33
Slightly soluble (SS)	From 100 to 1000	1–10
Very slightly soluble (VSS)	From 1000 to 10,000	0.1–1
Practically insoluble (PI)	>10.000	<0.1

Biopharmaceutics Classification System

The Biopharmaceutics Classification System (BCS) divides drugs into four main classes according to their aqueous solubility and intestinal permeability (Figure 1.4). The BCS is based on the understanding that the dissolution of a drug is chiefly determined by its intrinsic aqueous solubility while its absorption is determined by its permeability properties (Amidon et al, 1995). The BCS is widely used in the design and development of innovative drugs, new dosage forms, clinical pharmacology and drug regulation. Aqueous solubility is assessed by measuring the volume of aqueous solvent required to dissolve the highest dose of drug at 37°C in the pH range of 1 to 7.5. Intestinal permeability refers to the ability of a compound to transverse the gastrointestinal membrane by passive diffusion, active or facilitated transport. In order to assess intestinal permeability, pharmacokinetic data from humans, human perfusion data, data from *in vivo* or *in situ* animal models or validated cell cultured monolayers are frequently used. Computational methods such as calculation of log P have also been employed.

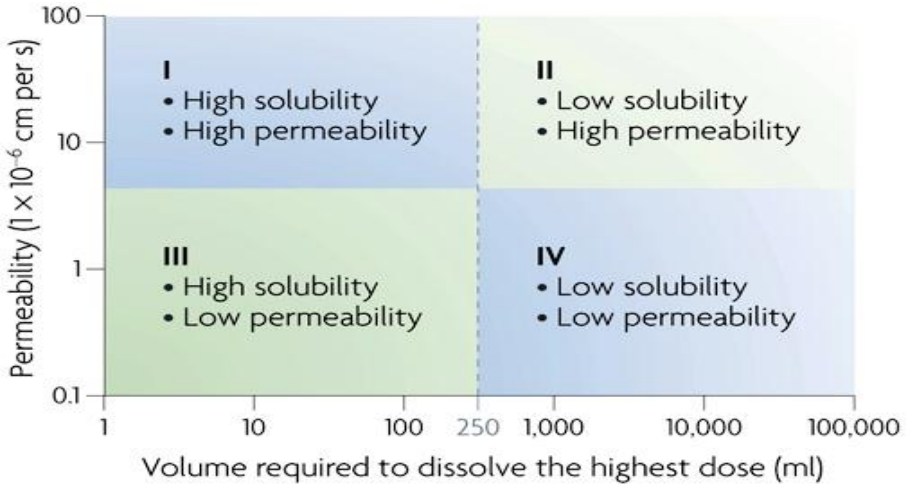

Figure 1.4: Biopharmaceutics classification system (Rautio et al, 2008).

BCS class I drugs are highly soluble and highly permeable. A drug is termed highly permeable when a 90% bioavailability is achieved relative to an intravenously administered dose. A highly soluble drug is one in which the highest dose strength is soluble in 250 mL water over the pH range 1-7.5. Such compounds are suitable for oral delivery as they exhibit both a high dissolution rate and high bioavailability.

Activity may only be limited by gastric emptying time. Examples of BCS class I drugs include metoprolol, propanolol and verapamil.

BCS class II drugs are highly permeable but poorly water-soluble and display dissolution rate limited activity. Current research into dissolution enhancement techniques e.g. micronization, complexation, solubilisation among others, often involves the use of many drugs from this class. Examples of BCS class II drugs include griseofulvin, cephalexin, carbamazepine and naproxen.

BCS class III drugs are highly water-soluble but poorly permeable. Their activity is permeability rate limited and consequently their formulation frequently involves the use of penetration enhancers. Examples of BCS class III drugs include amoxicillin, ranitidine, methyl dopa, losartan and atenolol.

BCS class IV drugs display both low water-solubility and permeability. These are the most difficult drugs to formulate; portraying both dissolution and permeability rate limited activity. Nonetheless a number of compounds in this class are available on the market. Examples of BCS class IV drugs include frusemide and hydrochlorothiazide (Lenneras et al, 2007).

The FDA issued guidance to industry on waivers of *in vivo* bioavailability and bioequivalence studies on immediate release solid dose forms of BCS class I drugs in August 2000 (Guidance CHER/FDA, 2000). Since then, further extensions to the biowaivers have been proposed for rapidly dissolving BCS class III compounds provided that the excipients do not affect drug permeability (Yu et al, 2002). These extensions have been adopted in recent WHO guidelines (WHO 2006).

Developablility Classification System

The Developability Classification System (DCS) is a recent revision of the BCS and attempts to categorise drugs according to factors which limit their oral absorption. It is not designed as a regulatory classification for assurance of bioavailability, but rather as a guideline in early product development. The DCS incorporates an estimate of human fasted intestinal solubility as a primary measure of *in vivo* solubility using biorelevant dissolution media, a solubility limited absorbable dose (SLAD) and dissolution rate expressed as a target drug particle size rather than the dose/solubility ratio. The introduction of a target particle size provides additional information on any potential dissolution rate sensitivity.

Assumptions necessary for the DCS include the use of single values for solubility and permeability in the upper small intestine as the region of interest for oral absorption, a total volume of fluid available in the GI tract in the fasted state for drug dissolution of about 500 mL, a compensatory permeability and solubility for highly permeable/low solubility compounds and a dissolution number (Dn) relating dissolution rate and solubility.

SLAD is the product of an estimate of small intestine solubility, fluid volume (500 mL) and a permeability dependent multiplier. It provides an estimate of the dose above which oral absorption is likely to be limited by intestinal solubility. SLAD divides class II compounds into classes IIa and IIb, and shifts the boundaries between class I and II high permeability drugs and between class III and IV low permeability drugs (Figure 1.5). The subdivision of class II drugs can help define optimal formulation strategies in product development. Class IIa drugs display dissolution rate limited activity. Control of factors affecting drug release such as particle size, surface area and wettability are critical in their formulation. Class IIb compounds on the other hand are solubility limited and therefore these drugs may need to be formulated in an already solubilised form (Butler et al, 2010). Table 1.2 shows the DCS reclassification of selected drugs across the BCS classes.

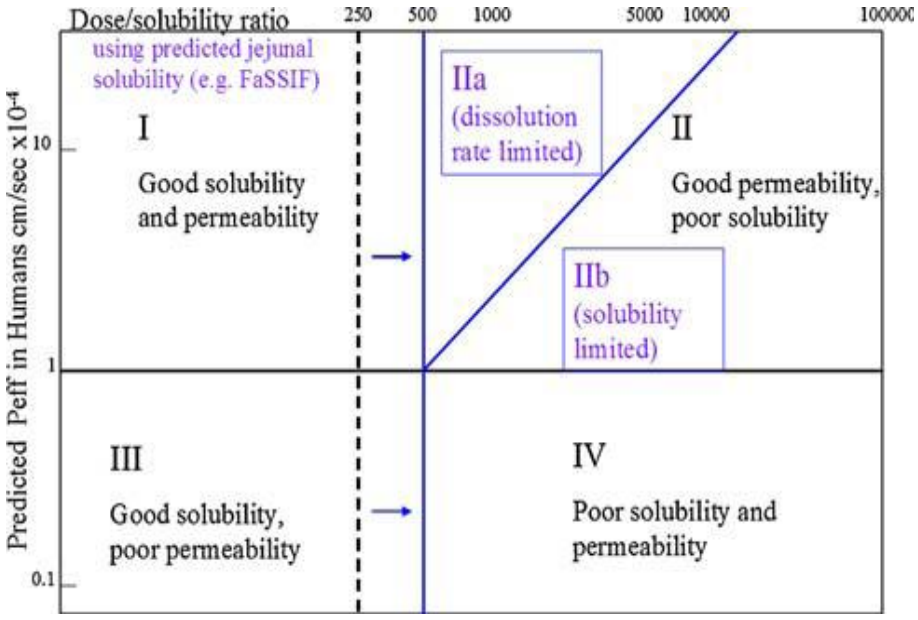

Figure 1.5: Developability classification system (Butler et al, 2010).

Table 1.2: DCS reclassification of selected drugs (Butler et al, 2010).

Drug and Dose	BCS Category	FaSSIF[d] Solubility (mg/mL)	Estimated Human P_{eff}[f] ($cm/s \times 10^{-4}$)	DCS Category	SLAD[a] (mg)	Max Particle Size (µm D_{90}[e])
Digoxin 0.5 mg	I/III	0.017	0.9	I/III	8.5	32
Paracetamol 500 mg	I	14	1.3	I	9100	900
Griseofulvin 500 mg	II	0.019	8.7	IIb	83	34
Mefenamic acid 250 mg	II	0.036	14	IIa	280	42
Ibuprofen 400 mg	II	1.46	12	I	8800	300
Dipyridamole 100 mg	II	0.023	1.5	IIb	17[b]	37[b]
Acyclovir 800 mg	IV	1.3	0.25	IV	650	280
Furosemide 80 mg	IV	1.7	0.6	III	850	120[c]

a: Solubility limited absorbable dose. b: For dipyridamole, which is soluble in the stomach, these intestinal solubility derived parameters will be of less significance. c: For furosemide, the target particle size was calculated using a shorter intestinal transit time (0.5 h), assuming absorption is limited to the upper small intestine. d: Fasted state simulated intestinal fluid. e: particle size below which 90% of the particle size distribution (by volume) is found f: permeability coefficient.

1.3 Dissolution enhancement

Dissolution is the process by which a solid substance undergoes mass transfer from a solid surface into a liquid phase. Dissolution rate is measured under standardized conditions of temperature, solvent volume and composition.

The widely accepted drug dissolution theory is the Film Theory. This theory postulates a two step process; firstly formation of a stagnant diffusive layer saturated with drug substance around the particle, followed by the diffusion of drug from this stagnant phase into the bulk solution (Figure 1.6).

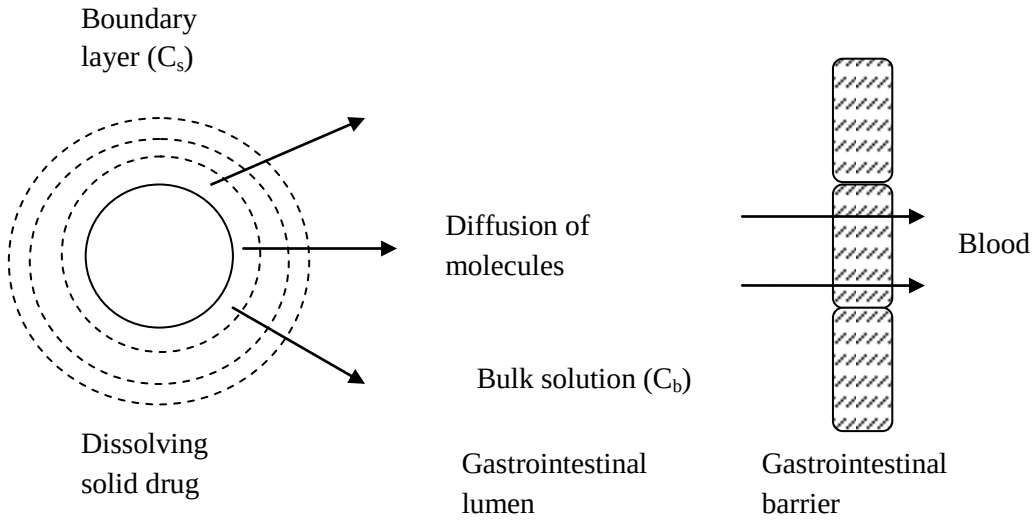

Figure 1.6: Diffusion layer model for drug dissolution showing the boundary layer with drug concentration C_s and the bulk solution with drug concentration C_b.

Drug dissolution may follow first order kinetics under non-sink conditions (dissolution rate is dependent on drug concentration in bulk) whereby the volume of the dissolution media is less than three times that required to form a saturated drug solution. However, under sink conditions (*in vivo)* where the drug is rapidly absorbed and the drug concentration in bulk approaches zero, dissolution follows zero order kinetics (dissolution rate is independent of drug concentration in bulk).

The kinetics of drug dissolution can be described by the Noyes Whitney Equation;

$$\frac{dQ}{dt} = \frac{D}{h} SA\left(C_s - C_b\right) \qquad \text{(Equation 1.1)}$$

where dQ/dt is the dissolution rate, D is the diffusion coefficient of drug, SA is the effective surface area, C_s is the concentration of drug at boundary layer, C_b is the concentration of drug in bulk and h is the thickness of diffusion boundary.

Dissolution rate can thus be enhanced by increasing the diffusion coefficient of the drug, the saturation concentration of the drug in the bulk solution, its surface area and/or by decreasing the thickness of boundary layer.

Increasing saturation solubility

1.3.1 Polymorphism

Many classes of drugs are known to exhibit polymorphism. Polymorphs possess different lattice energies and physico-chemical properties such as melting point, solubility, heat of fusion, density, e.t.c. Enhanced dissolution rates of a drug can be achieved by the selection of metastable polymorphs with higher apparent solubilities than the stable, crystalline form.

The use of the term polymorphic forms variably refers to crystalline forms that have different arrangements and/or conformations of the molecules in the crystal lattice, amorphous forms consisting of disordered arrangements of molecules that do not possess a distinguishable crystal lattice, or solvates which are crystal forms containing either stoichiometric or nonstoichiometric amounts of a solvent. If the incorporated solvent is water, the solvate is commonly known as a hydrate (Byrn et al, 2000). Examples of drugs exhibiting polymorphism include steroids, barbiturates, and sulphonamides (Higuchi et al, 1967). Commercial exploitation of metastable polymorphs is limited by their inter-conversion into the less soluble, crystalline form.

1.3.2 Solubilization

Solubilization is defined as the preparation of a thermodynamically stable isotropic solution of a substance normally insoluble or very slightly soluble in a given solvent by the introduction of additional amphiphilic component(s). The amphiphilic component, namely a surfactant, must be introduced either at the critical micellar concentration (cmc) or a concentration above it.

Micelles are surfactant aggregates with an anisotropic water distribution within their structure. In aqueous solvents, the water concentration decreases from the surface

towards the core of the micelle, where it is completely excluded from the hydrophobic core. Consequently, the average spatial position of a solubilized drug in a micelle will depend on its polarity - nonpolar molecules will be solubilised in the micellar core, and substances with intermediate polarity will be distributed along the surfactant molecules in intermediate positions (Rangel-Yagui et al, 2005).

Microemulsions are single phase, optically isotropic, thermodynamically stable solutions of water, oil and amphiphile (Danielsson et al, 1981). By virtue of their oil core, oil-in-water microemulsions generally have a greater solubilising power than their corresponding micellar solutions.

Nanoemulsions are often confused with microemulsions but differ in that they are kinetically (as opposed to thermodynamically) stable and comprise of slightly larger sized droplets. (Anton et al, 2011).

The inclusion of hydrophobic drugs in micelles, microemulsions or nanoemulsions to increase their apparent aqueous solubility has been widely used in drug delivery (Lawrence et al, 2000). Surfactant toxicity and formulation instability upon dilution are major challenges faced with this technique of increasing the apparent aqueous solubility of a drug.

1.3.3 pH adjustment

The majority of drugs are either weak acids or bases. The degree of ionization of these drugs is governed both by their dissociation constants (pKa) and the pH of the dissolution medium. The pKa, which can be calculated from the Henderson-Hasselbalch Equation, is the pH at which 50% of the drug is ionized. pH modification can be used to increase the presence of the ionized species of drug in solution thereby enhancing its dissolution rate and solubility (Otzurk et al, 1988). Drugs that make good candidates for increasing their solubility by this method are those that ionize between pH 2-8. Examples of drugs formulated in buffer systems include; amikacin sulphate (pH 3.5-5.5 citrate buffer), midazolam hydrochloride (pH 3) and acetylsalicylic acid (magnesium oxide or calcium carbonate buffer). Precipitation of a drug upon dilution with the intestinal contents, which may be at pH at which drug is less soluble, as well as toxicity and tolerability issues associated with extreme pHs, are among the drawbacks of this technique.

1.3.4 Salt formation

Salts of acidic/basic drugs usually have a higher aqueous solubility than their corresponding free acid or base. This is due to their higher ionization causing a rapid saturation of the diffusion layer surrounding the drug. A careful assessment of the interrelationship between the intrinsic solubility, pKa and possible salt forms is necessary when formulating poorly water-soluble drugs as salts. With the increased number of extremely poorly water-soluble drug compounds currently in development, strong anions or cations are required for effective salt formation.

About 77% of the salts of basic drugs approved by FDA (1995-2006) were prepared using relatively strong counterions, namely the hydrochloride, methanesulfonate, hydrobromide/bromide, sulfate/bisulfate and nitrate. Similarly, 73% of the salts of acidic drugs were prepared with strong alkalis such as NaOH and KOH (Serajuddin 2007). The use of these strong counterions may lead to toxicity concerns when the salt is administered orally. Examples of drugs formulated as salts to increase dissolution include theophylline as the isobutanolamine salt and penicillin V as the potassium salt, among others. Pharmaceutical salts also have other actions e.g. reducing drug toxicity, organoleptic properties, prolonging drug action and improving drug stability (Berge et al, 1977).

1.3.5 Complexation

Poorly water-soluble drugs can be complexed with a soluble intermediate (such as a cyclodextrin, caffeine or donor acceptor) to form a soluble intermolecular complex. Cylodextrins are cyclic oligosaccharides formed by the enzymatic hydrolysis of starch. They generally contain 6, 7 or 8 glucose units, linked by α-(1, 4) bonds and are known as α-, β-, γ- cyclodextrins respectively. Cyclodextrins possess a hydrophilic exterior with a hydrophobic interior cavity into which poorly water-soluble drugs can be incooperated. The interaction between the drug and cyclodextrin is governed by hydrophobic interactions, van der Waals forces and hydrogen bonding. The water-soluble inclusion complexes formed by cyclodextrins frequently exhibit new, physico-chemical characteristics compared with the original guest molecules, including better stability, higher water solubility, increased bioavailability and/or decreased undesirable side effects. β-cyclodextrin has been widely used for drug delivery because it is readily available and interacts with a wide variety of pharmaceutical compounds. However, the low water solubility and

nephrotoxicity of β-cyclodextrin has lead to development of more water-soluble alternatives such as 2-hydroxypropyl-β-cyclodextrin, methyl-β-cyclodextrin and sulfobutyl ether-β-cyclodextrin.

There are currently over 30 cyclodextrin-linked drugs on the market. These include alprostadil, cefotiam hexetil HCl (α-cyclodextrin); dexamethasone, nicotine, nitroglycerin, piroxicam (β-cylodextrin); cisapride, indomethacin, mitomycin (2-hydroxypropyl-β-cyclodextrin); diclofenac sodium (2-hydroxypropyl-γ-cyclodextrin) (Loftsson et al, 2005).

1.3.6 Prodrugs

Prodrugs are inactive derivatives of a drug that undergo enzymatic or chemical conversion *in vivo* to yield the active parent drug moiety which then exerts its desired pharmacological action. Common functional groups that are amenable to prodrug design include carboxylic, hydroxyl, amine, phosphate/phosphonate and carbonyl groups, which can be modified to esters, carbonates, carbamates, amides, phosphates and oximes.

49% of all prodrugs in the market are esters (Ettmayer et al, 2004). Phosphate esters of hydroxyl and amine functionalities are commonly used to improve drug solubility e.g. sulindac, miproxfene phosphate TAT-59, fosamprenavir, estramustine phosphate, prednisolone phosphate and fludarabine phosphate (Rautio et al, 2008).

1.3.7 Solid dispersions

Solid dispersions are two component systems comprising of a hydrophilic matrix (amorphous or crystalline) and hydrophobic drug (amorphous, crystalline or molecularly dispersed). Categories of solid dispersions include simple eutectic mixtures, glass solutions, solid solutions and amorphous precipitates in a crystalline carrier (Chiou et al, 1971; Brientechbach 2002).

Techniques such as the fusion method, hot melt extrusion, the solvent method and supercritical fluid technologies are used to produce solid dispersions. Limitations encountered with solid dispersions include laborious, expensive preparation methods and scale up of manufacture as well as the difficulty in further formulating the solid dispersion into a dosage form. Gris-PEG by Novartis (griseofulvin in polyethylene glycol), Cesamet by Lily (nabilone in polyvinylpyrrolidone), Sporanox by Janssen Pharmaceutica (itraconazole in hypromellose and polyethylene glycol 20,000

sprayed on sugar spheres), Rezulin by Parke-Davis (troglitazone formulation), Zoladex parenteral implants (geoserelin in polylactidecoglycolide), Depotprofact (buserelin in polylactidecoglycolide), Kaletra by Abbott (lopinavir/ritonavir) and Norvir by Abbott (ritonavir) are among the solid dispersion products currently on the market (Dhihendra et al, 2009).

Increasing surface area

The surface area of a drug is a critical factor in determining its dissolution rate. The effective surface area available for dissolution is a function of both particle size and the ability of the fluid to wet the drug particles.

1.3.8 Wetting

Most poorly water-soluble drugs are also poorly wetted. Low levels of surfactant have historically been included in many drug formulations to improve drug wetting properties (Singh et al, 1968). The beneficial effect of surfactants on the drug wetting processes is as a result of their adsorption at the solid drug-liquid interface resulting in a change of interfacial tension - surfactants can reduce the liquid-air and/or liquid-solid interfacial tension. The hydrophobic chains of the surfactant typically adsorb onto the hydrophobic surface of the drug particle, while their hydrophilic head extends towards the aqueous solution. Native surfactants present in the gastrointestinal tract e.g. bile salts, have also been shown to improve drug wetting.

1.3.9 Particle size reduction

In comparison to other factors in the Noyes Whitney equation, particle size reduction has the greatest impact on drug dissolution. A reduction of particle size leads to an increase in surface area, thereby increasing dissolution rate. Micronisation, which is reduction of particle size to within the 1-10 μm size range, is widely exploited in the pharmaceutical industry. The required reduction in particle size is generally achieved by mechanical processes such as milling, cutting, crushing, and grinding. Equipment used for comminution includes ball mills, hammer mills, fluid energy mills, pin mills, rotary cutters and colloid mills. The selection of the type of mill to be used depends on factors such as the physical properties of the material, the operation process, auxillary equipment and safety. A further reduction of particle size to within

the nanometer size range is envisaged to further increase dissolution rate and bioavailability as depicted in Figure 1.7.

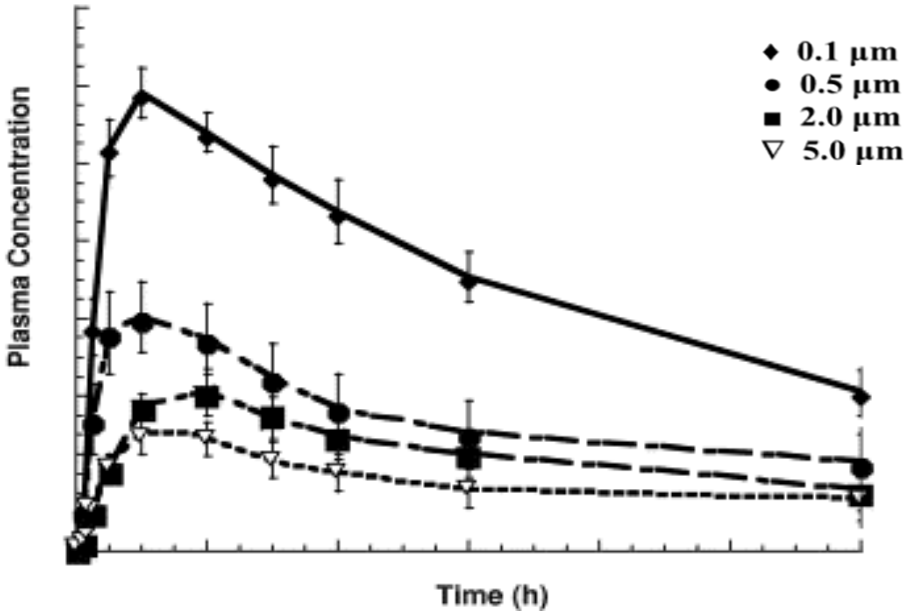

Figure 1.7: Variation of drug bioavailability with particle size (Merisko-Liversidge et al, 2003).

However dry milling, often used for micronisation, can only yield microparticles, i.e. particles within the 1-10 µm size range. Attempts to further reduce particle size below 1 µm, leads to aggregation and clumping of powder in the mill due to high van der Waals forces (Parrott 1974).

1.4 Nanoparticle production

Recent technological advances in the understanding of colloidal systems has allowed the formulation of nanometre sized crystalline drug particles in a reproducible manner. These nano-sized drug crystals are often stabilized by surfactants and/or polymers adsorbed onto their surfaces thereby overcoming the high surface energy of nanoparticles.

Nanoparticles may be manufactured by 'top down' approaches which involve breaking down of large particles into smaller ones e.g. media milling, high pressure homogenization or by 'bottom up' approaches involving controlled precipitation/crystallization to obtain the desired particle size (Figure 1.8).

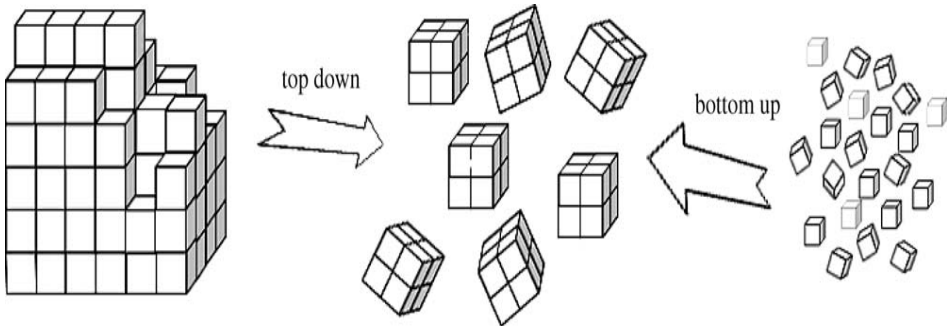

Figure 1.8: Schematic representation of top down and bottom up approaches to nanoparticle production (Verma et al, 2009).

Table 1.3 lists the nanocrystalline drugs currently on the market. The nanoparticles are all produced via the 'top down' approaches namely media milling and high pressure homogenization. Nanoparticle formulations exhibit a rapid onset of action, a reduced fed-fasted ratio, improved bioavailability and an increased therapeutic effectiveness (Chaubal 2004). Nanoparticles enhance dissolution by increasing not only surface area, but also by increasing the saturation solubility of the drug. Such nanoparticulate systems can also be used to target drug delivery to specific sites. For example, thiamine coated nanoparticles have demonstrated a preferential uptake in the brain, utilising the blood-brain barrier thiamine transporters (Lockman et al, 2003).

The nanosuspensions can be transformed into solid products using well-defined unit operations such as freeze-drying, spray drying, pellization and granulation (Mersiko-Liversidge et al, 2003, 2008; van Eerdenburgh et al, 2008; Yunhui et al, 2007).

Table 1.3: Key characteristics of nanoparticle formulations currently available in the market (van Eerdenburgh et al, 2008; FDA 2009).

Product, active ingredient, company	Date of FDA approval	Manufacturing approach, manufacturing technique	Dose, dosage form	Rationale for development as a nanocrystalline dosage form
Rapamune®, Sirolimus, Wyeth	August 2000	Top-down, media milling	1 and 2 mg, tablets	Re-formulation of the oral solution that requires refrigeration storage and is less easy to administer.
Emend®, Aprepitant, Merck	March 2003	Top-down, media milling	80 and 125 mg, capsules	New chemical entity, formulation as nanocrystals reduces fed/fasted variability.
TriCor®, Fenofibrate, Abbott	November 2004	Top-down, media milling	48 and 145 mg, tablets	Re-formulation for a more flexible dosing regime and to prevent the need of administration with a meal
Megace® ES, Megestrol acetate, Par Pharmaceutical	July 2005	Top-down, Media milling	125 mg/mL, nanosuspension	Re-formulation of the oral suspension to obtain a higher dissolution rate, bioavailability and ease of administration (reduced dosing volume and suspension viscosity).
Invega® Sustenna®, Paliperidone palmitate, Janseen	July 2009	Top-down, Media milling	Once monthly injection	Monthly dosing to improve compliance by patients.
Triglide®, Fenofibrate, Skye Pharma	May 2005	Top-down, high-pressure homogenization	50 and 160 mg, tablets	Reduce fed/fasted variability, as for TriCor®.

Techniques for nanoparticle production include:

1.4.1 Precipitation

Typically, the drug is first dissolved in a solvent followed by the addition of a miscible anti-solvent. The drug then precipitates out of solution and is recovered by solvent evaporation. The resultant nanoparticles are stabilised by surfactants added to the drug solution and/or anti-solvent during processing. Controlled conditions are required to achieve a high nucleation rate and a low growth rate. Mixing processes vary and include the infusion of anti-solvent into solvent ensuring low levels of supersaturation and a narrow size range of the resultant nanoparticles (Violante et al, 1991), while the rapid addition of solvent to anti-solvent leads to high levels of supersaturation and consequently rapid nucleation producing smaller nanoparticles (Mahajan et al, 1993).

The disadvantages of the precipitation method include the difficulty in controlling crystal growth, the difficulty in obtaining a narrow size distribution, the requirement that the drug is soluble in one solvent, toxicity and environmental concerns of the non-aqueous solvents used (Kipp 2004). Recent advances in precipitation technology include the use of gravity (Chen et al, 2004), ultrasonication (Kumar et al, 2009), liquid nitrogen for freeze drying (Waard et al 2008; Yanga et al, 2008), and acid-base neutralization reactions (Chen et al, 2008). Precipitation has also been coupled to high pressure homogeniztion using NANOEDGE technology (Kipp 2004). Nanoparticles have also been obtained by the evaporation of the solvent from emulsions and microemulsions, which contain drug in the hydrophobic phase.

1.4.2 High pressure homogenisation

High pressure homogenization is patented by Skyepharma under the tradename Disso Cubes®. Currently one drug formulated using the 'Disso Cubes' formulation technology, namely Triglide®, is available on the market (Table 1.3). A suspension containing drug and stabiliser solution is pumped through a narrow gap at high pressure (15,000-30,000 psi). The suspension flows through the very thin aperture (about 25 μm) at extremely high velocity. To maintain constant energy, this high flow is compensated by a dramatic decrease in static pressure below the vapor pressure of water, causing boiling of the suspension to occur. As the suspension exits the gap, the pressure suddenly rises to ambient pressure and the vapor bubbles

implode (or cavitate). This implosion generates considerable local energy as turbulent flow and heat.

Particle size reduction variously occurs via implosion (cavitation) forces, high shear forces and interparticle impact. The high pressure homogenizer consists of a high-pressure plunger pump and a subsequent homogenezing valve (Figure 1.9). Homogenizers are available in different capacities ranging from 40 mL (for lab use) to several thousand litres (for industrial use).

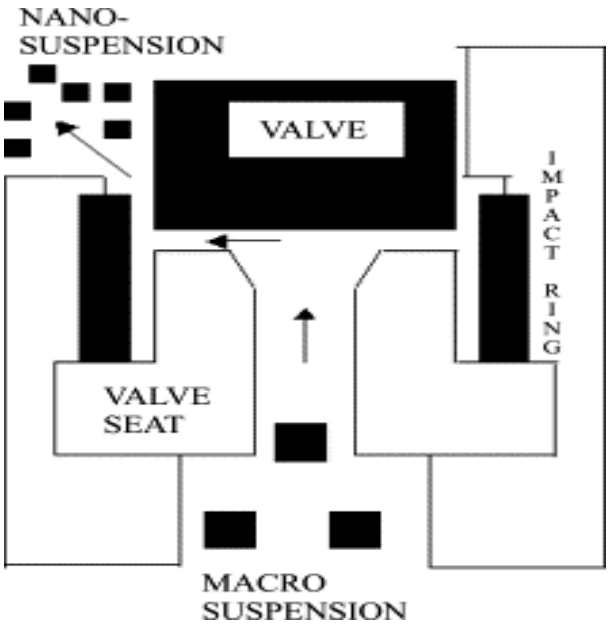

Figure 1.9: Schematic representation of high-pressure homogenization process (Patravale et al, 2004).

The particle size reduction achieved is dependent on the number of homogenisation cycles used, the temperature and the power density of the homogeniser. Advantages of this technique include low contamination levels, ease of scale-up, little batch-batch variation and a narrow size distribution of the resultant nanoparticles. Drawbacks include the clogging of the gaps with concentrated drug formulations and a prerequisite for micronisation of the drug before loading into the homogeniser (Muller et al, 1999; Kipp 2004).

1.4.3 Supercritical fluid processing

Supercritical fluids (SCFs) such as CO_2 have been used for nanoparticle production due to their mix of gas-like and liquid-like properties. In addition to advantages such as gas-like diffusivities, tunable solvent power/selectivity and ease of elimination,

SCFs can be employed as solvents, anti-solvents or reaction media (Reverchon et al, 2006).

Rapid expansion of supercritical solutions

Rapid expansion of supercritical solutions (RESS) is employed for drugs soluble in SCFs. Supercritical CO_2 is the preferred solvent for RESS though other solvents such as propane, pentane, methane, acetone amongst others may be used. The process entails saturation of the supercritical fluid with the drug substrate. The resultant solution is then depressurised through a heated nozzle into a low pressure chamber resulting in a high degree of drug supersaturation leading to homogeneous nucleation (Figure 1.10).

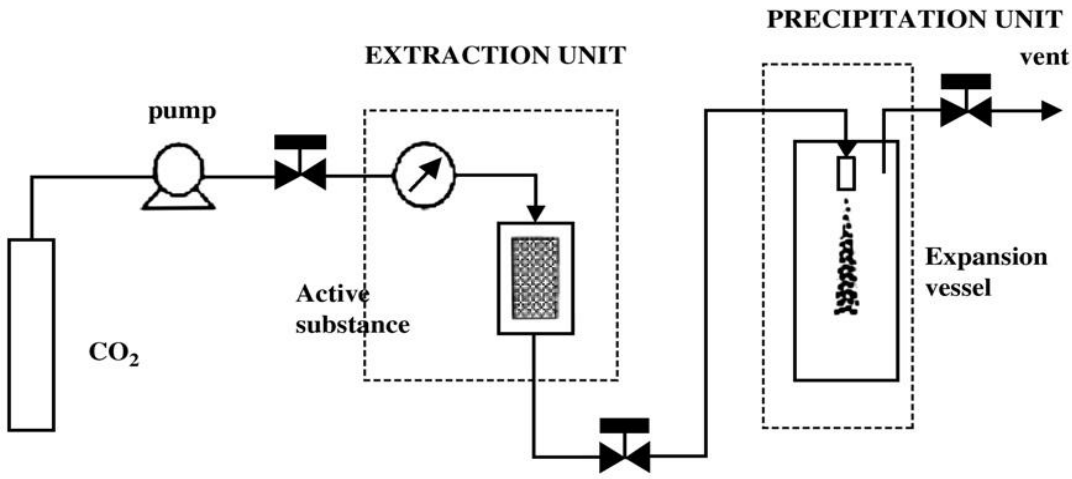

Figure 1.10: The rapid expansion supercritical solution process is shown in a schematic representation (Byrappa et al, 2008).

The RESS parameters such as temperature, pressure drop, e.t.c. as well as the chemical nature of the drug influence the morphology of the resultant nanoparticles. RESS is particularly attractive as it eliminates the need for organic solvents in nanoparticle production. A major limitation of RESS is that many high molecular weight drug compounds with polar bonds have negligible solubility in supercritical CO_2 (Byrappa et al, 2008). In addition, it is also difficult to control particle size and morphology using this technique.

Supercritical anti-solvent precipitation

For CO_2 insoluble drugs, supercritical anti-solvent (SAS) entails first dissolving the drug in an organic solvent, then atomizing the solution in an excess continuum of

flowing supercritical fluid (Figure 1.11). The underlying principle being that when a drug solution is expanded sufficiently by an anti-solvent, supersaturation and nucleation occurs due to the lower solubility strength (Byrappa et al, 2008). The prerequisites for a successful SAS process are the complete miscibility of the liquid solvent and the anti-solvent and the insolubility of the solute in the anti-solvent.

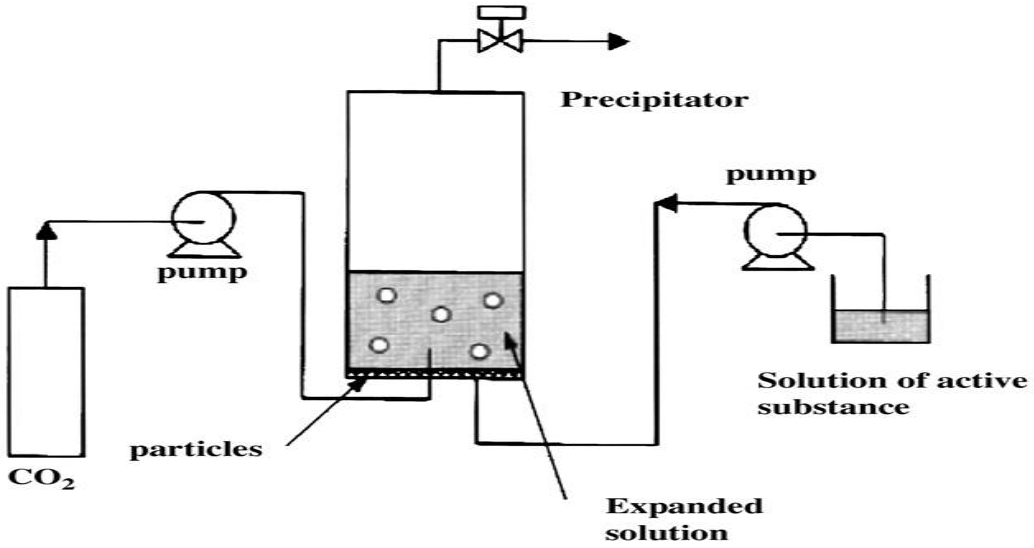

Figure 1.11: The supercritical anti-solvent precipitation process is shown schematically (Byrappa et al, 2008).

Recently, several modifications of the RESS and SAS processes have been employed for nanoparticle production. These include supercritical assisted atomization, sol/gel formation among others (Reverchon 2003).

1.4.4 Media milling

Wet bead milling (WBM) utilises the Elan 'Nanocrystal' technology in which crystalline drug is milled in the presence of a solution of stabilisers yielding nanometer sized drug particles. Currently five drugs formulated using 'Nanocrystal' formulation technology namely Rapamune®, Emend®, TriCor®, Megace®, Sustenna® are available in the market (van Eeerdenburgh et al, 2008; FDA 2009).

In order to wet bead mill a drug, a slurry consisting of drug, water and stabiliser along with milling media are loaded into the mill. Figure 1.12 shows a cross section of the media mill. The drug concentration used generally ranges from 1 to 400 mg/mL. The milling media consists of spherical glass, yttrium zirconia stabilised, ceramic or plastic (highly cross linked polystyrene resin) beads of 0.4-3 mm

diameter. The slurry and milling media are rotated at a very high shear rate either by paddles in the milling chamber, or by oscillation of the milling chamber. Mills can be operated in either the re-circulation or batch mode. The milling media fractures the drug crystals into a homogeneous nanocrystalline dispersion, which is then screened to separate it from the milling media. Milling is usually carried out under controlled temperature by the use of coolants. Particle size reduction is achieved mainly by mechanical attrition and impact (Kipp 2004 and Merisko-Liversidge et al, 2003; 2008).

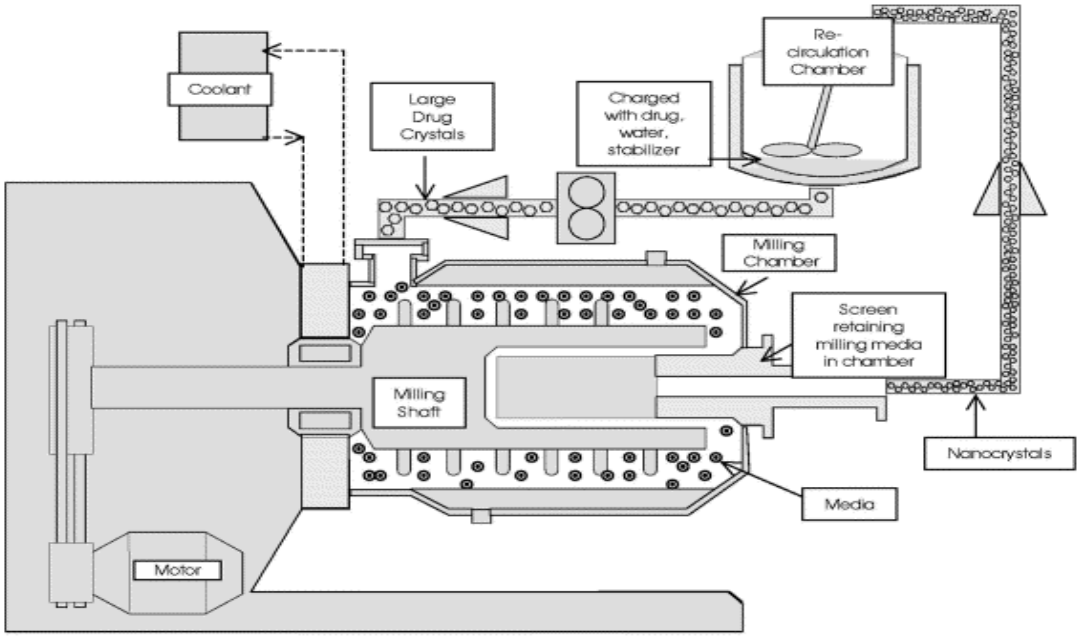

Figure 1.12: The media milling process is shown schematically (Merisko-Liversidge et al, 2003).

WBM offers advantages over other nanosizing techniques, such as minimal batch-to-batch variation, eliminating the need for the pre-micronization of drugs, avoiding the need for the use of organic solvents, the resultant narrow particle size polydispersity and the easy scale up to industrial level.

The main drawbacks in this technique are product contamination by the milling media and the possibility of milling induced disorder in the drug crystalline lattice. There is a need to test the milling process in order to ensure that any shedding by the milling media is minimal and any product contamination is below acceptable levels for pharmaceutical products. Secondly, the nanocrystalline drug has to be screened for any amorphous transitions or crystal defects using techniques such as solution

calorimetry, dynamic scanning calorimetry, moisture sorption and X-ray powder diffraction (Iaccocca et al, 2009).

1.5 Nanoparticle stabilisation

Owing to their high surface area to volume ratio, nanoparticles have a tendency to aggregate due to van der Waals forces. Stabilisers act to cancel out the attractive nature of the van der Waals forces by introducing repulsive steric or electrostatic forces at the nanoparticle surface.

Adsorption

Adsorption usually occurs at interfaces be it the air-liquid, the liquid-liquid or the solid-liquid interface. At the solid-liquid interface, adsorption results from the interplay of electrostatic interactions, van der Waals forces, hydrogen bonding and covalent bonding between the adsorbing species and the solid surface as well as interactions between the adsorbed species. It is an equilibrium process with depletion and adsorption occurring simultaneously.

Adsorption can either be classified as physical or chemical. Physical adsorption usually occurs due to van der Waals forces or electrostatic charges between the adsorbate and the adsorbent and is usually weak and reversible. Chemical adsorption on the other hand is much stronger and irreversible and occurs due to covalent bonding between the adsorbate and the adsorbent.

Adsorption isotherms have been extensively used to characterise adsorption and they represent the amount adsorbed as a function of adsorbate concentration at a constant temperature. Adsorption density, which is the amount of adsorbate deposited at the interface, is usually measured by depletion of the adsorbate from solution.

Adsorption density is defined by the following equation:

$$\Gamma = \left(C_f - C_i\right)\frac{V}{W} \qquad \text{(Equation 1.2)}$$

where Γ is the adsorption density, C_i and C_f are the initial and final concentrations of adsorbate in solution, V is the volume of solution, and W is the mass of the adsorbent.

1.5.1 Electrostatic (ionic) stabilisation

Colloidal particles may bear a surface charge originating from the ionization of surface groups, the differential loss of ions from the crystal lattice or the adsorption of charged species (ions or ionic surfactants). A negatively charged particle attracts positive counterions surrounding the particle. The electrical double layer is the layer surrounding a dispersed particle and includes the ions adsorbed directly onto the particle surface and an outer layer of countercharged ions in the dispersion medium. As shown in Figure 1.13, the electrical double layer is overall electrically neutral and consists of three parts:

- **Surface charge:** charged ions adsorbed on the particle surface.
- **Stern layer:** counterions (charged opposite to the surface charge) attracted to the particle surface and closely attached to it by the electrostatic force.
- **Diffuse layer:** a film of the dispersion medium (solvent) adjacent to the particle. The diffuse layer contains a higher concentration of the counterion than in the bulk. The charge of the ions in the diffuse layer is influenced by the electrostatic force of the charged particle.

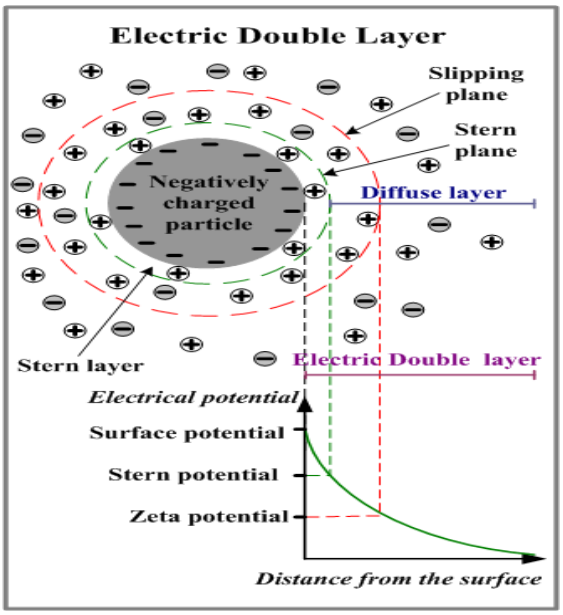

Figure 1.13: The electrical double layer (Kopeliovich 2011).

The electrical potential within the electric double layer has a maximum value at the surface of the particle (surface potential). The potential drops with an increase in distance from the particle surface and reaches zero at the boundary of the electric

double layer. When a colloidal particle moves in the dispersion medium, a layer of the surrounding liquid- whose boundary is known as the slipping plane remains "attached" to the particle. The value of the electric potential at the slipping plane is called zeta potential, which is a very important parameter in the theory of the interaction of colloidal particles. Stable, charged, particles typically possess zeta potentials of above +30 mV or below -30 mV. Zeta potential is affected by pH, conductivity and the concentration of functional component (Li et al, 2007).

DVLO theory

In considering the interaction between two hydrophobic colloidal particles Derjaguin, Landau, Verwey and Overbeek came up with a theory (Derjaguin et al, 1941; Verwey et al 1948). This theory assumes that the total force (V_T) acting on the particles is a summation of the attractive (V_A) and repulsive forces (V_R) between the two particles as depicted in Figure 1.14.

$$V_T = V_R + V_A \qquad \text{(Equation 1.3)}$$

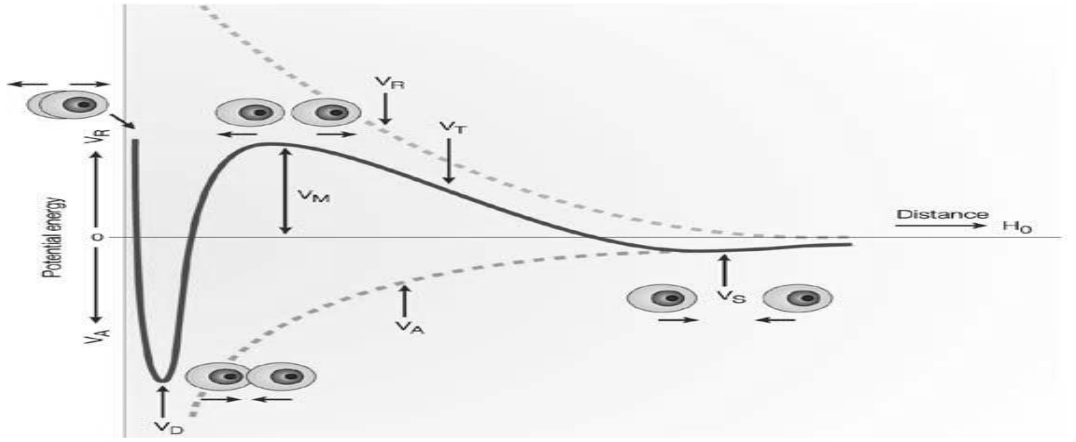

Figure 1.14: Potential energy curve for two approaching nanoparticles (Rabinow 2004).

The repulsive forces on the particles arise due to the osmotic effect brought about by increase in the number of charged species on the overlap of diffuse parts of the electrical double layer. These repulsive forces are a function of the interparticulate distance as shown:

$$V_R = 2\pi\varepsilon a\xi^2 \exp(-kD) \qquad \text{(Equation 1.4)}$$

where π is the solvent permeability, ε is the permittivity of the polar liquid, a is the radius of the spherical particle, k is a function of the ionic composition, ξ is the zeta potential and D is the distance between particles.

The attractive forces present in the system are mainly van der Waals forces, which vary as the inverse of the distance between particles.

$$V_A = \frac{-A}{12\pi D^2} \qquad \text{(Equation 1.5)}$$

where A is the Hamaker constant.

As the particles approach each other, there is a greater increase in the repulsive forces relative to the attractive forces. The maximum repulsion between the particles occurs at a separation known as the primary maximum (V_M). In order for the particles to aggregate (which occurs at the primary minimum (V_D)) the particles have to overcome these repulsive forces. The higher the intensity of the primary maxima, the more stable the suspension (Rabinow 2004).

The secondary minima (V_S) is the point at which weak, reversible flocculation occurs. Ionic stabilisers introduce an electrostatic charge on the particle surface leading to repulsion between particles. Ionic stabilisation can be achieved by ionic surfactants and/or polymers e.g. sodium dodecyl sulphate, dodecyl trimethyl ammonium bromide and hypromellose acetate succinate.

The DVLO theory only holds for dilute colloidal suspensions in which no other forces besides van der Waals and electrostatic forces are present and if the geometry of the particles is simple and the electrical double layer is purely diffusive.

Disadvantages of electrostatic stabilisation include sensitivity to the presence of electrolytes, decreased efficacy in non-aqueous dispersion media and high solid content. In addition, electrostatically-stabilised systems will overtime undergo aggregation as they are thermodynamically metastable (Napper 1983).

1.5.2 Steric stabilisation

Stabilisation of lyophobic colloids by non-ionic polymers/surfactants (a result of steric forces, V_S) was not originally described by the DLVO theory. Equation 1.3 was later modified to account for steric stabilisation by non-ionic polymers/surfactants (Figure 1.15).

$$V_T = V_A + V_R + V_S \qquad \text{(Equation 1.6)}$$

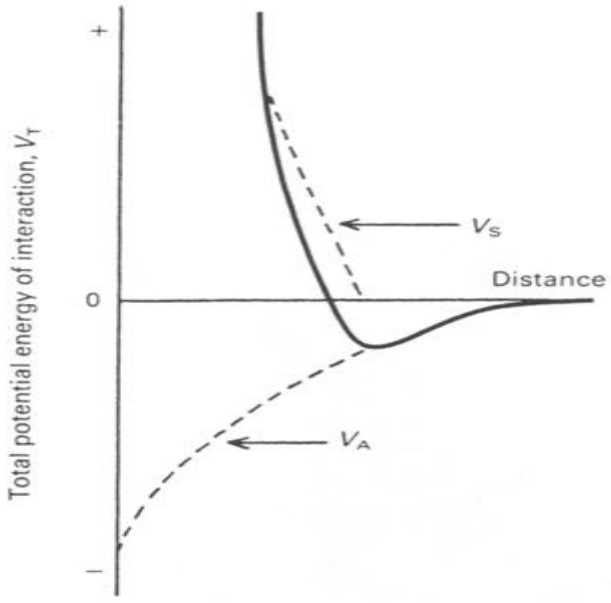

Figure 1.15: Potential energy curve for two approaching nanoparticles showing influence of steric forces (Birdi 2009).

As with charged stabilisers, steric stabilisers adsorb on the particle surface and provide a physical barrier to aggregation. However in this case, the stabilisation is provided by the entropic or osmotic constraints imposed by the stabilisers. For two particles coated with non-ionic polymers or surfactants to aggregate, the hydrophilic chains of the stabiliser have to be compressed which is entropically unstable and causes a repulsion between the particles. In other cases, the osmotic stress created by the encroaching steric layers leads to an influx of solvent molecules, which serve to keep the particles apart (Osmond et al, 1975). Steric stabilisation of particles can be achieved by a range of non-ionic surfactants and/or polymers including the Tweens®, Brij®, hypromellose and polyvinylpyrrolidone.

Figure 1.16 shows particles stabilised sterically by a polymer, where the thickness of polymer chain adsorbed on the particle is *d*. At a distance of 2*d* the polymer chains

either interpenetrate or are compressed, causing the two approaching particles to repel each other.

Steric stabilisation comprises of two main contributors; an entropic term (repulsive) which is due to change of conformation of polymers as they approach each other and an enthaphic term, which depends on the polymer-polymer versus polymer-solvent interactions. When two hydrated polymer molecules approach each other, the water of hydration is released leading to an energetically unfavourable positive enthalpy change.

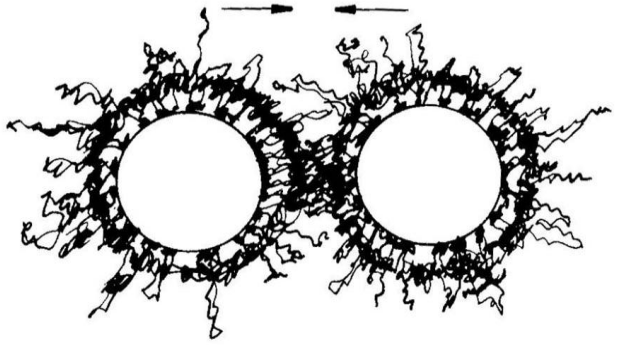

Figure 1.16: Steric stabilisation of particles by polymer layer with thickness of *d* (Shi 2002).

Steric stabilisation offers several advantages over electrostatic stabilisation including: equal efficacy in both aqueous and non aqueous dispersion media, relative insensitivity to the presence of electrolytes, equal efficacy at both high and low solid conditions and reversibility of flocculation. Sterically stabilised systems are thermodynamically stable (Napper 1983).

Polymeric stabilisation may also occur via other mechanisms including depletion flocculation, bridging flocculation and electrostatic stabilisation.

Depletion flocculation

Flocculation refers to the formation of reversible loosely packed aggregates within a colloidal suspension. Polymers can stabilise colloids via this mechanism without necessarily being adsorbed onto the colloidal particles. In such a case, the polymers exist freely in solution. As two colloidal particles approach each other, the intercolloidal distance is depleted of polymer, leading to an osmotic gradient which causes an influx of solvent between the two particles, which acts to keep the particles apart (Figure 1.17).

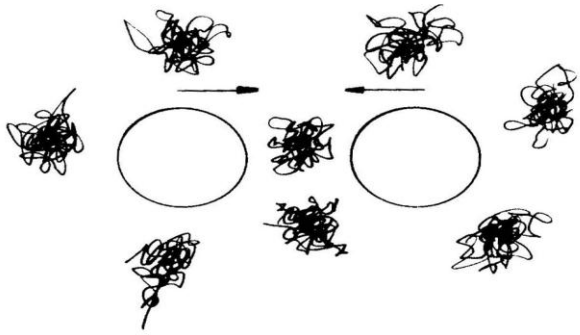

Figure 1.17: Depletion flocculation (Shi 2002).

Bridging flocculation

When a polymer chain is long enough to adsorb onto the surface of two particles (Figure 1.18A) or long enough to interact with another polymer chain absorbed on a different particle (Figure 1.18B), loosely formed aggregates of particle are formed.

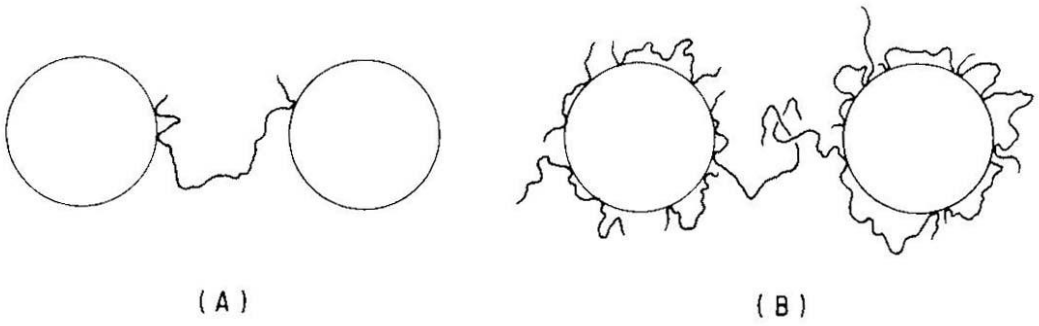

Figure 1.18: Bridging flocculation (Shi 2002).

1.5.3 Electrosteric stabilisation

Electrosteric stabilisation is achieved by the combined use of non-ionic polymers and ionic surfactants, which often complement each other in terms of their mechanism of stabilisation. Firstly, entropic steric interactions are more sensitive to temperature fluctuations than electrostatic stabilisation. Therefore the inclusion of an ionic surfactant could help protect a polymer-stabilised formulation from temperature cycling effects. Secondly, there is a synergy between ionic and non-ionic stabilisers e.g. inclusion of a polymer in a formulation stabilised by an ionic surfactant could decrease self-repulsion and thereby allow greater coverage by the surfactant (Rabinow 2004). Electrosteric stabilisation can also be achieved using charged polymers or polymeric surfactants. Although not much literature is currently available on electrosteric stabilisation, interest in it as a mechanism of stabilisation is growing.

1.6 Surfactants

1.6.1 Surfactant classification and properties

Surfactants are amphiphilic molecules; having a polar/hydrophilic head group and a non-polar/hydrophobic tail group (Figure 1.19). As such surfactants, in the monomeric form, have limited solubility in any solvent and instead tend to adsorb at interfaces; air-liquid, liquid-liquid or liquid-solid.

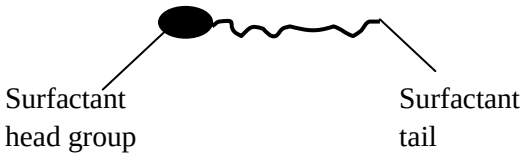

Figure 1.19: The structure of a surfactant.

Surfactants are divided into four classes according to their head group charge (Table 1.4). Anionic surfactants have a negatively charged head group e.g. sulphate, sulphonate, while cationic surfactants have a positively charged group e.g. amine. Anionic/cationic surfactants are usually incompatible with other charged compounds, as well as sensitive to hard water, salts and preservatives. These charged surfactants, in particular cationics, are frequently irritating to physiological membranes.

In zwitterionic surfactants the head group bears both a positive and negative charges in close proximity, thus they behave as effectively neutral. Zwitterionics are compatible with other charged compounds, display low skin/eye irritation and are thus widely used in dermatological preparations.

Non-ionic surfactants bear no head group charge, are compatible with other charged compounds and are unaffected by electrolytes or hard water. These surfactants are widely used in drug delivery; however they are particularly sensitive to temperature changes (Attwood et al, 1983; Rosen 2004).

Table 1.4: Classification of surfactants by head group charge.

Class	**Head group charge**	**Examples**
Anionic	**-**	Sodium dodecyl sulphate (SDS) 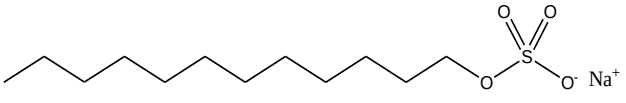
Cationic	**+**	Dodecyl trimethyl ammonium bromide (DTAB) 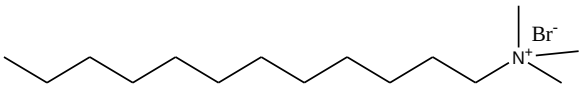
Zwitterionic	**+ and -**	Dimethyl dodecyl amino propane sulphate (DDAPS) 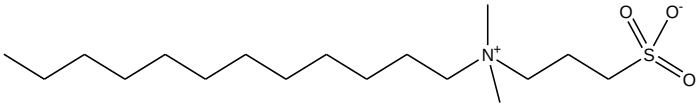
Non ionic	**none**	TWEEN 80 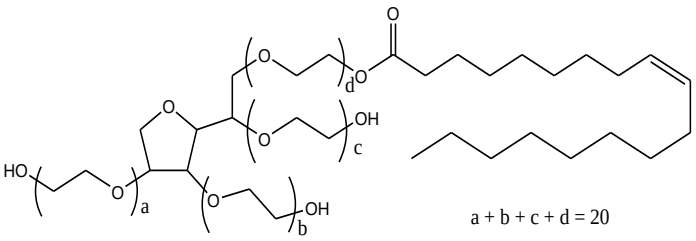

1.6.2 Surfactant adsorption at the air-liquid interface

Surfactant adsorption at the air-liquid interface depends on the polarity of the liquid. When dissolved in an aqueous solvent such as water, the hydrophobic tail aligns itself towards the air while hydrophilic head remains in contact with the water. This alignment leads to a reduction in surface tension due to disruption of the ordered water structure. As the surfactant concentration is increased, more and more of the surfactant is adsorbed at the air-water interface leading to a further reduction in surface tension. The surfactant in the bulk is in constant equilibrium with that on the surface. Once the surfactant monolayer at the air-water interface is saturated, there is no appreciable change in surface tension upon the addition of further surfactant.

At this point any more surfactant monomers in the bulk tend to come together to form aggregates known as micelles (Figure 1.20). These micelles will be in dynamic equilibrium with surfactant monomers in solution and will constantly break down and reform (Attwood et al, 1983). In a polar solvent such as water, the hydrophilic head groups of the surfactant molecules comprising the micelle are oriented towards the solvent, while the hydrophobic tails form the core of the aggregate. Micelle formation involves a balance between hydrophilic forces (including hydration and head group charge) which oppose aggregation, and hydrophobic forces (e.g. the increase in entropy of the system) which promote aggregation. Micellisation is inherently an 'energy saving' process as the hydrophobic portion of the surfactant molecule is "protected" from contact with the bulk phase. In the core of the micelle, the fluidity of the hydrophobic portion of the surfactant molecule resembles that of hydrocarbon oil thereby increasing the entropy of the system. In non-polar solvents, reverse micelles with a hydrophilic core and hydrophobic tails oriented towards the solvent, may be formed.

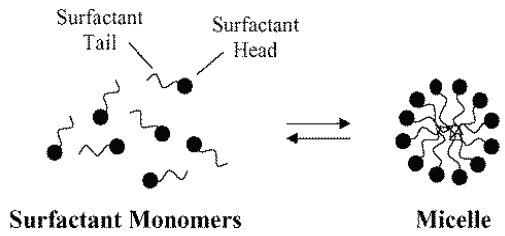

Figure 1.20: The formation of micelles (Liu et al, 1996).

The concentration at which the surfactants form micelles is known as the critical micelle concentration (*cmc*). The *cmc* is usually marked by a sudden change in physical properties of the solution e.g. light scattering, conductivity, osmotic pressure and surface tension. These properties are either sensitive to surfactant monomers e.g. surface tension and osmotic pressure or micelles e.g. light scattering, explaining why some discrepancy is seen between the *cmc* determined using different techniques. Surface tension is widely used to study the micellisation properties of surfactants. The surface tension of a liquid decreases with increasing surfactant concentration upto the *cmc* above which no further appreciable decrease in surface tension is noticed (Figure 1.21).

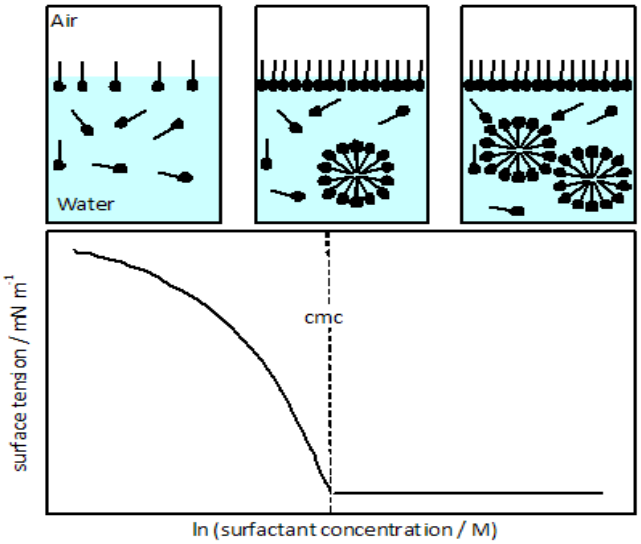

Figure 1.21: Change in the surface tension of water with increasing surfactant concentration. The attached illustrations show surfactant orientation and the onset of micellisation.

1.6.3 Surfactant adsorption at the liquid-solid interface

Surfactants are self-assembled systems that may adopt various types of aggregate in solution depending on the molecular architecture of the surfactant and the properties of the dispersion media. Figure 1.22 shows some aggregate structures that may be formed by surfactants in solution.

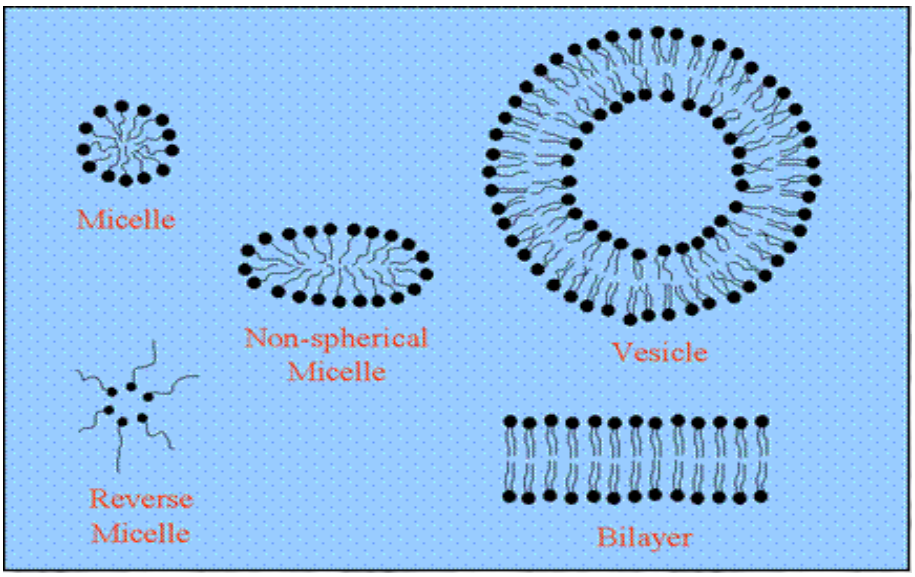

Figure 1.22: Various aggregates that may be formed by surfactants in solution.

The fact that surfactants self-assemble, coupled to the fact that surfactants may cause adsorbent ionization makes the interpretation of surfactant isotherms challenging.

The nature of adsorbent and the surfactant charge are critical determinants in the adsorption process (Duro et al, 1999).

Surfactants may adsorb onto a solid surface via mechanisms including electrostatic interaction, covalent bonding, lateral surfactant chain-chain interactions, hydrogen bonding and non-polar bonding between surfactant and solid surface. In addition solvation or desolvation of any species during adsorption may contribute to the net free energy of adsorption (Somasundaran et al, 1998).

The net driving force for surfactant adsorption is given by the equation:

$$\Delta G_{ads}{}^{o} = \Delta G_{elec}{}^{o} + \Delta G_{chem}{}^{o} + \Delta G_{c-c}{}^{o} + \Delta G_{c-s}{}^{o}\,\Delta G_{H} + \Delta G_{H2O}{}^{o} \qquad \text{(Equation 1.7)}$$

where $\Delta G_{ads}{}^{o}$ is the adsorption force, $\Delta G_{elec}{}^{o}$ is the electrostatic interaction, $\Delta G_{chem}{}^{o}$ is the covalent bonding, $\Delta G_{c-c}{}^{o}$ is the cohesive lateral chain – chain interactions among the adsorbed species, $\Delta G_{c-s}{}^{o}$ interaction between hydrocarbon chains of the adsorbate and the hydrophobic sites on the solid surface, $\Delta G_{H}{}^{o}$ is the hydrogen bonding and $\Delta G_{H20}{}^{o}$ is the hydration of the adsorbate during adsorption.

Ionic surfactants

Ionic surfactants usually adsorb onto oppositely charged surfaces via electrostatic interactions to form a typical log-log Somasudaran Fleutcher type isotherm (Figure 1.23). This isotherm is divided into four distinct regions, namely Regions I-IV (Chandar et al, 1986; Somasundaran et al, 1966; 1997; 1998).

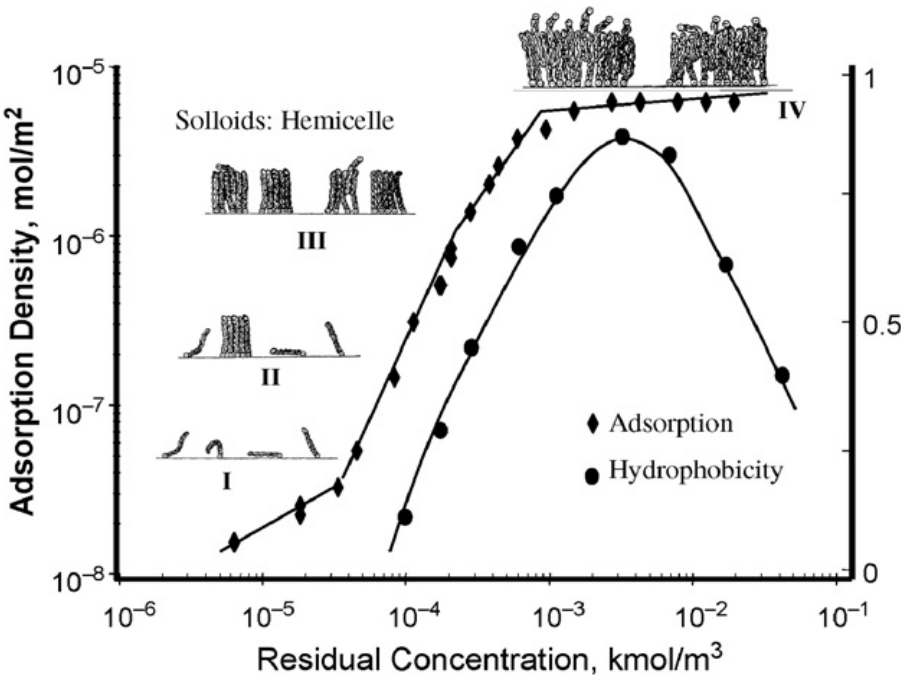

Figure 1.23: The adsorption isotherm of sodium dodecyl sulfate onto positively charged alumina at pH 6.5. The illustrations show the growth of surface aggregates and orientation of surfactant molecules (Chandar et al, 1986).

Region I:

At low surfactant concentrations, adsorption is governed by electrostatic interactions between the surfactant head group and the solid surface. The adsorption isotherm in this region has a slope of unity as there are no inhibitions to the adsorption process. The surfactant molecules are usually lying flat on the surface at this stage.

Region II:

A marked increase in adsorption is observed. This can be attributed to surfactant aggregation due to lateral chain-chain interactions and the formation of solloids (surface colloids) e.g. hemimicelles and admicelles. Electrostatic interactions between the solid surface and the surfactant head group are still in play. The area per surfactant molecule decreases with surfactant adsorption due to surfactant-surfactant repulsion and association.

Region III:

A decrease in surfactant adsorption is observed. Electrostatic adsorption forces are no longer operative due to the neutralisation of the charged

surface by the pre-adsorbed surfactant. In this region surfactant adsorption is governed only by the lateral attraction between the adsorbed surfactant molecules.

Region IV:

This region is denoted by the formation of a plateau, which indicates maximum surface coverage due either to micelle formation in the bulk or monolayer coverage. Higher surfactant concentrations may lead to multilayer formation due to the reversal of the orientation of charge at the solid surface.

Adsorption of ionic surfactants is usually reversible. There is not much literature describing the adsorption of ionic surfactants onto neutral or oppositely charged surfaces, though it would be expected that the adsorption of ionic surfactant onto these surfaces would be minimal.

Non-ionic surfactants

Non-ionic surfactants usually adsorb onto solid surfaces due to hydrogen bonding and not electrostatic or covalent bonding. Most non-ionic surfactants possess polar groups capable of forming hydrogen bonds with hydroxyl groups on the solid surface. Their adsorption is usually lower and weaker as compared to ionic surfactants. Thus the absorption of non-ionic surfactants is easily reversible with only a weak hysteresis. One marked difference in the adsorption isotherms obtained for non-ionic surfactants in comparison to that of ionic surfactants is that Region III is characterised by a sharp increase in adsorption. This is due to absence of an electrostatic repulsion by the adsorbed surfactant molecules (Somasundaran et al, 1997; 1998).

Zwitterionic surfactants

Zwitterionic surfactants adsorb onto solid surfaces due to both hydrophobic interactions of the tail group and ion dipole interactions between the adsorbent and zwitterionic head group (Zajac et al, 1997).

1.7 Polymers

1.7.1 Polymer classification and properties

Polymers are high molecular weight macromolecules with self-repeating units (monomers). They are usually classified according to their

- molecular structure:

Linear Branched Cross-linked

- charge: uncharged and charged (known as polyelectrolytes)
- substitution pattern:
  - homopolymers constituting the same monomer unit
    AAAAAAA
  - copolymers made up of different monomer units, which could be

Random: BAABBABA Alternate: ABABABAB

Block: AABBAABB Graft: AAAAAAA
B
BBBA

- origin: natural or synthetic – cellulose or rubber

Polymers soluble in a particular liquid, first undergoes imbibition, which is swelling due to ingress of solvent, followed by the formation of a true solution. The formation of a true solution is governed by polymer chain-solvent interactions, which must exceed the interaction between the polymer-polymer chains and the solvent-solvent molecules. The conformation which a polymer adopts in solution depends on the interaction between polymer and solvent (Figure 1.24).

Coiled
in a bad solvent

Ideal polymer chain
in a theta solvent

Extended
in a good solvent

Figure 1.24: Conformation of a polymer chain in different solvents.

The ideal polymer chain conformation is one in which there can be no interaction between the individual monomer units; this can only be achieved in what is known as a theta solvent. In good solvents, the monomer-solvent interaction is more favourable than the monomer-monomer interaction resulting in an extended polymer conformation. In bad solvents, the monomer-monomer interaction is greater than that between the monomer-solvent leading to a collapse of the polymer chains and their phase separation from the solvent (Jannick et al, 1990). In a theta solvent the monomer-monomer interactions exactly balance the monomer-solvent interactions leading to the random flight configuration of the polymer chain.

The conformation of a polymer in solution is also influenced by its concentration. In dilute polymer solutions, two critical concentrations C^{*} and C^{**} are observed. C^{**} divides the dilute and semi-dilute concentrations, while C^{*} separates the range between extremely dilute and dilute polymer solutions. C^{*} is the concentration at which polymer molecules begin to overlap (Dondos et al, 1992; 1993).

1.7.2 Polymer adsorption at the air-liquid interface

Polymers such as the cellulosics are surface active due to presence of partially charged groups on the cellulose backbone (Mezdoura et al, 2007; Nahringbauer 1995; Um et al, 1997; Pereza et al, 2008). The resultant surface activity of the polymer is dependent upon its concentration, with high polymer concentrations reaching equilibrium very quickly (seconds), while low polymer concentrations reach equilibrium much slower (hours). Variation in the surface tension of the polymer solution with time follows a sigmoidal curve (Figure 1.25).

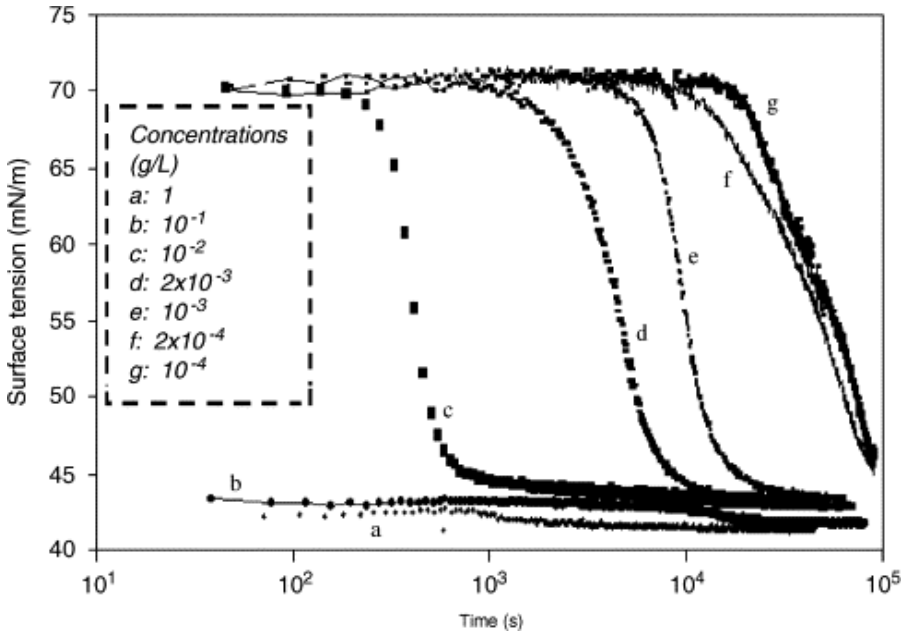

Figure 1.25: Evolution of surface tension of hydroxypropyl cellulose (HPC) in water versus time. HPC concentration: (a) 1, (b) 10^{-1}, (c) 10^{-2}, (d) 2×10^{-3}, (e) 10^{-3}, (f) 2×10^{-4}, (g) 10^{-4} g/L at 20 °C (Mezdoura et al, 2007).

Three distinct phases in the conformation of the polymer chains are observed during the aging of the liquid surface.

Induction period:

The first phase is the induction period in which the surface tension does not change. This indicates that there is an energy barrier to the adsorption of polymer at the air-liquid interface.

Surface coverage:

A rapid decrease in surface tension occurs as the polymer starts to adsorb at the liquid surface. In this region, the kinetics of absorption depends on the surface coverage. Polymer adsorption at the surface occurs via: (i) transport of the molecules from the bulk to the subsurface by diffusion, (ii) spreading or unfolding of the adsorbed molecules, (iii) attachment of molecules/polymer segments from the subsurface to the surface, (iv) rearrangement of the adsorbed molecules/polymer segments between the surface and the subsurface. Here, the subsurface represents the very thin region of the bulk solution immediately next to the surface Macromolecules adsorbed at the air–water interface appear as trains, loops, and tails. Trains are sequences of macromolecule segments in actual contact with the surface, whereas loops and tails are sequences of

macromolecule segments located in the solution. Loops have both ends connected to trains, whereas a tail occurs at one or both ends of the macromolecule chain (Nahringbauer 1995). The reduction in surface tension depends on the number of train segments adsorbed at the surface. This means that the surface properties of a macromolecule depends upon the length and distribution of trains, loops, and tails

Mesophase region:

The last region is the mesophase region at which there is no change in surface tension. Here, the system is in equilibrium and only reordering of the polymer segments within the surface layer takes place.

1.7.3 Polymer adsorption at the liquid-solid interface

Polymer adsorption onto a solid surface occurs when the polymer-solid interactions are more favourable than those between the polymer-polymer and the polymer-solvent. Polymers are composed of many monomer units therefore a slight attractive force between the monomer and solid surface is amplified many times in the polymer (Rao et al, 2003). Note that polymer adsorption can be governed by electrostatic interactions, hydrogen bonding, van der Waals and hydrophobic forces (Duro et al, 1999).

The adsorption energy parameter (x_s) is a dimensionless unit used to assess the probability of polymer adsorption.

$$x_s = \frac{\left(u_s - u_p\right)}{kT} \qquad \text{(Equation 1.8)}$$

where x_s is the adsorption energy parameter, u_s is the adsorption energy of solvent molecule, u_p is the adsorption energy of polymer molecule, k is a constant and T is temperature.

Adsorption can only occur when x_s is greater than zero. For a value of x_s less than or equal to zero, polymer adsorption cannot occur since the gain in the free energy is not sufficient to compensate for the loss of translational entropy of the chains upon adsorption.

An isolated neutral polymer chain next to a surface adsorbs in form of loops, trains and tails. The points of attachment to the solid are known as trains, separated by the non-adsorbing segments – known as loops and tails. Adsorption of polymers is characteristically different from that of small molecules due to the large number of possible conformations that can be attained upon adsorption (Figure 1.26). The structure of an adsorbed film depends upon the inherent characteristics of the polymer as well as the quantity of polymer adsorbed. At low levels of coverage the polymer chains predominantly lie flat forming 'trains' at the surface, while at high levels of coverage the hydrophilic groups project towards the aqueous phase forming 'loops' or 'tails' (Duro et al, 1999).

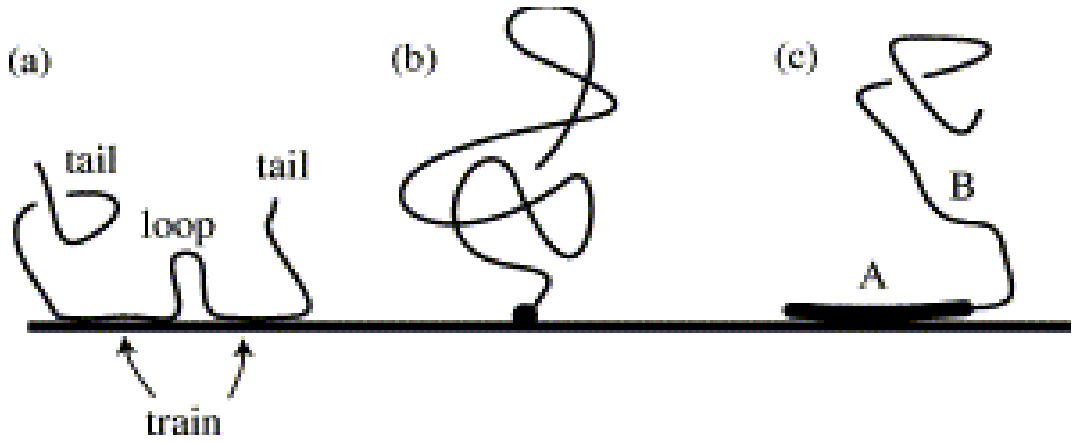

Figure 1.26: The different polymer adsorption mechanisms: (a) adsorption of a homopolymer, where each monomer has the same interaction with the substrate. The 'tail', 'train' and 'loop' sections of the adsorbing chain are shown; (b) grafting of an end-functionalized polymer via a chemical or a physical bond, and; (c) adsorption of a diblock copolymer where one of the two block is attached to the substrate surface, while the other is not (Netz 2003).

Polymer adsorption isotherms generally display a high affinity of the polymer for the surface and a plateau level in the order of a few mg/m^2. Polymer adsorption onto a solid surface tends to increase with decreasing solvent quality and increasing temperature or polymer concentration. In theta solvents, polymer adsorption increases with polymer molecular weight, regardless of whether the polymer has a low or high molecular weight.

Adsorption kinetics are dependent on polymer molecular weight with low molecular polymers adsorbing first, but being replaced by better adsorbing higher molecular polymers.

Adsorption energy depends on both the nature of the solvent and the surface, as well as the competition between the polymer and solvent for binding sites. Polymer adsorption can often be accompanied by a change in the conformation of the chain compared to that in the bulk (Netz 2003).

1.8 Polymer-surfactant mixtures

1.8.1 Polymer-surfactant systems and properties

Polymer-surfactant systems have widely been used in cosmetology, mineral processing, petroleum, detergency, paint, pharmaceutical industries among other fields. The synergy between polymers and surfactants is often used to achieve the desired result. Polymers and surfactants associate in solution thus modifying its solution, rheological and interfacial properties. Interactions in these systems are governed by the charge, hydrophobicity, hydrophilicity, size and concentration of both polymer and surfactant. Electrostatic charge is the most important characteristic forming the basis for classification of polymer-surfactant systems (Table 1.5).

Table 1.5: Classification of polymer-surfactant systems according to charge.

	Anionic surfactant (S^-)	Cationic surfactant (S^+)	Non-ionic surfactant (S^0)	Zwitterionic surfactant ($S^{+/-}$)
Anionic polymer (P^-)	P^-S^-	P^-S^+	P^-S^0	$P^-S^{+/-}$
Cationic polymer (P^+)	P^+S^-	P^+S^+	P^+S^0	$P^+S^{+/-}$
Non-ionic polymer (P^0)	P^0S^-	P^0S^+	P^0S^0	$P^0S^{+/-}$

From the nature of the ionic charges, the polymer-surfactant system interactions can be deduced. No or minimal interaction is expected in polymer-surfactant systems bearing similar charge (P^-S^-, P^+S^+), those with no charge (P^0S^0) as well as cases in which the polymer is rigid and sterically hindered.

When polymer-surfactant systems bear opposite charges (P^+S^-, P^-S^+), complexes are formed due to mutual electrostatic interactions. Single surfactant molecules may be bound linearly along the polymer chain or onto multiple polymer sites leading to intra/intermolecular bridging.

Interactions between uncharged-charged systems (P^0S^+, P^0S^-) are governed by the polymer molecule wrapping its self around the surfactant micelles. The polymer chains are known to partially penetrate the polar head group of micelles, reducing their water content, forming a 'pearl necklace' arrangement. Techniques such as NMR, neutron scattering, fluorescence spectroscopy have been used to elucidate structure of polymer-surfactant complexes.

1.8.2 Polymer-surfactant adsorption at the air-liquid interface

Surface tension can be used to study polymer-surfactant interactions at the air-liquid interface with characteristic changes in the surfactant adsorption isotherm being observed in the presence of different types of polymer (Goddard 2002). These variations in surface tension are dependent on the charge and concentration of both the polymer and surfactant in solution.

Weakly interacting systems

Interactions between neutral polymers and ionic surfactants (P^0S^+, P^0S^-) are mainly governed by 'weak' hydrophobic forces. In such systems, three transition/break points in the surface tension (T_1, T_2 and T_3) are observed (Figure 1.27). The first break point (T_1), which occurs at a concentration lower than the surfactant *cmc*, is known as the critical aggregation concentration (*cac*). At this concentration, mixed complexes comprising of surfactant micelles and polymer are formed in the bulk solution. The *cac* typically occurs at a lower concentration than the *cmc*, implying that polymer-surfactant complexation is energetically more favourable than micellisation. At T_2 the polymer chains are saturated with surfactant micelles, any more surfactant added to the system is not bound onto the polymer chains and thus leads to further decrease in surface tension. T_2 is not very well defined in most cases. The interval between T_1 and T_2 increases with polymer concentration/chain length. T_3 denotes the 'normal' *cmc*, at which time normal surfactant micelles are formed after saturation of the polymer chains with surfactant (Bell et al, 2007, 2010; Taylor et al, 2007).

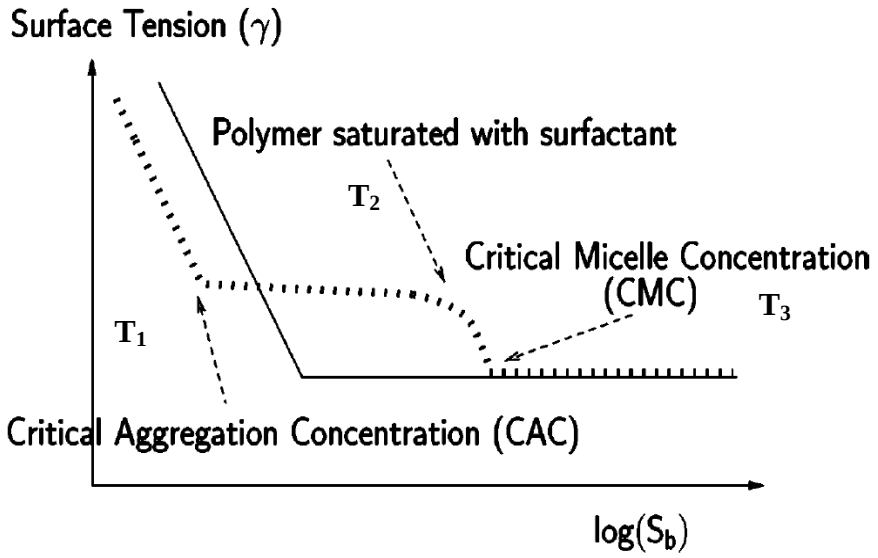

Figure 1.27: Variation in the surface tension of an anionic surfactant solution with surfactant concentration in absence (—) and presence (---) of a weakly interacting neutral polymer (Bell et al, 2007).

Anionic surfactant-neutral polymer systems have been widely investigated in literature by a number of authors including Chari et al (1991) and Sesta et al (1997) who investigated the anionic surfactant, sodium dodecyl sulphate (SDS) and the non-ionic polymer, polyvinylpyrrolidone (PVP); Hou et al (1999) and Bahadur et al (1995) who studied the anionic surfactant, sodium dodecyl sulphate (SDS) and the non-ionic polymer, polyethylene oxide (PEO). Less literature is available on interactions in mixed cationic surfactant and neutral polymer systems.

S***trongly interacting systems***

Strong electrostatic interactions are observed between oppositely charged ionic polymer and surfactant (P^+S^-, P^-S^+). Surface tension curves of these systems may show a peak due to competition between the bulk polymer-micelle complex and the polymer-surfactant monomer complex (Taylor et al, 2007). Five surface active species namely; surfactant monomer, free surfactant micelle, free polymer chain, polymer-surfactant monomer complex and polymer-surfactant micelle complex, are all involved in determining surface activity. In the literature concerning weakly interacting polymer-surfactant systems, there is less mention of the polymer-surfactant monomer complex with focus being on the polymer-surfactant micelle 'pearl necklace' complex.

The surface tension curve of the cationic surfactant, tetradecyltrimethylammonium bromide (C_{14}TAB), and the anionic polymer, sodium poly(styrene sulfonate), exhibits four break points, namely T_1-T_4 (Figure 1.28).

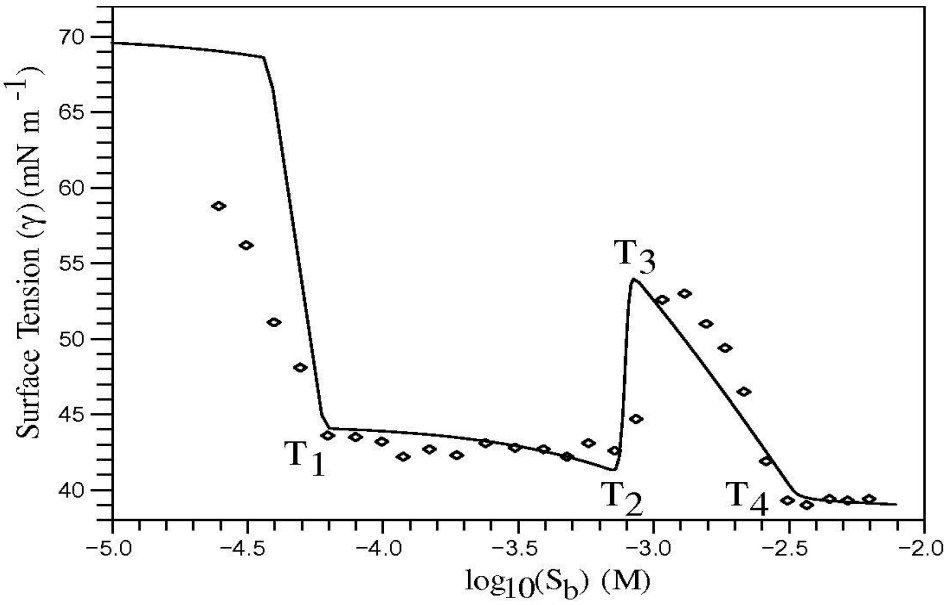

Figure 1.28: Schematic diagram showing the changes in surface tension with changing surfactant concentration in a strongly interacting cationic polymer-anionic surfactant system (Bell et al, 2010).

T_1 corresponds to the saturation of the polymer-monomer complex at the surface, T_2 and T_3 to the formation and saturation of the polymer-micelle complex in the bulk (and corresponding dissolution of the polymer-monomer complex at the surface), respectively while T_4 corresponds to the formation of free surfactant micelles in the bulk (Bell et al, 2007; 2010; Taylor et al, 2007). Reports of strongly interacting systems in the literature include; the anionic surfactant, SDS, and the cationic polymer, polydimethyldiallylammonium chloride (Staples et al, 2002), the cationic surfactant, C_{14}TAB, and the anionic polymer, NaPSS (Bell et al, 2010), the cationic polymer polyvinylpyridium chloride (PVPmCl) and the anionic surfactant, SDS, (Taylor et al, 2002) among others.

The peak (T_3) in surface tension is not observed with all strongly interacting systems. The appearance of a peak is dependent on the stability of the polymer-monomer and the polymer micelle complexes, the polymer concentration as well as the surface active parameters of the surfactant and the polymer-monomer complex (Bell et al, 2010).

1.8.3 Polymer-surfactant adsorption at the liquid-solid interface

Polymer/surfactant adsorption onto solid surfaces has been studied using various experimental techniques including neutron scattering, nuclear magnetic resonance, photon correlation spectroscopy, fluorescence spectroscopy, atomic force microscopy, microscopy among others (Goddard 2002).

Adsorption kinetics of polymer/surfactant mixtures at the liquid/solid interface largely depends on the interplay of polymer-surfactant-substrate interactions, their concentration in the bulk solution as well as the order of addition of the various components (Claesson et al, 2003). Cooperative or/and competitive polymer-surfactant adsorption may occur in any particular system.

Order of addition

Two distinct scenarios can be envisaged; one in which surfactant/polymer is pre-adsorbed onto substrate before the addition of the second component and the other in which polymer-surfactant complexes are preformed in bulk solution before introduction of a substrate.

Interesting surface modifying effects have been observed with polymer/surfactant mixtures whereby one entity is preadsorbed. Preadsorbtion of a polymer/surfactant on a solid surface may lead to co-adsorption of the corresponding entity, even when the latter does not usually adsorb on that surface. For example non-ionic polymer PEO does not usually adsorb on alumina but in presence of pre-adsorbed SDS it does. Similarly SDS does not adsorb on silica, however if the non-ionic polymer, polyethylene oxide, is pre-adsorbed on silica, SDS will subsequently be adsorbed (Maltesh et al, 1992).

In cases where the polymer and surfactant are premixed and their complexation occurs in bulk solution, their adsorption onto the solid depends on the competition between the formation of the polymer/surfactant complexes in the bulk and on the nature of the solid surface. Kronberg et al (1986) observed that low amounts of polyacrylic acid inhibited the adsorption of polyethylene oxide onto kaolinite, while higher amounts of the polymer enhanced surfactant adsorption. In a different study, Otsuka et al (1994) observed the opposite effect. The adsorption of the non-ionic polymer, PVP, in the presence of the anionic surfactant, lithium dodecyl sulphate (LiDS) on alumina was enhanced at low LiDS concentrations and decreased at higher surfactant concentrations. This observation was attributed to the preferential

formation, at higher surfactant concentrations, of LiDS-PVP complexes in the bulk solution as opposed to on the solid surface.

Polymer-surfactant interactions

Polymer-surfactant combinations, which exhibit weak interactions in bulk, may compete for adsorption e.g. the competitive adsorption of the non-ionic polymer, polyethylene oxide, and the cationic surfactants, dodecyltrimethylammonium bromide and 1,2-bis(dodecyltrimethyl ammonio) ethane dibromide, on silica studied by Esumi et al (1998). On the other hand, if the polymer-surfactant combinations interact strongly in the bulk, the simultaneous adsorption of polymer and surfactant will be favoured e.g. the system consisting of the non-ionic polymer, PVP, and the anionic surfactant, SDS (Duro et al, 1999).

1.9 Techniques

Particle size analysis

Particle size is the most fundamental property used to describe any nanosized formulation. If defined as a 'characteristic linear dimension', it is largely an ambiguous quantity for non-spherical particles, as size obtained depends on the physical response of the instrument used to measure particle size in relation to the size and shape of the particles (Shekunov et al, 2006). Huge discrepancies in the particle sizes obtained are often observed among different techniques or instruments.

The concept of equivalent particle diameters was therefore evolved to try and solve this challenge. Equivalent particle diameters are diameters of calibrated spheres that yield the same size when analysed under the same conditions as the irregularly sized particles. Equivalent particle diameters may be geometrical e.g. surface area, volume or behavioural e.g. sedimentation, inertia (Figure 1.29).

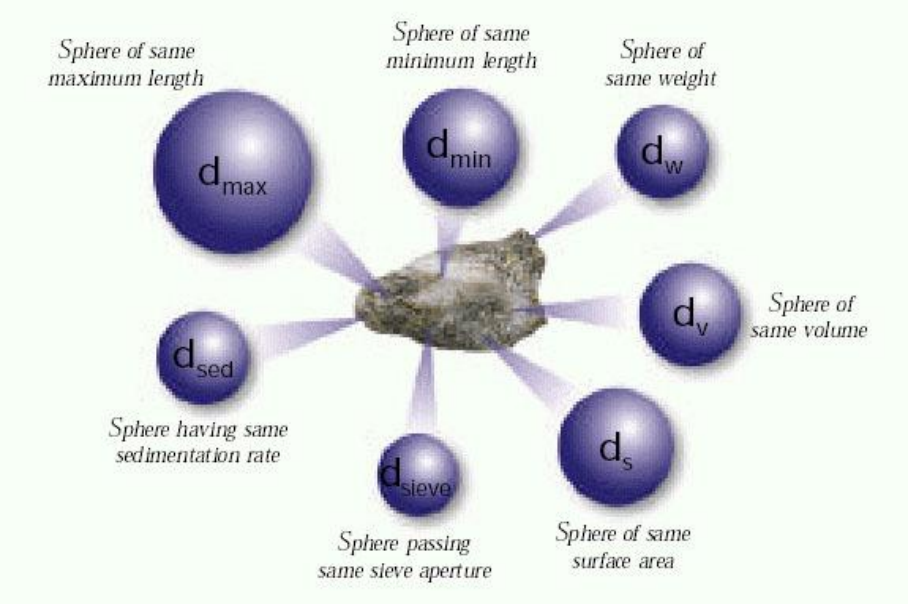

Figure 1.29: Figure illustrating a range of equivalent particle diameters from Rawle (2002).

With the exception of microscopy, which is a direct measure of size, a variety of indirect techniques utilising the concept equivalent diameters are available for particle sizing (Table 1.6). When measuring particle size it is usually advisable to use more than one technique.

Table 1.6: Characteristics of some commonly used particle sizing techniques from Shekunow et al (2006).

Technique	Method	Equivalent Particle Diameter	Effective Measuring Range, μm	Most Representative PSD[a]
Optical image analysis	Direct imaging	Projected area	3-150	Number-weighted
Scanning electron microscopy	Direct imaging	Projected area	0.01-150	Number-weighted
Laser diffraction	Fraunhofer diffraction rings measurement	Angular-averaged linear (Feret's)	0.5-1000	Volume-weighted
Dynamic light scattering	Measurement of light intensity correlations from particles in Brownian motion	Hydrodynamic	0.003-3	Volume-weighted
Coulter counter	Electrical zone-sensing	Volume	0.6-1,200	Volume-weighted
Time-of-flight	Measurement of particle velocity in expanding air flow	Aerodynamic, ultra-Stokesian	0.5-200	Number-weighted
Cascade impactor	Inertial particle impaction as a function of air velocity	Aerodynamic, ultra-Stokesian	0.5-10	Mass -weighted

a: particle size distribution.

1.9.1 Photon correlation spectroscopy

Photon correlation spectroscopy (PCS) is also known as dynamic light scattering or quasi-elastic light scattering. Colloidal particles in solution undergo random 'Brownian' motion due to constant bombardment by the solvent molecules surrounding them. The motion of particles is inversely proportional to particle size with small particles moving faster and further than large particles in the same time period. The velocity of Brownian motion is defined as the translational diffusion coefficient (D), which is related to particle size by the Stokes Einstein Equation.

$$d(H) = \frac{k_B T}{3\pi\eta D} \qquad \text{(Equation 1.9)}$$

where *d(H)* is the hydrodynamic diameter, *D* is the translational diffusion coefficient, k_B is the Boltzmann's constant, *T* is the absolute temperature in degrees Kelvin and η is the liquid viscosity.

PCS measures the apparent hydrodynamic radius of the particles dispersed in solution, by assessing the variation in the intensity of light scattering with time using an auto correlator. For large particles, which result in slow fluctuations in the intensity of the scattered light, the correlation persists longer than that of smaller particles, which result in rapid intensity fluctuations of the scattered light. A monodisperse population of particles produces an autocorrelation function in the form of a single exponential decay. Mixtures of particles of more than one size population produce an autocorrelation function that is the sum of exponentials. Algorithms, e.g. non-negatively constrained least squares (NNLS) and CONTIN (Tscharnuter 2000), are available to extract the "true" size distribution from complex samples.

$$C(\tau) = Ae^{-2\Gamma t} + B \qquad \text{(Equation 1.10)}$$

where $C(\tau)$ is the autocorrelation function, and A, B are instrumental constants.

$$\Gamma = q^2 D \qquad \text{(Equation 1.11)}$$

where q is the scattering vector and D is the translational diffusion coefficient.

$$q = \frac{4\pi n \sin\left(\frac{\theta}{2}\right)}{\lambda} \qquad \text{(Equation 1.12)}$$

where n is the refractive index, θ is the scattering angle and λ is the laser wavelength.

The main components of a PCS instrument include the laser, which provides the light source, a cell in which the sample is placed, a detector to measure the

fluctuations in scattered light, an attenuator to reduce the intensity of light scattering with concentrated samples, an autocorrelator for digital processing of the scattered light signal and finally a computer software package to analyze this data and derive particle size (Figure 1.30).

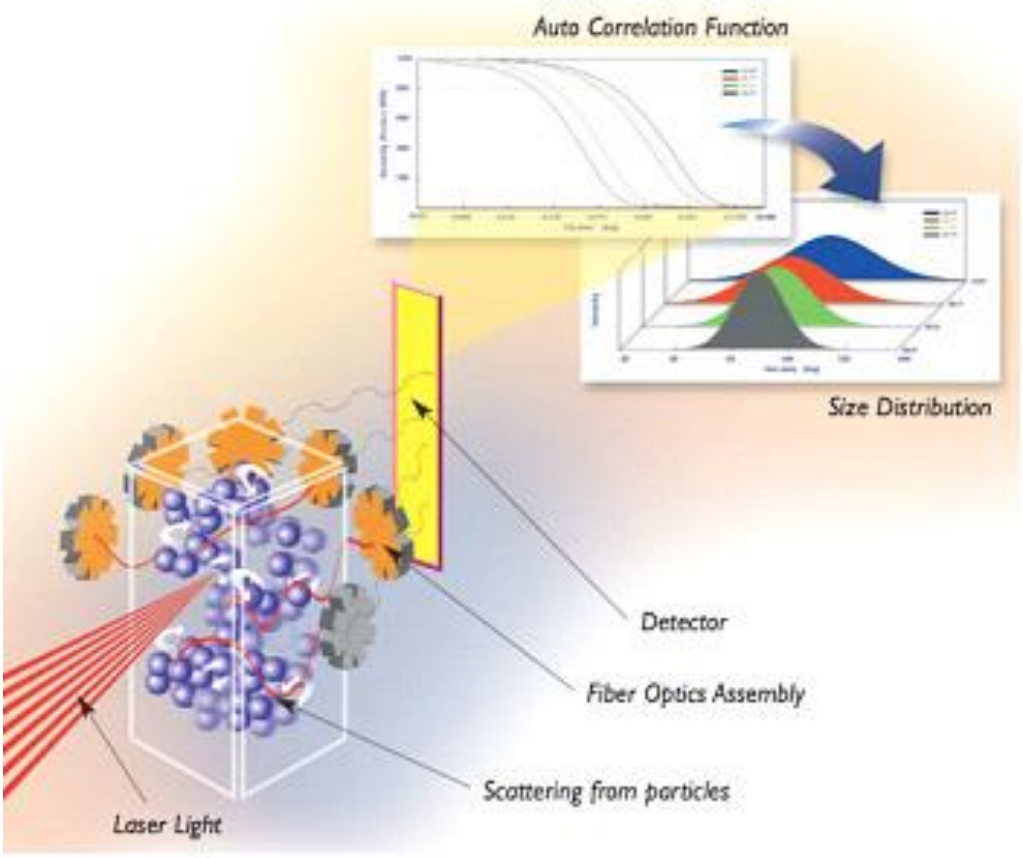

Figure 1.30: Main components of a photon correlation spectrometer.

PCS is widely used for particle sizing because it is rapid and requires a (relatively) small amount of sample. Furthermore it is an absolute method were size is obtained from first principles and can be performed in a variety of suspending liquids. Drawbacks are that the technique does not typically provide any particle shape information, nor does it produce a high resolution histogram of size distribution, while small quantities of dust can make measurements and interpretation difficult (Tscharnuter 2000). In addition, the particle size obtained by PCS is affected by factors such as temperature, viscosity, and the ionic strength of media, all of which must be taken into account during the measurement and subsequent analysis.

1.9.2 Scanning electron microscopy

Microscopy is the only particle sizing method that allows for the direct observation of particle size, shape and surface. Scanning electron microscopy (SEM) employs a high energy beam of electrons under vacuum conditions thereby allowing for very high magnification and image resolution. It can efficiently detect clusters and agglomerates of particles in a sample.

SEM can be used to scan large areas of sample using magnification ranges that can be changed rapidly. It also has the advantage of possessing a large depth of focus due to small probe aperture and can utilise various contrast mechanisms e.g. magnetic or voltage contrasts (Newbury et al, 2000).

Drawbacks of SEM include errors due to insufficient particles being measured to give a representative size and possible sample artefacts due to the vacuum conditions.

1.9.3 X-ray powder diffraction

X-ray diffraction (XRD) is a non-destructive technique that is used for characterisation, quantification and identification of crystalline substances. Crystalline substances comprise an orderly periodic arrangement of atoms, with a unit cell being the basic repeating unit.

When X-rays come in contact with a substance, they may be reflected, transmitted, absorbed, scattered or diffracted. Diffraction is defined as the constructive interference of coherent scattering and occurs when Bragg's law (Equation 1.13) is satisfied (Figure 1.31).

$$n\lambda = 2d\sin\theta \qquad \text{(Equation 1.13)}$$

where n is an integer number, λ is the wavelength of the electromagnetic radiation, d is the distance between the atomic layers in the crystal (d-spacings) and θ is the angle of incidence.

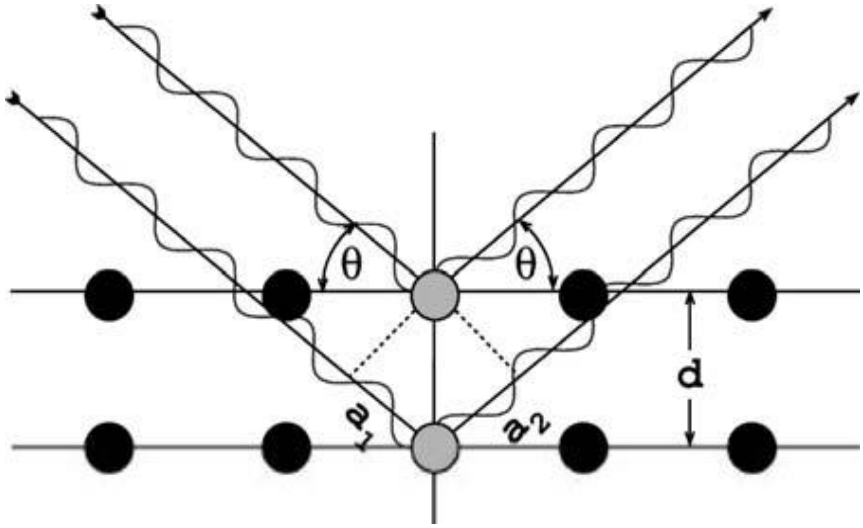

Figure 1.31: Geometric derivation of Bragg's law: Constructive interference occurs when the delay between waves scattered from adjacent lattice planes given by $a1 + a2$ is an integer multiple of the wavelength λ (Stanjek et al, 2004).

Crystalline substances act as three-dimensional diffraction gratings for X-ray wavelengths similar to the spacing of planes in a crystal lattice. The characteristic d-spacings and their intensity provides a 'fingerprint' for crystalline substances, while the presence of non crystalline (disordered nanocrystalline, glassy or amorphous) material is observed as a specific wide 'halo' on the diffraction pattern.

The occurrence, in the diffraction pattern, of peak broadening without a change in peak position or intensity is characteristic of a disordered nanocrystalline material and is related to loss of long range order in a crystalline microstructure. With glassy materials, the position of the diffuse halo moves in respect to its parent crystalline peaks although the overall intensity envelope is maintained. Amorphous materials present as broad diffuse halos, which are not correlated in position or intensity envelope to the parent crystalline peaks (Bates et al, 2006).

A diffractometer consists of an x-ray beam source, sample holder, and an x-ray detector. X rays are typically generated by heating a filament in a cathode ray tube in order to produce electrons of high energy which are then accelerated to a target material. The specific wavelengths of x-rays produced are characteristic of the target material (Cu, Fe, Mo, Cr). Beam optics are then used to filter, collimate and direct the monochromatic x-rays to the sample. A goniometer is used to rotate the sample and detector through a range of 2 θ angles such that all possible diffraction directions are attained. The detector then records the x-ray signal, which is then processed as a count rate.

1.9.4 Viscosity

Viscosity is the resistance of a fluid to flow. It is normally determined by measuring the time taken for a liquid to flow through a capillary of a defined length and width at a specific temperature relative to a standard solution, frequently water.

The relative viscosity (η_{rel}) is given by:

$$\eta_{rel} = \frac{time\ taken\ by\ solution\ to\ \ flow}{time\ taken\ by\ solvent\ to\ \ flow} = \frac{t}{t_0} \qquad \text{(Equation 1.14)}$$

where specific viscosity (η_{sp}) is:

$$\eta_{sp} = (\eta_{rel} - 1) = \frac{t}{t_0} - 1 \qquad \text{(Equation 1.15)}$$

Reduced viscosity is given by the Huggins equation

$$\left(\frac{\eta_{sp}}{c}\right) = (\eta) + k_H\ \ (\eta)_C^2 \qquad \text{(Equation 1.16)}$$

where k_H is Huggins constant, c is concentration and ($\frac{\eta_{sp}}{c}$) is reduced viscosity.

Inherent viscosity is calculated using the Kraemer equation:

$$\left(\frac{\ln \eta_{rel}}{c}\right) = (\eta) + k_K (\eta)_c^2 \qquad \text{(Equation 1.17)}$$

where k_K is Kraemer constant, c is concentration and ($\frac{\ln \eta_{rel}}{c}$) is inherent viscosity.

The intercept of the Huggins and Kraemar plots give the intrinsic viscosity (η):

$$\eta = \lim_{c \to 0} \frac{\eta_{sp}}{c} = \lim_{c \to 0} c^{-1} \ln \eta_{rel} \qquad \text{(Equation 1.18)}$$

Intrinsic viscosity is related to polymer molecular weight by the Mark Houwink equation (Mc Crackin 1987):

$$\eta = km^{\alpha} \qquad \text{(Equation 1.19)}$$

where η is intrinsic viscosity, m is the polymer molecular weight and k, α are polymer dependent constants.

1.9.5 Surface tension

Liquid molecules near the air surface interact with fewer liquid molecules as compared to those in bulk. As a consequence molecules at the interface of a liquid tend to experience an inward force resulting in the spontaneous curvature of the surface. This inward force corresponds to surface tension and is determined by the amount of work needed to increase the surface area by one m^2.

Surfactants reduce the surface tension of liquids by adsorbing at the air-liquid interface. The resultant change in surface tension is given by:

$$d\gamma = -\sum_i \Gamma_i \, d\mu_i \qquad \text{(Equation 1.20)}$$

where $d\gamma$ is the change in surface tension, Γ_i is surface excess concentration of i, and $d\mu_i$ is change in chemical potential of i.

At equilibrium:

$$d\mu_i = RTd \ln a_i \qquad \text{(Equation 1.21)}$$

where a_i is the activity of i in the bulk phase given by the molar concentration of the surfactant in the bulk

Therefore

$$d\gamma = -RT \sum_i \Gamma_i \, d \ln C \qquad \text{(Equation 1.22)}$$

where C is molar concentration of the surfactant

The slope of surface tension against surfactant concentration can be used to determine the surface excess, which is related to the Gibbs equation (Scatchard 1962) by:

$$\Gamma = -\frac{1}{2.303} RT \left(\frac{d\gamma}{d \log c} \right) TP \qquad \text{(Equation 1.23)}$$

where Γ is surface excess concentration (mol m^{-2}), $\frac{d\gamma}{d \log c}$ is the slope of surface tension reduction versus log surfactant concentration in premicellar region, R is the gas constant (8.314 J/Kmol) and T is temperature in K.

The surface excess is related to the area per surfactant molecule by the following equation:

$$A = \frac{1 * 10^{20}}{N_A \, \Gamma_{\max}} \qquad \text{(Equation 1.24)}$$

where A is the area per surfactant molecule in $Å^2$, Γ is surface excess concentration (mol m^{-2}) and N_A is Avogadro's number (6.023×10^{23} molecules mol^{-1}).

The area per surfactant molecule provides information about the degree of packing and orientation of the adsorbed surfactant molecules.

1.9.6 Optical rotatory dispersion

Chiral substances rotate the plane of polarized light due to different refractive indexes for left and right handed circularly polarized light. Optical rotatory dispersion (ORD) is defined as the rate of change in optical rotation with the

wavelength of light. The angle of rotation is dependent on the nature of substance, the thickness of sample, sample concentration, temperature and wavelength. This rotation may be clockwise (dextrorotary) or anti clockwise (levorotatory).
The specific rotation of a compound is given by:

$$[\alpha]_{\lambda}^{T} = 100\,\frac{\alpha}{c.l} \qquad \text{(Equation 1.25)}$$

where α is rotation in degrees, c is concentration in g/mL, l is pathlength in dm, T is temperature in °C and λ is wavelength in nm.

Optical rotation of chiral substance in solution depends linearly on the pathlength and its concentration at low concentrations making it ideal for quantification. However, at high concentrations this linearity is lost due to intermolecular interactions such as association or dimerization. Molecular rotation is used to compare optical activity of different substances (Schreier et al, 1995).
The molecular rotation of a compound is given by:

$$[M]_{\lambda}^{T} = [\alpha]_{\lambda}^{T}\,\frac{M}{100} \qquad \text{(Equation 1.26)}$$

where α is the rotation in degrees, M is the molecular weight of compound, T is the temperature in °C and λ is the wavelength in nm.

The basic set up of a polarimeter is shown in Figure 1.32. Major components include a monochromator, two polarizers (a fixed one before the sample and another after the sample which can be rotated relative to the first), a sample holder and a detector. The angle between the two polarizers is measured.

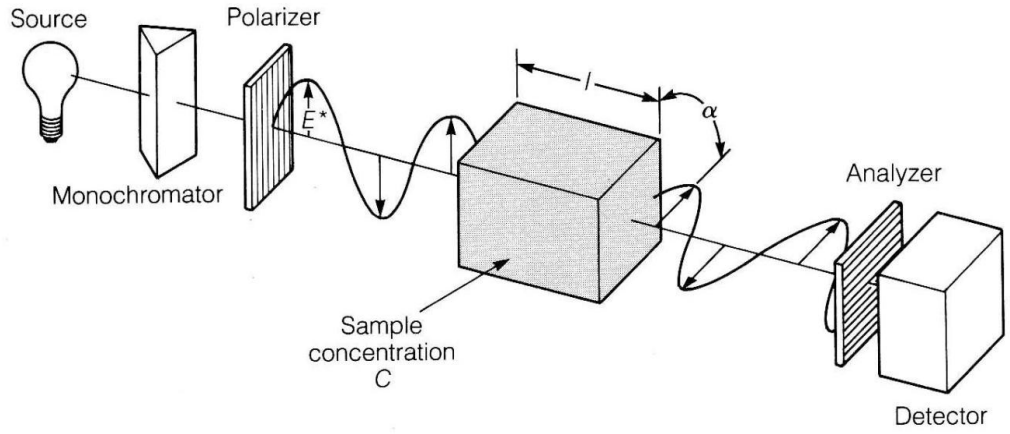

Figure 1.32: Basic set up of a polarimeter.

1.9.7 Zeta potential

When an electric field is applied across an electrolyte, any charged particles suspended in the electrolyte are attracted towards the electrode of opposite charge. Viscous forces acting on the particles tend to oppose this movement. When equilibrium is reached between these two opposing forces, the particles move with constant velocity. The velocity of a particle in a unit electric field (referred to as its electrophoretic mobility) is dependent upon the strength of the electric field or voltage gradient, the dielectric constant of the medium, the viscosity of the medium and the zeta potential (Li et al, 2007).

Zeta potential is related to the electrophoretic mobility by the Henry equation:

$$U_E = \frac{2\varepsilon z f(\kappa a)}{3\eta} \qquad \text{(Equation 1.27)}$$

where U_E is the electrophoretic mobility, z is the zeta potential, ε is the dielectric constant, η is viscosity, κ is the Debye length (often taken as a measure of the "thickness" of the electrical double layer), a is the particle radius and f(κa) is Henry's function.

Electrophoretic determinations of zeta potential are most commonly made in aqueous media and at moderate electrolyte concentration. If f(κa) is 1.5, as with particles (> 200 nm) dispersed in moderate electrolytes (> 10^{-3} molar salt),

calculation of zeta potential from the mobility is carried out using the Smoluchowski model. For small particles in low dielectric constant media (e.g. non-aqueous media), f(κa) becomes 1.0 and the Huckel approximation is used to calculate zeta potential.

Equipment for measuring zeta potential comprises of six main components, namely the laser which provides the light source, a cell in which the sample is placed, a detector to measure the scattered light, an attenuator to reduce the scattered light intensity when measuring concentrated samples, a digital processor to compile the scattered light signals and finally computer software to analyze fluctuations of scattered light from which electrophoretic mobility and hence zeta potential are calculated.

1.9.8 Contact angle

The surface energetics of a solid is related to its wettability via the Young's equation. Wetting of a solid surface involves the replacement of corresponding liquid-vapour and solid-vapour interfaces by a liquid-solid interface. The contact angle formed by a drop of liquid on a horizontonally positioned, planar, chemically inert, homogeneous solid surface represents an equilibrium between the solid vapour interfacial tension (γ_{SV}) favouring wetting, alongside the solid liquid (γ_{SL}) and the tangent to the liquid vapour (γ_{LV}) interfacial tensions opposing wetting (Figure 1.33).

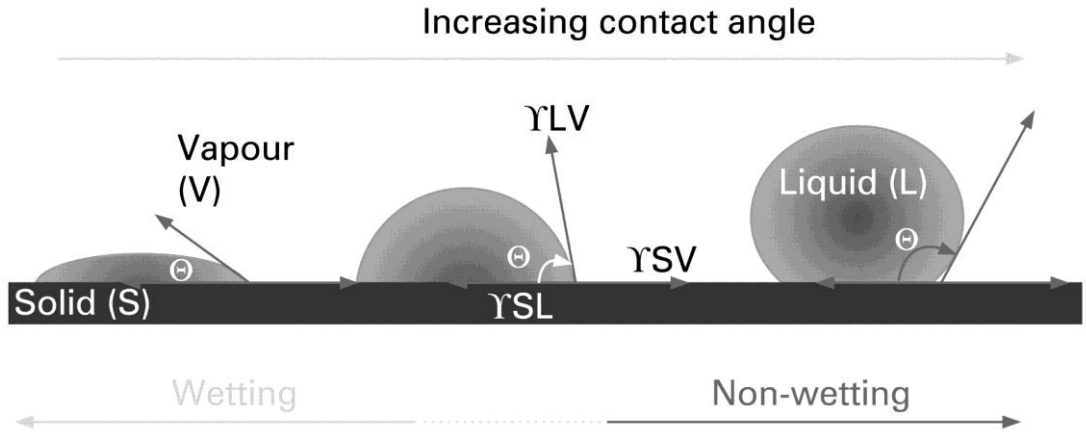

Figure 1.33: Schematic diagram of drops of liquid (L), with increasing contact angles (Θ), on a solid surface (S) showing the solid vapour (γ_{SV}), solid-liquid (γ_{SL}) and liquid-vapour (γ_{LV}) interfacial tensions acting on them (Wong et al, 2009).

Complete wetting is observed at a contact angle of 0°, while complete non-wetting occurs at an angle of 180°. The rate/speed of wetting is dependent on factors such as capillary forces, the viscosity of the liquid, thermal conditions of the system and reactions occurring at the liquid-solid interface (Attwood et al, 1983).

Young's Equation represents the condition at equilibrium when no further spreading occurs:

$$\gamma_{SL} = \gamma_{SV} - \gamma_{LV} \cos \theta \qquad \text{(Equation 1.28)}$$

where γ_{SV}, γ_{SL} and γ_{LV} are respectively, the solid vapour, solid-liquid and liquid-vapour interfacial tensions and θ is the contact angle.

The contact angle and γ_{LV} can easily be determined, leaving two unknown parameters in Equation 1.28, that is γ_{SL} and γ_{SV}. Surface tension is postulated to be composed of two components namely dispersive and polar interactions (Kwok et al, 1999) giving the Equation 1.29 below:

$$\gamma_{SL} = \gamma_{LV} + \gamma_{SV} - 2\sqrt{\gamma_S^d \gamma_L^d} - 2\sqrt{\gamma_S^p \gamma_L^p} \qquad \text{(Equation 1.29)}$$

where γ_S^d, γ_L^d, γ_S^p, γ_L^p are the dispersive and polar components of the solid surface energy and liquid surface energy respectively.

Combining equations 1.28 and 1.29 gives the Owens-Wendt equation (Owens et al, 1969) below:

$$(1 + \cos \theta)\gamma_{LV} = 2\sqrt{\gamma_S^d \gamma_L^d} + 2\sqrt{\gamma_S^p \gamma_L^p} \qquad \text{(Equation 1.30)}$$

Equation 1.30 can be used to calculate γ_S^d and γ_S^p by measuring the contact angles of two or more different liquids (with known γ_L^d, γ_L^p) on the same solid and solving the equations simulatenously.

The sessile drop technique allows the direct measurement of contact angle. Basic equipment includes a light source, sample stage, lens and image capture device. A 'back-lit' drop of liquid deposited on a solid is imaged and the angle formed at solid-

liquid interface estimated either manually or by computerized image analysis. The sessile drop method has been widely used in pharmaceutical wetting studies. Its advantages include minimal sample requirements (both liquid and solid), versatility and ease.

The main setback when attempting to measure contact angle is encountered when the drop is absorbed by porous substrates leading to erroneous results. Saturation of the solid phase with the wetting liquid has been used to try and counteract this absorption, although its success is debatable.

1.9.9 X-ray photoelectron spectroscopy

X-ray photoelectron spectroscopy (XPS) is a surface chemical analysis technique in which the surface of a solid sample is bombarded with high energy X-ray photons in ultra high vacuum, resulting in the photoemission of core level electrons. Core level electrons are those electrons close to the nucleus that have binding energies characteristic of a particular element. The kinetic energy of the ejected electrons is analysed by an electron detector, allowing their binding energies to be calculated according to the following equation:

$$E_{BE} = h_p \nu - E_{KE} - \Phi \qquad \text{(Equation 1.31)}$$

where E_{KE} is the kinetic energy of the ejected electrons, E_{BE} is the binding energy of the electron in the solid, Φ is the work function, h_p is the Planck's constant (6.626×10^{-34} m^2 kg/s) and v is the frequency of the electromagnetic radiation.

XPS data is presented as a graph of electron current (intensity) against electron binding energy to give an X-ray induced photoelectron spectra. Electrons that are ejected without energy loss contribute to the characteristic peaks in the spectrum, whereas those that undergo inelastic scattering or energy loss form the background of the spectra. Since the binding energies of core level electrons are unique to elements present in a sample, XPS can detect chemical functionalities with extreme sensitivity (Tougaard 2005). Though X-rays may penetrate bulk, the ejected electrons cannot escape from within a few nanometres of the surface, limiting XPS to surface characterisation (to a depth of ~1-10 nm).

The binding energies of core level electrons for organic compounds are typically between 200-700 eV. These core level electrons have specific binding energies depending on their chemical state. For instance while the binding energy of unfunctionalised carbon in an aliphatic hydrocarbon is 285.00 eV, a chemical shift occurs in presence of adjoining functionalities to the main carbon such as in amines, alcohols or carbonyls to give higher binding energy values of 285.94, 286.55 and 287.90 eV respectively.

X-ray photoelectron spectrometers consist of a moderate vacuum sample introduction chamber, an ultra-high vacuum measurement chamber, the specimen holder, specimen manipulators, a source of X-rays or electron beam as well as an electron analyser and detection system (Figure 1.34).

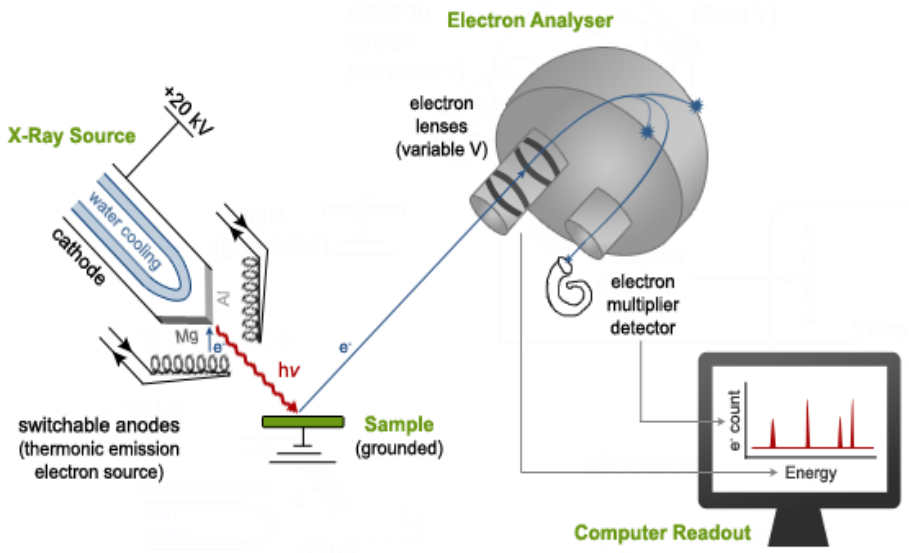

Figure 1.34: Schematic diagram of an X-ray photoelectron spectrometer.

1.10 Work plan

1.10.1 Current problem

Formulation of poorly water-soluble drugs poses a significant challenge to the pharmaceutical industry. These drugs often have sub-optimal clinical outcome due to poor dissolution and bioavailability, high fed to fasted variability as well as high inter patient variability. Over the years many methods including micronisation, complexation and solubilisation have been used in an attempt to increase their dissolution rate and consequently their bioavailability.

Recent technological advancements and understanding of colloidal systems has enabled the formulation of poorly water-soluble drugs as nanoparticles. Various techniques such as media milling, homogenization, precipitation and supercritical fluid processing have been employed to obtain drug nanoparticles. Media milling has had the most favourable outcome with five drugs formulated in this way reaching the market (van Eeerdenburgh et al, 2008; FDA 2009). Media milling is a relatively simple technique that can be conveniently employed for screening purposes by the researcher. Wet-bead milling achieves particle size reductions of drug to within the nanometer size range using a high impact bead mill to fracture drug particles dispersed in a crude concentrated suspension in presence of stabilisers (Kipp 2004 and Merisko-Liversidge et al, 2003; 2008).

Despite its success, mastery of the mechanism behind nanoparticle stabilization is lacking. Selection of stabilisers for a particular formulation is an empirical process involving a lot of trial and error. This is compounded by the fact that each drug demonstrates a unique stabilisation profile, which may vary according to the production process employed (Verma et al, 2009). Previous attempts to relate drug-stabilizer interactions to stabiliser surface tension and viscosity or drug log P, solubility and density have not been successful (van de Eerdenburgh et al, 2009).

The current research aims to elucidate the mechanism of nanoparticle stabilisation and enable prediction of suitable stabilisers for drug formulation by wet bead milling. Eight, structurally disimilar, low water solubility drugs and a range of ionic, non-ionic polymers and surfactants were used to investigate the relationship between the drug and the stabilizer. Furthermore, the effect of stabilizer concentrations on nanoparticle production, stability and adsorption kinetics were determined.

1.10.2 Drug selection

Screening drug-stabiliser relationships for nanoparticle production via wet bead milling was carried out using eight poorly water-soluble drugs namely; albendazole, carbamazepine, frusemide, griseofulvin, halofantrine, indomethacin, nabumetone and phenytoin (Table 1.7). The majority of these drugs exhibit poor water-solubility but high permeability (BCS II), except frusemide, which displays both low water-solubility and permeability (BCS IV). The selected drugs are structurally different and include acids (indomethacin, phenytoin), bases (albendazole, frusemide, halofantrine) and neutral compounds (carbamazepine, griseofulvin, nabumetone).

Pharmaceutically acceptable stabilisers employed in this screen included anionic, cationic, non-ionic polymers and surfactants.

Albendazole is a broad spectrum antihelminthic, carbamazepine and phenytoin are both anticonvulsants, frusemide is a diuretic, griseofulvin an antifungal, halofantrine an antimalarial while indomethacin and nabumetone are both non steroidal anti-inflammatory drugs. These drugs undergo slow and erratic dissolution leading to unpredictable performance, thereby necessitating high drug dosing which increases the incidence of side effects.

Table 1.7: Chemical structure and properties of selected drugs. Table continued on next page.

Drug and chemical structure	**Molecular weight**	**Melting point (C)**	**Water solubility**	**BCS**
1. Albendazole $C_{12}H_{15}N_3O_2S$ 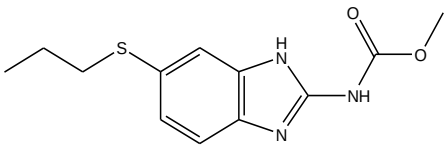	265.33	208-210	0.16 µg/mL at 25°C	II/IV
2. Carbamazepine $C_{15}H_{12}N_2O$ 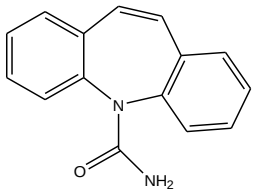	236.28	190-192	18 µg/mL at 25°C	II
3. Frusemide $C_{12}H_{11}ClN_2O_5S$ 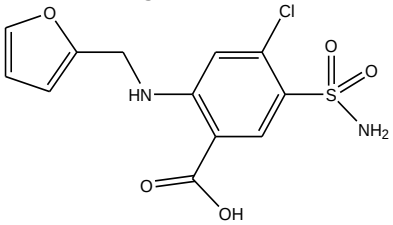	330.74	295	70 µg/mL at 30°C	IV
4. Griseofulvin $C_{17}H_{17}ClO_6$ 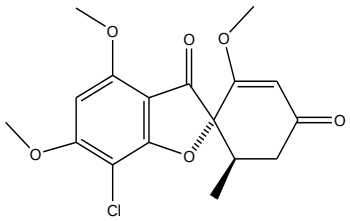	352.77	220	64 µg/mL at 25°C	II

Table 1.7: Chemical structure and properties of selected drugs. Table continued on next page.

Drug and chemical structure	**Molecular weight**	**Melting point (C)**	**Water solubility**	**BCS**
5. Halofantrine $C_{26}H_{30}C_{l2}F_3NO$ 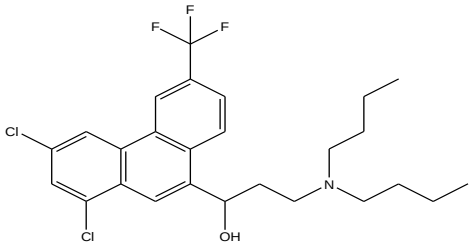	536.9	199-202	< 1.0 µg/mL at 25°C	II
6. Indomethacin $C_{19}H_{16}ClNO_4$ 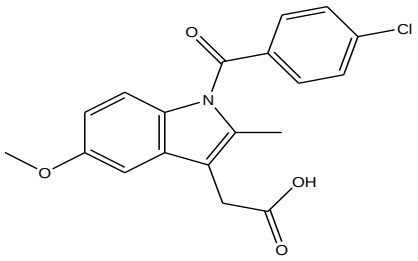	357.79	151-155	0.94 µg/mL at 25°C	II
7. Nabumetone $C_{15}H_{16}O_2$ 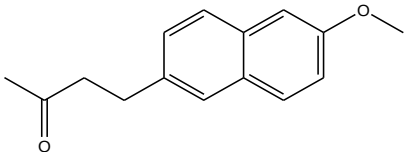	228.3	78-83	4.7 µg/mL at 25°C	II

Table 1.7: Chemical structure and properties of selected drugs. Table continued from previous page.

Drug and chemical structure	Molecular weight	Melting point (C)	Water solubility	BCS
8. Phenytoin $C_{15}H_{12}N_2O_2$ 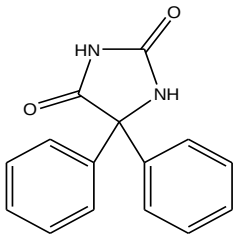	252.27	294	32 μg/mL at 22°C	II

The majority of the work outlined in this thesis was carried out using griseofulvin, which was found to only be stabilised in presence of either an anionic polymer or surfactant. The major indication for griseofulvin is in treatment of various dermatomycosis. It has been the choice agent in stubborn fungal infections for many years. Interest in this drug is re-emerging due to reports of anti-inflammatory activity and synergy with some chemotherapeutic agents. Griseofulvin is available in tablets of 500 mg, 250 mg, 125 mg and in the form of a paediatric suspension. Previous research demonstrated that micronization of griseofulvin led to a 50% reduction in dose (Atkinson 1962). All griseofulvin formulations have since been micronized. Recent attempts to improve the formulation of griseofulvin have included use of self micro-emulsifying drug delivery systems (Ofokanski et al, 2009), solid dispersions (Stachurek et al, 2009), micellar solubilisation (Pierri et al, 2005), complexation with cyclodextrins (Kata et al, 1998) and supercritical fluid nanoparticle production (Thakur et al, 2005). None of these products have reached the market.

1.10.3 Aims

1. To understand the relationship between surfactant/polymer and drug structure on the formation of nanoparticles by wet bead milling.

Screening for drug-stabiliser relationships was carried out using eight poorly water-soluble drugs namely; albendazole, carbamazepine, frusemide, griseofulvin, halofantrine, indomethacin, nabumetone and phenytoin. Using pre-defined

experimental parameters (Goodwin, 2006) a range of ionic and non-ionic polymers and/or surfactants were used to determine stabiliser efficacy for nanoparticle formation. The stabilisers used in the screen included aerosol-OT (AOT), sodium dodecylsulphate (SDS), hydroxypropylmethylcellulose acetate succinate (HPMCAS), hydroxypropylmethylcellulose (HPMC), hydroxypropylcellulose (HPC), hydroxyethylcellulose (HEC), polyvinylpyrorolidine (PVP) Pluronic F 127, Tween 80 and dodecyltrimethylammonium bromide (DTAB); chosen to determine the effect of stabiliser head group charge on nanoparticle stabilisation. An alternative approach would be to select a homologous series of stabilisers in order to determine the effect of hydrocarbon length on nanoparticle stabilisation.

2. To determine the effect of polymer and/or surfactant concentration and polymer molecular weight on production of griseofulvin nanoparticles by wet bead milling.

Griseofulvin, which could only be stabilised by either an anionic polymer or surfactant, was selected for all subsequent research. Unfortunately anionic stabilisers are unsuitable for oral delivery. Anionic surfactant/non-ionic polymer co-stabilisation using the non-ionic polymer, HPMC, was therefore investigated with the view of reducing the amount of ionic surfactant required for nanoparticle production. Reports of polymer-surfactant synergy have been widely used in the cosmetology, mineral processing and other industries. The effects of varying surfactant/polymer concentration and polymer molecular weight on nanoparticle formation and stability were assessed.

3. To ascertain the effect of polymer/surfactant concentration and polymer molecular weight on the amount of stabiliser adsorbed onto griseofulvin nanoparticles.

In order to obtain an adequate understanding of stabilisation of colloidal systems it is imperative to quantify the stabiliser absorded onto these particles. Polymer/surfactant adsorption isotherms were studied by the depletion method using spectroscopic techniques. Adsorption was studied as a function of polymer/surfactant concentration and polymer molecular weight. Small angle neutron scattering was used to provide more detailed information on the adsorbed polymer/surfactant layer.

4. To investigate the crystal surface properties of the various drugs used.

The majority of pharmaceutical drugs are crystalline solids. Each crystal face exhibits its own physical and chemical properties. Knowledge of surface properties of drug crystal faces may help predict its interaction with other molecules of interest, in this case polymer/surfactants used as stabilisers of drug nanoparticles. Macroscopic griseofulvin crystals were grown in acetone and surface energies of the individual crystal facets determined experimentally using contact angle measurements and X-ray photoelectron spectroscopy.

Computer modelling was used to predict the morphology and facet-specific surface energies of the albendazole, carbamazepine, griseofulvin, indomethacin, frusemide and nabumetone crystals.

Chapter 2
Wet bead milling

2.1 Introduction

2.1.1 Wet bead milling

Media milling has been used widely for fine and ultrafine milling of materials such as minerals, ceramics, paint pigments, plant products and microorganisms. Generally stirred media mills are preferred over tumbling and vibrating ball mills due to their lower energy consumption (Kwade 1999). These stirred, tumbling or vibrating media

mills are operated ‘wet’ thus providing advantages of temperature regulation and product containment.

Wet Bead milling (WBM) is also used in the pharmaceutical industry to formulate poorly water-soluble drugs as nanocrystalline particles in order to improve their bioavailability. Elan ‘Nanocrystal’ technology, in which micron sized drug crystals are media milled in the presence of a solution of pharmaceutically acceptable stabilisers yielding nanometer sized drug particles, is employed. WBM efficiently overcomes the challenges of aggregation and powder clumping due to high van der Waals forces, which are associated with dry milling by incorporating stabilisers in the milling process. The nanoparticles are thus stabilised immediately on formation. The presence of effective and sufficient stabilisation is paramount for the success of the milling process.

The stabiliser used should promote wetting and generate a physically stable form of the milled material by providing a steric or ionic barrier cancelling out the effect of the van der Waals forces at the surface of the particles. Stabilisers used include celluloses, pluronics, povidones, polysorbates, and combinations of ionic and non-ionic surfactants. Physically stable nanocrystalline formulations have been widely reported to occur at within specific ranges of drug to stabilizer weight ratios, with lower amounts of stabiliser leading to aggregation, and higher amounts of stabiliser promoting Ostwald ripening (Merisko-Liversidge et al, 2003). The geometrical shape of the resultant nanoparticles is determined by drug/stabilizer interactions, the morphology and the fracture plane of the drug crystals (Merisko-Liversidge et al, 2003, 2008).

2.1.2 Production of nanoparticles

WBM is a highly versatile technique that can handle quantities of drugs from mg to kg, and thus can be used by the research scientist for formulation screening (Kesisoglou et al, 2007) as well as routine production of nanoparticles in the pharmaceutical industry. The studies outlined in the present study were carried out on a micro-scale using 10 g of drug per milling experiment.

Operating parameters such as bead size, bead loading, drug loading and energy input all influence the milling efficiency (Kwade 1999; Fadhel et al, 2001). Sepassi (2003) in our group investigated the effect of varying these parameters. Energy input and drug loading were found to have the most dramatic effect on nanoparticle

production, with nanoparticles no longer being produced if either parameter was reduced. A high drug loading is critical to increase the chance of the beads impacting the drug particles (Rabinow 2004).

The mixer mill used in the present study operates such that the contents of two jars are milled simultaneously, with the jars oscillating in the horizontal plane. During the milling process, the YTZ beads (milling media) bombard the drug particles from all directions breaking them down, mainly by impact and attrition.

Milling induced disorder

It is important to realise that the milling of pharmaceutical crystalline materials may introduce a degree of amorphicity into the material due to exposure to mechanical stresses during the processing. The physical properties of amorphous structure are dramatically different from those of crystalline structure in terms of flow, solubility, stability and bioavailability. It is therefore critical to verify if a process has introduced any amorphous material and, if so, to quantify the amount. Various analytical techniques such as powder x-ray diffraction (XRD), differential scanning calorimetry, isothermal microcalorimetry, solution calorimetry, solid-state nuclear magnetic spectroscopy, fourier transform raman spectroscopy and dynamic vapour sorption have all been used to quantify amorphous and crystalline content in solid drugs. Of these techniques, XRD is the most widely used due to its relative simplicity and ability to detect amorphous material down to levels of ~ 5% (Shah et al, 2006). Amorphous material indicates isotropic material without any translational, orientational or conformational characteristic of the crystalline state. Crystal defects on the other hand include point defects involving a few atoms, line defects comprising crystal lattice misalignments, planar defects characterised by change in crystallographic direction of the lattice and bulk defects (Chamarthy et al, 2008). Both the drug crystal morphology and the mill type used are known to have an effect on the degree of milling disorder induced (Chikhalia et al, 2005).

Ostwald ripening

Ostwald ripening occurs in polydisperse systems of particles, when smaller particles dissolve and recrystallize around the larger particles. As time increases, the number of particles decreases and the average size of the particles increases, although the volume fraction occupied by the particles remains constant. Ostwald ripening occurs

as a result of the system trying to reduce its interfacial energy by diffusion of the small particles to the surface of the larger ones (Yao et al, 1993). Ostwald ripening occurs to a higher extent when the particles have some degree of solubility in the disperse phase.

Ostwald ripening is a disadvantage in nanoparticle formulations as the increase in particle size it causes negates the advantages conferred by particle size reduction. Ostwald ripening can be eliminated or reduced by the tight control of formulation parameters such as particle size, particle-size distribution, solids content, choice of stabilizer, and the use of a fluid phase with minimal solubilising potential of the dispersed phase (Merisko-Liversidge et al, 2008).

Nanosuspensions of poorly water-soluble drugs (< 1 mg/mL) generated by media milling are generally stable on storage, although Ostwald ripening may occur over time or at increased temperatures, particularly when the nanosuspensions are prepared from more water-soluble (> 10 mg/mL) drugs (Gennaro 1995) or if excess stabiliser has not been removed from the nanosuspension. Ostwald ripening occurs as a consequence of uncontrolled precipitation or crystallization of drug leading to a growth in the overall particle size (Boistelle et al, 1988).

2.1.3 Existing challenges

Despite the relative success of WBM for the production of drug nanoparticle formulations, mastery of the stabilisation mechanism is still lacking. Selection of stabilisers for a particular formulation is still an empirical process entailing the use of time and money resources. The current chapter presents a systematic investigation into the effect of a range of stabilisers on the production by WBM of nanoparticles of eight poorly water-soluble drugs, namely albendazole, carbamazepine, frusemide, griseofulvin, halofantrine, indomethacin, nabumetone and phenytoin. The milling results are analysed for trends that would enable the prediction of stabilisers suitable for drug nanoparticle production.

2.2 Methodology

2.2.1 Materials

Griseofulvin was purchased from Acros Organics (Geel, Belgium). Nabumetone was supplied by GlaxoSmithKline (Harlow UK) batch no. 00N60141. Hydroxypropylmethylcellulose (HPMC) with a nominal molecular weights of 8K

(Methocel E3LV (HPMC 8)) and 15K (E15 (HPMC 15000)) were obtained from Dow Company (Michigan, USA) and Colorcon Limited (Dartford, UK), respectively. Hydroxypropylmethylcellulose acetate succinate (HPMCAS), an anionic polymer comprising a mixture of acetic and monosuccinic acid esters of HPMC, was kindly donated by Shin-etsu Co. Limited (UK). It was supplied in three micronized grades differing in weight ratio of acetyl:succinoyl substitution, low LF possesses an acetyl:succinoyl weight ratio substitution of 8:15, medium MF, a weight ratio of 9:11 and high HF, a weight ratio of 12:7. Regardless of the weight ratio of acetyl:succinoyl, HPMCAS, whose trade name is AQOAT, had a weight-average molecular weight of 18000 daltons. All other chemicals were purchased from Sigma-Aldrich Co. Limited (Poole, UK).

Yttrium zirconia (YTZ) beads of size 0.44 mm (0.35-0.5 mm range), which have minimal contamination levels acceptable for pharmaceuticals (Ruddy et al, 1998), were obtained from GlaxoSmithKline (Harlow, UK). Ultra pure water (UPW), obtained from a well seasoned, all glass still (D4000 Distinction, Sterling, UK) was used for all experiments. All chemicals were of the highest grade available and were used as received without further purification.

2.2.2 Preparation of crude drug suspensions

Stabiliser solutions were prepared by weighing the required amount of polymer and/or surfactant and making up to weight with UPW. The only exception to this method was when using the water insoluble HPMCAS polymers, where the polymer was suspended in an aqueous 10 mM sodium citrate (alkaline) solution prior to its use in milling. Note that the dispersed HPMCAS polymer systems were sometimes turbid, although in these cases caution was exercised to ensure the effective dispersion of the polymer before the addition of the drug so that no solid particles of polymer remained. Regardless of the nature of the stabiliser used, its dispersion/dissolution was achieved by constant magnetic stirring. The HPMC polymer solutions were kept in the fridge for 2 hours prior to use to aid polymer dissolution.

40 g of the initial stabiliser solution was added to 10 g of drug to make up 50 g of the crude drug suspension or slurry, which was stirred overnight prior to milling. A 20% w/w drug concentration in the crude suspension increased the chances of the YTZ beads impacting the drug particles during milling. The amount of stabiliser is quoted

hereafter as a weight percentage of the initial stabiliser solution before the addition of drug.

2.2.3 Wet bead milling

Wet bead milling was carried out using the Retsch MM 200 mixer mill (Glen Creston Ltd, Stanmore UK) illustrated in Figure 2.1. The milling parameters used in the present study were adapted from those of Sepassi-Ashtiani (2003) and utilised 0.44 mm YTZ beads, a frequency setting of 30 Hz, a milling time of 6 hours and a 50:50 vol % bead:slurry loading. Specifically 10 mL of YTZ beads (0.44 mm diameter) followed by 10 mL of slurry (crude drug suspension) were loaded into a milling jar (Nylube, Nylecast,UK) of 25 cm^3 capacity. The jar was then well sealed with sufficient parafilm and clamped into the mixer mill and milled at room temperature. The temperature of the milling jar contents would rise to ~ 45 ± 0.1°C after 6 hours of continuous WBM, necessitating stopping the mill for a few minutes every hour.

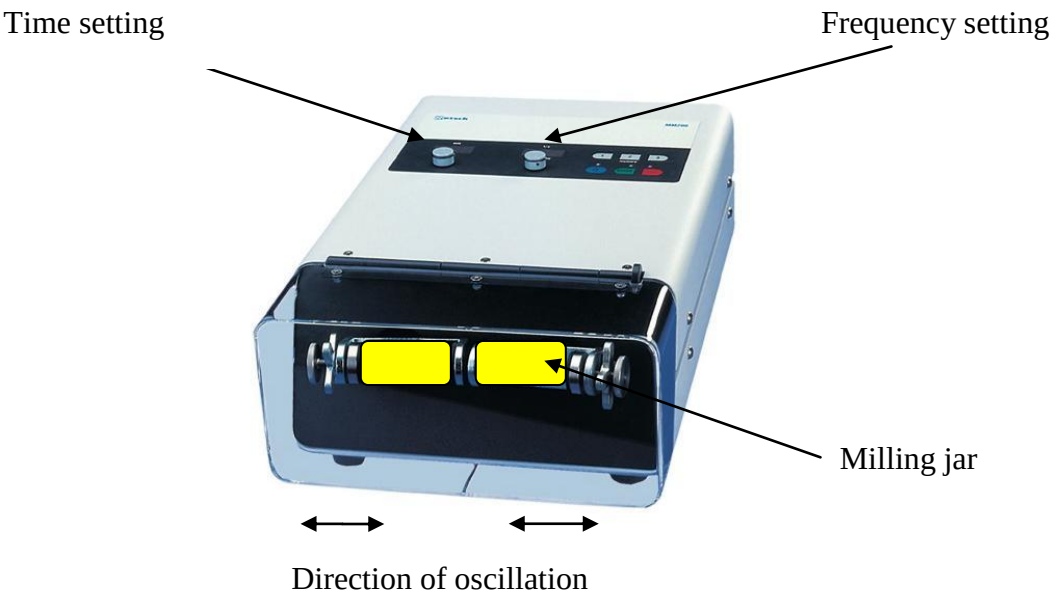

Figure 2.1: Retsch MM200 Mixer Mill.

Milling was stopped every hour, the jar opened and two drops of suspension collected and diluted with UPW for particle size analysis. The jars were then resealed with parafilm and the milling resumed. After 6 hours the YTZ beads were separated from the nanosuspension using a 60 mesh sieve (0.25 mm nominal aperture), the nanosuspension collected and stored for further analysis. The beads

were then cleaned with copious amounts of water, rinsed in methanol, oven dried and re-used.

2.2.4 Particle size analysis

Photon correlation spectroscopy (or light scattering) was performed using a Brookhaven ZetaPlus particle sizer v2.29 (Brookhaven instruments, UK) consisting of a He-Ne laser operating at 677 nm, in order to determine the apparent hydrodynamic size (i.e. effective diameter) and polydispersity index (i.e. width of the particle size distribution) of the drug nanoparticles. The particle size range accessible with this equipment, as quoted by the manufacturer, is 10 nm to 10 μm depending on the particle density.

The experiments were performed at 25 ± 0.1°C using a light scattering detection angle of 90°. Values for viscosity and refractive index of aqueous media were set at 0.89 cp and 1.33 respectively. 2-3 drops of the drug nanosuspensions were added to 10 mL water to give a suitable count rate (i.e. 50-80 kcps). The diluted nanosuspensions were placed in clear, 4-sided, 10 mm path length disposable polystyrene cuvettes for particle size analysis. Each measurement was performed for 30 seconds with ten repetitions. Particle size analysis was performed every hour in order to follow the milling kinetics. For each formulation studied, three individual nanosuspensions were prepared and their size measured. Therefore results are expressed as the mean of three individual measurements ± the standard deviation.

2.2.5 Zeta potential

Zeta potential was measured using a Zetasizer Nano ZS (Malvern instruments, UK), which utilises the Malvern M3-PALS (phase analysis light scattering) technology to give high sensitivity, accuracy and resolution of measurements. The detection angle was large (173º) as the Zetasizer Nano ZS is a back scattering instrument. Zeta potential measurements were carried out both in presence and absence of excess polymer/surfactant.

Experiments were performed at 25 ± 0.1°C in water and zeta potential calculations carried out using the Smoluchowski theory. 2-3 drops of the crude drug nanosuspensions were added to 10 mL water. The samples were placed in disposable, folded capillary cells with gold electrodes for analysis. Each measurement was carried out for 30 seconds with ten repetitions.

2.2.6 Viscosity

Viscosity measurements were carried out using the AVS 350 unit (Schott-Gerate, Hofheim, Germany) coupled to the AVS 20 viscodoser for automated dilutions. A Ubbelohde dilution vessel with a fill volume of 75 mL and capillary length 290 mm was used. The viscometer was cleaned with copious amounts of soap and water, ensuring it was dry and dust free before any measurements were made. Six dilutions were preselected and the time for temperature equilibration after dilution and prior to measurement was set at 10 minutes. The initial, concentrated solutions for viscosity measurement were filtered using a 0.22 micron cellulose acetate membrane filter prior to introduction into the viscometer. In addition, the flow time of UPW was also measured. Flow measurements were made in triplicate. All viscosity measurements were performed at 25 ± 0.1°C.

For polymer molecular weight determination, it is important to ensure that the relative viscosity (i.e. the flow time of the solution relative to the flow time of the solvent) of the diluted polymer solutions was in the range 1.1 to 2. In this dilute region intermolecular interactions are not operative and there is a linear variation between viscosity and concentration. The intercept of the Huggins and Kraemar plots on the y-axis yield the intrinsic viscosity, which is then used to calculate viscosity average molecular weight by means of the Mark Houwink equation.

2.2.7 Surface tension

Surface tension measurements were performed by the Wilhelmy plate method using the automated K11 tensiometer (KRUSS GmbH Hamburg, Germany). A roughened platinum plate was used to allow the assumption of complete wetting (contact angle of zero) of the plate to be satisfied. About 3 mL of the solution whose surface tension was to be measured was poured into a scrupulously clean, metal vessel, which was then placed into a temperature controlled chamber (25 ± 0.1°C).

All the glassware with which the solution whose surface tension was to be measured was to come in contact with, was soaked overnight in detergent, copiously rinsed initially with distilled water and then UPW and dried before use. Prior to the measurement of sample surface tension, the surface tension of the UPW used to prepare the samples was determined with a value of 72.8 ± 0.5 mN/m being deemed acceptable. Between measurements the platinum plate was cleaned and flamed to

ensure no residual surface active material remained to interfere with the measurement of surface tension.

Surface tension was measured as a function of surfactant concentration in order to obtain the critical micelle concentration of SDS, AOT, Tween 80 and DTAB. Stock solutions of 10% w/w surfactant were prepared and serially diluted in the same container to avoid loss of surfactant by its adsorption onto the container walls. The surface tension of the anionic surfactants as a function of surfactant concentration was also measured in the presence of the non-ionic polymer, HPMC, to determine the critical aggregation concentration. For the polymer/surfactant studies, 0.1% w/w HPMC solution was used in place of UPW as the diluent. The surface tensions of 1% w/w polymer (HEC, HPC, HPMC, PVP 30 and F127) solutions were also measured. Each measurement was performed on three individual solutions and therefore the results are expressed as the mean of these three measurements ± standard deviation.

Surface tension was taken every 30 seconds until an equilibrium value was attained. The more dilute solutions took markedly longer times to reach equilibrium e.g. 5 and 15 min equilibration times for 1.0% w/w and 0.01% w/w of SDS solutions respectively.

2.2.8 Scanning electron microscopy

Scanning electron microscopy (SEM) images of griseofulvin nanosuspensions prepared by 6 hours WBM in presence of 0.5% w/w SDS, 0.5% w/w AOT, 0.5% w/w SDS + 1.88% w/w HPMC 8000, 0.5% w/w AOT + 1.88% w/w HPMC 8000 and 0.5% w/w HPMCAS-LF were obtained. These samples were selected to investigate effect of stabiliser on the morphology of resultant nanoparticles. SEM images of a suspension of unmilled griseofulvin stirred in UPW were also taken to establish griseofulvin morphology prior to milling.

A drop of the sample to be examined was placed on the surface of a small cover glass (ca. 5 x 5 mm) mounted on a specimen stub and allowed to dry before being mounted in the electron microscope. A FEI Quanta 200 ESEM FEG scanning electron microscope operating at accelerating voltage of 7.5 kV under low vacuum conditions at 1.00 Torr chamber pressure was used to visualize the samples.

2.2.9 X-ray powder diffraction

Griseofulvin nanosuspensions prepared by 6 hours WBM in presence of 0.5% w/w SDS, 0.5% w/w AOT, 0.5% w/w SDS + 1.88% w/w HPMC 8000, 0.5% w/w AOT + 1.88% w/w HPMC 8000 and 0.5% w/w HPMCAS-LF, MF and HF were snap frozen using liquid nitrogen and subsequently dried using a Heto PowerDry® LL3000 freeze dryer (Thermo Fisher Scientific, UK) operating at 55 ± 0.1°C for 24 hours. X-ray diffraction (XRD) patterns of the powders were obtained, alongside that of unmilled drug to investigate whether milling induces any changes in the crystalline nature of the drug.

An X'Pert PRO X-ray diffractometer (PANalytical B.V) with Cu-K_α targets was used to record the XRD patterns of the samples. The powders to be examined were first coarsely ground using a mortar and pestle to break any loose powder clumps. About 50 mg of powder was then loaded into the sample holder before mounting it into the machine. XRD measurements were then carried out from 5 to 60 2θ degrees using a step size of 0.1 2θ degrees and a dwell time of 10 s at each step.

2.2.10 Time stability studies

Griseofulvin nanosuspensions prepared in sections 2.3.3-2.3.5 were stored in their original milled state, i.e. in presence of excess polymer/surfactant, at room temperature for 1 year and particle size periodically monitored.

2.2.11 pH stability studies

pH stability studies were carried out to understand the effect of pH changes on the nanoparticle size during transit through the gastrointestinal tract. The sizes of griseofulvin nanoparticles prepared in sections 2.3.3 and 2.3.5 were measured by PCS immediately after dilution in hydrochloric acid (pH 1-6) or water (pH 7) at 25 ± 0.1°C and 37 ± 0.1°C. Of particular interest was the effect of inclusion of the non-ionic polymer, HPMC, on stability of the electrostatically stabilised nanoparticle formulations.

2.3 Results

2.3.1 Stabiliser screen

Selection of stabilisers for the production of drug nanoparticles is an empirical process involving trial and error. Difficulty in the selection process is compounded

by the fact that each drug demonstrates a unique stabilisation profile, which may vary according to the production process employed to produce the nanoparticles (Verma et al, 2009).

Eight structurally different, poorly water-soluble drugs namely; albendazole, carbamazepine, frusemide, griseofulvin, halofantrine, indomethacin, nabumetone and phenytoin (Table 1.7) with varying physical properties (molecular weights, melting points, aqueous solubility's) were studied for their ability to be formulated into nanoparticles using a range of stabilisers. The selected drugs included acids (indomethacin, phenytoin), bases (albendazole, frusemide, halofantrine) and neutral compounds (carbamazepine, griseofulvin, nabumetone). All drugs had a mean particle size of above 10 microns prior to milling.

Appropriate amounts of stabiliser, sufficient to prepare a 1.5% w/w aqueous solution were weighed and mixed with the required amount of water. Wet bead milling of the crude drug solutions was performed as outlined in sections 2.2.2-2.2.3 and resultant particle size determined. The stabilisers investigated were the non-ionic polymers - hydroxylpropylmethylcellulose (HPMC), hydroxylpropylcellulose (HPC), hydroxylethylcellulose (HEC) and polyvinylpyrolidine (PVP); the polymer non-ionic surfactant - Pluronic 127 (F127); and the low molecular weight surfactants - sodium dodecyl suphate (SDS), dodecyl trimethylammonium bromide (DTAB) and Tween 80. The structures and molecular weights of the stabilisers used are shown in Table 2.1. The stabiliser concentration of 1.5% w/w was chosen after preliminary studies deemed it to be a sufficiently high concentration to provide sufficient coverage of the nanoparticles while at the same time not producing too viscous a solution as to impede the collision of the drug particles and beads. The screen was adapted from methodology developed by Goodwin (2006).

Table 2.1: Chemical structures and physicochemical properties of stabilisers investigated. Table continued on next page.

Compound	Chemical structure	Molecular weight (Daltons)
1. Hydroxypropyl methylcellulose	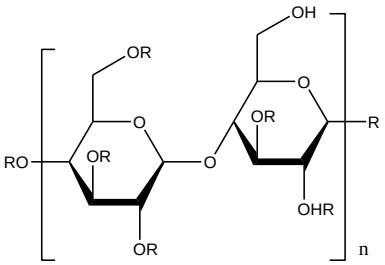 R= H, CH_3 or $CH_2CH(OH)CH_3$	8000 15000 86000
2. Hydroxypropyl cellulose	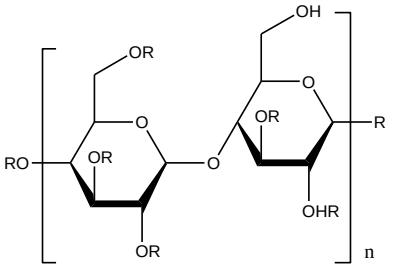 R= H or $CH_2CH(OH)CH_3$	34000
3. Hydroxyethyl cellulose	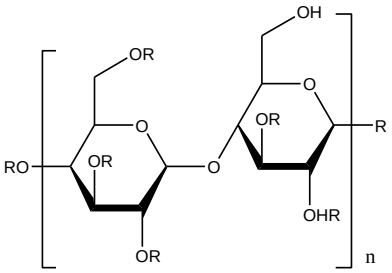 R= H or $CHCH_2OH$	33000

Table 2.1: Chemical structures and physicochemical properties of stabilisers investigated. Table continued on next page.

Compound	Chemical structure	Molecular weight (Daltons)
4. Polyvinyl pyrollidine	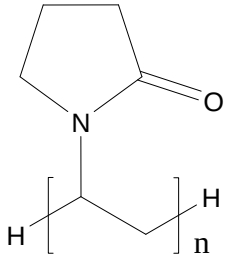	42000
5. HPMCAS	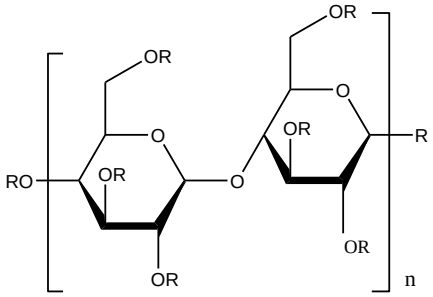 R= H or CH_3 or $CH_2CH(CH_3)OH$ or $COCH_3$ or $C0CH_2CH_2COOH$ or $CH_2CH(CH_3)OCOCH_3$ or $CH_2CH(CH_3)OCOCH_2CH_2COOH$	18000
6. Tween 80	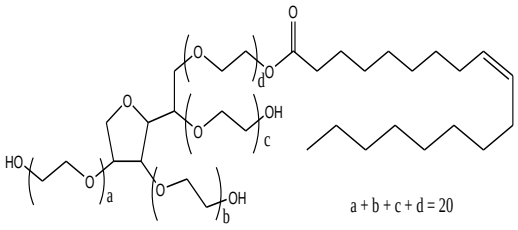 a + b + c + d = 20	1310
7. Sodium dodecyl sulphate	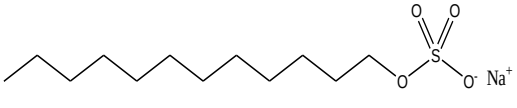	288.38

Table 2.1: Chemical structures and physicochemical properties of stabilisers investigated. Table continued from previous page.

Compound	Chemical structure	Molecular weight (Daltons)
8. Aerosol-OT	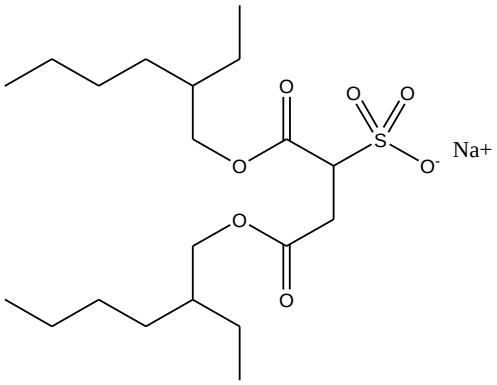	444.56
9. Dodecyl trimethyl ammonium bromide	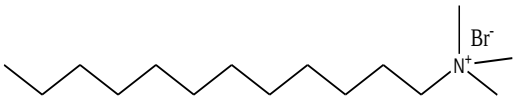	308.34
10. Pluronic F 127	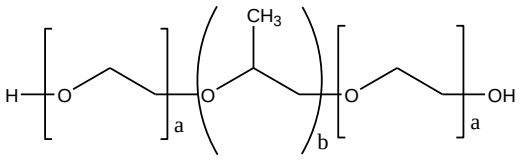 a = 100, b = 65	12000

Table 2.2 shows the results obtained after 6 hours wet bead milling of the eight drugs studied with the various drug-stabiliser combinations tested. The milled nanoparticles generally exhibited a relatively narrow polydispersity (PI of less than 0.2), except when the particle size was above 400 nm. Formulations denoted 'M' indicate those in which stabilisation was ineffective producing micron sized particles after the 6 hours of milling. In some of these cases, formulations solidified in the jars e.g. with halofantrine-SDS – the occurrence of solidification is not specifically

indicated in the table. Milling of halofantrine was only carried out in presence of 4 stabilisers, namely HPMC, PVP 30, SDS and DTAB, due to a shortage of drug. Unfortunately no apparent trend was visible from the milling results. As can be seen most of the drugs displayed different stabilisation profiles. Indeed only the non-ionic drugs, nabumetone and carbamazepine had similar stabilisation profiles, despite the fact that they are structurally quite distinct (Table 1.7).

Table 2.2: Particle size (nm) obtained using photon correlation spectroscopy after 6 hours wet bead milling of 8 structurally different drugs in presence of a range of stabilisers (stabiliser concentration used 1.5% w/w).

Drug	HPMC 8000	HPC 34000	HEC 33000	PVP 30	F127	Tween 80	SDS	DTAB
Albendazole	513.4	316.2	406.8	440	M	M	309.4	463.5
Carbamazepine	482.9	730.0	M	M	M	M	M	M
Frusemide	246.4	199.6	380	234.9	347.8	417.3	M	M
Griseofulvin	M	M	M	M	M	M	276.0	M
Halofantrine	522.7	ND	ND	501.4	ND	ND	M	407.8
Indomethacin	237	210	320	260	640	308.9	M	M
Nabumetone	388.3	359.1	M	M	M	M	M	M
Phenytoin	355	218	309	234	641	M	M	M

M: micron sized particles thus stabiliser not effective. ND: not determined

The drug-stabiliser relationships will be discussed further as a function of stabiliser and drug properties:

Stabiliser properties

The screen revealed that the non-ionic polymers, particularly the cellulosics, HPMC and HPC, were the most efficient stabilisers forming nanoparticles with all drugs tested, except griseofulvin (Table 2.2). The non-ionic polymers, HEC and PVP 30, were also successful stabilisers, stabilising all but 3 of the drugs tested while Pluronic F 127 stabilised 3 drugs out of the 7 drugs it was tested with. The low molecular weight surfactants stabilised a narrower range of drugs in comparison to the non-ionic polymers and polymeric surfactants, with Tween 80, SDS and DTAB stabilising only 2 drugs each. The observed differences in resultant particle size of the nanoparticles obtained with the various drugs are probably a result of the difference in the hardness of the drugs and drug/stabiliser interactions. It is important to note that in the present study because one representative stabiliser concentration

was tested, the differences in sizes obtained for the drugs with the various stabilisers may be, in part, a consequence of the use of a sub-optimal amount of stabiliser.

Drug properties

Most of the drugs examined displayed unique stabilisation profiles that were not obviously possible to predict. For example although the non-ionic drugs, carbamazepine and nabumetone could both be stabilised by the non-ionic polymers, HPMC and HPC, the drugs exhibited widely varying structures and physical properties, in particular different solubilities and lipophilicites. Frusemide and indomethacin formed the smallest nanoparticles of about 200 nm, probably indicating these drugs were easily fractured. It must be noted however that the one representative concentration of stabiliser used for the screen, possibly explaining the variation in the size of the nanoparticles obtained with the different stabilisers. Interestingly griseofulvin only formed nanoparticles with one of the stabilisers examined, namely the anionic surfactant, SDS.

The number of successful stabilisers for each drug was plotted against the physico-chemical properties of the drugs examined, namely molecular weight, solubility, melting point, surface tension and functional groups (groups containing nitogen, oxygen, sulpur or halogens) to see if any trends were visible (Figures 2.2 to 2.6). Halofantrine was excluded from the plots due to an incomplete set of data being obtained.

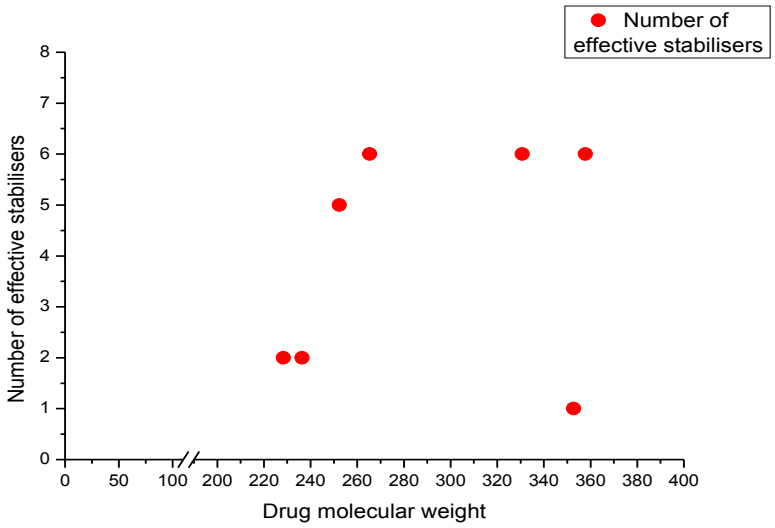

Figure 2.2: Plot of number of effective stabilisers against drug molecular weight.

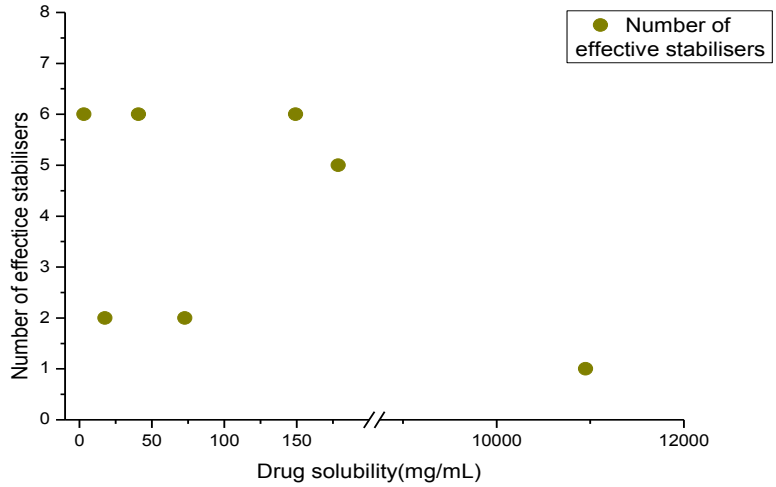

Figure 2.3: Plot of number of effective stabilisers against drug aqueous solubility.

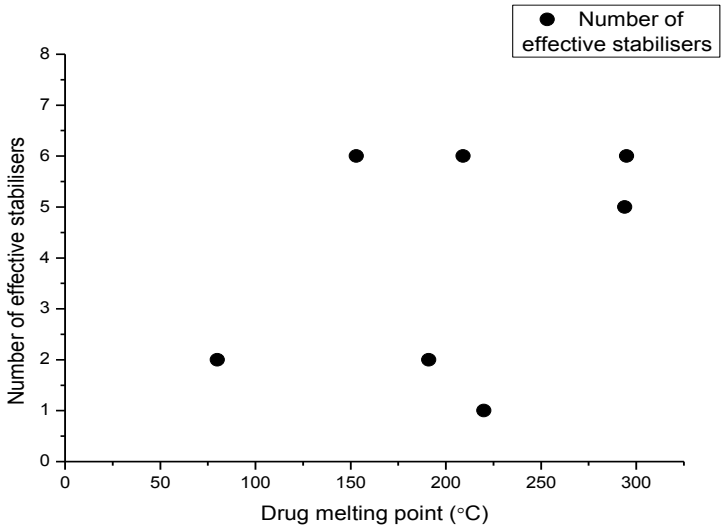

Figure 2.4: Plot of number of effective stabilisers against drug melting point.

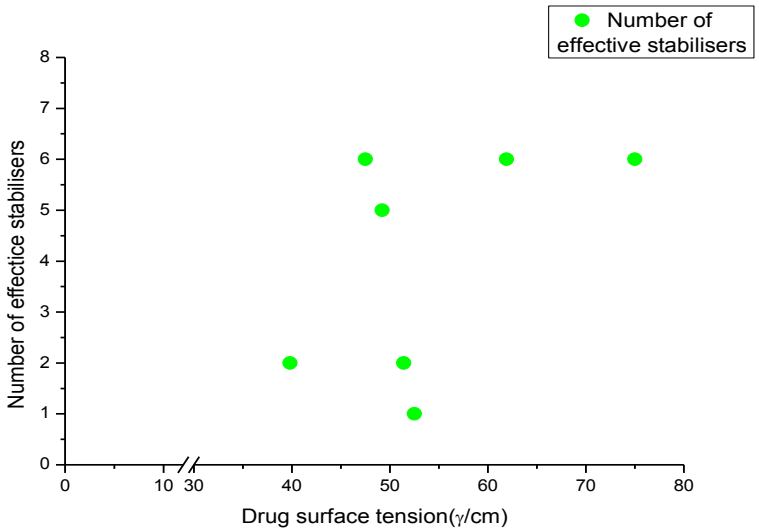

Figure 2.5: Plot of number of effective stabilisers against drug surface tension.

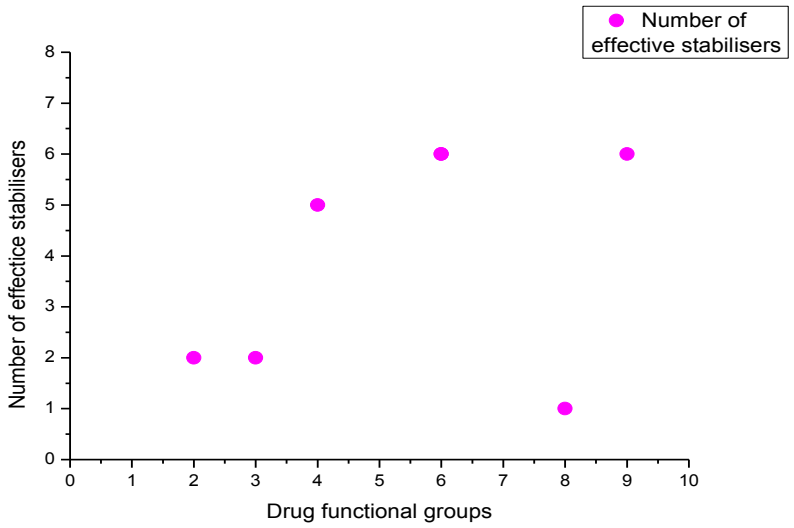

Figure 2.6: Plot of number of effective stabilisers against drug functional groups.

With the exception of one outlier, a relationship was observed in the plots of the number of effective stabilisers against drug molecular weight and functional groups (Figures 2.2 and 2.6). In general, the number of effective stabilisers and thus ease of stabiliser selection was found to increase with both the drug's molecular weight and the number of functional groups it contains. Interestingly, despite griseofulvin's high molecular weight and number of functional groups, it did not follow the observed trends and was the noticeable outlier in both Figures 2.2 and 2.6.

As the number of effective stabilisers tended to be higher for the less water-soluble drugs (Figure 2.3), this suggests that it should be relatively easier to select stabilisers for very poorly water-soluble drugs. No relationship between the melting point or surface tension of a drug and the number of effective stabilisers was clear (Figure 2.4, 2.5). Lee et al (2008) performed drug-stabiliser studies using 11 drugs and 5 polymers and 2 surfactants and observed an increase in number of successful stabilisers with increasing drug molecular weight and melting point and decreasing water solubility. Using the results obtained from milling 9 structurally different drugs using 13 stabilisers, van de Eerdenburgh et al (2009) attempted to relate drug-stabilizer interactions using the surface tension and viscosity of the stabiliser solution, and the log P, solubility and density of the drug. Recently Liu et al (2011) also carried out a similar screen on 2 drugs namely indomethacin and itraconazole using 4 different stabilisers at 4 different concentrations. In neither of the latter

studies did a pattern emerge for the prediction of which stabilisers were suitable for production of nanoparticles using a particular drug.

Griseofulvin nanoparticles

All subsequent milling experiments in the present study were performed using griseofulvin. Although griseofulvin is a neutral drug, possessing no charged groups, during the stabiliser screen, it was only stabilised by the anionic surfactant, SDS. To this end, other anionic molecules, namely aerosol-OT (AOT) and hypromellose acetate succinate (HPMCAS), were also investigated for their ability to produce griseofulvin nanoparticles. The molecular structure of AOT and HPMCAS are shown in Table 2.1.

SDS is a monoalkyl surfactant with a sulphate head group. It is very hydrophilic (HLB 40) and dissolves rapidly in water to form micelles. AOT on the other hand is a dialkyl surfactant with a sulfo-succinate head group. It is hydrophobic and requires sonication to disperse it in water. On dispersion in water, it forms a lamellar phase. HPMCAS is an anionic polymer with a hypromellose backbone and acetate and succinate ester side groups. Various grades of HPMCAS are available differing in levels of acetyl and succinoyl substitution and particle size (Table 2.3).

Table 2.3: Parameters of various HPMCAS grades from Shin-etsu (2005).

Grade	Description		Mean particle size	Application
	Dissolving pH*	**Acetyl (%) / Succinoyl (%)**		
Aqoat AS-LF	≥ 5.5	8 / 15	5 μm	Micronized grades or aqueous and dry coating.
Aqoat AS-MF	≥ 6.0	9 / 11		
Aqoat AS-HF	≥ 6.5	12 / 7		
Aqoat AS-LG	≥ 5.5	8 / 15	1 mm	Granular grades for solvent-based coating.
Aqoat AS-MG	≥ 6.0	9 / 11		
Aqoat AS-HG	≥ 6.5	12 / 7		

* In Mcllvaine's buffer (citric acid-Na_2HPO_4) and USP Phosphate Buffer (NaOH-KH_2PO_4)

A preliminary milling of griseofulvin in the presence of either 1.5% w/w AOT or HPMCAS led to the production of nanoparticles, further confirming that the presence of anionic groups was paramount for the stabilisation of griseofulvin nanoparticles. The size of the griseofulvin nanoparticles produced in presence of AOT and HPMCAS will be presented and discussed in a latter section, namely 2.3.3.

2.3.2 Characterisation of polymers/surfactants

2.3.2.1 Viscosity measurements

Capillary viscometry measurements of dilute polymer solutions of HPC, HEC, HPMC or PVP 30 were used to obtain their intrinsic viscosity in order to calculate polymer viscosity averaged molecular weight. The Mark Houwink parameters ‘k’ and ‘a’ (defined in Equation 1.19) used in the calculations are given in Table 2.4.

Table 2.4: Mark Houwink parameters of various polymers determined in water.

Polymer	Temperature (ºC)	Mark Houwink parameter k	Mark Houwink parameter a	Reference
HPMC	20	$3.39 * 10^{-4}$	0.88	Dow chemical 1975
HPC	25	$6.25 * 10^{-5}$	0.84	Law et al, 1983
HEC	25	$9.49 * 10^{-5}$	0.87	Brown et al, 1963
PVP 30	25	$6.76 * 10^{-4}$	0.55	Ahmad et al, 1990

The Huggins and Kraemer plots of the polymers studied intercepted on or close to the y-axis (Figure 2.7 to 2.12), thereby enabling an accurate determination of the intrinsic viscosities of the polymer solutions. Table 2.5 gives the intrinsic viscosity and viscosity averaged molecular weights calculated in this manner. As can be seen from the Table there was good agreement between the nominal molecular weight (M_n) quoted by the manufacturer and the experimentally determined value (M_v), with the exception of HPMC 8000 and PVP 30 whose experimentally determined molecular weight was much lower than that quoted by the manufacturer.

Table 2.5: Polymer intrinsic viscosities (η) and viscosity averaged molecular weights (M_v) as determined by capillary viscometry at 25 ± 0.1°C (n = 3 ± s.d.).

Formulation	Nominal molecular weight (M_n) (kg/mol)	Intrinsic viscosity (η) mL/g	Viscosity averaged molecular weight (M_v) (kg/mol)
HPMC 8000	8000	52.7 ± 1.4	4200 ± 110
HPMC 15000	15000	153.1± 2.1	14000 ± 190
HPMC 86000	86000	770.5 ± 1.2	89000 ± 140
HEC 33000	33000	90.7 ± 2.3	38000 ± 220
HPC-SSL 34000	34000	44.1 ± 1.2	38000 ± 110
PVP 30 42000	42000	19.2 ± 1.1	29000 ± 170

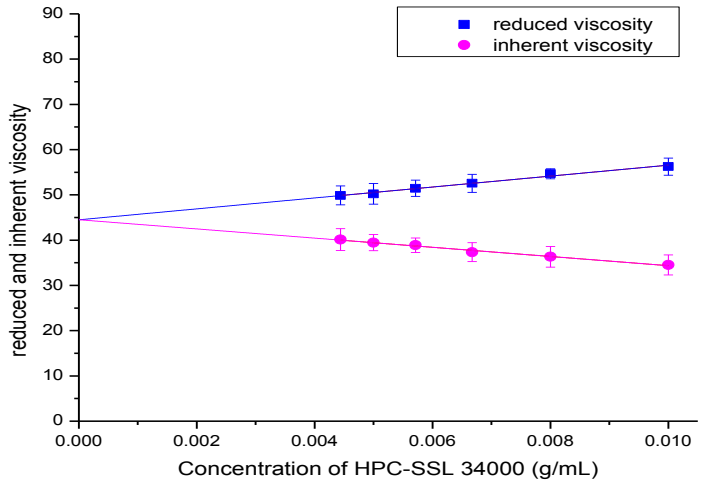

Figure 2.7: Huggins/Kraemer plots for aqueous solutions of HPC-SSL 34000 at 25 ± 0.1°C (n = 3 ± s.d.). Error from measurements on three separate solutions.

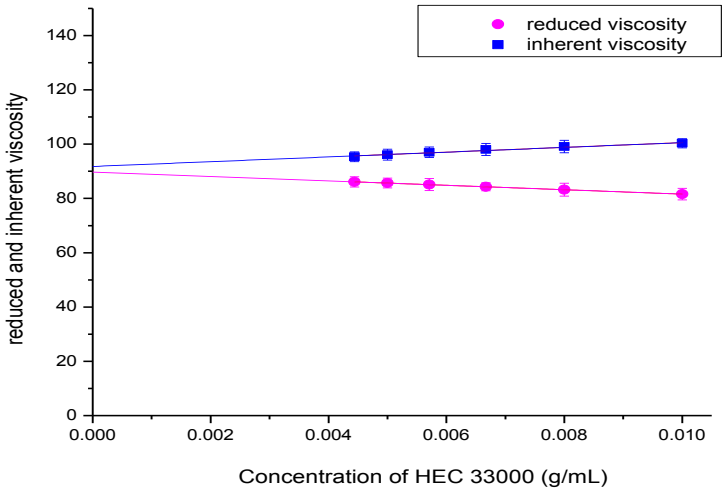

Figure 2.8: Huggins/Kraemer plots for aqueous solutions of HEC 33000 at 25 ± 0.1°C (n = 3 ± s.d.). Error from measurements on three separate solutions.

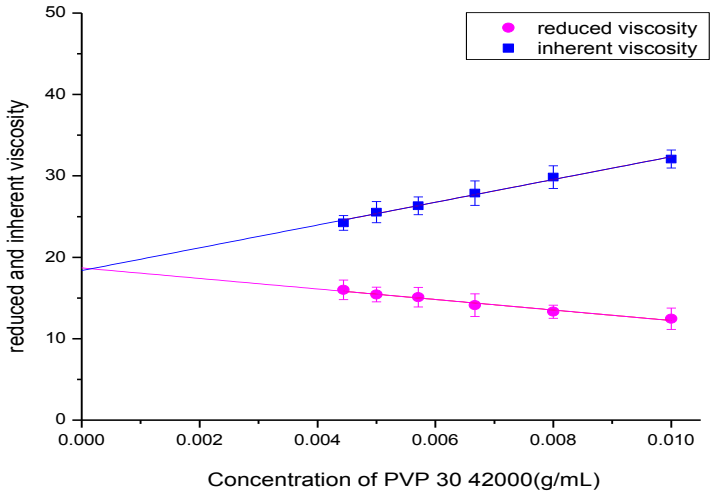

Figure 2.9: Huggins/Kraemer plots for aqueous solutions of PVP 30 42000 at 25 ± 0.1°C (n = 3 ± s.d.). Error from measurements on three separate solutions.

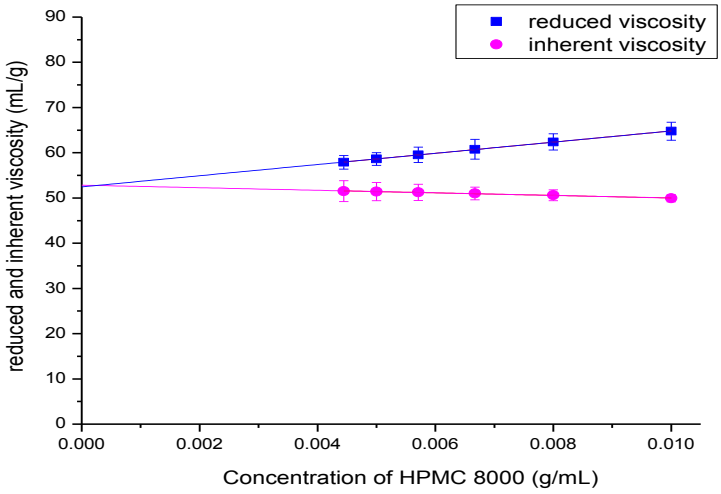

Figure 2.10: Huggins/Kraemer plots for aqueous solutions of HPMC 8000 at 25 ± 0.1°C (n = 3 ± s.d.). Error from measurements on three separate solutions.

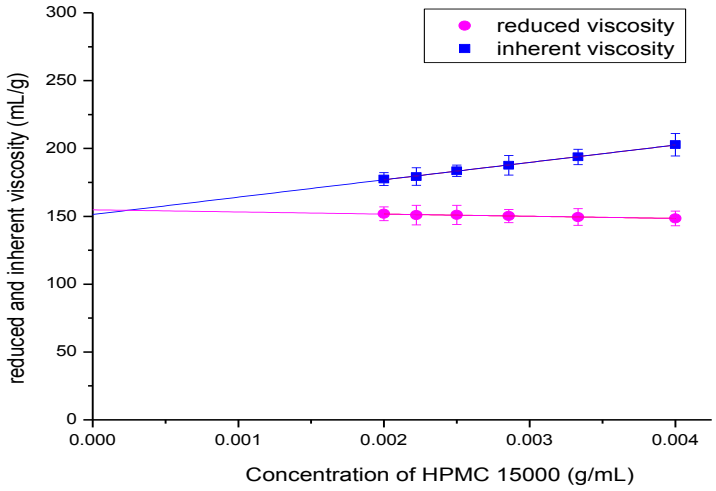

Figure 2.11: Huggins/Kraemer plots for aqueous solutions of HPMC 15000 at 25 ± 0.1°C (n = 3 ± s.d.). Error from measurements on three separate solutions.

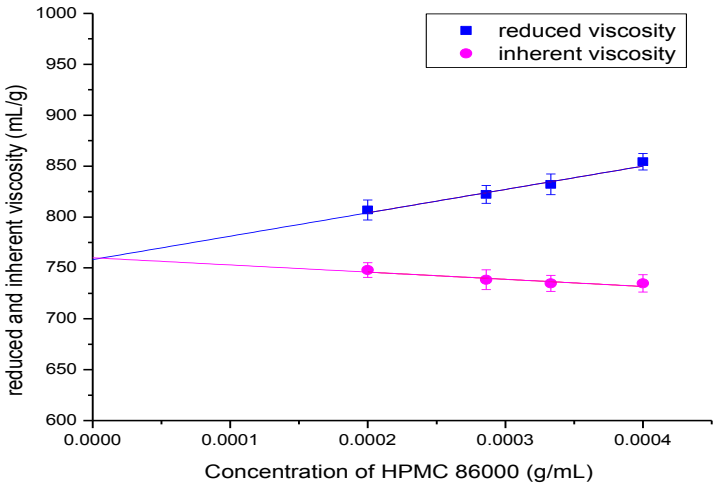

Figure 2.12: Huggins/Kraemer plots for aqueous solutions of HPMC 86000 at 25 ± 0.1°C (n = 3 ± s.d.). Error from measurements on three separate solutions.

2.3.2.2 Surface tension

Surfactants

The surface tension of SDS, AOT, DTAB and Tween 80 in water was measured as a function of surfactant concentration in order to obtain the various surfactants' critical micelle concentration (cmc), i.e. the concentration at which surfactant micelles are formed in the bulk solution. Characteristic surface tension isotherms (where surface tension reduced monotonically with increasing surfactant concentration up to a

certain concentration beyond which there was no appreciable change in surface tension) were obtained for each of the surfactants (Figures 2.13 to 2.16). The break in surface tension corresponds to the critical micelle concentration of the surfactant. Surface excess and area per molecule were calculated to obtain an understanding of surfactant packing at the air-water interface (Table 2.6).

As can be seen from Table 2.6, the dichain, anionic surfactant, AOT is more surface active than its single chain counterpart, SDS, displaying both a lower cmc and a lower surface tension at the cmc. This result was expected due the higher ionisation potential of the sulphate head group relative to the sulfosuccinate (Attwood et al, 1983; Chatterjee et al, 2001), coupled with the larger/more hydrophobic chain region present in AOT compared to SDS. Secondly, AOT occupies a larger area per molecule at the air-water interface in comparison to SDS, which again is predictable from a consideration of their respective molecular structures.

The cationic surfactant, DTAB, exhibited a cmc value similar to that of SDS (Table 2.6), which is perhaps not unexpected considering that these two surfactants have a similar hydrophobic chain length, differing only in their head group - SDS possess a sulphate group and DTAB a trimethylammonium group. The DTAB surfactant exhibited a larger area per molecule than SDS, which is expected from a consideration of their respective head groups. The non-ionic surfactant, Tween 80, possessed a lower cmc than any of the ionic surfactants (Table 2.6). This observation was as expected since non-ionic surfactants tend to possess a lower cmc than ionic surfactants, because of the lower nature of the repulsive forces between the non-ionic head groups. Perhaps surprisingly, because of the polymeric nature of its head group, Tween 80, possessed the lowest area per molecule of all the surfactants examined.

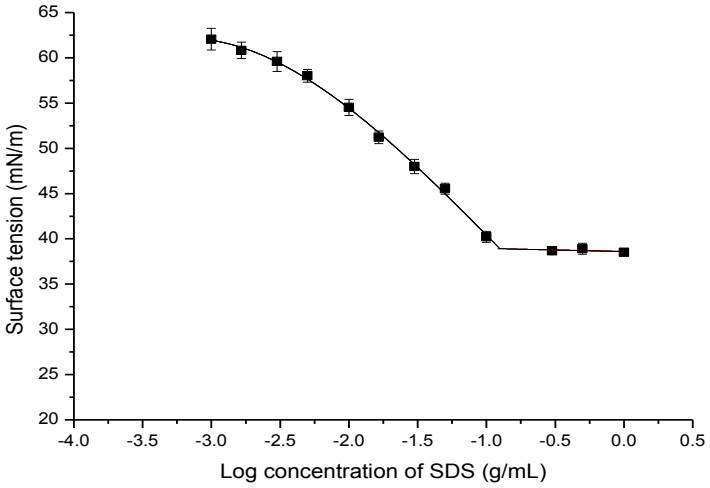

Figure 2.13: Variation in surface tension against log concentration for SDS (■) in water at 25 ± 0.1°C (n = 3 ± s.d.). Error from measurements on three separate solutions.

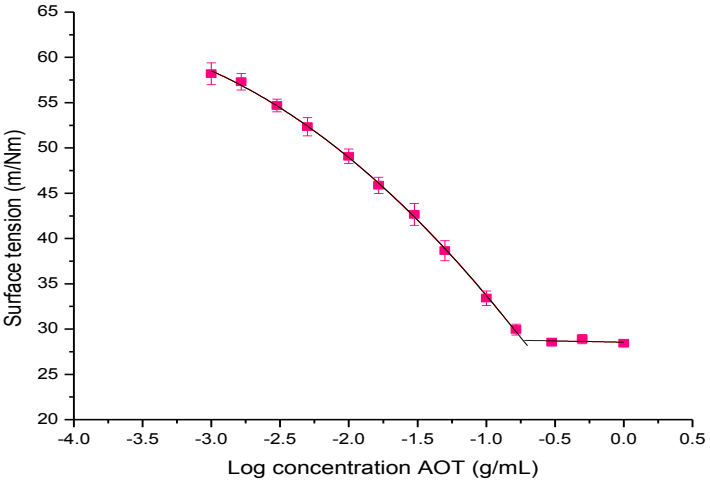

Figure 2.14: Variation in surface tension against log concentration for AOT (■) in water at 25 ± 0.1°C (n = 3 ± s.d.). Error from measurements on three separate solutions.

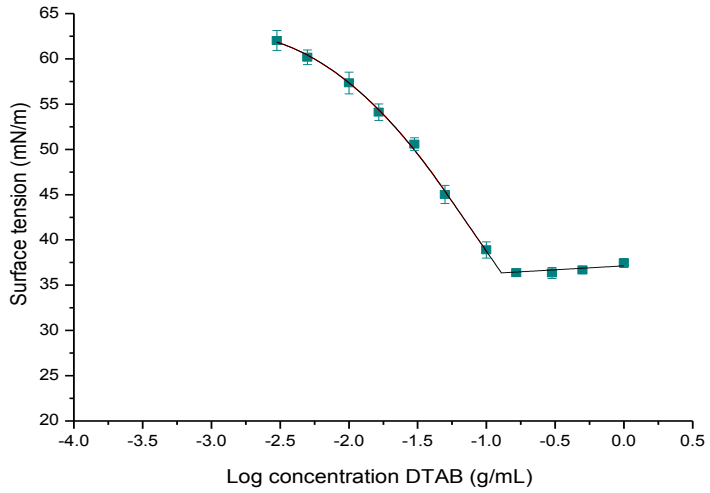

Figure 2.15: Variation in surface tension against log concentration for DTAB (■) in water at 25 ± 0.1°C (n = 3 ± s.d.). Error from measurements on three separate solutions.

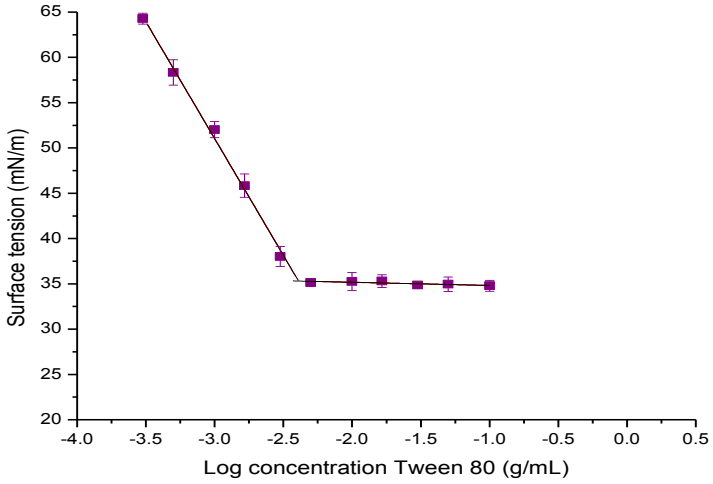

Figure 2.16: Variation in surface tension against log concentration of Tween 80 (■) in water at 25 ± 0.1°C (n = 3 ± s.d.). Error from measurements on three separate solutions.

Table 2.6: Surface parameters of SDS, AOT, DTAB and Tween 80 in water at 25 ± 0.1°C (n = 3 ± s.d.).

Surfactant	**cmc (g/mL)**	**Cmc (mM)**	**Surface tension at cmc (mN/m)**	**Surface excess (mol/m^2)**	**Area per molecule ($Å^2$)**
AOT	0.107 ± 0.02	2.418 ± 0.04	29 ± 0.3	$1.845 * 10^{-6} \pm 0.01$	89 ± 0.6
SDS	0.128 ± 0.03	4.425 ± 0.05	38.7 ± 0.2	$3.082 * 10^{-6} \pm 0.03$	53.9 ± 0.7
DTAB	0.128 ± 0.03	4.145 ± 0.04	36.4 ± 0.2	$3.489 * 10^{-6} \pm 0.04$	47.6 ± 0.5
Tween 80	0.004 ± 0.00	0.028 ± 0.00	34.9 ± 0.4	$4.512 * 10^{-6} \pm 0.03$	36.8 ± 0.8

Polymers

As outlined in section 1.7.2, some of the hydrophilic polymers used in the present study are surface active, consequently the surface tension of the aqueous polymer solutions of HPMC, HEC, HPC, PVP 30 and F127 were measured at a concentration of 1% w/w (Table 2.7). The results in Table 2.7 indicate that all polymers used as stabilisers in the present study were surface active. The cellulosics, HPMC, HPC, and HEC, all exhibited similar surface tension values of ~ 44-45 mN/m. PVP 30 was the least surface active polymer, with F127 being the most surface active, which is perhaps not surprising as F127 is a non-ionic, polymeric surfactant.

Table 2.7: Surface tension of 1% w/w polymer solutions in water at 25 ± 0.1°C (n = 3 ± s.d.).

Formulation	**Surface tension (mN/m)**
HPMC 8000	45.5 ± 0.3
HPMC 15000	45.6 ± 0.2
HPMC 86000	45.7 ± 0.4
HEC 33000	44.5 ± 0.5
HPC 34000	44.0 ± 0.4
PVP 30	56.3 ± 0.3
F127	36.8 ± 0.3

Polymer-surfactant mixtures

The surface tension of SDS and AOT in the presence of 0.1% w/w HPMC (nominal molecular weight either 8000, 15000 or 86000) was measured as a function of surfactant concentration in order to elucidate any polymer-surfactant interactions. In presence of polymer, two transition points, namely a cmc and cac, were observed, indicative of weak interactions between the non-ionic polymer and anionic surfactant (Figures 2.17 and 2.18). As anticipated, the cac occurred at a lower concentration than the cmc, this is because the complexation between the polymer and surfactant is more energetically favourable than the micellisation of the surfactant. The cac/cmc ratio is inversely proportional to the strength of the polymer-surfactant interactions (Yan et al, 2004).

From the experimentally determined values listed in Table 2.8, it can be deduced that the complexation between SDS and the HPMC polymer is stronger relative to the interaction of the polymer with AOT. Notable differences between the results shown in Figures 2.17 and 2.18, suggests differences in the mechanism of polymer

complexation between the two surfactants. Interestingly polymer molecular weight did not appear to have an effect on the mechanism of polymer complexation with the anionic surfactant, with the cac varying only slightly with polymer molecular weight- $F(2, 6) = 2.362$, $p = 0.175$.

The surface tension of neutral polymer-ionic surfactant systems at the air-water interface have recently been studied by other workers who also reported the presence of both cac and cmc transition points (Bell et al, 2007; Taylor et al, 2007; Touhami et al, 2001).

Table 2.8: Surface parameters of AOT and SDS in the presence of 0.1% w/w HPMC (molecular weight 8000, 15000 or 86000) at 25 ± 0.1°C (n = 3 ± s.d.).

Formulation	**cac (g/mL)**	**cac (mM)**	**cac/cmc ratio**	**Surface tension at cac (mN/m)**
AOT/HPMC 8000	0.093 ± 0.00	2.083 ± 0.03	0.862 ± 0.02	29.68 ± 0.4
SDS/HPMC 8000	0.096 ± 0.00	3.319 ± 0.05	0.75 ± 0.0	37.29 ± 0.3
AOT/HPMC 15000	0.097 ± 0.00	2.172 ± 0.04	0.898 ± 0.03	30.45 ± 0.2
SDS/HPMC 15000	0.101 ± 0.01	3.491 ± 0.04	0.789 ± 0.02	36.86 ± 0.3
AOT/HPMC 86000	0.090 ± 0.00	2.016 ± 0.05	0.834 ± 0.01	29.21 ± 0.5
SDS/HPMC 86000	0.105 ± 0.00	3.630 ± 0.02	0.82 ± 0.02	37.43 ± 0.5

cmc data shown in Table 2.6

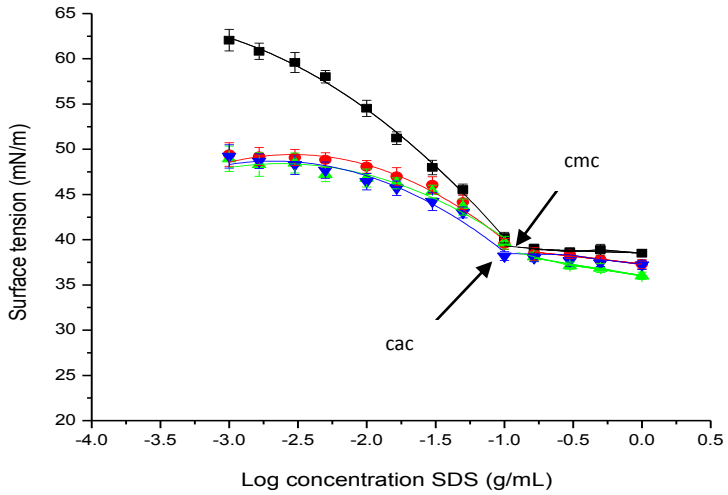

Figure 2.17: Variation in surface tension against log concentration of SDS in water (■) and in 0.1% HPMC 8000 (●), HPMC 15000 (▲), and HPMC 86000 (▼) at 25 ± 0.1°C (n = 3 ± s.d.). Error from measurements on three separate solutions.

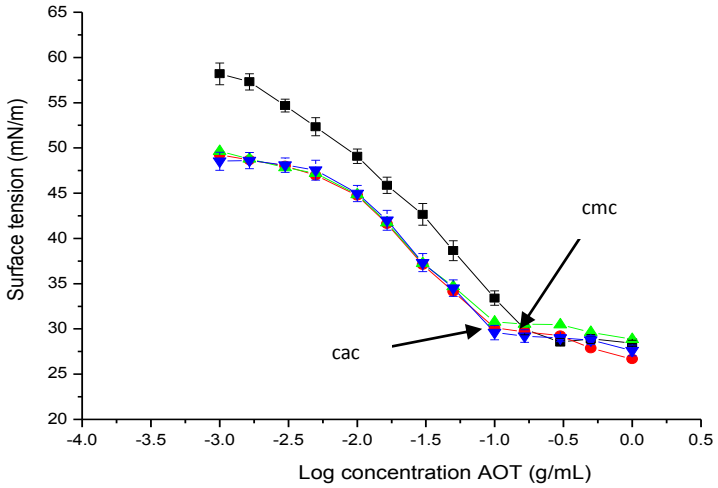

Figure 2.18: Variation in surface tension against log concentration of AOT in water (■) and in 0.1% HPMC 8000 (●), HPMC 15000 (▲), and HPMC 86000 (▼) at 25 ± 0.1°C (n = 3 ± s.d.). Error from measurements on three separate solutions.

2.3.3 Effect of anionic surfactant/polymer concentration on griseofulvin nanoparticle production

The stabiliser screen in section 2.3.1 revealed that griseofulvin nanoparticles could only be produced in presence of SDS, AOT or HPMCAS. It is apparent that anionic stabilisation is necessary for WBM production of griseofulvin nanoparticles. The cationic surfactant, DTAB, differs from SDS only in its head group. In this case, replacement of the anionic sulphate group with a cationic trimethylammonium group leads to the loss of stabilisation efficacy. Interestingly, none of the non-ionic polymers or surfactants provided effective stabilisation of griseofulvin nanoparticles.

The effect of varying concentration (0.1-10 %w/w) of AOT, SDS and HPMCAS on the production of griseofulvin nanoparticles by WBM is reported in Table 2.9. The WBM of griseofulvin using crude drug suspension was performed as outlined in sections 2.2.2-2.2.3 and resultant particle size determined by laser light scattering. Zeta potential measurement was performed simultaneously, on the same suspensions as used for PCS, as described in section 2.2.5. Any interference in zeta potential measurement from the excess surfactant/polymer was investigated by centrifuging the milled nanosuspensions, removal of the supernatant containing excess surfactant/polymer and resuspending the nanoparticles with an equivalent volume of

UPW prior to measurement. In no case was any marked difference observed between the zeta potential obtained for the nanosuspensions in the absence and presence of excess stabiliser. This is probably because, although the surfactant micelles were negatively charged (-78.3 mV and -105.7 mV for 0.5% w/w SDS and AOT solutions respectively), the copious dilution of nanosuspensions prior to zeta potential measurement negated any interference from any surfactant micelles or excess monomeric surfactant present.

Table 2.9: Effect of concentration of anionic surfactant/polymer on griseofulvin particle size after 6 h milling (n = 3 ± s.d.). Concentrations expressed in % w/w. Table continued on next page.

Stabiliser and concentration used (% w/w)	Weight ratio of drug: stabiliser	Particle size (nm) 6 h milling (PCS)	Zeta potential (mV) at pH 7
	SDS		
10.0% SDS	2.5:1	425.3 ± 9.8	- 42.2 ± 0.4
5.0% SDS	5:1	320.9 ± 7.5	- 38.0 ± 0.5
2.0% SDS	12.5:1	275.9 ± 4.8	- 31.8 ± 0.8
1.5% SDS	16.7:1	276.0 ± 4.3	- 30.9 ± 0.4
1.0% SDS	25:1	264.6 ± 3.4	- 28.3 ± 0.3
0.5% SDS	50:1	269.2 ± 4.3	- 27.6 ± 0.4
0.25% SDS	100:1	304.3 ± 4.2	- 25.1 ± 0.3
0.1% SDS	250:1	> 1000	ND
	AOT		
10.0% AOT	2.5:1	ND	ND
5.0% AOT	5:1	324.5 ± 8.2	- 48.3 ± 0.3
2.0% AOT	12.5:1	270.3 ± 4.2	- 46.1 ± 0.4
1.5% AOT	16.7:1	266.7 ± 5.7	- 45.7 ± 0.3
1.0% AOT	25:1	265.8 ± 6.1	- 44.4 ± 0.5
0.5% AOT	50:1	254.4 ± 3.3	- 37.6 ± 0.4
0.25% AOT	100:1	290.5 ± 2.6	- 34.8 ± 0.5
0.1% AOT	125:1	> 1000	ND
	HPMCAS-LF		
10.0% HPMCAS-LF	2.5:1	434.7 ± 8.8	- 43.8 ± 0.8
5.0% HPMCAS-LF	5:1	328.8 ± 6.5	- 42.4 ± 1.2
2.0% HPMCAS-LF	12.5:1	321.9 ± 4.9	- 38.8 ± 0.8
1.5% HPMCAS-LF	16.7:1	326.3 ± 3.0	- 37.1 ± 0.9
1.0% HPMCAS-LF	25:1	300.0 ± 3.0	- 35.8 ± 1.3
0.5%HPMCAS-LF	50:1	274.4 ± 3.0	- 31.1 ± 1.6
0.25%HPMCAS-LF	100:1	310.8 ± 3.0	- 32.2 ± 0.9
0.1 %HPMCAS-LF	125:1	>1000	ND

ND = not determined

Table 2.9: Effect of concentration of anionic surfactant/polymer on griseofulvin particle size after 6 h milling (n = 3 ± s.d.). Concentrations expressed in % w/w. Table continued from previous page.

Stabiliser and concentration used (% w/w)	Weight ratio of drug: stabiliser	Particle size (nm) 6 h milling (PCS)	Zeta potential (mV) at pH 7
HPMCAS-MF			
10.0% HPMCAS-MF	2.5:1	416.5 ± 9.7	- 44.9 ± 1.4
5.0% HPMCAS-MF	5:1	328.6 ± 5.8	- 41.6 ± 1.3
2.0% HPMCAS-MF	12.5:1	273.8 ± 3.2	- 38.2 ± 1.1
1.5% HPMCAS-MF	16.7:1	288.9 ± 4.1	- 36.4 ± 0.8
1.0% HPMCAS-MF	25:1	304.5 ± 3.0	- 35.2 ± 0.9
0.5% HPMCAS-MF	50:1	284.6 ± 3.0	- 32.8 ± 1.4
0.25% HPMCAS-MF	100:1	274.5 ± 3.0	- 32.7 ± 0.7
0.1 % HPMCAS-MF	125:1	430.4 ± 3.0	- 30.4 ± 0.8
HPMCAS-HF			
10.0% HPMCAS-HF	2.5:1	489.6 ± 9.8	- 42.6 ± 1.1
5.0% HPMCAS-HF	5:1	472.2 ± 10.1	- 40.1 ± 0.5
2.0% HPMCAS-HF	12.5:1	464.5 ± 8.3	- 37.7 ± 1.3
1.5% HPMCAS-HF	16.7:1	496.8 ± 9.2	- 35.8 ± 0.9
1.0 % HPMCAS-HF	25:1	415.4 ± 3.0	- 34.7 ± 1.5
0.5%HPMCAS-HF	50:1	413.0 ± 3.0	- 32.6 ± 1.1
0.25%HPMCAS-HF	100:1	484.3 ± 3.0	- 33.0 ± 0.8
0.1 %HPMCAS-HF	125:1	>1000	ND

ND = not determined

As can be seen from Table 2.9, the surfactants SDS and AOT displayed a similar trend in nanoparticle production with surfactant concentration. For example for both surfactants, there was a minimum starting surfactant concentration of 0.25% w/w below which nanoparticles could not be produced. This was due to insufficient amount of surfactant being present to coat the particle surfaces leading to particle aggregation during milling. Increasing surfactant starting concentration to a level within the range 0.5-2.0% w/w lead to the production of the smallest nanoparticles. A simultaneous increase in the zeta potential of the nanoparticles suggests an increase in the amount of surfactant adsorbing onto their surface. The highly negative zeta potential of the nanoparticles suggests that they should be highly stable on storage, assuming that the pH (or electrolyte concentration) of the system does not change.

Any further increase in surfactant concentration led to an increase in particle size indicating a decrease in milling efficiency, possibly due to higher specific energy

consumptions (Kwade 1999). The highest concentration of AOT studied was 5% w/w, above which a highly viscous initial stabiliser solution, unsuitable for milling, was formed. Bilgili et al (2004) studied the effect of varying the concentration of the anionic surfactant, sodium N-methyl N-oleyl taurate, on the production of pigment nanoparticles by WBM and obtained similar results in that intermediate surfactant concentrations produced the smallest nanoparticles.

As with SDS and AOT, when WBM griseofulvin in the presence of HPMCAS, there was a minimum starting concentration of HPMCAS, i.e. 0.25% w/w for HPMCAS-HF, LF and 0.1% w/w for HPMCAS-MF, below which nanoparticles could not be produced (Table 2.9). This was due to insufficient amounts of polymer being present on the nanoparticle surfaces leading to particle aggregation during milling. In addition, there were notable differences in the nanoparticle stabilisation profiles obtained with the three HPMCAS grades. HPMCAS-MF with the intermediate acetyl/succinoyl substitution was the most efficient at stabilising the griseofulvin nanoparticles. This grade produced the smallest nanoparticle sizes across the whole concentration range studied. In contrast, the polymers, HPMCAS-LF and HF were not effective at producing nanoparticles across the whole concentration range with HPMCAS-HF producing the largest griseofulvin nanoparticles. The zeta potential of the resultant nanoparticles increased with an increase in starting HPMCAS concentration suggesting that more polymer was adsorbed onto the nanoparticle surfaces. Interestingly there was no effect of polymer grade i.e HPMCAS LF, MF or HF on the zeta potential of nanoparticles produced at any given polymer concentration. The milled nanoparticles generally exhibited a relatively narrow polydispersity (PI of less than 0.2), except when the particle size was above 400 nm.

The weight ratio of drug to stabiliser is given in Table 2.9 due to reports of optimal drug:stabiliser weight ratios of 10:1 or lower quoted by Mersiko-Liversidge et al (2008), although in the present study nanoparticles are produced at higher drug:stabiliser weight ratios of up to 100:1. In fact the drug:stabiliser weight ratio is not felt to be a useful parameter in either predicting or understanding nanoparticle production.

Figures 2.19-2.21 show the kinetics of the milling process over time. The initial particle size of the drug in the crude initial suspension was in the micron size range. It is clear that the majority of the particle size reduction occurred within the first 2 hours of milling when the particles where reduced to the nanometre size range,

thereafter the reduction in size tapered off. No marked difference in the size reduction profile was seen with the different surfactant concentrations tested (Figure 2.19-2.20). However, with the HPMCAS-LF formulations, the size reduction was notably slower when the higher polymer concentrations, which were more viscous, were used (Figure 2.21). The effects on suspension viscosity on the milling process will be discussed in detail in section 2.3.4.

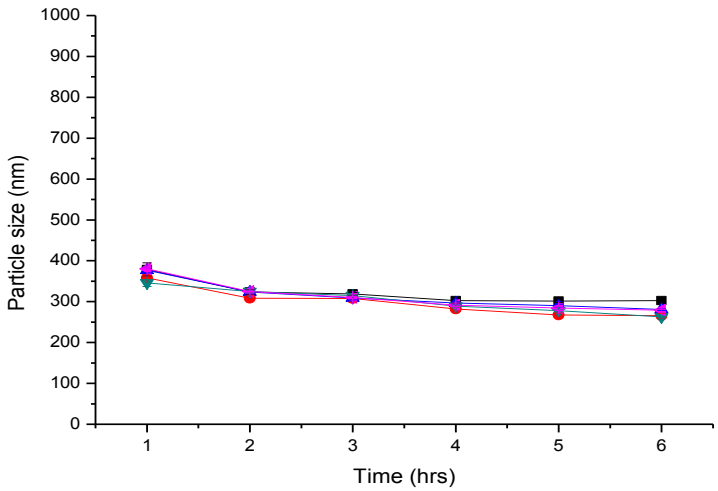

Figure 2.19: Particle size reduction of griseofulvin milled for 6 h in the presence of 0.25% w/w SDS (■), 0.5% w/w SDS (●), 1.0% w/w SDS (▼), 1.5% w/w SDS (▲), and 2.0% w/w SDS (◀) (n = 3 ± s.d.). Error from light scattering measurements on one nanosuspension.

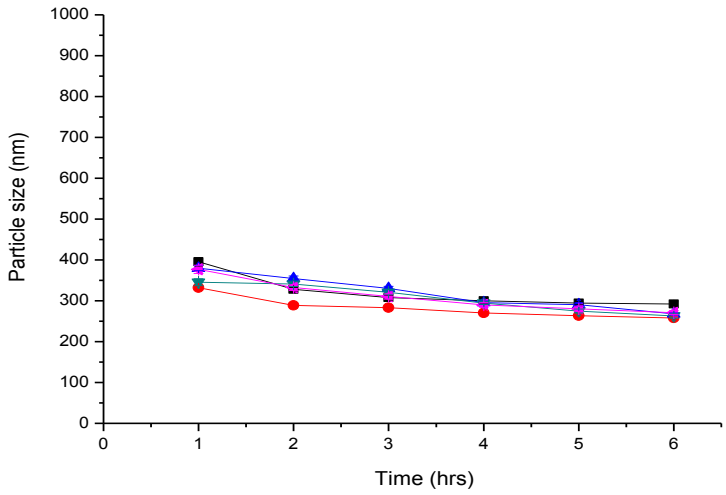

Figure 2.20: Particle size reduction of griseofulvin milled for 6 h in the presence of 0.25% w/w AOT (■), 0.5% w/w AOT (●), 1.0% w/w AOT (▼), 1.5% w/w AOT (▲), and 2.0% w/w AOT (◀) (n = 3 ± s.d.). Error from light scattering measurements on one nanosuspension.

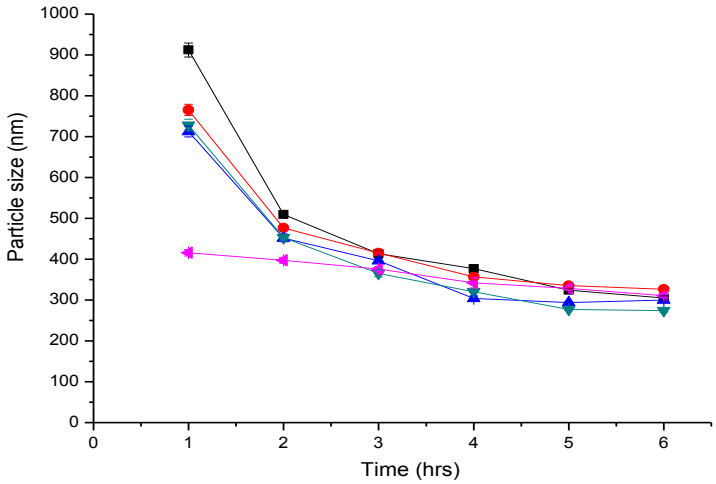

Figure 2.21: Particle size reduction of griseofulvin milled for 6 h in the presence of 0.25% w/w HPMCAS-LF (◀), 0.5% w/w HPMCAS-LF (▼), 1.0% w/w HPMCAS-LF (▲), 1.5% w/w HPMCAS-LF (●), and 2.0% w/w HPMCAS-LF (■)(n = 3 ± s.d.). Error from light scattering measurements on one nanosuspension.

Polymer-surfactant systems

The use of ionic surfactants in oral drug formulations presents challenges such as incompatibilities with other ionic molecules, sensitivity to pH, salt or temperature changes, GIT irritation and toxicity (Attwood et al, 1983). Despite a knowledge of the synergy which can be achieved when using polymers and surfactants, this synergism has not been widely utilised in pharmaceutical nanotechnology. Only a few literature reports exist employing polymer-surfactant combinations for the stabilisation of drug nanoparticles including albendazole, buparvaquone, cilostazol and other undisclosed drug moieties (van Eerdenbrugh et al, 2008).

In the present study, electrosteric stabilisation, tailored to take advantage of pH stability associated with steric stabilisers, has been investigated. Polymer-surfactant mixtures comprising of the non-ionic polymer, HPMC, and an anionic surfactant, either SDS or AOT, were employed. In this part of the study, HPMC of different molecular weights, namely 8000, 15000 and 86000, were studied. As reported previously screening experiments revealed that the use of HPMC as sole stabilising agent was unable to stabilise griseofulvin nanoparticles.

Polymer-surfactant stabilisation

2.3.4 Effect of non-ionic polymer molecular weight and concentration on griseofulvin nanoparticle production in presence of anionic surfactant

Keeping the surfactant concentration constant at 0.5% w/w SDS, the effect of varying polymer molecular weights and concentration on the size of the griseofulvin particles obtained by WBM was determined (Table 2.10). Note that the polymer molecular weights quoted are those given by the manufacturer.

Table 2.10: Effect of varying HPMC concentration in presence of constant surfactant concentration (0.5% w/w SDS) on griseofulvin particle size after 6 h milling (n = 3 ± s.d.). Concentrations expressed in % w/w.

Formulation and concentration used (% w/w)	Weight ratio of drug: stabilisers	Particle size (nm) HPMC 8000	Zeta potential (mV) at pH 7	Particle size (nm) HPMC 15000	Zeta potential (mV) at pH 7	Particle size (nm) HPMC 86000	Zeta potential (mV) at pH 7
0.5% SDS + 10.0% HPMC	2:1	> 1000	ND	NF	ND	NF	ND
0.5% SDS + 5.0% HPMC	4:1	460.7 ± 9.6	- 26.9 ± 0.5	NF	ND	NF	ND
0.5% SDS + 2.5% HPMC	8:1	306.5 ± 2.4	- 27.0 ± 0.6	NF	ND	NF	ND
0.5% SDS + 1.88% HPMC	11:1	250.4 ± 2.3	- 26.7 ± 0.7	> 1000	ND	NF	ND
0.5% SDS + 1.5% HPMC	13:1	245.7 ± 2.1	- 27.3 ± 0.9	471.1± 8.8	- 22.1 ± 0.6	NF	ND
0.5% SDS + 1.0% HPMC	17:1	239.0 ± 1.9	- 27.4 ± 0.4	326.0 ± 4.3	- 22.1 ± 1.1	NF	ND
0.5% SDS + 0.5% HPMC	25:1	232.4 ± 2.9	- 27.6 ± 0.5	247.3 ± 3.4	- 25.9 ± 0.7	NF	ND
0.5% SDS + 0.1% HPMC	42:1	258.4 ± 3.0	- 27.7 ± 0.7	262.2 ± 1.3	- 27.5 ± 0.5	> 1000	ND
0.5% SDS	50:1	265.8 ± 4.2	- 27.6 ± 0.4	265.8 ± 4.2	- 27.6 ± 0.4	265.8 ± 4.2	- 27.6 ± 0.4

ND = not determined, NF = not formed – nanoparticles not produced

As seen with the surfactant only formulations in section 2.3.3, nanoparticles could be produced outside the optimal drug:stabiliser weight ratio of 10:1 quoted by Merisko-Liversidge et al (2008). Indeed nanoparticles could be formulated at drug:stabiliser weight ratios of up to 42:1, depending on the molecular weight of the non-ionic polymer used. This observation illustrates the uselessness of using a drug:stabliliser weight ratio to predict nanoparticle formation.

For both HPMC 8000 and 15000, the smallest particle size was produced when 0.5% w/w of both surfactant and polymer was used. Thereafter, an increase in polymer concentration led to a gradual increase in particle size and a corresponding slower rate of nanoparticle production. In addition, regardless of the polymer molecular weight, there was a maximum polymer concentration above which nanoparticles could not be produced. This maximum concentration reduced with increasing polymer molecular weight, such that the range over which nanoparticles could be produced narrowed with increasing polymer molecular weight. As seen in Table 2.10, the maximum effective concentration of HPMC 8000 was 5% w/w, while for HPMC 15000 the maximum was 1.5% w/w – in both cases the minimum HPMC concentration was 0.1% w/w. It is of note that nanoparticles were not produced in presence of HPMC 86000, even at polymer concentrations as low as 0.1% w/w. Similar polymer molecular weight effects were recorded by Sepassi (2003) and Goodwin (2006) who investigated stabilisation of nabumetone nanoparticles, using HPMC and HEC, respectively.

These observations can be partly attributed to the increasing viscosity of the initial crude suspensions with increasing polymer molecular and/or concentration. The increase in viscosity of crude suspension leads to a cushioning of drug particles from impact by YTZ beads thereby decreasing milling efficiency (Kwade 1999; Yokohama et al, 1996). Secondly, in order to stabilise the drug nanoparticles, the stabiliser must undergo migration to the freshly exposed drug surface. Higher molecular weight polymers tend to undergo slower diffusion to the freshly cleaved drug surfaces during milling than their lower molecular weight equivalents.

Figures 2.22 and 2.23 show the change in particle size with WBM in the presence of 0.5% w/w SDS and varying concentrations of HPMC polymer of molecular weights of 8000 and 15000 respectively. As can be seen a dramatic reduction of particle size was observed within the first 2 hours of milling, with a reduction in particle size from microns to nanometers. Furthermore, regardless of molecular weight, an

increase of polymer concentration in the initial crude suspension resulted in a slower production of nanoparticles, attributable to an increased suspension viscosity.

There was no marked difference in the zeta potential of the nanoparticles produced with 0.5% w/w SDS either in the absence or the presence of either HPMC 8000 or low HPMC 15000 concentrations (i.e. < 1.0% w/w). However, the nanoparticles prepared in the presence of high concentrations (> 1.0% w/w) of HPMC 15000 and 0.5% w/w SDS exhibited a zeta potential that was 5 mV lower than that of nanoparticles prepared in absence of polymer (Table 2.10). This zeta potential reduction could be due to a thicker co-adsorbing HPMC 15000 layer partially masking the charge due to SDS. The milled nanoparticles generally exhibited a relatively narrow polydispersity (PI of less than 0.2), except when the particle size was above 400 nm.

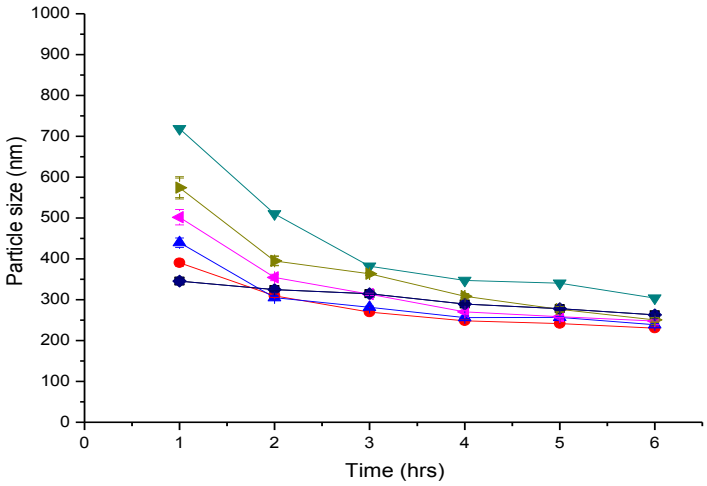

Figure 2.22: Effect of varying HPMC 8000 concentration in presence of 0.5% w/w SDS on size reduction profile of griseofulvin milled for 6 h: 0.5% w/w SDS (■), 0.5% w/w SDS + 0.1% w/w HPMC 8000 (♦), 0.5% w/w SDS + 0.5% w/w HPMC 8000 (●), 0.5% w/w SDS + 1.0% w/w HPMC 8000 (▲), 0.5% w/w SDS + 1.5% w/w HPMC 8000 (◄), 0.5% w/w SDS + 1.88% w/w HPMC 8000 (►), 0.5% w/w SDS + 2.5% w/w HPMC 8000 (▼)(n = 3 ± s.d.). Error from light scattering measurements on one nanosuspension.

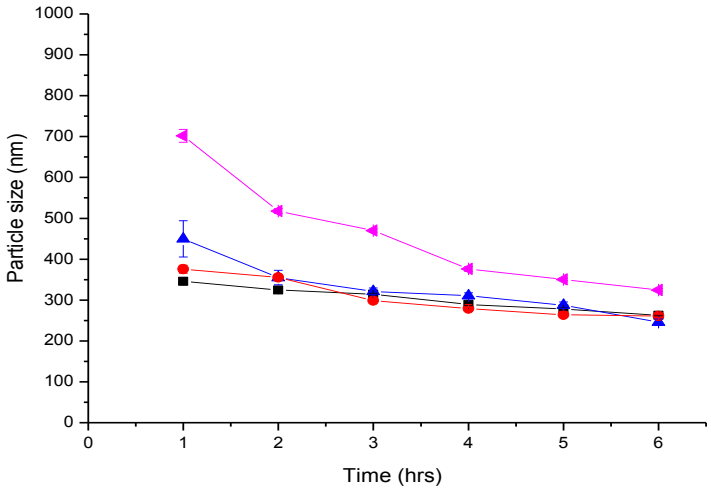

Figure 2.23: Effect of varying HPMC 15000 concentration in presence of 0.5% w/w SDS on size reduction profile of griseofulvin milled for 6 h: 0.5% w/w SDS (■), 0.5% w/w SDS + 0.1% w/w HPMC 15000 (●), 0.5% w/w SDS + 0.5% w/w HPMC 15000 (▲), 0.5% w/w SDS + 1.0% w/w HPMC 15000 (◀)(n = 3 ± s.d.). Error from light scattering measurements on one nanosuspension.

2.3.5 Effect of anionic surfactant concentration on griseofulvin nanoparticle production in presence of non-ionic polymer

Using the previously determined highest optimal concentration of 1.88% w/w HPMC 8000 (Table 2.10), the effect of varying surfactant concentration at constant polymer concentration was studied (Table 2.11). As can be seen, the inclusion of HPMC 8000 in the milling suspension allowed a reduction in the amount of surfactant required for effective stabilisation. Whereas in presence of either SDS or AOT alone, nanoparticles could only be produced above a surfactant concentration of 0.25% w/w (section 2.3.3), in the presence of HPMC, lower surfactant concentrations were effective. There was a reduction in the minimum SDS concentration required to 0.05% w/w and that of AOT to 0.1% w/w. This potentiation of stabilisation efficiency in presence of HPMC is thought to be the result of the formation of polymer surfactant complexes at the nanoparticle surfaces. Surface tension measurements (section 2.3.2) have confirmed the interaction between the anionic surfactants and HPMC of varying molecular weight in bulk solution. On the basis of these results, it can be postulated that polymer-surfactant interactions also occur at the solid-liquid interface. Interestingly, in the presence of HPMC, the smallest nanoparticles were produced using a surfactant concentration of

0.5% w/w, thereafter an increase in nanoparticle size occurred with an increase or decrease in surfactant concentration. This result possibly suggests that polymer-surfactant surface interactions were optimal at this surfactant concentration. The milled nanoparticles generally exhibited a relatively narrow polydispersity (PI of less than 0.2), except when the particle size was above 400 nm.

Table 2.11: Effect of anionic surfactant concentration on griseofulvin particle size after 6 h milling in the presence of various concentrations of surfactant + 1.88% w/w HPMC 8000 (n = 3 ± s.d.). Concentrations expressed in % w/w.

Polymer/ Surfactant combination and concentration used (% w/w)	Weight ratio of drug: stabiliser	Particle Size (nm) 6 h milling	Zeta potential (mV) at pH 7
SDS/HPMC			
1.88% HPMC 8000 + 10.0%SDS	2.1:1	433.4 ± 8.3	-32 ± 1.1
1.88% HPMC 8000 + 5.0%SDS	3.6:1	298.7 ± 3.6	-27.7 ± 0.8
1.88% HPMC 8000 + 2.0%SDS	6.4:1	297.4 ± 3.1	- 28.7 ± 0.5
1.88% HPMC 8000 + 1.5%SDS	7.4:1	296.7 ± 3.3	- 28.7 ± 0.3
1.88% HPMC 8000 + 1.0%SDS	8.7:1	282.0 ± 2.7	- 28.3 ± 0.9
1.88% HPMC 8000 + 0.5%SDS	11:1	250.4 ± 2.3	- 26.7 ± 0.6
1.88% HPMC 8000 + 0.25%SDS	12:1	306.1 ± 4.7	- 25.5 ± 0.5
1.88% HPMC 8000 + 0.1%SDS	13:1	321.4 ± 4.3	- 24.6 ± 0.7
1.88% HPMC 8000 + 0.05%SDS	13:1	330.5 ± 3.6	- 23 ± 0.9
1.88% HPMC 8000 + 0.025%SDS	13:1	> 1000	ND
AOT/HPMC			
1.88% HPMC 8000 + 10.0% AOT	2.1:1	ND	ND
1.88% HPMC 8000 + 5.0% AOT	3.6:1	389.4 ± 7.8	-37.8 ± 1.4
1.88% HPMC 8000 + 2.0% AOT	6.4:1	350.3 ± 5.3	- 35.5 ± 0.5
1.88% HPMC 8000 + 1.5% AOT	7.4:1	332.9 ± 6.1	- 35.4 ± 0.7
1.88% HPMC 8000 + 1.0% AOT	8.7:1	308.6 ± 5.6	- 29.9 ± 1.3
1.88% HPMC 8000 + 0.5% AOT	11:1	274.1 ± 4.8	- 27.1 ± 0.3
1.88% HPMC 8000 + 0.25% AOT	12:1	301.9 ± 3.3	- 26.4 ± 0.8
1.88% HPMC 8000 + 0.1% AOT	13:1	335.8 ± 3.2	- 25.9 ± 0.4
1.88% HPMC 8000 + 0.05% AOT	13:1	>1000	ND

ND = not determined

The zeta potentials of nanoparticles prepared in presence of 1.88% w/w HPMC 8000 were lower than those prepared in absence of polymer throughout the AOT concentrations studied and at SDS concentrations above 1.0% w/w SDS (Table 2.9, 2.11). The reduction of zeta potential suggests that the non-ionic polymer is co-adsorbing onto the drug surfaces. No marked change in zeta potential was seen with nanoparticles prepared in absence or presence of 1.88% w/w HPMC 8000 at SDS

concentrations of 1.0% w/w or below, possibly due to the low amount of co-adsorbing non-ionic polymer at the drug surface.

Figures 2.24-2.25 show the change in particle size with milling. Again a dramatic reduction of particle size was observed within the first 2 hours of milling, when particle size decreased from microns to nanometers. However the reduction in particle size was slowest in formulations prepared using lower surfactant concentrations. This result suggests that the presence of anionic surfactant promotes a rapid size reduction, most probably because of its rapid diffusion to the freshly exposed surface of the nanoparticles.

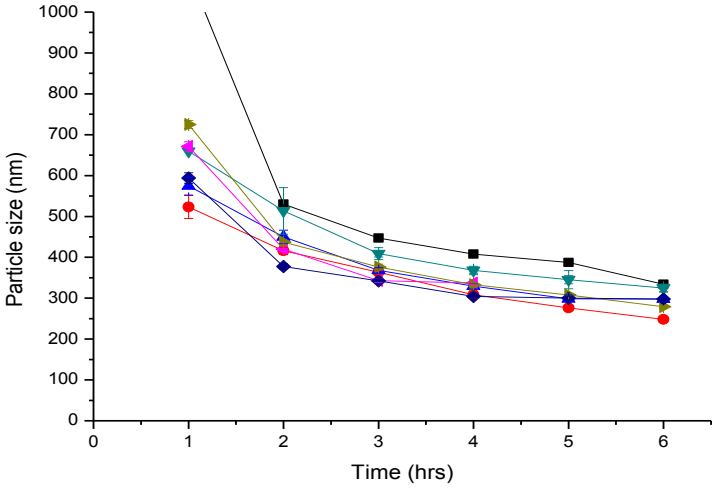

Figure 2.24: Effect of varying SDS concentration in presence of 1.88% w/w HPMC 8000 on size reduction profile of griseofulvin milled for 6 h: 0.05% w/w SDS + 1.88% w/w HPMC 8000 (■), 0.1% w/w SDS + 1.88% w/w HPMC 8000 (●), 0.25% w/w SDS + 1.88% w/w HPMC 8000 (▲), 0.5% w/w SDS + 1.88% w/w HPMC 8000 (▼), 1.0% w/w SDS + 1.88% w/w HPMC 8000 (◄), 1.5% w/w SDS + 1.88% w/w HPMC 8000 (►), 2.0% w/w SDS + 1.88% w/w HPMC 8000 (♦)(n = 3 ± s.d.). Error from light scattering measurements on one nanosuspension.

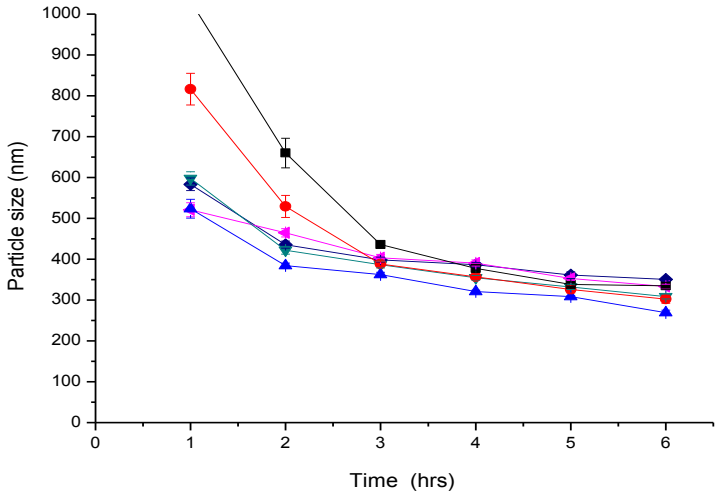

Figure 2.25: Effect of varying AOT concentration in presence of 1.88% w/w HPMC 8000 on size reduction profile of griseofulvin milled for 6 h: 0.1% w/w AOT + 1.88% w/w HPMC 8000 (■), 0.25% w/w AOT + 1.88% w/w HPMC 8000 (●), 0.5% w/w AOT + 1.88% w/w HPMC 8000 (▲), 1.0% w/w AOT + 1.88% w/w HPMC 8000 (▼), 1.5% w/w AOT + 1.88% w/w HPMC 8000 (◄), 2.0% w/w AOT + 1.88% w/w HPMC 8000 (♦) (n = 3 ± s.d.). Error from light scattering measurements on one nanosuspension.

2.3.6 Morphology of nanoparticles

Scanning electron microscopy (SEM) was used to assess the morphology of the nanoparticles. The geometrical shape of milled nanoparticles is known to be dependent on various factors including drug/stabiliser interactions, the fracture plane of crystal and the morphology of the starting drug material (Merisko-Liversidge et al, 2003).

SEM images of griseofulvin before milling and of resultant nanosuspensions after milling for 6 hours in presence of the various stabilisers were taken. Figure 2.26 (a-f) shows the images obtained. These images were very crowded with overlapping of some of the nanoparticles making it difficult to carry out accurate size and shape analysis. In retrospect, the nanoparticle samples should have been diluted prior to the examination by SEM. In addition, the nanoparticles appeared to 'melt', an observation attributable to decrease of the drug melting point under experimental vacuum conditions. As can be seen the melting was dependent on particle size; with the unmilled micron sized griseofulvin particles showing no evidence of melting, suggesting that there is a size dependent effect of the vacuum on melting. Griseofulvin has a melting point of 218-222°C under ambient conditions. As a

consequence of this 'melting', gold coating of nanoparticles could have been used to reduce thermal damage and preserve sample integrity.

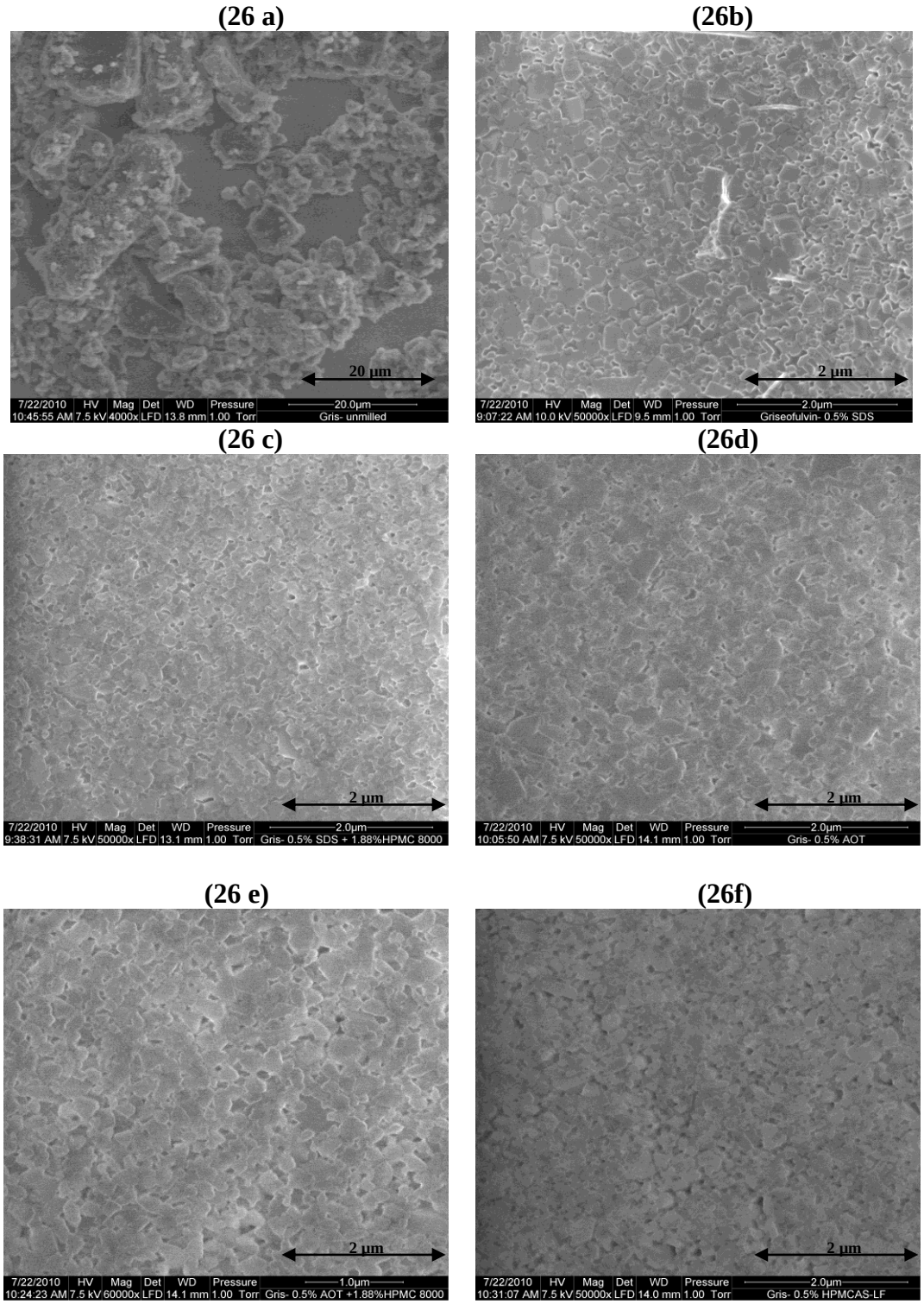

Figures 2.26 (a-f): Scanning electron micrographs of griseofulvin before milling (a), and after milling for 6 hours in presence of 0.5% w/w SDS (b), 0.5% w/w SDS + 1.88% w/w HPMC 8000 (c), 0.5% w/w AOT (d), 0.5% w/w AOT + 1.88% w/w HPMC 8000 (e), and 0.5% w/w HPMCAS-LF (f).

Despite these problems the SEM images of unmilled griseofulvin revealed a range of micron sized, irregular shaped particles (Figure 2.26 a). The unmilled particles were quite polydisperse with sizes ranging from ~ 5 micron to greater than 20 microns. The resultant milled nanoparticles (Figures 2.26 b-f) were also irregular in shape and exhibited a particle size in good agreement with that obtained by PCS, namely 250-300 nm. There were no differences in the resultant nanoparticle shape attributable to the use of different stabilisers. In the literature, the effect of stabiliser on the resultant shape of the nanoparticles seems to be drug specific. For example, Sepassi et al (2007) observed differences in nanoparticle shape when using different stabilisers to produce nanoparticles of halofantrine using WBM. While Liu et al (2011) observed changes in the resultant nanoparticle shape with stabiliser when WBM itraconazole but not indomethacin.

With regard to polydispersity, the nanoparticles produced in the presence of AOT appeared to be most polydisperse when examined by SEM. Although interestingly PCS measurements of the suspensions used for the SEM study indicated that all nanoparticle suspensions (including those stabilised by AOT) exhibited a relatively narrow polydispersity (PI of less than 0.2). The observed non-sphericity and polydisperse nature of the milled nanoparticles may be expected to introduce an error in the calculation of surface area required for adsorption isotherm determination. However, when Sepassi et al (2007) determined HPMC and PVP adsorption isotherms onto milled drug nanoparticles assuming the presence of spherical, cuboidal or rodlike particles, they deduced that shape differences did not impart much error to the adsorption calculations.

2.3.7 X-ray diffraction

X-ray diffraction (XRD) was used to determine whether WBM induced disorder into the griseofulvin nanoparticles. High energy milling can cause amorphous conversion or crystal defects in the lattice of crystalline materials (Chamarthy et al, 2008). Figure 2.27 (a-h) shows XRD patterns of griseofulvin obtained before milling and after milling in presence of the various stabilisers used to produce griseofulvin nanoparticles. The XRD pattern obtained before milling was that of a highly crystalline substance as evidenced by the presence of distinct peaks. This diffraction pattern was in good agreement with the griseofulvin XRD pattern obtained from the Cambridge structural database (Allen 2002) confirming the identity and purity of the

compound. Similar crystalline patterns in terms of nature and position of the peaks were observed before and after milling of griseofulvin confirming that crystallinity was largely, if not totally, maintained during milling. Furthermore, no peak broadening or halos were observed indicating that no significant long-range crystalline disorder or amorphous transformation had occurred. A slight decrease in the intensity of peaks 1 and 3 was, however, observed in all of the milled samples, regardless of the stabiliser used. As a consequence of this, after milling the intensity of the first three peaks was comparable, with the relative intensity of the second peak having appeared to increase compared to the situation prior to milling. These changes may indicate the formation of crystal defects. Furthermore, a reduction in the intensity of peak 4 was seen in samples stabilised in the presence of polymer, either HPMC with AOT or SDS and HPMCAS. Again this could possibly indicate the formation of different crystal defects in griseofulvin when milled in the presence of polymer. Chamarthy et al (2008) and Feng et al (2008) investigated the crystallinity of griseofulvin after cryrogenic milling and did not observe any features attributable to an amorphous transition. They did, however observe changes in the pattern of the XRD obtained for griseofulvin, which they deduced to be due to crystal defects.

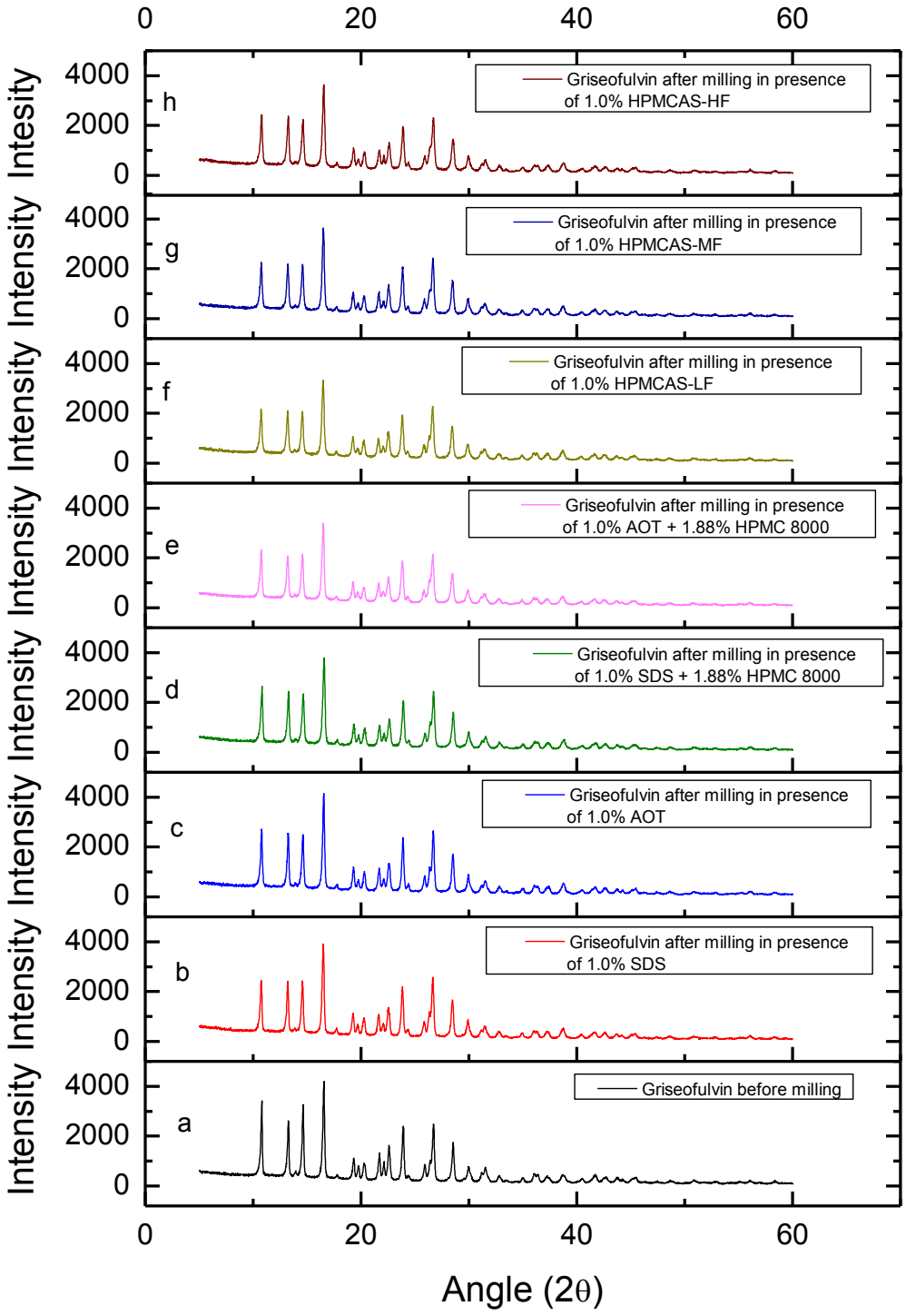

Figure 2.27 (a-h): XRD of griseofulvin samples before milling (a), after 6 h milling in presence of 1.0% w/w SDS (b), 1.0% w/w AOT (c), 1.0% w/w SDS + 1.88% w/w HPMC 8000 (d), 1.0% w/w AOT + 1.88% w/w HPMC 8000 (e), 1.0% w/w HPMCAS-LF (f), 1.0% w/w HPMCAS-MF (g) and 1.0% w/w HPMCAS-HF (h).

2.3.8 Time stability studies

The size of griseofulvin nanosuspensions stored in their original milled state, i.e. in presence of excess polymer/surfactant, at room temperature was monitored over time. As can be seen in Figures 2.28 to 2.33 Ostwald ripening was observed in all formulations, irrespective of the stabilising agent used in their preparation.

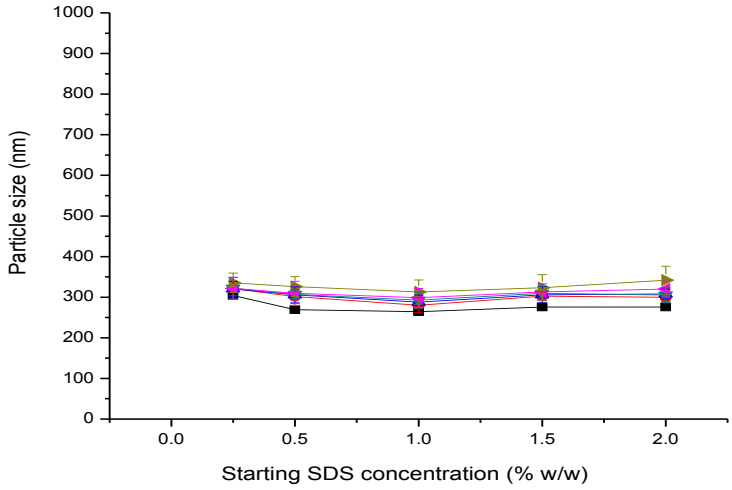

Figure 2.28: Particle size of griseofulvin nanoparticles prepared by 6 h milling in presence of varying SDS concentrations at production (■), 1 month (●), 3 months (▲), 6 months (▼), 9 months (◄) and 12 months (►) (n = 3 ± s.d.). Error from particle sizes obtained with three separate nanosuspensions.

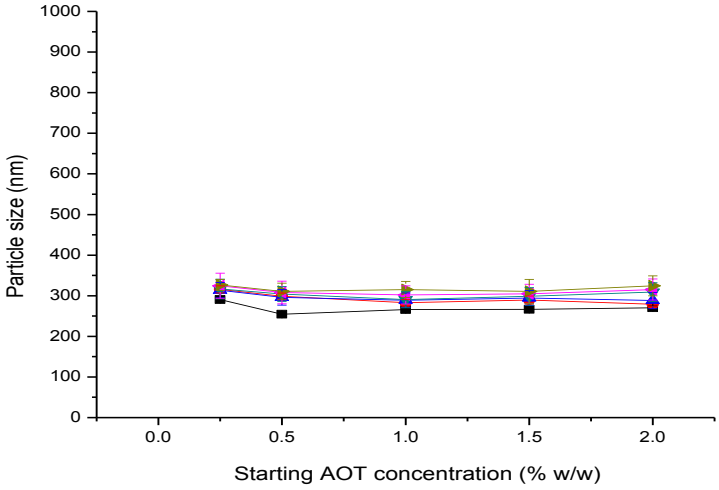

Figure 2.29: Particle size of griseofulvin nanoparticles prepared by 6 h milling in presence of varying AOT concentrations at production (■), 1 month (●), 3 months (▲), 6 months (▼), 9 months (◄) and 12 months (►) (n = 3 ± s.d.). Error from particle sizes obtained with three separate nanosuspensions.

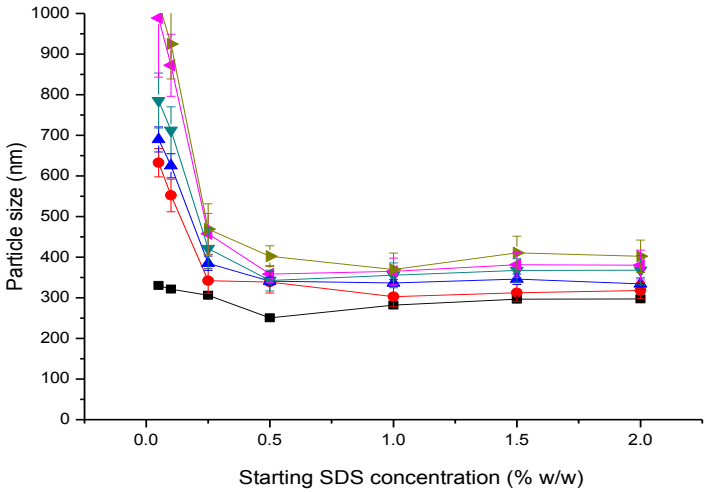

Figure 2.30: Particle size of griseofulvin nanoparticles prepared by 6 h milling in presence of 1.88% w/w HPMC 8000 and varying SDS concentrations at production (■), 1 month (●), 3 months (▲), 6 months (▼), 9 months (◀) and 12 months (▶) (n = 3 ± s.d.). Error from particle sizes obtained with three separate nanosuspensions.

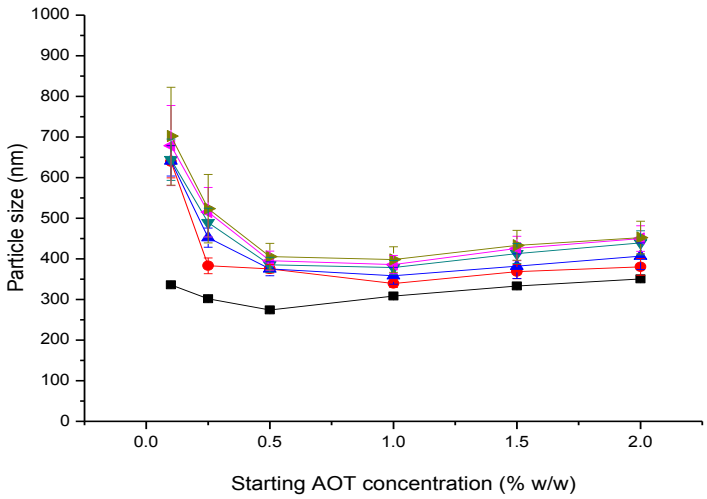

Figure 2.31: Particle size of griseofulvin nanoparticles prepared by 6 h milling in presence of 1.88% w/w HPMC 8000 and varying AOT concentrations at production (■), 1 month (●), 3 months (▲), 6 months (▼), 9 months (◀) and 12 months (▶) (n = 3 ± s.d.). Error from particle sizes obtained with three separate nanosuspensions.

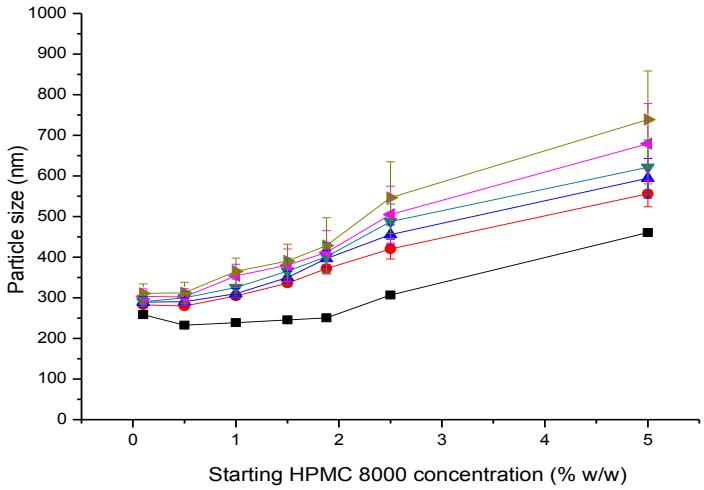

Figure 2.32: Particle size of griseofulvin nanoparticles prepared by 6 h milling in presence of 0.5% w/w SDS and varying HPMC 8000 concentrations at production (■), 1 month (●), 3 months (▲), 6 months (▼), 9 months (◄) and 12 months (►) (n = 3 ± s.d.). Error from particle sizes obtained with three separate nanosuspensions.

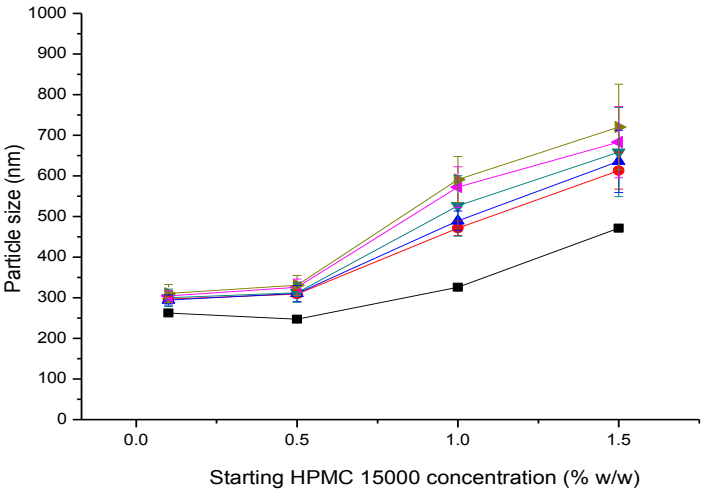

Figure 2.33: Particle size of griseofulvin nanoparticles prepared by 6 h milling in presence of 0.5% w/w SDS and varying HPMC 15000 concentrations at production (■), 1 month (●), 3 months (▲), 6 months (▼), 9 months (◄) and 12 months (►) (n = 3 ± s.d.). Error from particle sizes obtained with three separate nanosuspensions.

Figures 2.28-2.29 show the change in particle size of nanoparticles prepared in the presence of SDS and AOT, respectively. In both cases, the surfactant stabilised nanoparticles displayed only slight increases in size over the 12 months. The surfactant stabilised particles were relatively stable as can be predicted by their high zeta potentials of between -25.1 to -42.2 mV (SDS stabilised nanoparticles) and between -34.8 to -48.3 mV (AOT stabilised nanoparticles) on production (Table 2.9). Electrostatically stabilised particles of nominal zeta potential of 30 mV are normally

regarded as physically stable, whereas for electrosterically stabilised particles a value of 20 mV is usually considered adequate for stabilisation (Jacobs et al, 2002).

As can be seen from Figures 2.30-2.33, nanoparticle growth was much higher in the systems stabilised by a combination of HPMC polymer and surfactant. This observation could be attributed to the higher griseofulvin solubilising capacity of HPMC. Indeed it is clear that nanoparticle growth was greatest in the formulations prepared using the higher concentrations of HPMC, supporting this assumption. In addition, the presence of non-ionic polymer on the surface of the drug would be expected to reduce the amount of anionic surfactant adsorbed and thereby lower the particle zeta potential and decrease charge stability, although the presence of a steric stabilisation due to the hydrophilic polymer chains may, at least in part, be expected to counteract this situation.

When a constant amount of HPMC 8000 was used to prepare the nanoparticles (Figures 2.30-2.31), nanoparticle size growth was highest in formulations prepared using the lowest surfactant concentrations (i.e. < 0.5% w/w). When a constant amount of surfactant was used, nanoparticle size growth was highest in those formulations containing either the higher molecular weight HPMC, HPMC 15000 and/or the higher HPMC concentrations (Figures 2.32-2.33), most probably due to the higher solubilising capacity of the HPMC polymer. Notably nanoparticles at both extremes (i.e. lowest surfactant concentration or highest polymer molecular weight/concentration) contained the largest and most polydisperse particles, making Ostwald ripening more probable. The zeta potentials of the polymer/surfactant formulations at production were all above -20 mV and thus the value of zeta potential alone did not give a clear prediction to the stability of the polymer/surfactant stabilised nanosupensions (Tables 2.10-2.11).

Nanoparticles prepared using HPMCAS were the least stable of all nanoparticles with the majority of the systems solidifying within 1-3 months of storage. These formulations were very viscous on preparation, a fact most likely contributing to the aggregation due to low interparticle distances. Zeta potentials of the HPMCAS nanoparticles at production were above -30 mV (Table 2.9) supporting the observation seen with polymer/surfactant stabilised nanoparticles that zeta potential alone was not a good indicator of nanoparticle stability.

Drug aqueous solubility is a critical factor in determining the relative stability of the drug nanoparticles. WBM nanoparticles of nabumetone stabilized by HPMC or HPC

and halofantrine nanoparticles stabilised by HPMC or PVP 30 were found to be stable for one year under similar storage conditions (Sepassi 2003; Goodwin 2006). Both nabumetone (4.7 µg/mL) and halofantrine (< 1.0 µg/mL) have a much lower aqueous solubility at 25 ± 0.1ºC in comparison to griseofulvin (64 µg/mL) and as a consequence Ostwald ripening was considered less likely.

The solubilising effect of the disperse phase is also an important factor affecting stability. To investigate the effect of an excess amount of polymer/surfactant on stability a selection of griseofulvin nanosuspensions were centrifuged, the excess polymer/surfactant removed and the nanoparticles re-suspended in water before storage at room temperature. The nanosuspensions tested were those prepared in the presence of 0.5% w/w SDS, 0.5% w/w AOT, 0.5% w/w SDS + 1.88% w/w HPMC 8000, 0.5% w/w AOT + 1.88% w/w HPMC 8000 and 0.5% w/w HPMCAS-MF. As can be seen in Figure 2.34, any increase in nanoparticle size with time was tended to be slightly lower (although not significantly so) in the formulations re-suspended in water compared to those stored in the presence of an excess of polymer/surfactant. However, interestingly the griseofulvin nanoparticles prepared in presence of HPMCAS aggregated (> 1000 nm) when stored both in excess polymer and when re-suspended in water.

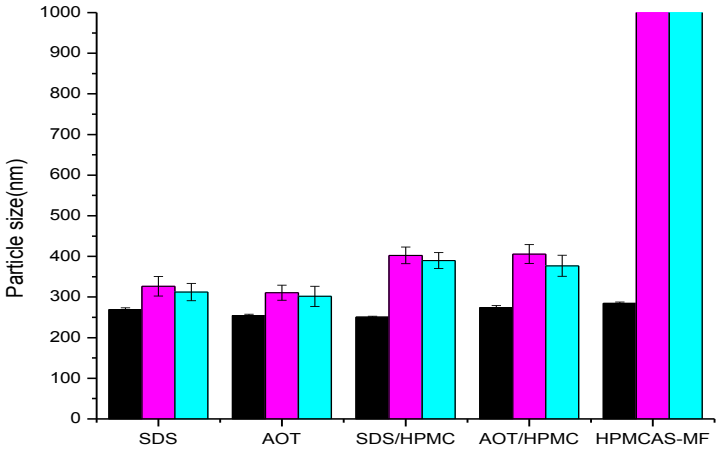

Figure 2.34: Particle size of griseofulvin nanoparticles prepared by 6 h milling in presence of 0.5% w/w SDS, 0.5% w/w AOT, 0.5% w/w SDS + 1.88% w/w HPMC 8000, 0.5% w/w AOT + 1.88% w/w HPMC 8000 and 0.5% w/w HPMCAS-MF at production (■), after 12 months storage in excess polymer/surfactant (■) and after 12 months storage in water after removal of excess polymer/surfactant (■) (n = 3 ± s.d.). Error from particle sizes obtained with three separate nanosuspensions.

With the exception of the HPMCAS formulation, the rest of the nanosupensions chosen for investigation were fairly stable upon storage in excess polymer/surfactant. In retrospect it may have been more beneficial to study the more unstable formulations in order to fully elucidate any advantage conferred by removal of excess polymer/surfactant.

All griseofulvin nanoparticles, regardless of stabiliser used for production, were observed to sediment over the year's storage and had to be re-suspended by shaking prior to PCS measurements which could partly explain the observed increase in particle size.

Rao et al (1997) determined the solubility of crystalline griseofulvin in water and in SDS solutions of varying concentrations at 25 ± 0.1ºC. The solubility of crystalline griseofulvin in water (12.1 gm/L) increased to 44.7 gm/L, 57.4 gm/L and 598.6-2340.8 gm/L below, at and above critical micellar concentration of SDS, respectively. In another study Murdande et al (2011) found that the solubility of crystalline griseofulvin in water (8.6 gm/L) increased to 11.4 gm/L and 22.9 gm/L in solutions of 1% w/w HPMC (E5) and HPMCAS-HF, respectively at 25 ± 0.1ºC. The increased solubility of griseofulvin in SDS, HPMC and HPMCAS was therefore likely to be a contributing factor to the Ostwald ripening observed.

Kumar et al (2009) studied the stability of itraconazole and odanacatib nanoparticles under a range of different conditions; namely temperature, nanoparticle size, drug solubility and nature of the stabiliser used. They found that nanoparticle size, drug solubility and temperature were important factors with nanoparticles stored at room temperature growing faster than those stored at 5 ± 0.1^{o}C. These workers attributed an increase in formulation instability seen with polymeric surfactant stabilisers to solubilisation of drug within the polymeric micelles formed by these molecules.

2.3.9 pH stability studies

Simulation of the stability of a nanoparticle formulation in the gastrointestinal tract is critical as it may help predict whether the formulation is stable and does not undergo aggregation *in vivo*, which, if it occurred, would negate the benefits conferred by particle size reduction. Numerous studies of *in vitro* gastrointestinal stability of various nanoformulations using simulated gastric and intestinal fluids are available in literature e.g. palcitaxel lipid nanocapsules (Roger et al 2009), solid lipid nanoparticles (Zimmerman et al, 2001) among others.

The microclimate of the stomach favours particle aggregation due to its high ionic strength and/or acidity (Mehnert et al, 2001; Zimmerman et al, 2001). The fasted stomach is highly acidic with a mean pH of 1-2.5, as determined by Evans et al, 1988. This pH may rise with food intake and in disease states such as achlorrhydia. The rest of the gut has a pH value ranging from 6.6 to 7.5, 6.6 for proximal ileum, 7.5 for terminal ileum and 6.4 in the caecum (Evans et al, 1988).

Figures 2.35-2.36 show the particle sizes of nanoparticles prepared in the presence of AOT and SDS respectively when suspended in solutions of pH 1-7 at 25 ± 0.1^{o}C. In all these formulations there was a marked increase in particle size at pH 1, with aggregation (> 1000 nm) seen in the formulations prepared using surfactant concentrations of < 2.0% w/w, in keeping with their lower zeta potentials. In addition, some of the SDS (but none of the AOT) stabilised formulations displayed aggregation at pH values of 2-3. On production, SDS stabilised nanoparticles generally had lower zeta potentials in comparison to those stabilised by AOT (Table 2.9). In these electrostatically stabilised particles, a high zeta potential seemed beneficial in preventing particle aggregation at low pH's of between 1-3. Similarily high zeta potential was predictive of the stability of these surfactant stabilised nanoparticles over time (section 2.3.8).

PCS measurements of the nanoparticles measured at 37 ± 0.1^{o}C (Figures 2.37-2.38) yielded particle sizes larger than those obtained at 25 ± 0.1^{o}C due to the increased solubility of griseofulvin at higher temperature.

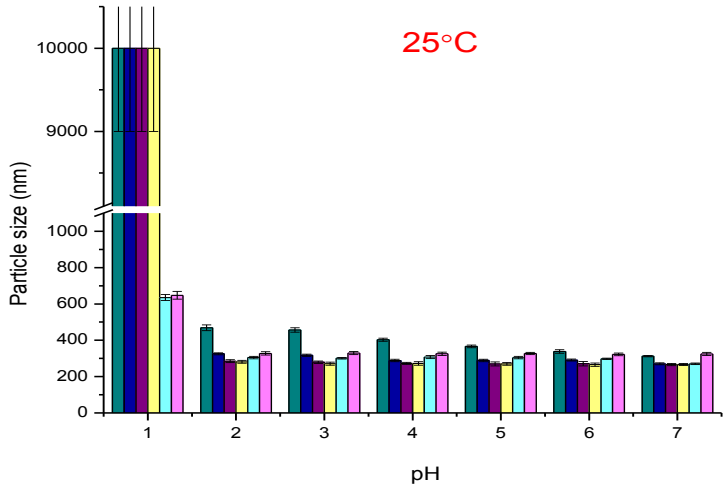

Figure 2.35: Particle sizes of griseofulvin nanoparticles prepared in presence of 0.25% w/w AOT (■), 0.5% w/w AOT (■), 1.0% w/w AOT (■), 1.5% w/w AOT (■), 2.0% w/w AOT (■) and 5.0% w/w AOT (■) when suspended in solutions of pH 1-7 at 25 ± 0.1°C (n = 3 ± s.d.). Error from particle sizes obtained with three separate nanosuspensions.

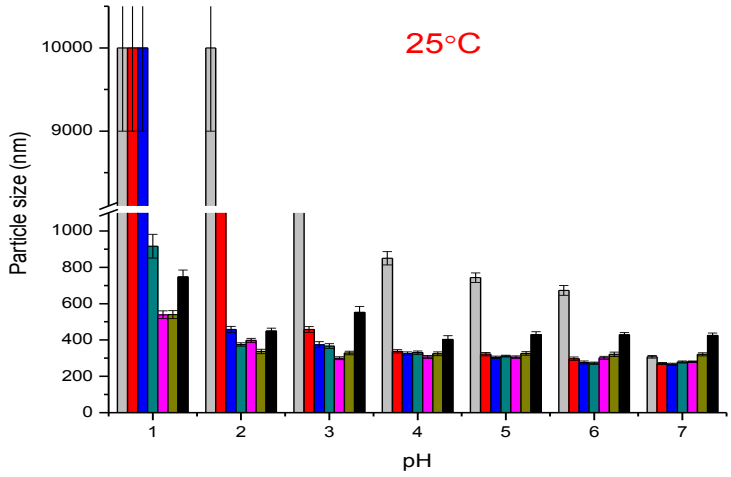

Figure 2.36: Particle sizes of griseofulvin nanoparticles prepared in presence of 0.25% w/w SDS (■), 0.5% w/w SDS (■), 1.0% w/w SDS (■), 1.5% w/w SDS (■), 2.0% w/w SDS (■), 5.0% w/w SDS (■) and 10.0% w/w SDS (■) when suspended in solutions of pH 1-7 at 25 ± 0.1°C (n = 3 ± s.d.). Error from particle sizes obtained with three separate nanosuspensions.

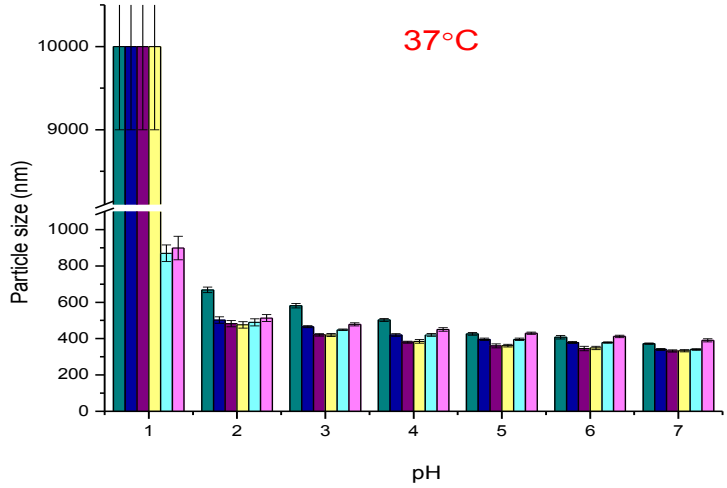

Figure 2.37: Particle sizes of griseofulvin nanoparticles prepared in presence of 0.25% w/w AOT (■), 0.5% w/w AOT (■), 1.0% w/w AOT (■), 1.5% w/w AOT (■), 2.0% w/w AOT (■) and 5.0% w/w AOT (■) when suspended in solutions of pH 1-7 at 37 ± 0.1°C (n = 3 ± s.d.). Error from particle sizes obtained with three separate nanosuspensions.

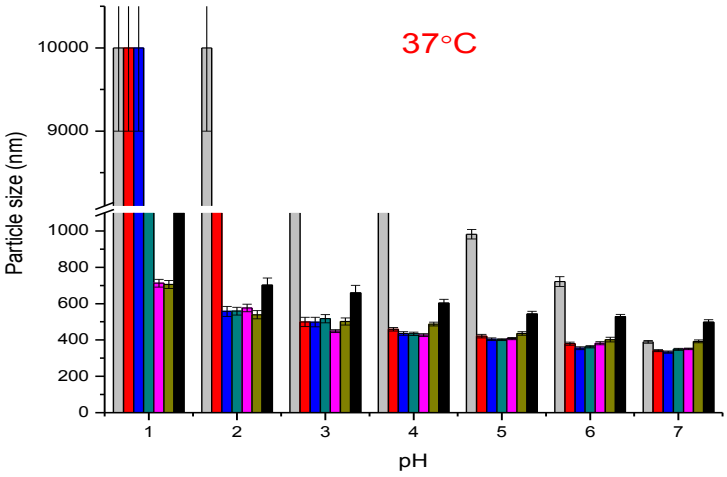

Figure 2.38: Particle sizes of griseofulvin nanoparticles prepared in presence of 0.25% w/w SDS (■), 0.5% w/w SDS (■), 1.0% w/w SDS (■), 1.5% w/w SDS (■), 2.0% w/w SDS (■), 5.0% w/w SDS (■) and 10.0% w/w SDS (■) when suspended in solutions of pH 1-7 at 37 ± 0.1°C (n = 3 ± s.d.). Error from particle sizes obtained with three separate nanosuspensions.

Figures 2.39-2.40 show particle sizes of nanoparticles prepared in the presence of AOT + 1.88% w/w HPMC 8000, and SDS + 1.88% w/w HPMC 8000, respectively when suspended in solutions of pH 1-7 at 25 ± 0.1°C. In all these formulations there was a marked increase in nanoparticle size at pH 1-2, with aggregation (> 1000 nm) seen in the formulations prepared using surfactant concentrations > 2.0% w/w AOT

and > 0.5% w/w SDS, despite their higher zeta potentials upon production. This contradicts the scenario with the surfactant stabilised formulations whereby the nanopartcles with higher zeta potential were less likely to under aggregation at low pH. In these polymer/surfactant formulations, the zeta potentials (Table 2.11) did not predict aggregation behaviour. Rather the amount of surfactant used in nanoparticle production was a more useful predictor, with lower starting amounts of surfactant appearing to be more beneficial when a polymer was present, in preventing particle aggregation at low pHs of between 1-3. Once again PCS measurements on nanoparticles stored at 37 ± 0.1°C (Figures 2.41-2.42) yielded particle sizes larger than those obtained at 25 ± 0.1°C.

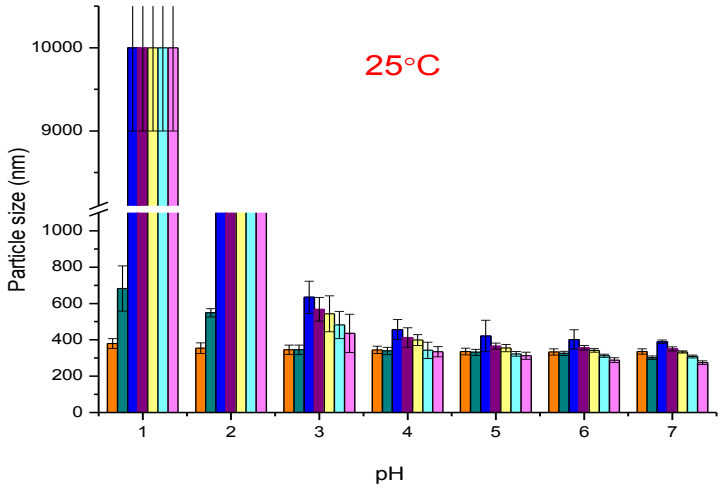

Figure 2.39: Particle sizes of griseofulvin nanoparticles prepared in presence of 0.1% w/w AOT + 1.88% w/w HPMC 8000 (■), 0.25% w/w AOT + 1.88% w/w HPMC 8000 (■), 0.5% w/w AOT + 1.88% w/w HPMC 8000 (■), 1.0% w/w AOT + 1.88% w/w HPMC 8000 (■), 1.5% w/w AOT + 1.88% w/w HPMC 8000 (■), 2.0% w/w AOT + 1.88% w/w HPMC 8000 (■) and 5.0% w/w AOT + 1.88% w/w HPMC 8000 (■) when suspended in solutions of pH 1-7 at 25 ± 0.1°C (n = 3 ± s.d.). Error from particle sizes obtained with three separate nanosuspensions.

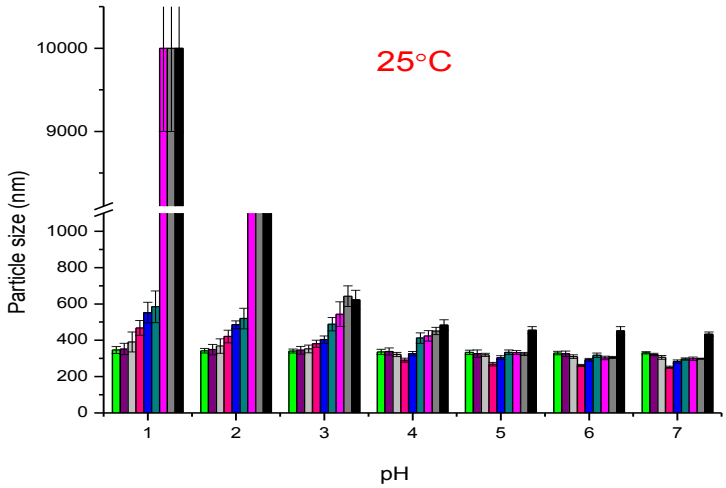

Figure 2.40: Particle sizes of griseofulvin nanoparticles prepared in presence of 0.05% w/w SDS + 1.88% w/w HPMC 8000 (■), 0.1% w/w SDS + 1.88% w/w HPMC 8000 (■), 0.25% w/w SDS + 1.88% w/w HPMC 8000 (■), 0.5% w/w SDS+ 1.88% w/w HPMC 8000 (■), 1.0% w/w SDS + 1.88% w/w HPMC 8000 (■), 1.5% w/w SDS + 1.88% w/w HPMC 8000 (■), 2.0% w/w SDS+ 1.88% w/w HPMC 8000 (■), 5.0% w/w SDS + 1.88% w/w HPMC 8000 (■) and 10.0% w/w SDS + 1.88% w/w HPMC 8000 (■) when suspended in solutions of pH 1-7 at 25 ± 0.1°C (n = 3 ± s.d.). Error from particle sizes obtained with three separate nanosuspensions.

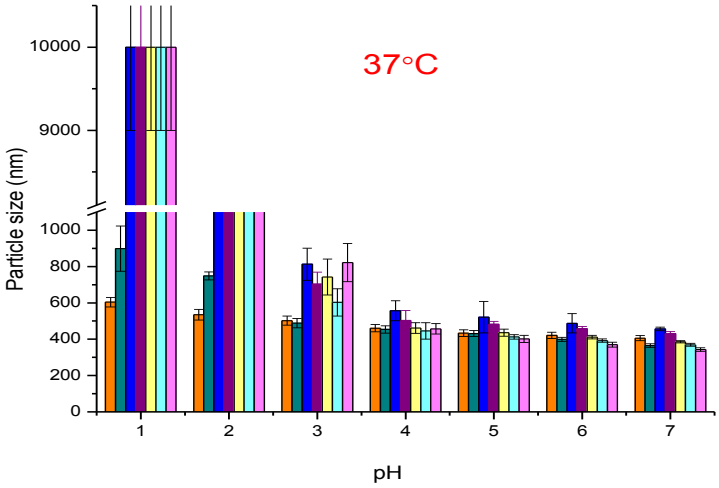

Figure 2.41: Particle sizes of griseofulvin nanoparticles prepared in presence of 0.1% w/w AOT + 1.88% w/w HPMC 8000 (■), 0.25% w/w AOT + 1.88% w/w HPMC 8000 (■), 0.5% w/w AOT + 1.88% w/w HPMC 8000 (■), 1.0% w/w AOT + 1.88% w/w HPMC 8000 (■), 1.5% w/w AOT + 1.88% w/w HPMC 8000 (■), 2.0% w/w AOT + 1.88% w/w HPMC 8000 (■) and 5.0% w/w AOT + 1.88% w/w HPMC 8000 (■) when suspended in solutions of pH 1-7 at 37 ± 0.1°C (n = 3 ± s.d.). Error from particle sizes obtained with three separate nanosuspensions.

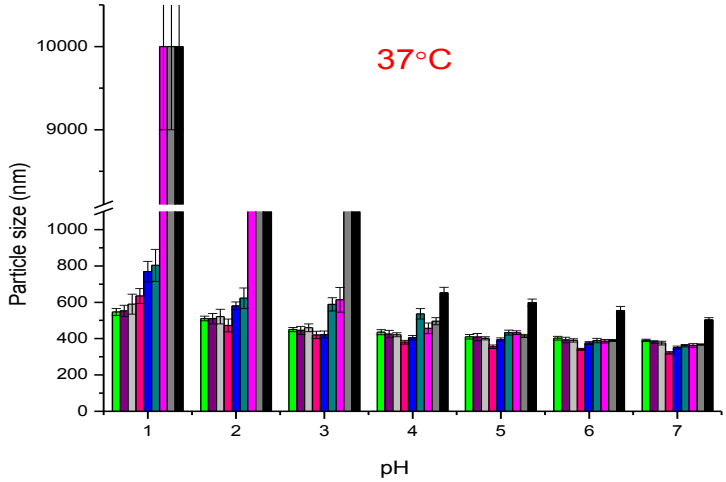

Figure 2.42: Particle sizes of griseofulvin nanoparticles prepared in presence of 0.05% w/w SDS + 1.88% w/w HPMC 8000 (■), 0.1% w/w SDS + 1.88% w/w HPMC 8000 (■), 0.25% w/w SDS + 1.88% w/w HPMC 8000 (■), 0.5% w/w SDS+ 1.88% w/w HPMC 8000 (■), 1.0% w/w SDS + 1.88% w/w HPMC 8000 (■), 1.5% w/w SDS + 1.88% w/w HPMC 8000 (■), 2.0% w/w SDS+ 1.88% w/w HPMC 8000 (■), 5.0% w/w SDS + 1.88% w/w HPMC 8000 (■) and 10.0% w/w SDS + 1.88% w/w HPMC 8000 (■) when suspended in solutions of pH 1-7 at 37 ± 0.1^{o}C (n = 3 ± s.d.). Error from particle sizes obtained with three separate nanosuspensions.

Nanoparticles prepared in the presence of HPMCAS (one grade i.e. HPMCAS-MF plotted) were the least stable when suspended in solutions of pH 1-4 (Figures 2.43-2.44). For example, when dispersed in a solution of pH 4, at either 25 ± 0.1^{o}C or 37 ± 0.1^{o}C, the nanoparticles aggregated, with particle sizes of > 1000 nm being observed. When dispersed in a solution of pH between 1-3, at either 25 ± 0.1^{o}C or 37 ± 0.1^{o}C, the same nanoparticles produced a visible cloudy precipitate, with particle sizes of greater than 10000 nm being recorded. These results predict that the HPMCAS would be the least suitable stabiliser for nanoparticles of griseofulvin intended for oral use.

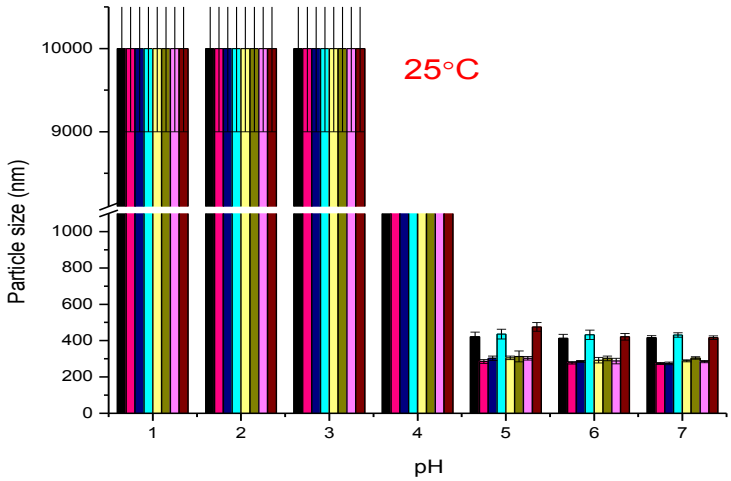

Figure 2.43: Particle sizes of griseofulvin nanoparticles prepared in presence of 0.1% w/w HPMCAS-MF (■), 0.25% w/w HPMCAS-MF (■), 0.5% w/w HPMCAS-MF (■), 1.0% w/w HPMCAS-MF (■), 1.5% w/w HPMCAS-MF (■), 2.0% w/w HPMCAS-MF (■), 5.0% w/w HPMCAS-MF (■) and 10.0% w/w HPMCAS-MF (■) when suspended in solutions of pH 1-7 at 25 ± 0.1°C (n = 3 ± s.d.). Error from particle sizes obtained with three separate nanosuspensions.

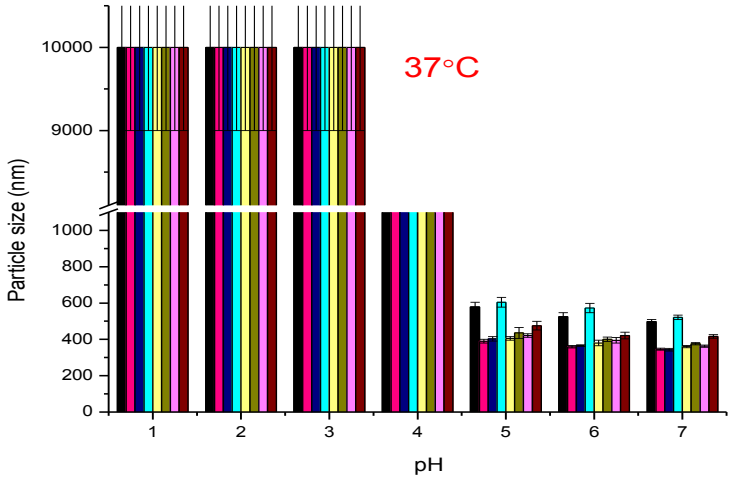

Figure 2.44: Particle sizes of griseofulvin nanoparticles prepared in presence of 0.1% w/w HPMCAS-MF (■), 0.25% w/w HPMCAS-MF (■), 0.5% w/w HPMCAS-MF (■), 1.0% w/w HPMCAS-MF (■), 1.5% w/w HPMCAS-MF (■), 2.0% w/w HPMCAS-MF (■), 5.0% w/w HPMCAS-MF (■) and 10.0% w/w HPMCAS-MF (■) when suspended in solutions of pH 1-7 at 37 ± 0.1°C (n = 3 ± s.d.). Error from particle sizes obtained with three separate nanosuspensions.

2.4 Summary

Wet bead milling (WBM) of eight poorly water-soluble drugs namely albendazole, carbamazepine, frusemide, halofantrine, griseofulvin, indomethacin, nabumetone and phenytoin was carried out in presence of a range of ionic and non-ionic polymers and surfactants. The most effective stabilisers of drug nanoparticles produced by WBM could not be attributed to either the physico-chemical properties of the drug and/or stabiliser therefore making prior prediction of stabiliser difficult.

Further, detailed studies were performed using griseofulvin whose nanoparticles could only be produced in presence of anionic stabilisers namely sodium dodecyl sulphate (SDS), aerosol-OT (AOT) and hypromellose acetate succinate (HPMCAS). A minimum effective concentration of anionic stabiliser below which nanoparticles could not be produced was observed. Below this concentration there was insufficient anionic stabiliser to coat nanoparticles and prevent aggregation during milling. Any further increase in the anionic stabiliser concentration in the crude drug suspension prior to milling lead to an increase in the zeta potential of the resultant nanoparticles, suggesting that increasing amounts of the anionic stabiliser were being adsorbed onto the drug nanoparticles. The use of anionic surfactants or polymers in formulations intended for oral use is suboptimal due to their incompatibility with other ionics, salt and pH changes within the gastrointestinal tract.

Polymer-surfactant synergy was investigated by including both the non-ionic polymer hypromellose (HPMC) and the anionic surfactant in the crude drug suspensions before milling. HPMC on its own was unable to stabilise griseofulvin nanoparticles during WBM. Incorporation of a constant amount of HPMC 8000 (namely 1.88% w/w) into surfactant stabiliser solution prior to milling led to a reduction of the minimal effective surfactant concentration at which nanoparticles could be produced, suggesting that non-ionic polymer and surfactant were co-adsorbing onto drug surfaces. Lower zeta potentials were measured for the nanoparticles milled in presence of non-ionic polymer and anionic surfactant relative to those milled with anionic surfactant only, further supporting this hypothesis. Using a constant SDS concentration, the effect of polymer molecular weight and concentration was investigated. An increase in polymer concentration and molecular weight in the crude drug suspension prior to milling was found to decrease milling efficiency due to an increase slurry viscosity and polymer diffusion effects. X-ray

diffraction was used to screen for milling induced disorder and revealed that in all cases tested, crystallinity of griseofulvin was maintained after milling.

Ostwald ripening was observed in all the griseofulvin nanoparticle formulations when stored for a year in their original milled state, that is in presence of excess polymer and/or surfactant, at room temperature. Particle growth was higher in particles prepared in presence of HPMC and anionic surfactant, particularly when either the lowest surfactant concentration was used and/or when the highest polymer concentration/molecular weight was used. The nanoparticles at these extremes were larger and more polydisperse at production. Nanoparticles prepared in presence of HPMCAS were the least stable and aggregated at 1-3 months storage. The HPMCAS formulations were quite viscous on production, which probably contributed to aggregation due to low interparticle distances.

The stability of nanoparticles in the gastrointestinal tract, particularly the stomach, was investigated by resuspending them in HCl solutions of pH 1-6 and determining particle size at 25 ± 0.1ºC and 37 ± 0.1ºC. When the nanoparticles were prepared in presence of anionic surfactant, the measured zeta potential was predictive of stability with aggregation being seen at low pH's in the range 1-3 for nanoparticles possessing the lowest zeta potentials. For the nanoparticles prepared in presence of HPMC and anionic surfactant, low amounts of anionic surfactant seemed beneficial, as nanoparticles prepared with the higher amounts of surfactant tending to aggregate at low pH's of 1-3. As noted earlier the inclusion of HPMC in the milling slurry enabled a reduction in the minimum effective surfactant concentration, thereby resulting in a better pH stability of the nanoparticles. The nanoparticles prepared in presence of HPMCAS were the least stable of all, with all of these nanoparticles aggregating at pH of 4 or less. HPMCAS was thus found to be the least suitable stabiliser for nanoparticles intended for oral delivery.

Chapter 3
Polymer/surfactant adsorption isotherms

3.1 Introduction

3.1.1 Determination of adsorption isotherms

Adsorption of solute molecules onto solid surfaces has been important in enabling a better understanding of a range of processes in fields as diverse as cosmetology, medicine, the pharmaceutical industry and environmental science. The characteristic adsorption behaviour of a material is normally described by means of an adsorption isotherm, which describes the amount of the adsorbate adsorbed onto a known

amount of adsorbent as a function of the adsorbate concentration, at a fixed temperature.

Adsorption isotherms are typically determined *indirectly* by the depletion method (Dejardin, 1982), which measures the amount of adsorbate left in solution after adsorption using techniques such as surface tension (Lin et al, 2002; Fainerman et al, 2009), PCS (Zhao et al, 1995), conductometric titration (Nodehi et al, 2007) and colorimetric assays (Govender et al, 2005) amongst others. Many of these techniques are not without problems. For example although surface tension measurements have been used to determine surfactant adsorption isotherms (Lin et al, 2002; Fainerman et al, 2009), measurement errors are very likely because surface tension is sensitive to changes in temperature, salt, traces of dust, and the presence of other surface active molecules e.g. polymers and some drugs.

The amount of solute molecule adsorbed can also be established *directly* using more sophisticated techniques such as small angle neutron scattering (SANS) (Qui et al, 2009), atomic force microscopy (Lipatov et al, 2006) and Fourier transform infrared spectroscopy (Habich et al, 2010). These more advanced techniques often provide very useful, additional information over that obtained using an indirect method. SANS for example, can provide information both on the thickness of an adsorbed layer as well as the conformation of the adsorbing molecules (Goodwin 2006). In addition, computer modelling programs e.g. Monte Carlo simulations, have been used to predict adsorption isotherms (Arnold et al, 2011).

3.1.2 Challenges faced with the present systems

Despite the successful formulation of a range of poorly water-soluble drugs as nanoparticles, mastery of the mechanisms behind nanoparticle stabilisation is lacking. In order to fully elucidate the stabilisation mechanism of the nanoparticles, it is important to determine the adsorption isotherm of polymer/surfactants on nanoparticle surfaces. In comparison to model systems such as polystyrene latex beads, the determination of adsorption onto drug nanoparticles prepared by milling, as is the case in the present study, is challenging due to particle polydispersity both in terms of particle size and shape as well as surface heterogeneity. This chapter reports work aimed at determining adsorption isotherms of polymer and/or surfactant on the WBM griseofulvin nanoparticles.

3.1.3 Surfactant assay

In the present study a colorimetric method was used to quantify sodium dodecyl sulphate (SDS) in µL volume samples (Rusconi et al, 2001). The method is based on the use of a cationic carbocyanine dye, called Stains All, whose colour changes from an intense fuschia to yellow upon interaction with the sulphate head group present in SDS. The colour change of the dye on interaction with SDS is dose proportionate, allowing the quantification of SDS by visible light spectroscopy. Furthermore, a wide variety of biological compounds such as proteins, nucleic acids and other materials such as detergents, salts, buffers, solvents, acids and reducing agents have been found not to interfere with the assay (Rusconi et al, 2001). Figure 3.1 shows the chemical structure of Stains All.

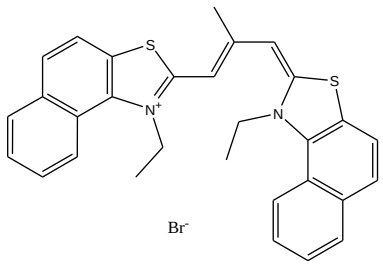

Figure 3.1: Chemical structure of Stains All.

3.1.4 Polymer assay

The assay of cellulose polymers is particularly difficult because they lack a chromophore and cannot therefore be studied using UV/Vis spectroscopy. Colorimetric assays (performed by means of complexation of the cellulose polymer with a chromophore-containing molecule), size exclusion chromatography and gas chromatography are among the many techniques that have been used to quantify cellulose polymers in solution. Unfortunately however, most of these techniques have problems, for example they are expensive, time consuming and/or grossly inaccurate. For example, colorimetric assays of cellulose polymers based on the complexation with chromophore-containing molecules have been reported to possess standard errors exceeding 40% (Shea et al, 1994). Such methods are particularly problematic for low molecular weight and/or polydisperse polymers, as the terminal groups of the polymer chains greatly influence the extent of its complexation with the chromophore-containing molecules leading to the inaccurate assessment of polymer molecular weight and therefore erroneous measurements (Sepassi 2003). An

accurate assessment of polymer molecular weight is essential for the present studies due to the preferential adsorption, at equilibrium, of higher molecular weight polymers onto the drug surface and the possible fractionation, by molecular weight, of polymer during milling (Sepassi et al, 2007).

Previously, an optical rotatory dispersion (ORD) assay method has been described for quantification of cellulose polymers in solution. Indeed Sepassi (2003) and subsequently Goodwin (2006) have successfully employed ORD methodology to determine the extent of the adsorption of hydroxypropylmethylcellulose (HPMC) and hydroxypropylmethylcellulose (HPC), respectively onto milled drug nanoparticles. Significantly, as the ORD assay Sepassi (2003) and Goodwin (2006) developed was found to be molecular weight independent (at least over a wide range of polymer molecular weights) it was considered ideal for the present study.

3.2 Methodology

3.2.1 Sample preparation

Polymer/surfactant isotherms in the present study were obtained by measuring the depletion of the respective entity from solution after contact with the absorbent. The WBM drug nanosupensions, prepared as discussed in section 2.2.2-2.2.3, were centrifuged for 1.5 hours at 13000 rpm using a Heraus Biofuge Pico ultracentrifuge (Fischer scientific Leicestire, UK) in an attempt to completely precipitate the nanoparticles. The resultant supernatant was removed from contact with the drug nanoparticles and then centrifuged again for 30 minutes to ensure the complete sedimentation of the nanoparticles.

A range of spectroscopic techniques was then used to determine the amount of polymer/surfactant remaining in the supernatant, assumed to be the total amount of non-absorbed material. The amount of polymer/surfactant adsorbed was calculated by subtracting the amount experimentally determined to be non-absorbed from the known starting concentration. When determining the surface area of the griseofulvin nanoparticles available for adsorption, the nanoparticles were assumed to be spherical. This assumption has been previously shown not to introduce significant errors into the value of surface area and hence the amount of polymer/surfactant absorbed per unit surface area (Sepassi et al, 2007). Calculations used for the determination of the nanoparticle's surface area are detailed in Appendix 1. The

value for griseofulvin density used in these calculations was 1.455 g/cm^3 (Martin, 2005).

3.2.2 Stains All colorimetric assay

Initially a Stains All stock solution (1.8 mM) was prepared by dissolving 1 mg of Stains All in 1 mL of isopropanol:water 50:50 (v/v). 1 mL of this stock solution was then mixed with 1 mL of formamide and 18 mL of ultrapure water (UPW) to form the Stains All intermediate solution (90 µM). The Stains All quantification solution (56.25 µM) used for analysis was prepared by diluting 5 mL of the intermediate Stains All solution (90 µM) with 3 mL UPW to yield a fuschia coloured solution. The UV/Vis spectrum of this quantification solution over the wavelength range 400-750 nm in a 1 cm path length cell was measured immediately using a Perkin Lambda 2 UV/Vis spectrophotometer with UPW as blank. The remainder of the quantification solution, which had been kept in the dark, was then immediately used for analysis.

In order to obtain a calibration curve 0.4 µL samples containing known amount of SDS (0.1-0.5% w/w) and 1.0 µL of AOT (0.1-0.5% w/w) were added into a cuvette containing 3 mL of the 56.25 µM Stains All quantification solution. The resultant solution was then thoroughly mixed with a Gilson P-1000 pipette and its absorbance measured immediately using the same conditions as for the Stains All quantification solution. All measurements were made in triplicate.

The same protocol was followed for analysis of the amount of surfactant remaining in the supernatant solution after nanoparticle production, the only differences being that in some instances it was necessary first to dilute the supernatant solution to ensure that the surfactant concentration was in the quantifiable range for the assay and that the blank was the corresponding supernatant solution in the absence of Stains All.

3.2.3 Optical rotatory dispersion

The UV/Vis spectra of solutions of HPMC 8000, 11000, 15000 dissolved in water were measured using a Perkin Lambda 2 UV-Vis spectrophotometer in polystyrene cuvettes of 10 mm pathlength. The measurements of the UV/Vis spectra were made over a wavelength range of 230-650 nm, with a step size of 2 nm, time per point of 0.5 sec, and total time per spectrum of 7 min. UPW was used as the blank. Scans

were carried out on three separate solutions; therefore the results are expressed in triplicate.

The ORD spectra of solutions of HPMC 8000, 11000, 15000 dissolved in water were measured. The samples to be examined were placed in 10 mm path length quartz cells and their ORD spectra measured over the wavelength range 230-650 nm using a Chirascan spectropolarimeter (Applied Photophysics, UK) with a step size of 2 nm, band width 2 nm, time per point of 0.5 sec, and total time per spectrum of 7 min. UPW was used as the blank. Scans were carried out on three separate solutions; therefore the results are expressed in triplicate.

3.2.4 Circular dichroism

Circular dichroism (CD) spectra of griseofulvin dissolved in water, 2% w/w HPMC 8000 aqueous solution and supernatants of griseofulvin nanosuspensions prepared in presence of 0.5% w/w SDS and, 0.5% w/w SDS + 1.88% w/w HPMC 8000, were obtained. The samples to be examined were placed in 10 mm path length quartz cells and their CD spectra measured over the wavelength range 200-500 nm using a Chirascan spectropolarimeter (Applied Photophysics, UK) with a step size of 1 nm, band width 1 nm, time per point of 0.5 sec, and total time per spectrum of 5 min. UPW was used as the blank. Due to their high CD signal, the supernatants of the griseofulvin nanosuspensions were diluted prior to analysis.

3.3 Results

3.3.1 Development of Stains All colorimetric surfactant assay

Figure 3.2 shows the absorbance spectrum of the quantification solution of Stains All (56.25 μM) and absorbance of 56.25 μM Stains All in the presence of varying concentrations of SDS. As can be seen the Stains All spectrum shows a major absorption band at 510 nm, which decreases linearly upon the addition of SDS, while at the same time a peak at 453 nm and a shoulder at 438 nm appear (Figure 3.2). The shoulder at 438 nm was selected for quantification due to the high linearity between its absorbance value and the amount of SDS added (Rusconi et al, 2001).

The above methodology was adapted for quantification of aerosol-OT (AOT). Like SDS, AOT is an anionic surfactant, possessing a sulfosuccinate head group, which can interact with the cationic Stains All dye. While the methodology employed was the same, a higher volume (1.0 μL) of the corresponding AOT stock solution and

sample was required due to the lower sensitivity of the assay for AOT. The scans incorporating AOT samples are shown in Figure 3.3.

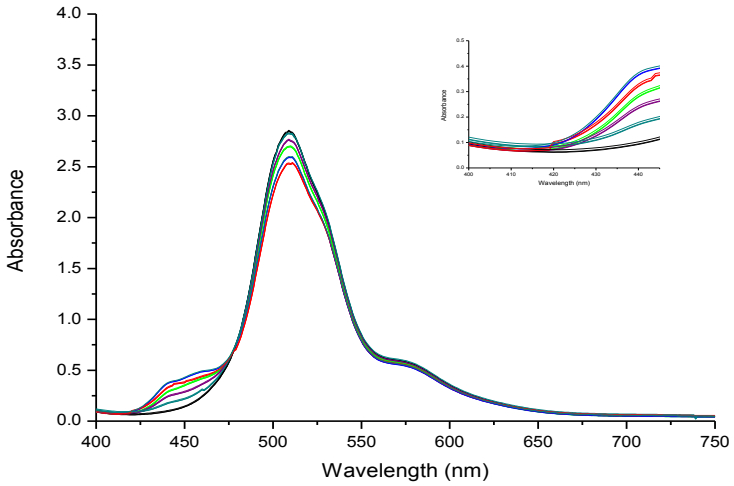

Figure 3.2: UV scans (wavelength range 400-750 nm) of 56.25 µM Stains All alone (3 mL), and in the presence of 0.4 µL of a known concentration of SDS solution. (—) Stains all, (—) 0.1% w/w SDS, (—) 0.2% w/w SDS, (—) 0.3% w/w SDS, (—) 0.4% w/w SDS and (—) 0.5% w/w SDS. Figure inset shows UV scans in the wavelength range 400-450 nm.

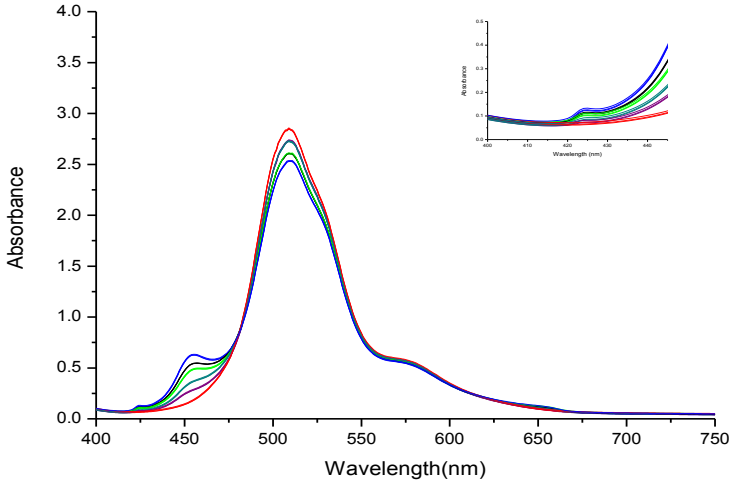

Figure 3.3: UV scans (wavelength range 400-750 nm) of 56.25 µM Stains All alone (3 mL) and in the presence of 1.0 µL of known concentration of AOT solution. (—) Stains all, (—) 0.1% w/w AOT, (—) 0.2% w/w AOT, (—) 0.3% w/w AOT, (—) 0.4% w/w AOT and (—) 0.5% w/w AOT. Figure inset shows UV scans in the wavelength range 400-450 nm

Figure 3.4 shows the calibration curves obtained for the determination of surfactant concentration in solution using the Stain All assay. As can be seen the variation of absorbance with surfactant concentration was linear at the measurement wavelength of 438 nm and over the range of surfactant concentrations tested. The curves were fitted by linear regression yielding correlation coefficients (R^2) of 0.9989 and of 0.9983 for SDS and AOT, respectively. A 56.25 µM solution of Stains All had an absorbance of ~ 0.098 and is therefore responsible for the y-intercept of the calibration curves at zero surfactant concentration.

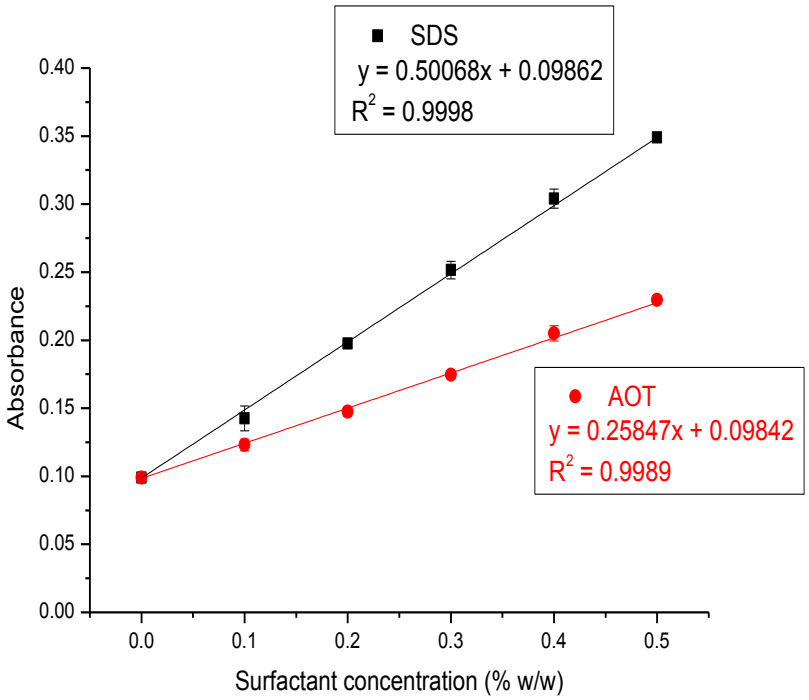

Figure 3.4: Calibration curve at 438 nm of 0.4µL of SDS (■) and 1.0 µL of AOT (●) surfactant solutions (concentration in the range 0-0.5% w/w) in 3 mL of 56.25 µM Stains All solution at 438nm. (n = 3 ± s.d.).

The interference, if any, of HPMC polymer (used in the polymer-surfactant stabilisation studies) in the Stains All assay was investigated by dissolving surfactant in HPMC 8000 or HPMC 15000 solutions in place of water and repeating the assay using the appropriate polymer solution as blank. Although the presence of both molecular weights of HPMC in the solutions lead to a higher absorbance of the Stains All solutions, as can be seen from Figures 3.5 (SDS as surfactant) and 3.6 (AOT as surfactant), the linearity of the calibration curve was maintained when using the appropriate polymer solution as blank.

The interference, if any, to the Stains All assay by griseofulvin was also evaluated by repeating the experiments in the presence of 0.01% w/w griseofulvin. The presence of griseofulvin at this concentration did not alter the absorbance of the Stains All or the linearity of the calibration curves (Figures 3.5 and 3.6).

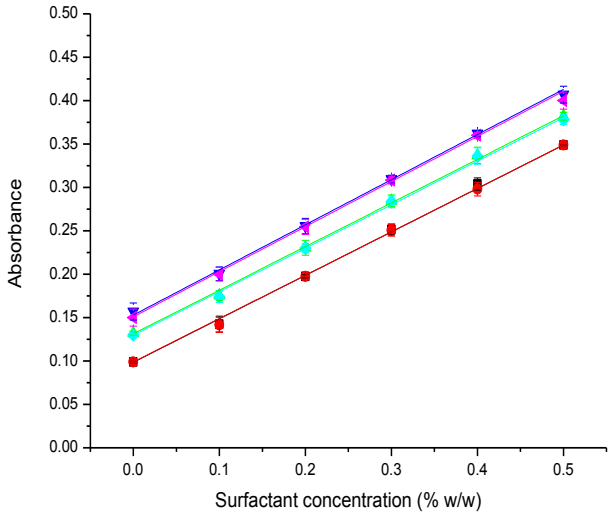

Figure 3.5: Calibration curves of the absorbance at 438 nm of 0.4 µL SDS surfactant solutions (concentration range 0-0.5% w/w) in 3 mL of a 56.25 µM Stains All solution in water (■), in 1% w/w HPMC 8000 (▲), in 2% w/w HPMC 8000 (▼). Overlaid are the corresponding calibration curves in the presence of griseofulvin; in water (●), in 1% w/w HPMC 8000 (♦) and in 2% w/w HPMC 8000 (◄). (n = 3 ± s.d.)

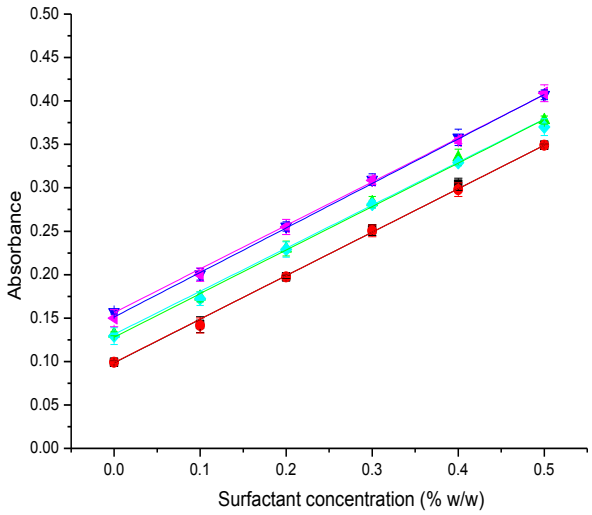

Figure 3.6: Calibration curves of the absorbance at 438 nm of 1.0 µL AOT surfactant solutions (concentration range 0-0.5% w/w) in 3 mL of a 56.25 µM Stains All solution in water (■), in 1% w/w HPMC 8000 (▲), in 2% w/w HPMC 8000 (▼). Overlaid are the corresponding calibration curves in the presence of griseofulvin; in

water (●), in 1% w/w HPMC 8000 (♦) and in 2% w/w HPMC 8000 (◄). (n = 3 ± s.d.)

3.3.2 Development of optical rotatory dispersion polymer assay

The UV scans of HPMC 8000, 11000 and 15000 are illustrated in Figures 3.7, 3.8 and 3.9, respectively. Irrespective of polymer molecular weight, the UV/Vis spectra (225 – 650 nm) of the polymer solutions all exhibited an absorbance which peaked at ~ 275 nm. As HPMC is not expected to exhibit a chromophore over this wavelength range, the recorded absorbance may be due to an impurity in the polymer samples that possess a chromophore or due to the high polymer concentrations tested. In order to ensure that the observed absorbance did not interfere with the ORD measurements, the wavelength selected for analysis of the ORD measurements was 350 nm, a wavelength where the various polymer samples exhibited a low absorbance.

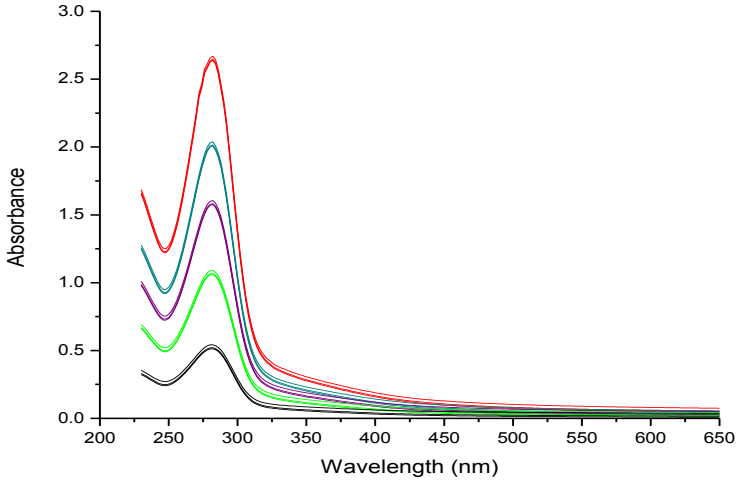

Figure 3.7: UV/Vis spectra of aqueous solutions of varying HPMC 8000 concentration HPMC. (—) 1% w/w HPMC 8000, (—), 2% w/w HPMC 8000 (—), 3% w/w HPMC 8000, (—) 4% w/w HPMC 8000, (—) 5% w/w HPMC 8000 (n = 3).

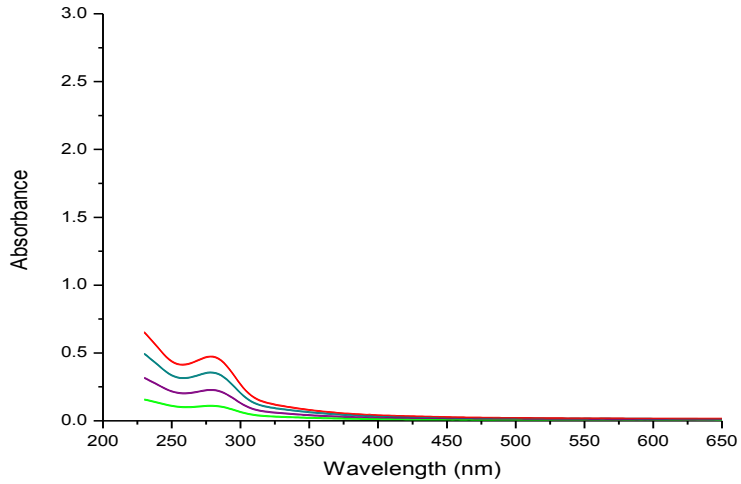

Figure 3.8: UV/Vis spectra of aqueous solutions of varying HPMC 11000 concentration. (—) 0.5% w/w HPMC 11000, (—) 1% w/w HPMC 11000, (—) 1.5% w/w HPMC 11000, (—) 2% w/w HPMC 11000 (n = 3).

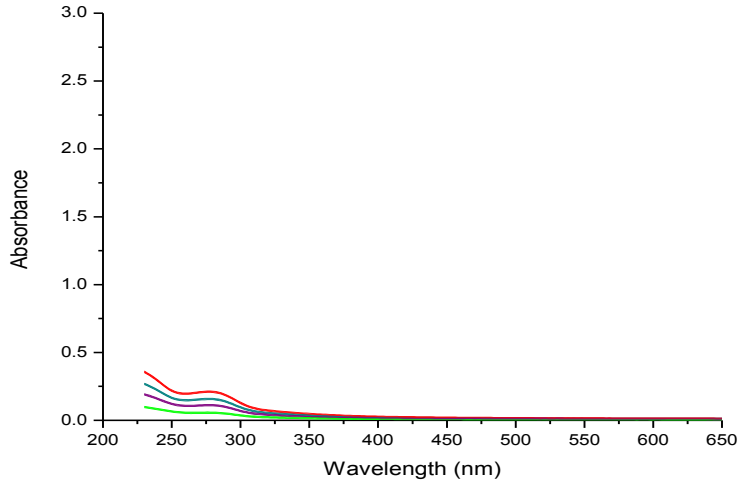

Figure 3.9: UV/Vis spectra of aqueous solutions of varying HPMC 15000 concentration. (—) 0.5% w/w HPMC 15000, (—) 1% w/w HPMC 15000, (—) 1.5% w/w HPMC 15000, (—) 2% w/w HPMC 15000 (n = 3).

ORD scans of polymer, namely HPMC 8000, 11000 or 15000, dissolved in water are shown in Figures 3.10, 3.11 and 3.12, respectively.

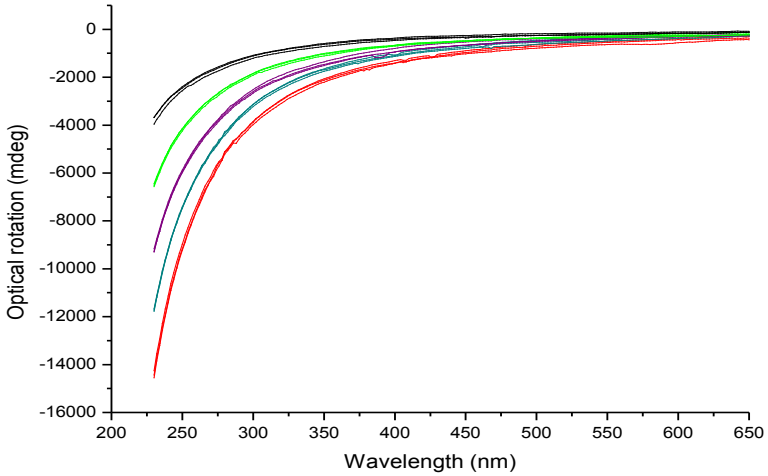

Figure 3.10: ORD spectra of aqueous solutions of varying HPMC 8000 concentration. (—) 1% w/w HPMC 8000, (—), 2% w/w HPMC 8000 (—), 3% w/w HPMC 8000, (—) 4% w/w HPMC 8000, (—) 5% w/w HPMC 8000 (n = 3).

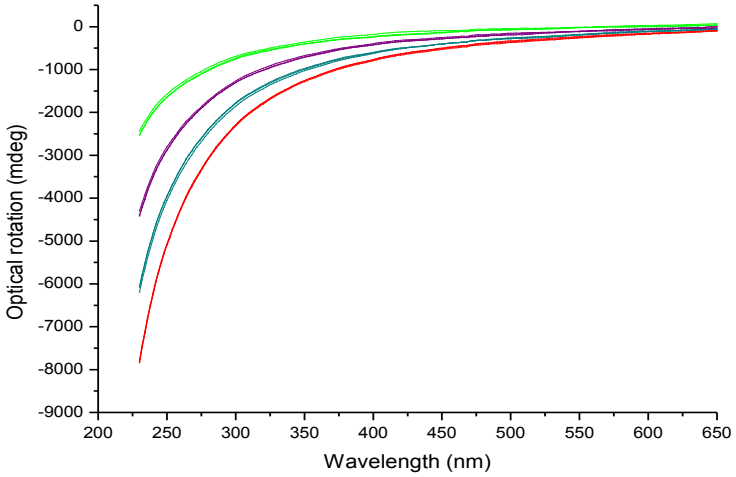

Figure 3.11: ORD spectra of aqueous solutions of varying HPMC 11000 concentration. (—) 0.5% w/w HPMC 11000, (—) 1% w/w HPMC 11000, (—) 1.5% w/w HPMC 11000, (—) 2% w/w HPMC 11000 (n = 3).

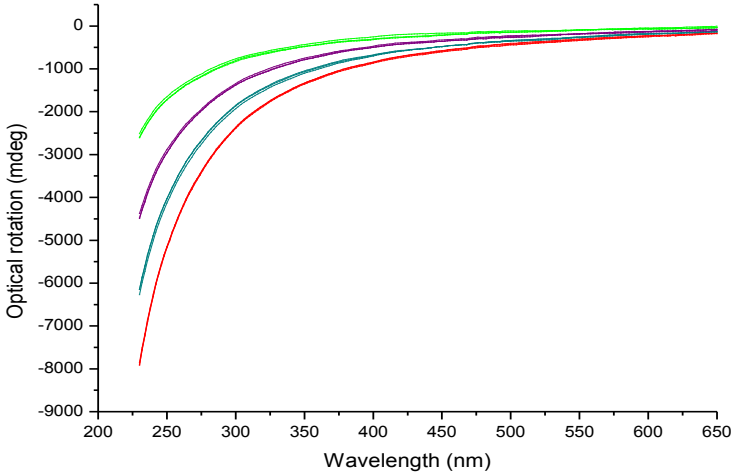

Figure 3.12: ORD spectra of aqueous solutions of varying HPMC 15000 concentration. (—) 0.5% w/w HPMC 15000, (—) 1% w/w HPMC 15000, (—) 1.5% w/w HPMC 15000, (—) 2% w/w HPMC 15000 (n = 3).

The ORD scans of the aqueous HPMC 8000, HPMC 11000 and HPMC 15000 solutions (concentration range 1-5% w/w for the HPMC 8000 solutions and 0.5-2.0% w/w for the HPMC 11000 and 15000 solutions) showed a linear variation in ORD with concentration, with correlation coefficients of above 0.9985 being obtained for the three polymer samples (Figure 3.13). However, in contrast to previous ORD measurements on similar polymers (Shadi 2003, Goodwin 2006), the variation in ORD with concentration of the three molecular weight polymers did not overlay each other. In fact only the curves obtained for the HPMC 11000 and 15000 polymer solutions were comparable, while the curve obtained for the HPMC 8000 polymer solutions possessed a much lower negative slope. Analysis of variance (ANOVA) of the ORD results for the polymer solutions showed that the differences between the curves obtained for the HPMC 8000, 11000 and 15000 solutions were significant, $F(2, 6) = 21.71$, $p = 0.00179$. The Tukey HSD test was used to analyse the differences between the various polymer solutions and showed that any differences between the results obtained for the aqueous solutions of HPMC 11000 and HPMC 15000 were not significant. There where however significant differences ($p < 0.01$) obtained between the aqueous HPMC 8000 and HPMC 11000 polymer solutions and between the aqueous HPMC 8000 and HPMC 15000 solutions.

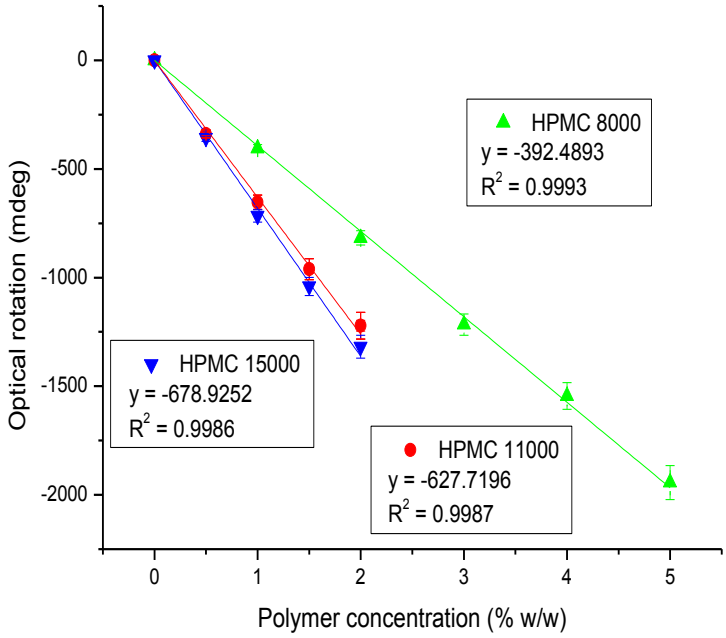

Figure 3.13: ORD calibration curves of aqueous HPMC polymer solutions: (▲) HPMC 8000 (1-5% w/w), (●) HPMC 11000 (0.5-2.0% w/w), (▼) HPMC 11000 (0.5-2.0% w/w) at 350 nm (n = 3 ± s.d.).

The ORD results obtained lead to the suspicion that the differences in the values of ORD measured for the HPMC 8000 solutions were due to interference arising from the UV absorption seen with the HPMC 8000 solutions (Figure 3.7). In an attempt to determine the nature of the impurity, the NMR spectra of the three different molecular weight polymers (HPMC 8000, 11000 and 15000) dissolved in D_2O were measured using a Bruker Avance DRX 400 MHz NMR spectrometer (Bruker, UK), however the resultant NMR spectra did not reveal any notable differences in the spectra attributable to an impurity (Appendix 2-4).

It is also possible that the differences in the ORD spectra seen with HPMC 8000 relative to HPMC 11000 and 15000 could be due to a different substitution pattern. This hypothesis could be checked by degrading the three polymers using sonication (Goodwin 2006), to a similar molecular weight and measuring the ORD of the degraded polymers. This experiment was not performed in the present study.

Unfortunately, the HPMCAS polymer solutions were unsuitable for spectroscopy due to the turbidity of the solutions, which arose because HPMCAS is not entirely soluble in water or even in the presence of 10 mM sodium citrate.

3.3.3 Surfactant adsorption isotherms

3.3.3.1 Adsorption of anionic surfactant onto griseofulvin nanoparticles: effect of surfactant concentration and non-ionic polymer HPMC 8000

The adsorption isotherm of an anionic surfactant (either SDS or AOT) on griseofulvin nanoparticles as a function of starting surfactant concentration (i.e. the surfactant concentration used to mill the sample - 0.05-10% w/w) in the absence and presence of a constant amount of the non-ionic polymer, HPMC 8000 (namely 1.88% w/w, i.e. the starting concentration), has been determined.

Surfactant only systems

The lowest starting concentration of anionic surfactant (either SDS or AOT) that could produce stable grisofulvin nanoparticles was determined to be 0.25% w/w (Tables 3.1 and 3.2). Although surfactant adsorption on the griseofulvin particles may have occurred at concentrations below this limiting concentration, the amount of surfactant present was obviously not sufficient to coat the particles and prevent their subsequent aggregation.

Table 3.1: SDS adsorption parameters on griseofulvin nanoparticles prepared by 6 h milling in presence of varying starting surfactant concentrations (n = 3 ± s.d.). The three rows of data per formulation represent results obtained from three separate nanosupension formulations.

Formulation – starting concentration	**Surface area (m^2)**	**SDS in supernatant (%w/w)**	**SDS adsorbed (%w/w)**	**SDS adsorbed (mg/g)**	**SDS adsorbed (mg/m^2)**	**Average SDS adsorbed (mg/m^2)**
10.0% w/w SDS	96.7	9.575	0.425	4.25	2.197	2.285 ± 0.11
	97.97	9.561	0.439	4.39	2.245	
	95.66	9.538	0.462	4.62	2.233	
5.0% w/w SDS	128.51	4.426	0.574	5.74	2.34	2.224 ± 0.12
	126.73	4.407	0.593	5.93	2.1	
	130.17	4.451	0.549	5.49	2.168	
2.0% w/w SDS	152.53	1.329	0.671	6.71	2.2	2.079 ± 0.12
	147.83	1.385	0.615	6.15	2.08	
	148.2	1.42	0.58	5.8	1.957	
1.5% w/w SDS	146.93	0.909	0.591	5.91	2.011	2.085 ± 0.07
	150.03	0.856	0.644	6.44	2.146	
	151.46	0.865	0.635	6.35	2.096	
1.0% w/w SDS	154.12	0.51	0.49	4.9	1.59	1.628 ± 0.03
	158.08	0.478	0.522	5.22	1.651	
	155.4	0.489	0.511	5.11	1.644	
0.5% w/w SDS	155.12	0.222	0.273	2.78	0.895	0.986 ± 0.08
	150.42	0.191	0.309	3.09	1.029	
	150.47	0.189	0.311	3.11	1.033	
0.25% w/w SDS	133.34	0.087	0.163	1.63	0.613	0.627 ± 0.02
	136.34	0.073	0.177	1.77	0.65	
	133.26	0.085	0.165	1.65	0.619	

Table 3.2: AOT adsorption parameters on griseofulvin nanoparticles prepared by 6 h milling in presence of varying starting surfactant concentrations (n = 3 ± s.d.). The three rows of data per formulation represent results obtained from three separate nanosupension formulations.

Formulation – starting concentration	**Surface area (m^2)**	**AOT in supernatant (%w/w)**	**AOT adsorbed (%w/w)**	**AOT adsorbed (mg/g)**	**AOT adsorbed (mg/m^2)**	**Average AOT adsorbed (mg/m^2)**
5.0% w/w AOT	127.1	4.449	0.551	5.51	2.168	2.272 ± 0.16
	126.69	4.377	0.623	6.23	2.459	
	124.7	4.454	0.546	5.46	2.188	
2.0% w/w AOT	155.06	1.358	0.642	6.42	2.069	2.021 ± 0.06
	152.3	1.403	0.597	5.97	1.96	
	150.36	1.388	0.612	6.12	2.035	
1.5% w/w AOT	158.21	0.951	0.549	5.49	1.733	1.847 ± 0.11
	154.19	0.929	0.571	5.71	1.851	
	151.58	0.907	0.593	5.93	1.957	
1.0% w/w/ AOT	155.23	0.597	0.403	4.03	1.298	1.345 ± 0.09
	158.76	0.590	0.410	4.10	1.293	
	152.48	0.560	0.440	4.40	1.44	
0.5% w/w AOT	159.93	0.238	0.262	2.62	0.818	0.874 ± 0.06
	162.52	0.196	0.304	3.04	0.936	
	164.07	0.215	0.285	2.85	0.868	
0.25% w/w AOT	140.26	0.068	0.182	1.82	0.649	0.692 ± 0.04
	143.26	0.045	0.205	2.05	0.716	
	142.83	0.047	0.203	2.03	0.711	

When the amount of surfactant adsorbed was plotted against the initial concentration of surfactant, a typical 'Somasundaran–Fluerstenau' ionic surfactant isotherm (Somasudaran et al, 1997) was obtained for both surfactants on the griseofulvin nanoparticles (Figures 3.14 (for SDS) and 3.15 (for AOT)).

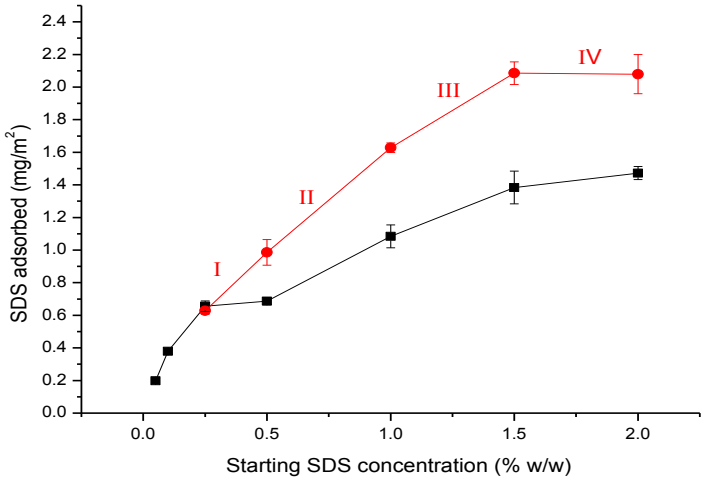

Figure 3.14: SDS adsorption isotherms on griseofulvin nanoparticles prepared by 6 h milling in the absence (●) and in the presence (■) of the non-ionic polymer, HPMC 8000, starting concentration 1.88% w/w (n = 3 ± s.d.).

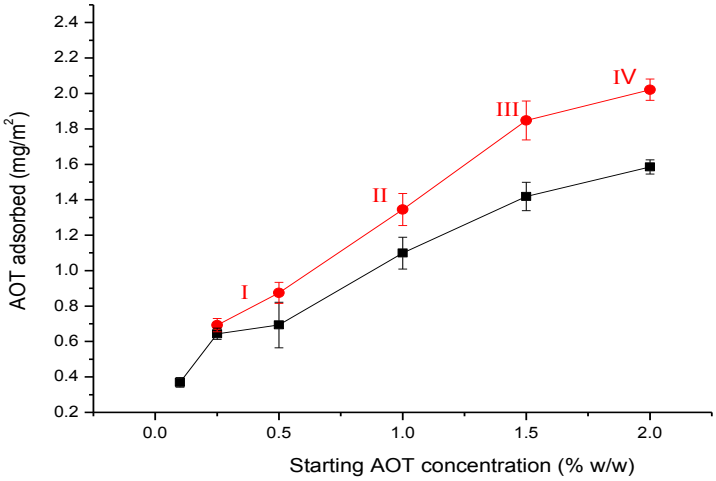

Figure 3.15: AOT adsorption isotherms on griseofulvin nanoparticles prepared by 6 h milling in the absence (●) and in the presence (■) of the non-ionic polymer, HPMC 8000, starting concentration (n = 3 ± s.d.).

The four regions of the Somasundaran-Fluerstenau adsorption isotherm (section 1.3.1), characteristic of a charged surfactant adsorbing onto an oppositely charged surface, could be observed in Figures 3.14 and 3.15. Region I, which occurs at the lowest surfactant concentrations, is characterised by a linear increase in surfactant

adsorption with concentration. In this region absorption is governed by electrostatic interactions between surfactant head group and the drug surface. Following this is Region II where there is a sudden increase in surfactant adsorption attributable to the formation of surface aggregates. In Region III there is a reduction in surfactant adsorption due to the electrical neutralization of the absorbing surface causing repulsion to the adsorption of more surfactant. At this stage in the adsorption isotherm, the lateral attractive forces between the surfactant molecules prevail. In Region IV the maximum amount of surfactant has been adsorbed and this region is characterised by the formation of a plateau. Griseofulvin is however a neutral compound; thus electrostatic interactions are unlikely to be driving to the surfactant adsorption. Instead the surfactants may be adsorbing with their tails onto the drug surfaces with the charged surfactant head groups stabilising the nanoparticles.

The amount of surfactant adsorbed onto the griseofulvin nanoparticles was similar for both surfactants, with maximum values for surfactant absorption of ~ 2.2 mg/m^2 being obtained. The area per surfactant molecule when adsorbed onto the drug nanoparticle was calculated in order to determine the likely conformation of the surfactant on the nanoparticle surface. The calculations used for determination of area per absorbed surfactant molecule are described in Appendix 5. Tables 3.3 and 3.4 show the areas per adsorbed surfactant molecule calculated for SDS and AOT, respectively when adsorbed on the surface of the griseofulvin nanoparticles. Surface tension measurements (2.3.2.2) determined that the area per molecule occupied by the surfactant when in a surfactant monolayer at the air-liquid interface – established to be 90 and 53 $Å^2$ for AOT and SDS, respectively. From the calculated surfactant area per molecule on the nanoparticle surfaces it is possible to postulate the conformation of the adsorbed surfactant molecules at the nanoparticle surfaces. Figures 3.16a and b give the possible adsorption mechanisms of SDS and AOT respectively onto griseofulvin nanoparticles.

Table 3.3: Area per adsorbed SDS molecule on griseofulvin nanoparticles prepared by 6 h milling in the absence and presence of 1.88% w/w of the non-ionic polymer, HPMC 8000 (n = 3).

Formulation (starting concentration in % w/w)	**Area per surfactant molecule ($Å^2$) without 1.88% w/w HPMC 8000**	**Area per surfactant molecule ($Å^2$) with 1.88% w/w HPMC 8000**
10.0% SDS	21	26.5
5.0% SDS	21.5	30.7
2.0% SDS	23	32.5
1.5% SDS	23	34.6
1.0% SDS	29.4	44.2
0.5% SDS	48.6	69.7
0.25% SDS	76.4	73
0.1% SDS	NF	126.4
0.05% SDS	NF	243.1

NF = not formed – no stable nanoparticles produced

Table 3.4: Area per adsorbed AOT molecule on griseofulvin nanoparticles prepared by 6 h milling in the absence and presence of the 1.88% w/w non-ionic polymer, HPMC 8000 (n = 3).

Formulation (starting concentration in % w/w)	**Area per surfactant molecule ($Å^2$) without 1.88% w/w HPMC 8000**	**Area per surfactant molecule ($Å^2$) with 1.88% w/w HPMC 8000**
5.0% AOT	32.5	44.1
2.0% AOT	36.5	46.6
1.5% AOT	40	52.2
1.0% AOT	54.9	70.2
0.5% AOT	84.5	106.4
0.25% AOT	106.7	114.8
0.1% AOT	NF	200.1

NF = not formed – no stable nanoparticles produced

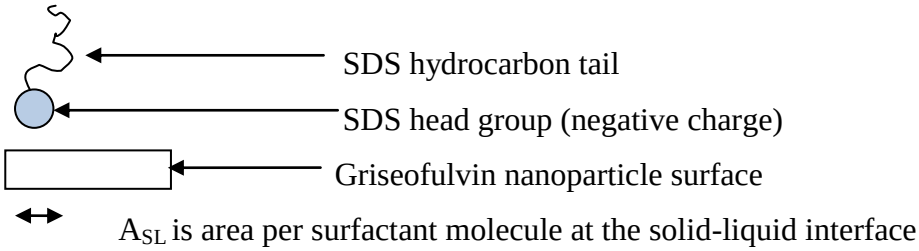

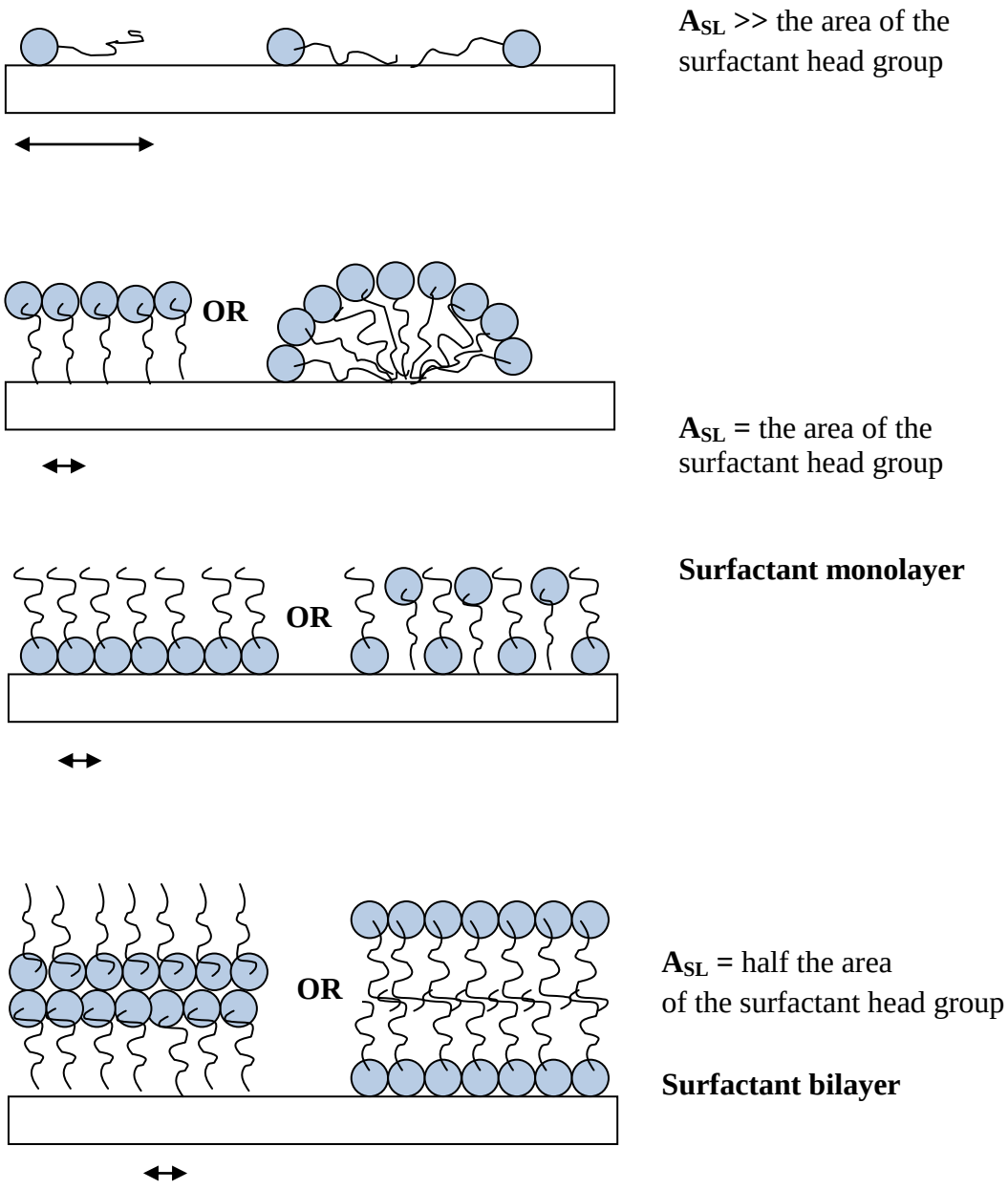

Figure 3.16 (a): Schematic diagram illustrating the proposed adsorption mechanism of SDS on griseofulvin nanoparticle surfaces with increasing surfactant adsorption.

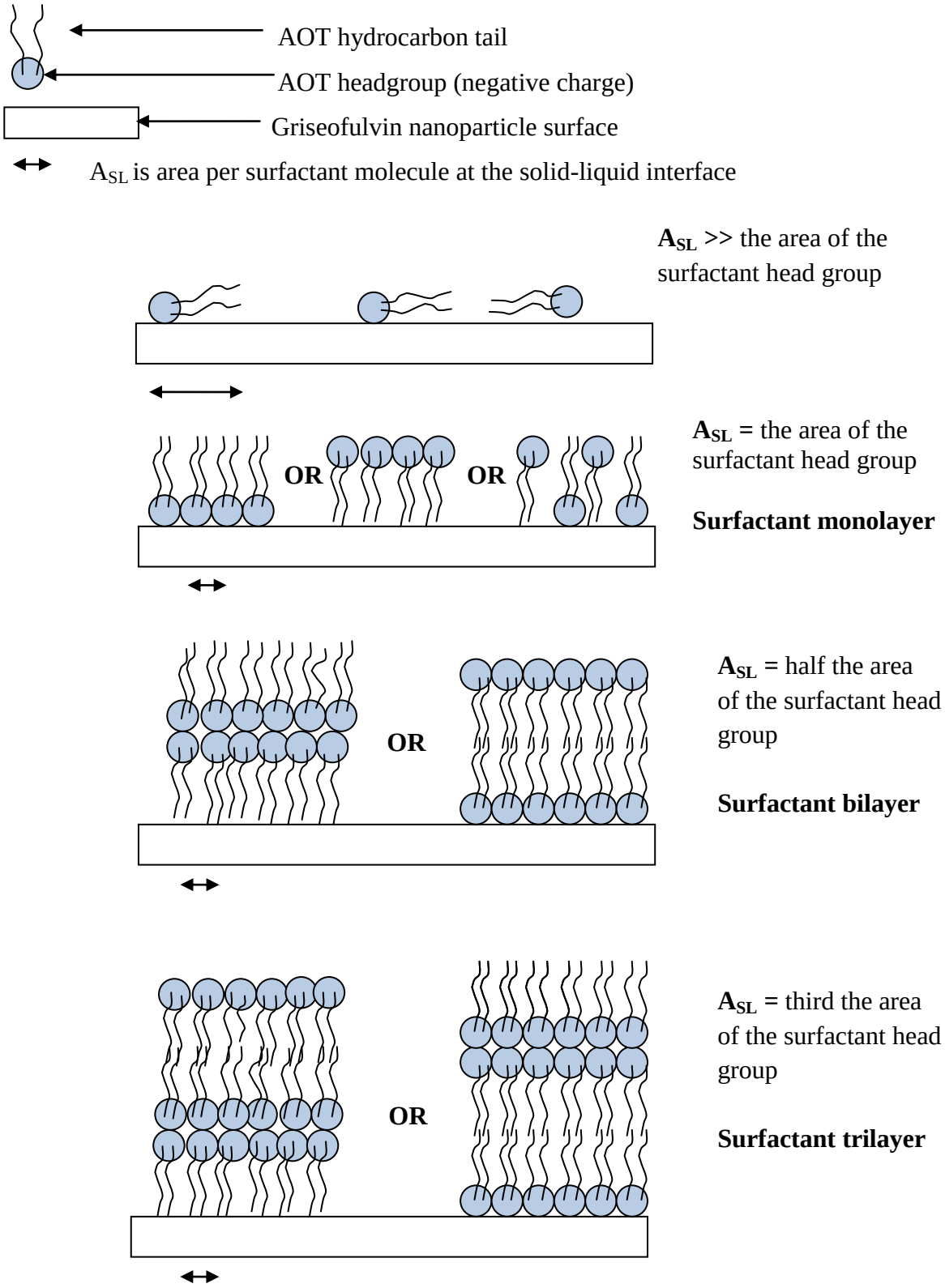

Figure 3.16 (b): Schematic diagram illustrating the proposed adsorption mechanism of AOT on griseofulvin nanoparticle surfaces with increasing surfactant adsorption.

At low levels of AOT or SDS adsorption (i.e. a starting surfactant concentration of 0.25% w/w), the area occupied by each surfactant molecule is greater than that of the cross sectional area of the surfactant at the air-water interface indicating a relaxed orientation of the surfactant with, most likely, the surfactant tails lying parallel or close to the surface of the griseofulvin nanoparticle. From a comparison of the area per molecule when the surfactants are close packed at the air-water interface (Table 2.6), the formation of a surfactant monolayer at the solid-liquid interface on the griseofulvin nanoparticles was considered to occur at surfactant concentrations of ~ 0.5% w/w AOT or SDS. It is thought that a surfactant monolayer is formed either by the charged surfactant head groups absorbing directly onto the griseofulvin surface such that the surfactant tails are orientated perpendicular to the solid-liquid interface or by the tail groups of the surfactant absorbing directly into the surface, or possibly the surfactant molecules adsorbing with head groups and hydrocarbon chains alternately anchoring on the drug surface. Another scenario that would lead to surfactant area per molecule equal to that of a surfactant monolayer is formation of hemi-micelles (assuming the surfactant is tightly packed within the hemi-micelle) with the hydrophobic surfactant chains anchored onto the drug surface. While the formation of hemimicelles is a possibility in the case of SDS, it is less likely to be the case with AOT, which forms bilayers as opposed to micelles when dispersed in water. At present, it is not possible to determine which scenario is correct.

The calculated area per surfactant molecule on the griseofulvin nanoparticles was found to decrease upon increasing surfactant adsorption, probably due to repulsion between the surfactant head groups. At the highest starting surfactant concentrations of between 1.5-10.0% w/w, the calculated area per surfactant molecule on griseofulvin nanoparticles is about half and a third of the values obtained for SDS and AOT, respectively, when the surfactant molecules are close packed at the air-water interface. This result possibly indicates the formation of surfactant bilayers and trilayers on the surface of the SDS and AOT-stabilised griseofulvin nanoparticles respectively. Knowledge of the packing of surfactant molecules at a drug surface can help predict the thickness of the adsorbed layer, for example when a monolayer of surfactant is present, the thickness of the layer will be approximately equal to the length of the surfactant molecule, while when a bilayer is present, the layer thickness will be approximately double that thickness.

As can be seen from Tables 3.1-3.2 the amount of surfactant remaining in the supernatant after its' adsorption onto the drug particles is, in most cases, greater than the cmc of the surfactants' (i.e. 0.107% w/w and 0.128% w/w for AOT and SDS, respectively). The presence of surfactant micelles in the drug nanosuspensions may be expected to promote drug solubilisation and lead to Ostwald ripening as observed in section 2.3.8.

Polymer-surfactant systems

Notable differences were observed in the adsorption of anionic surfactant onto the griseofulvin nanoparticles when milled in the presence of a starting concentration of 1.88% of the non-ionic polymer, HPMC 8000, compared to when griseofulvin was milled in the absence of polymer (Figures 3.14 and 3.15). Interestingly both anionic surfactants, once again behaved in a similar manner to each other.

Firstly, in the presence of the non-ionic polymer, HPMC 8000, griseofulvin nanoparticle production occurred at surfactant concentrations lower than the minimum effective surfactant concentration of 0.25% w/w determined with the surfactant only formulations. At low surfactant concentrations, namely 0.05, 0.1 % w/w SDS and 0.1% w/w AOT, virtually all of the surfactant present was adsorbed on the griseofulvin nanoparticles (Tables 3.5, 3.6). Nanoparticle stabilisation at these lower surfactant concentrations was only seen when the nanoparticles were prepared in the presence of non-ionic polymer, suggesting that polymer-surfactant co-adsorption is occurring at the griseofulvin nanoparticle surface. Indeed surface tension studies in section 2.3.2.2 revealed the presence of polymer surfactant interactions at the air-liquid interface, and thus we can also expect a corresponding interaction at the solid-liquid interface.

Table 3.5: SDS adsorption parameters on griseofulvin nanoparticles prepared by 6 h milling in presence of varying starting surfactant concentrations and non-ionic polymer (1.88% w/w HPMC 8000) (n =3 ± s.d.). The three rows of data per formulation represent results obtained from three separate nanosupension formulations. Table continued on next page.

Formulation (starting concentration in % w/w)	**Surface area (m^2)**	**SDS in supernatant (%w/w)**	**SDS adsorbed (%w/w)**	**SDS adsorbed (mg/g)**	**SDS adsorbed (mg/m^2)**	**Average SDS adsorbed (mg/m^2)**
1.88% HPMC 8000 + 10.0% SDS	95.15	9.641	0.359	3.59	1.886	1.809 ± 0.07
	96.24	9.656	0.344	3.44	1.787	
	93.23	9.673	0.327	3.27	1.754	
1.88% HPMC 8000 + 5.0% SDS	138.06	4.568	0.432	4.32	1.564	1.559 ± 0.03
	134.11	4.591	0.409	4.09	1.525	
	140.93	4.552	0.448	4.48	1.589	
1.88% HPMC 8000 + 2.0% SDS	138.59	1.587	0.413	4.13	1.490	1.472 ± 0.04
	140.19	1.58	0.42	4.2	1.498	
	137.3	1.608	0.392	3.92	1.428	
1.88% HPMC 8000 + 1.5% SDS	140.67	1.138	0.362	3.62	1.287	1.384 ± 0.10
	138.87	1.171	0.383	3.83	1.379	
	137.57	1.091	0.409	4.09	1.486	
1.88% HPMC 8000 + 1.0% SDS	147.46	0.659	0.341	3.41	1.156	1.084 ± 0.07
	146.57	0.69	0.3	3	1.023	
	144.72	0.694	0.31	3.1	1.071	
1.88% HPMC 8000 + 0.5% SDS	164.59	0.27	0.230	2.3	0.698	0.687 ± 0.02
	166.18	0.266	0.234	2.34	0.703	
	163.16	0.284	0.216	2.16	0.661	
1.88% HPMC 8000 + 0.25% SDS	132.66	0.075	0.175	1.75	0.661	0.656 ± 0.03
	136.79	0.063	0.187	1.87	0.685	
	132.69	0.085	0.165	1.65	0.622	

Table 3.5: SDS adsorption parameters on griseofulvin nanoparticles prepared by 6 h milling in presence of varying starting surfactant concentrations and non-ionic polymer (1.88% w/w HPMC 8000) (n =3 ± s.d.). The three rows of data per formulation represent results obtained from three separate nanosupension formulations. Table continued from previous page.

Formulation (starting concentration in % w/w)	**Surface area (m^2)**	**SDS in supernatant (%w/w)**	**SDS adsorbed (%w/w)**	**SDS adsorbed (mg/g)**	**SDS adsorbed (mg/m^2)**	**Average SDS adsorbed (mg/m^2)**
1.88% HPMC 8000 + 0.1% SDS	127.06	0.009	0.091	0.91	0.359	0.379 ±0.02
	129.53	0.001	0.099	0.99	0.383	
	127.09	0.0	0.1	1.0	0.393	
1.88% HPMC 8000 + 0.05% SDS	123.48	0.003	0.047	0.47	0.191	0.197 ±0.01
	126.05	0.0	0.05	0.5	0.198	
	123.52	0.0	0.05	0.5	0.202	

Table 3.6: AOT adsorption parameters on griseofulvin nanoparticles prepared by 6 h milling in presence of varying starting surfactant concentrations and non-ionic polymer (1.88% w/w HPMC 8000) (n =3 ± s.d.). The three rows of data per formulation represent results obtained from three separate nanosupension formulations.

Formulation (starting concentration in % w/w)	**Surface area (m^2)**	**AOT in supernatant (%w/w)**	**AOT adsorbed (%w/w)**	**AOT adsorbed (mg/g)**	**AOT adsorbed (mg/m^2)**	**Average AOT adsorbed (mg/m^2)**
1.88% HPMC 8000 + 5.0% AOT	105.9	4.618	0.382	3.82	1.804	1.673 ± 0.15
	107	4.677	0.323	3.23	1.509	
	104.29	4.644	0.356	3.56	1.707	
1.88% HPMC 8000 + 2.0% AOT	118.20	1.627	0.373	3.73	1.578	1.585 ± 0.04
	115.75	1.642	0.358	3.58	1.547	
	119.20	1.612	0.388	3.88	1.628	
1.88% HPMC 8000 + 1.5% AOT	126.28	1.175	0.325	3.25	1.285	1.415 ± 0.08
	123.59	1.153	0.347	3.47	1.404	
	121.73	1.175	0.325	3.25	1.333	
1.88% HPMC 8000 + 1.0% AOT	135.76	0.709	0.291	2.91	1.072	1.052 ± 0.07
	134.08	0.701	0.229	2.99	1.113	
	130.56	0.746	0.254	2.54	0.972	
1.88% HPMC 8000 + 0.5% AOT	153.27	0.331	0.169	1.69	0.551	0.694 ± 0.13
	147.67	0.285	0.215	2.15	0.729	
	154.27	0.253	0.247	2.47	0.801	
1.88% HPMC 8000 + 0.25%	136.48	0.08	0.170	1.7	0.624	0.643 ± 0.03
AOT	136.66	0.064	0.186	1.86	0.68	
	138.93	0.076	0.174	1.74	0.626	
1.88% HPMC 8000 + 0.1% AOT	123.22	0.014	0.086	0.86	0.35	0.369 ± 0.03
	125.01	0.0	0.1	1.0	0.4	
	125.47	0.01	0.09	0.9	0.359	

Interestingly, at the surfactant concentration that griseofulvin nanoparticles were prepared in the absence of polymer, namely 0.25% w/w, the amount of surfactant adsorbed was similar to that seen in the presence of polymer, possibly suggesting that the polymer was being adsorbed onto a pre-adsorbed surfactant layer on the griseofulvin nanoparticles.

In the presence of polymer, a short plateau in the level of surfactant adsorption was observed at a surfactant concentration of between 0.25-0.5% w/w. This plateau could be indicative of the formation of a monolayer of absorbate, possibly consisting of polymer/surfactant complexes. Upon further increasing the surfactant concentration, there was a further increase in surfactant adsorption before another plateau was reached at surfactant concentrations greater than 1.5% w/w. The second plateau is likely to be a consequence of the formation of layers of surfactant and polymer on the drug surface. The adsorption of surfactant on griseofulvin nanoparticles from polymer-surfactant systems was consistently lower than surfactant adsorption from surfactant only systems suggestive of the simultaneous adsorption of the polymer and surfactant. Simultaneous polymer-surfactant adsorption was also seen by Sakagami et al (2002) who studied the adsorption of poly (1-vinylpyrrolidone-co-acrylic acid) and SDS onto positively charged alumina.

The area per surfactant molecule calculated for the griseofulvin nanoparticles prepared using a mixture of polymer and surfactant was higher than that obtained in the corresponding surfactant only system (Tables 3.3 and 3.4) suggesting a more relaxed conformation of the surfactant, possibly due to a reduction in the repulsion between the surfactant head groups in the presence of co-adsorbed polymer. However, as before, the area per surfactant molecule at the nanoparticle surface decreased with an increase in the surfactant starting concentration, corresponding to a higher level of surfactant adsorption. The dramatic decrease in the area per surfactant molecule at the highest levels of surfactant adsorption, points towards the possible formation of surfactant multilayers on the surface of the griseofulvin nanoparticles, even in the presence of polymer.

3.3.3.2 Adsorption of anionic surfactant onto griseofulvin nanoparticles: effect of non-ionic polymer molecular weight

The variation of the amount of SDS adsorbed on griseofulvin nanoparticles prepared using 0.5% SDS, both in absence and presence of an increasing concentration of either HPMC 8000 and HPMC 15000 was investigated.

As can be seen from Tables 3.7-3.8, the amount of SDS adsorbed on the nanoparticles was less in the presence of polymer than in its absence, suggestive of the simultaneous adsorption of surfactant and polymer. Surface tension studies in section 2.3.2.2 revealed polymer surfactant interactions at the air-liquid interface, thus it is not unreasonable to propose a similar interaction between the surfactant and polymer at the solid-liquid interface. It is worth noting however, that regardless of polymer molecular weight, HPMC when used as sole stabiliser did not adsorbed onto griseofulvin and therefore did not allow the production of griseofulvin nanoparticles (section 2.3.1).

Table 3.7: SDS adsorption parameters on griseofulvin nanoparticles prepared by 6 h milling at a constant surface concentration of 0.5 % w/w SDS and in the presence of varying concentrations of the non-ionic polymer, HPMC 8000 (n = 3 ± s.d.). The three rows of data per formulation represent results obtained from three separate nanosupension formulations. Table continued on next page.

Formulation (starting concentration in % w/w)	**Surface area (m^2)**	**SDS in supernatant (%w/w)**	**SDS adsorbed (%w/w)**	**SDS adsorbed (mg/g)**	**SDS adsorbed (mg/m^2)**	**Average SDS adsorbed (mg/m^2)**
5% HPMC 8000 + 0.5% SDS	87.29	0.417	0.083	0.83	0.477	0.431 ± 0.05
	90.4	0.422	0.078	0.78	0.43	
	91.79	0.43	0.07	0.7	0.384	
2.5% HPMC 8000 + 0.5% SDS	136.28	0.327	0.173	1.73	0.636	0.653 ± 0.04
	132.99	0.333	0.167	1.67	0.627	
	134.83	0.312	0.188	1.88	0.696	
1.88% HPMC 8000 + 0.5% SDS	164.59	0.27	0.23	2.3	0.698	0.687 ± 0.02
	166.18	0.266	0.234	2.34	0.703	
	163.16	0.284	0.216	2.16	0.661	
1.5% HPMC 8000 + 0.5% SDS	166.38	0.27	0.23	2.3	0.69	0.696 ± 0.01
	169.32	0.262	0.238	2.38	0.702	
	167.74	0.266	0.234	2.34	0.696	
1.0% HPMC 8000 + 0.5% SDS	172.87	0.27	0.23	2.3	0.664	0.716 ± 0.05
	171.01	0.254	0.246	2.46	0.718	
	173.67	0.234	0.266	2.66	0.765	
0.5% HPMC 8000 + 0.5% SDS	178.95	0.224	0.276	2.76	0.77	0.789 ± 0.02
	175.97	0.22	0.28	2.8	0.794	
	175.3	0.218	0.282	2.82	0.803	

Table 3.7: SDS adsorption parameters on griseofulvin nanoparticles prepared by 6 h milling at a constant surface concentration of 0.5 % w/w SDS and in the presence of varying concentrations of the non-ionic polymer, HPMC 8000 (n = 3 ± s.d.). The three rows of data per formulation represent results obtained from three separate nanosupension formulations. Table continued from previous page.

Formulation (starting concentration in % w/w)	**Surface area (m^2)**	**SDS in supernatant (%w/w)**	**SDS adsorbed (%w/w)**	**SDS adsorbed (mg/g)**	**SDS adsorbed (mg/m^2)**	**Average SDS adsorbed (mg/m^2)**
0.1% HPMC 8000 + 0.5% SDS	158.82	0.198	0.302	3.02	0.949	0.978 ± 0.06
	161.75	0.163	0.337	3.37	1.043	
	158.21	0.202	0.298	2.98	0.94	
0.5% w/w SDS	155.12	0.222	0.273	2.78	0.895	0.986 ± 0.08
	150.42	0.191	0.309	3.09	1.029	
	150.47	0.189	0.311	3.11	1.033	

Table 3.8: SDS adsorption parameters on griseofulvin nanoparticles prepared by 6 h milling at a constant surface concentration of 0.5 % w/w SDS and in the presence of varying concentrations of the non-ionic polymer, HPMC 15000 (n = 3 ± s.d.). The three rows of data per formulation represent results obtained from three separate nanosupension formulations.

Formulation (starting concentration in % w/w)	**Surface area (m^2)**	**SDS in supernatant (%w/w)**	**SDS adsorbed (%w/w)**	**SDS adsorbed (mg/g)**	**SDS adsorbed (mg/m^2)**	**Average SDS adsorbed (mg/m^2)**
1.5% HPMC 15000 + 0.5% SDS	86.90	0.408	0.092	0.92	0.527	0.542 ± 0.06
	89.06	0.392	0.108	1.08	0.606	
	87.78	0.414	0.086	0.86	0.490	
1.0% HPMC 15000 + 0.5% SDS	127.36	0.294	0.206	2.06	0.808	0.807 ± 0.05
	124.94	0.308	0.192	1.92	0.769	
	127.88	0.284	0.216	2.16	0.845	
0.5% HPMC 15000 + 0.5% SDS	167.74	0.222	0.278	2.78	0.827	0.858 ± 0.03
	169.04	0.200	0.300	3.0	0.886	
	164.55	0.216	0.284	2.84	0.862	
0.1% HPMC 15000 + 0.5% SDS	158.03	0.204	0.296	2.96	0.935	0.978 ± 0.05
	156.53	0.179	0.321	3.21	1.027	
	157.19	0.194	0.306	3.06	0.972	
0.5% SDS	155.12	0.222	0.273	2.78	0.895	0.986 ± 0.08
	150.42	0.191	0.309	3.09	1.029	
	150.47	0.189	0.311	3.11	1.033	

Regarding the mechanism of adsorption of non-ionic polymer in the presence of anionic surfactant, it can be hypothesized that the negatively charged surfactant and the non-ionic polymer, HPMC, interact in solution to form a polymer-surfactant complex, which is then adsorbed onto the griseofulvin surface. There are several literature reports of surfactant/polymer mixtures altering adsorption profiles, whereby a non adsorbing entity is adsorbed on a surface by the anchoring effect of a co-adsorbent e.g. the non-ionic surfactant, pentadecylethoxylated nonyl phenol (NP15), only adsorbs onto alumina in the presence of the cationic surfactant, tetradecyl trimethyl ammonium chloride (TTAC) (Huang et al, 1996). Similarly the anionic surfactant, SDS, only adsorbs on alumina in the presence of polyethylene oxide (Maltesh et al, 1992) while hydroxypropylcellulose adsorbs on hydroxypatite only in presence of anionic SDS (Shimabayashi et al, 2002).

The amount of SDS adsorbed onto the griseofulvin nanoparticles in presence of the lowest polymer concentration, namely 0.1% w/w HPMC 8000 and 15000, was similar for both polymer molecular weights and similar to the amount of SDS adsorbed in the absence of polymer (Tables 3.7-3.8). As illustrated in Figure 3.17, SDS adsorption on the griseofulvin nanoparticles decreases with increasing polymer concentration. Comparing the two polymers, SDS adsorption tended to be higher on the griseofulvin nanoparticles prepared in presence of the higher molecular weight polymer with the exception of the highest HPMC 15000 concentration of 1.5 %w/w. However, the differences observed in the extent of surfactant adsorption onto the griseofulvin nanoparticles in the presence of the two polymers studied in the present project were not considered significant. Similarly, no polymer molecular weight effects on polymer-surfactant interactions were seen in the surface tension studies. Interestingly, literature reports suggest that, at equilibrium, higher molecular polymers tend to be adsorbed better onto surfaces than their lower molecular weight counterparts (Santhiya et al, 1998; Khraisheh et al, 2005).

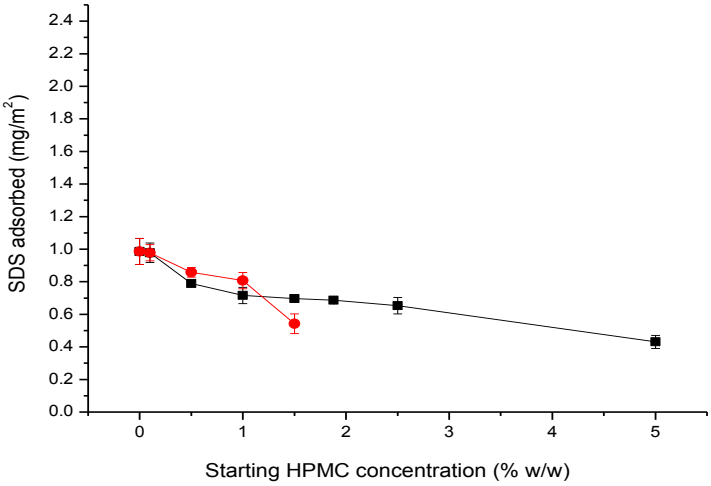

Figure 3.17: SDS adsorption isotherms on griseofulvin nanoparticles prepared by 6 h milling in the presence of varying concentrations of HPMC 8000 (■) and HPMC 15000 (●), SDS concentration kept constant at 0.5% w/w (n = 3 ± s.d.).

Table 3.9 shows the area per surfactant molecule obtained with the different polymer containing formulations. The area of the close packed SDS molecule at the air-water interface, as determined from surface tension measurements, was found to be 53 Å^2 (2.3.2.2) while the area per surfactant molecule calculated for the nanoparticles prepared in presence of 0.5% w/w SDS (no polymer) was very similar, which due to the assumptions made in the calculation is reassuring. In presence of an increasing concentration of polymer, the area per SDS molecule increases, suggesting a less constrained SDS conformation, possibly with the surfactant tails lying parallel to the drug surface. It is likely that the presence of co-adsorbed polymer decreases surfactant repulsion, thereby allowing a greater surface coverage by the surfactant.

Table 3.9: Area per surfactant molecule on griseofulvin nanoparticles prepared by 6 h milling at a constant surfactant concentration of 0.5% w/w SDS and in the presence of varying concentrations of the non-ionic polymers, HPMC 8000 and HPMC 15000 (n = 3).

Formulation (starting concentration in % w/w)	**Area per surfactant molecule ($Å^2$) (SDS / HPMC 8000)**	**Area per surfactant molecule ($Å^2$) (SDS / HPMC 15000)**
0.5% SDS + 10.0% HPMC	NF	NF
0.5% SDS + 5.0% HPMC	111.1	NF
0.5% SDS + 2.5% HPMC	73.3	NF
0.5% SDS + 1.88% HPMC	69.7	NF
0.5% SDS + 1.5% HPMC	68.8	88.4
0.5% SDS + 1.0% HPMC	66.9	59.3
0.5% SDS + 0.5% HPMC	60.7	55.8
0.5% SDS + 0.1% HPMC	49	49
0.5% SDS	48.6	48.6

NF = not formed – no stable nanoparticles produced

In general, the area per SDS molecule calculated was lower in nanoparticles prepared in presence of higher molecular weight polymer HPMC 15000, than those prepared using HPMC 8000. The reason for this finding is the larger surface area/smaller size of the nanoparticles prepared in presence of the lower molecular weight polymer.

3.3.4 Polymer adsorption isotherms

ORD measurements of the supernatants revealed a high level of interference around the wavelength of interest thereby rendering it impossible to determine the concentration of polymer remaining in the supernatant and therefore the amount absorbed onto the surface of the griseofulvin nanoparticle. Figure 3.18 shows the ORD spectra of griseofulvin dissolved in water and in a 1.88% w/w HPMC 8000 aqueous solution, as well as the spectra of supernatants of griseofulvin nanosuspensions prepared in presence of 0.5% w/w SDS, and 0.5% w/w SDS + 1.88% w/w HPMC 8000. (Note that griseofulvin is optically active exhibiting a positive peak in its ORD spectra at between 354 -364 nm (B.P 2010)).

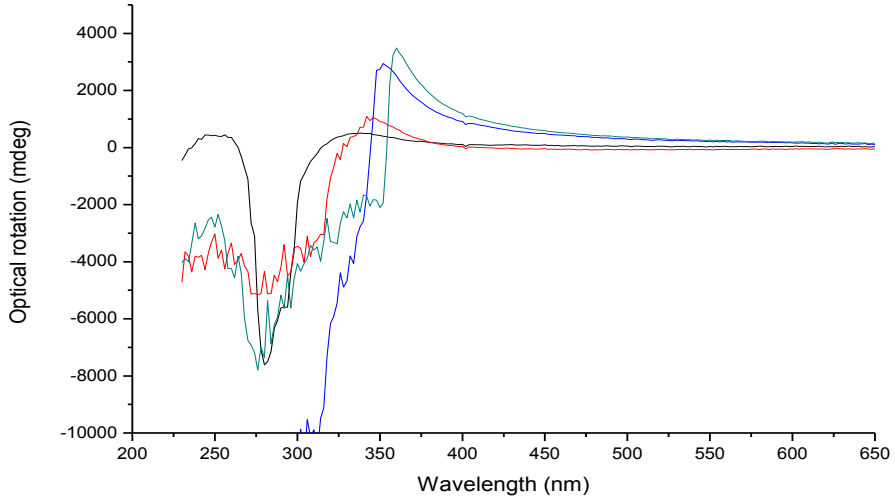

Figure 3.18: ORD spectra of griseofulvin dissolved in water (—), griseofulvin dissolved in an aqueous solution of 1.88% w/w HPMC 8000 (—), supernatant from a griseofulvin nanosuspension prepared using 0.5% w/w SDS (—) and supernatant from a griseofulvin nanosuspension prepared using 0.5% SDS w/w + 1.88% w/w HPMC 8000 (—).

The nature of this interference was further investigated by determining the circular dichroism (CD) of these supernatant systems and comparing them with the spectra obtained for a saturated solution of griseofulvin in water. The CD measurements revealed the presence of griseofulvin in the two supernatants as can be seen in Figure 3.19. Significantly, the amount of griseofulvin detected was higher in the supernatant from the nanoparticle preparation containing polymer, indicating that the polymer was solubilising more drug, probably via means of a polymer-surfactant complex, than could dissolve in water in its absence. This discovery suggested that griseofulvin might not be ideal for formulating as nanoparticles via WBM, - WBM is best for very water-insoluble drugs. The presence of dissolved drug in the various supernatants supports the hypothesis that the formulations might not exhibit a long term stability due to Ostwald ripening – see section 2.3.8.

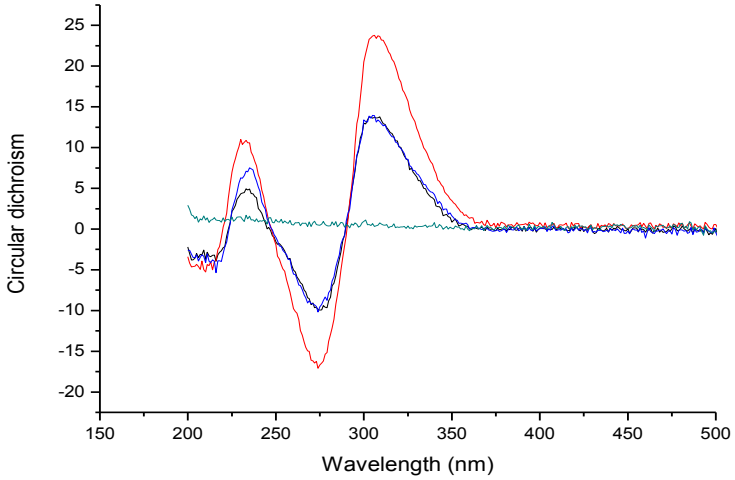

Figure 3.19: CD spectra of an aqueous solution of 2% w/w HPMC 8000 (—), griseofulvin dissolved in water (—), 1:2 diluted supernatant from griseofulvin nanosuspension prepared using 0.5% w/w SDS (—) and 1:10 diluted supernatant from griseofulvin nanosuspension prepared using 0.5% SDS w/w + 1.88% w/w HPMC 8000 (—).

Significantly, nanoparticles of the very water-insoluble drugs, nabumetone and halofantrine, prepared by WBM were stable for one year when stored under similar conditions to those used in the present study (Shadi 2003, Goodwin 2006). In the pharmaceutical industry, as the nanoparticles may be processed into dry powder within a day of preparation, the higher aqueous solubility of griseofulvin might not be a limitation. In addition, it should be realised that the fact that some griseofulvin 'dissolves' introduces a degree of error in the estimation of surface area necessary for the adsorption studies.

A programme of work was instigated to attempt to analyse the concentration of HPMC in the supernatants. This included:

- Liquid-liquid extraction

As griseofulvin is much more soluble in organic solvents than aqueous solvents and HPMC much more soluble in water, attempts were made to extract griseofulvin from the aqueous supernatant solutions using a range of organic solvents, namely chloroform, methylene chloride, pentane, hexane, toluene, diethyl ether, ethyl acetate. However all attempts were unsuccessful due to the surface active nature of the water-soluble polymer, HPMC, which tends to form a film at the liquid-liquid interface (Wollenweber et al, 2000). Attempts to break the HPMC films formed at

the water-organic solvent interface by the addition of electrolyte, changes in temperature and centrifugation were unsuccessful.

- Size exclusion chromatography

Taking advantage of the difference in molecular size between the polymer, surfactant and drug, size exclusion chromatography was investigated as a means of separating the polymer, surfactant and griseofulvin. Using a Sephadex 20 column and a range of solvent systems consisting of water:methanol (100:0, 20:80, 40:60, 80:20, 0:100), supernatants were eluted and the components of each eluent fraction determined. Although the surfactant and polymer were effectively separated, eluting in different fractions, griseofulvin was present in all fractions, possibly due to solubilisation of the drug within polymer and surfactant complexes. It had hoped that the addition of methanol may 'break' the complex but unfortunately when 100% of methanol was used the polymer did not exhibit sufficient solubility in the methanol for the extraction to take place.

- Weighing the freeze dried mass of sample supernatants

The most basic method of measuring adsorption by depletion is to freeze dry the supernatant and weigh the adsorbate remaining in solution. Sample supernatants in the current study were freeze dried and the amounts of surfactant and griseofuvin analytically determined to be present in the supernatant subtracted in order to quantify the amount of polymer in the supernatant. The amounts of surfactant and griseofulvin present were determined by means of the Stains All assay and UV spectroscopy, respectively. Unfortunately, however, the amount of polymer obtained was inaccurate due to very high standard errors and is thus not reported here.

Other techniques used to assay cellulose polymer were considered, although none of these techniques were considered ideal for the current samples.

- Fluorescently labelled polymers

Fluorescent probes such as fluorene, pyrene and fluorescein have been successfully used to label polymers (Winnik et al, 1987, 1989; Ahmed et al, 2001) for assay. However most of these labels impart a partial charge to the labelled polymer. The presence of a slight charge on the polymer chains would alter the polymer's adsorption profile on the drug particles making for erroneous results.

- Colorimetric assays

Previous attempts to quantify HPMC using colorimetric assays were grossly inaccurate due to the polymer molecular weight dependence of this technique (Sepassi 2003).

- High performance liquid chromatography

High performance liquid chromatography (HPLC) has been used to assay cellulosic polymers. However HPLC was unsuitable for the current systems comprising of different polymer molecular weights and the fractionation of polymers that may occur during milling which would make the data analysis extremely complicated. In addition, the presence of surfactant and dissolved griseofulvin in the samples would be a further challenge.

Though it was not possible to obtain polymer adsorption isotherms on the griseofulvin nanoparticles by the depletion method, due to interference by dissolved griseofulvin, the surfactant adsorption isotherms on the drug surfaces are highly suggestive of polymer-surfactant co-adsorption. Small angle neutron scattering experiments presented in Chapter 4 will be used to further investigate the adsorption profiles of polymer and surfactant on the griseofulvin nanoparticles.

3.4 Summary

This chapter presents work aimed at determining the adsorption isotherms of polymer and/or surfactant onto the milled griseofulvin drug nanoparticles by measuring the depletion of polymer and/or surfactant from solution. A colorimetric Stains All assay was used to determine the amount of anionic surfactant left in solution after milling, while optical rotatory dispersion was used to assay HPMC polymer remaining in solution after milling. Unfortunately the HPMCAS adsorption isotherms could not be determined due to the turbid nature of HPMCAS samples making them unsuitable for spectroscopy. The resultant surfactant adsorption isotherms revealed the adsorption of anionic surfactant onto the griseofulvin particle surfaces. Interestingly a characteristic 'Somasundaran-Fluerstenau' isotherm, for ionic surfactant adsorbing onto a surface of opposite charge, was obtained suggesting that electrostatic interactions were driving the adsorption process of SDS and AOT onto the griseofulvin nanoparticles.

Milling results in section 2.3.1 revealed that only anionic compounds (surfactants or polymers) could adsorb onto the surface of griseofulvin particles upon milling and provide effective stabilisation for nanoparticle production. None of the non-ionic or cationic stabilisers tested were effective in stabilising griseofulvin nanoparticles. Crystals of organic solids have been shown to have anisotropic surfaces, with the surface chemistry of each crystal facet being dependent on the differential exposure and concentration of the constituent chemical groups at the surface. Heng et al (2006) reported that milling of crystalline solids exposes the crystal facet with the weakest attachment energy, with the dominance of the surface properties of this facet increasing as particle size is reduced. Recent studies by Shariare et al (2012) have shown that inter-planar d-spacings and the corrugation of lattice slip planes are superior to attachment energy calculations in prediction of the fracture of crystalline material.

The amount of anionic surfactant adsorbed onto the griseofulvin particles increased with increasing starting surfactant concentration in the milling slurry. Calculating the area per surfactant molecule adsorbed on the drug surfaces and comparing it with area per surfactant molecule in the air-water monolayer as determined by surface tension measurements, allowed an assessment of the possible conformation of the surfactant molecules on the surface of griseofulvin. At low levels of surfactant adsorption, the surfactant molecules were considered to be either lying flat on the surface of griseofulvin or forming hemimicelles. As the amount of adsorbed surfactant increased there was formation of a surfactant monolayer and thereafter a surfactant bilayer/trilayer, on the surface of griseofulvin.

When the non-ionic polymer HPMC was included in the milling slurry containing anionic surfactant, the amount of surfactant adsorbed was consistently lower, indicating HPMC and anionic surfactant could be co-adsorbing onto the drug surfaces. In addition the area per surfactant molecule adsorbed onto the drug surfaces was slightly larger in the HPMC-surfactant formulations relative to the surfactant only formulations suggesting a more relaxed conformation of adsorbed surfactant – which we could reasonably assume to be due to presence of non-ionic polymer on the griseofulvin surfaces thus reducing surfactant charge repulsion.

It was not possible to determine the amount of the HPMC adsorbed onto the drug surface by measuring its concentration in the nanosuspension supernatant due to the interference arising from dissolved griseofulvin (which is optically active). However

the differences in the surfactant adsorption isotherms when nanoparticles were prepared in absence/presence of HPMC were suggestive of polymer-surfactant co-adsorption on the surface of griseofulvin. Further investigations into the adsorption of polymer and/or surfactant onto the griseofulvin nanoparticles using small angle neutron scattering will be described in Chapter 4.

Chapter 4
Small angle neutron scattering

4.1 Introduction

Small angle neutron scattering (SANS) is a sophisticated technique, which allows the determination of the size, shape and even orientation of colloidal particles in solution (King 1995). Neutrons can provide structural information on length scales from a fraction of an angstrom to tens of hundreds of angstroms (i.e. from the atomic scale through the macromolecular to the smaller end of the colloidal size range) and is useful for the study of polymers in solution, surfactant micelles, microemulsions

and adsorbed polymer and/or surfactant layers. Furthermore, the exploitation of contrast matching (or the 'neutron' refractive index, explained later) can provide very detailed information about structure/sub-structure in multi component systems.

Although depletion methods are frequently used to investigate the adsorption of polymer/surfactant onto solid surfaces, such methods can only give an indication of the adsorbed amounts of material. SANS on the other hand, allows the elucidation of not only adsorbed amounts but also the thickness and bound fraction of the adsorbate layer and thus provides a more complete picture of adsorption. In addition the volume fraction profile, which is variation in the concentration of adsorbate with distance from the surface, can also be obtained (King et al, 2000).

Numerous reports of SANS investigations into adsorption of polymers or surfactants onto solid particles are available in literature. However these studies are often performed using well characterised, monodisperse small spherical systems such as silica or latex beads. For example Qui et al (2008) studied the adsorption of polyethylene onto colloidal silica particles, while Penfold et al (1996) studied the adsorption of non-ionic surfactants on silica sol particles. SANS adsorption studies on milled particles, which are inherently polydisperse both in size and shape, have not been published.

Previous researchers in our group (Sepassi 2003; Goodwin 2006) successfully utilised SANS to characterise polymer adsorption on nabumetone and halofantrine nanopartices prepared by WBM. In these cases only polymer, namely HPMC, HPC or PVP, was used to stabilise the nanoparticles. In the present study however, a more complicated stabilising system was used consisting of polymer and surfactant, which are assumed to be co-adsorbed onto the griseofulvin nanoparticles. Although the depletion experiments in Chapter 3 confirmed the adsorption of anionic surfactant onto the nanoparticle surfaces, no quantiative results were obtained for polymer adsorption. The overarching aim of this part of the study therefore, was to determine the adsorption isotherm for the non-ionic polymer (HPMC) onto the surface of the griseofulvin nanoparticles. In addition, the absorption of anionic surfactant was also quantified in order to corroborate the results obtained from the depletion experiments. Finally, the thickness of the absorbed layer was established.

4.2 Neutrons and their sources

Neutrons, which were discovered by Chadwick (1932), have a zero charge, a mass of 1.0087 atomic mass units, a spin of 1/2 and a magnetic moment of -1.9132 nuclear magnetons. Each neutron has a half-life of 894 seconds and decays into a proton, an electron and an antineutrino. Neutrons are highly penetrating and are scattered by nuclei in samples, by unpaired electron spins (dipoles) in magnetic samples and reflected from some surfaces - properties which can be used to probe both bulk and surface sample characteristics (Hammouda 1995).

Neutron sources

Neutrons are mainly produced from fission reactors or spallation sources. There are currently about 200 neutron sources in the world across Europe, Asia, Africa and America. Figure 4.1 shows the neutron and X-ray sources in Europe which include ILL and PSI, both of which were used in the present study.

Figure 4.1: Map showing neutron and X-ray sources in Europe as of 2006 (Sinha 2006).

Fission reactors

In a fission reactor, heavy nuclides such as uranium-235 or plutonium-239 are bombarded by a neutron source which leads to fragmentation of the heavy nuclide, releasing fission fragments; gamma rays and fast (high energy) neutrons at 2 MeV. The fission chain reaction continues and thus reactor sources are a continuous flow of neutrons. These fast neutrons are subsequently shielded and slowed to produce cold (low energy) neutrons suitable for experiments.

Reactor sources around the world include HFIR-Oak Ridge National Laboratory, USA, HFBR-Brookhaven National Laboratory, USA, NIST-The National Institute of Standards and Technology, USA, MURR-The University of Missouri, USA, CRNL-Chalk River, Canada, IAE-Beijing, China, DRHUVA-Bombay, India, ILL-Grenoble, France, NLHEP-Tsukuba, Japan, NERF-Petten, The Netherlands, Bhabha ARC Bombay, India, IFF-Julich, Germany, JRR3-Tokai Mura, Japan, KFKI-Budapest, Hungary, HWRR-Chengdo, China, LLB-Saclay, France, HMI-Berlin, Germany and VVR-M Leningrad, Russia.

Spallattion sources

In spallation sources, high energy H^- are produced and linearly accelerated before being spun in a synchrotron to achieve very high energies (500-800 MeV). Once they reach this energy they are used to bombard a neutron rich target e.g. Tungsten-183 or Uranium-238. The result is the production of fast neutrons and few gamma rays. These high energy neutrons are then moderated before being used for experiments. Most spallation sources operate in pulsed mode.

Spallation sources around the world include IPNS-Argonne, USA, ISIS-Rutherford, UK, WNR/PSR LANSCE-Los Alamos, USA, and KENS-Tsukuba, Japan.

4.3 SANS instruments

Steady state instruments (reactor sources)

The main components of a SANS instrument on a steady state (or reactor source) are beam filters to remove unwanted gamma or epithermal neutrons, monochromators to select the wavelengths desired, a collimation chamber to focus the neutron beam, sample chamber with heating/cooling system, evacuated post sample flight path, an area detector and a set of beam stops to prevent the main (unscattered) neutron beam damaging the detector. Advantages of reactor source instruments include

straightforward data analysis and better resolution at high d-spacings (low Q) making such instruments suitable for studying magnetic samples, structures with large unit cells and *ab-initio* structures in solution (Hammouda 1995).

Time of flight instruments (PULSED spallation sources)

Time of flight (TOF) SANS instruments on a pulsed spallation source comprise many of the features described above (including collimation, sample chamber, flight paths, area detector, etc) as well as some specific features such as a source chopper which is used to define the starting neutron pulse and an area detector synchronized to the source chopper so that a number of wavelength frames are recorded for each pulse. No monochromator is necessary with TOF instruments at pulsed spallation sources. Supermirror benders and frame overlap mirrors can be used to remove short and high wavelength neutrons respectively. Prompt gamma rays emitted during the spallation reaction are eliminated by paralyzing the detection system for the first microsecond after each pulse.

Data reduction becomes more complex with TOF instruments since most corrections (transmission, monitor normalization, detector efficiency, linearity, uniformity, etc) are wavelength dependent. Time-of-flight instruments have the advantage, on the other hand, of measuring a wide Q range at the same time. Also the large number of wavelength frames can be kept separate therefore yielding very high wavelength resolution, which is useful for highly ordered scattering structures (Hammouda 1995).

Two steady state instruments were used in the present study namely D11 (ILL, France) and SANS 2 (PSI, Switzerland) are discussed in further detail below.

4.3.1 D11 at Institut Laue-Langevin

D11 at ILL (France) shown in Figures 4.2–4.3 offers the lowest momentum transfer and background of all the world's SANS instruments. D11 receives neutrons from the vertical cold source of the ILL high flux reactor, which is situated about 100 m from the first part of the instrument (the selector) and about 140 m from the sample position. The detector is hence in a very low background environment.

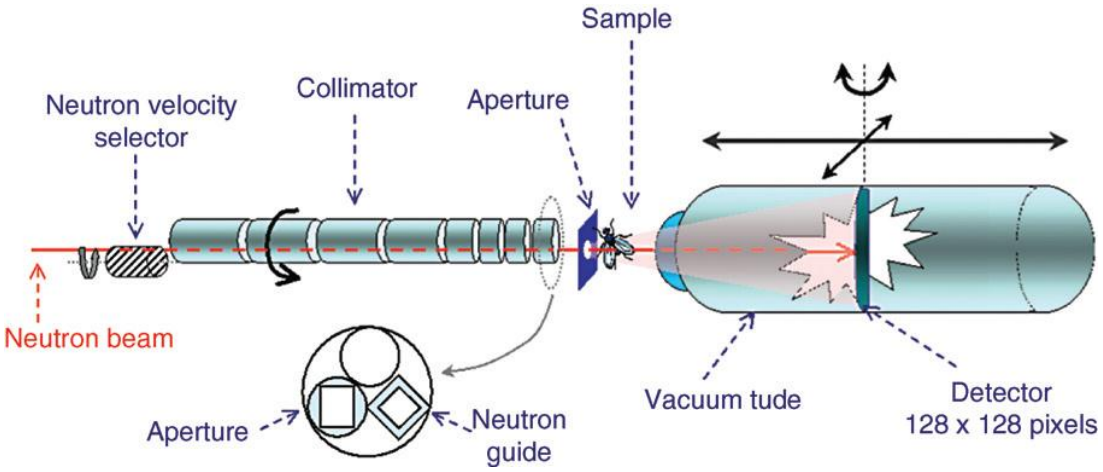

Figure 4.2: Geometry of a continuous source diffractometer, D11 at the ILL, France

The polychromatic beam from the cold source is monochromated by a helical slot (ASTRIUM) velocity selector, which selects neutrons of ± 9 % about a mean wavelength determined by the rotation speed of the drum. The neutrons are then collimated by a series of moveable glass guides. Guide sections are inserted into or removed from the beam depending on the incident beam divergence required. The sample zone, situated 40 m down-stream from the velocity selector, may be equipped with various sample environments such as an automatic temperature controlled sample changer, cryostat, magnet, shearing cell, Bohlin rheometer, dilution refrigerator, horizontal sample-changer under vacuum, etc.

Neutrons scattered from the sample are detected on a 96 x 96 cm^2 CERCA ^3He multi-detector mounted on a moveable trolley within the evacuated detector tube. The detector may be placed at any distance between 1.2 and 39 m from the sample position, giving a total accessible momentum transfer range of 0.0003 to 0.1 Å (D11 characteristics, ILL website).

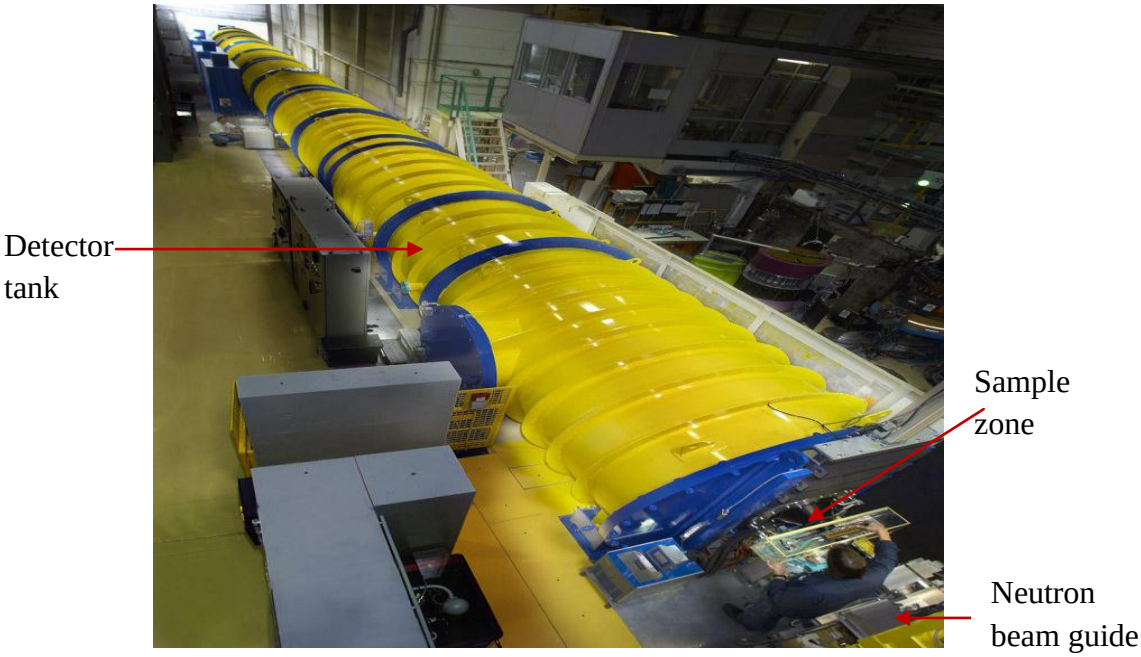

Figure 4.3: Photograph of the D11 instrument. Picture courtesy of ILL, France

4.3.2 SANS 2 at Paul Scherrer Institut

SANS 2 at PSI (Switzerland) shown in Figure 4.4 is one of the SANS instruments at the SINQ beam line, a *continous* spallation source, the first of its kind worldwide. The incoming neutrons are monochromized by a mechanical velocity selector to produce a neutron wavelength range of 4.5 - 20 Å. Collimation is performed in the six meter long collimation section, consisting of one fixed and five moveable one-meter sections allowing the neutron source pin-hole to be moved from one to six meters in steps of one meter away from the sample position. The whole system, i.e. collimators, sample chamber and detector tank can be operated in a single vacuum system without windows in order to lower background.

Scattered neutrons are detected on an area-sensitive multi-wire proportional neutron detector of 64 cm diameter and 128×128 pixels. The detector can be moved continuously from one to six meters away from the sample position. The accessible momentum range is 0.002 – 0.35 $Å^{-1}$ (SANS 2 characteristics, PSI website).

Figure 4.4: Photograph of the SANS 2 instrument. Picture courtesy of the PSI, Switzerland.

4.4 SANS in comparison with other techniques

Various forms of radiation scatter energy (Table 4.1) and can be used for experimental investigations. The choice of technique in a particular experiment is guided by structure, shape, size of domains of sample of interest.

Table 4.1: Characteristics of the various radiations used in scattering experiments (Hammouda 1995)

Radiation type	Light	X-Rays	Neutrons	Electrons
λ range	1 μm	0.1-5 Å	1-15 Å	0.1 Å
Probe	Refractive index	Electron density	Neutron density	Electron cloud
Scattering methods	Static light scattering	Small angle X-ray scattering	Small angle neutron scattering	Low-energy electron diffraction
Sample thickness	1-5 mm	< 1 mm	1-2 mm	100um
Problems	Dust scattering	Absorption, destructive	Low fluxes	Low penetration

Neutron scattering offers a range of advantages over other scattering techniques including a high penetration of most elements allowing the study of bulk properties, its non destructive nature allowing repetitive measurements and scattering length densities independent of atomic number leading to isotope effects e.g. deuterium hydrogen scattering differences (Figure 4.5). The differential ability of hydrogen and

deutrium to scatter neutrons (scattering length of D^2 is $0.6674e^{12}$ cm^{-1} as opposed to $-0.3741e^{12}$ cm^{-1} for H^1) is often used for contrast matching. Experimentally, there is no need to clarify SANS samples and opaque samples can be studied.

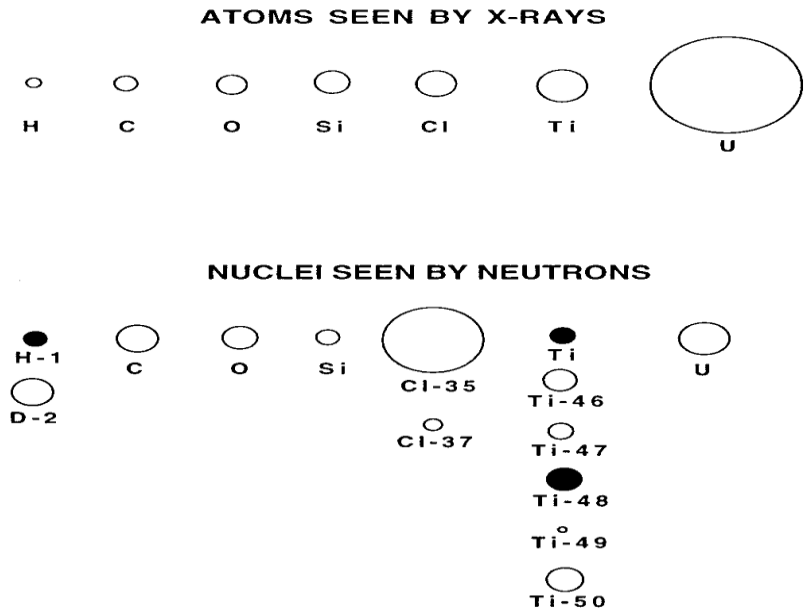

Figure 4.5: Neutrons are scattered from nuclei while X-rays are scattered from electrons. Scattering lengths for a few elements relevant to polymers are compared. Ti and U have also been included. Negative neutron scattering lengths are represented by dark circles (Hammouda 1995).

Disadvantages of SANS include the expense involved in building and maintaining neutron facilities as well as the expense of deuterating samples, low neutron fluxes from these facilities as well the need for relatively large volume of samples. Highly concentrated samples are liable to multiple scattering thereby making data analysis more difficult.

4.5 SANS theory and measurements

4.5.1 Scattering vector

When neutrons come into contact with a sample they may undergo one of a series of events, including absorption, multiple, coherent or incoherent scattering, or be transmitted through the sample. Figure 4.6 shows the coherent scattering of neutrons

through a sample. The scattering vector (or momentum transfer) is the modulus of the resultant between the incident and the scattered wave vectors (King et al, 2000).

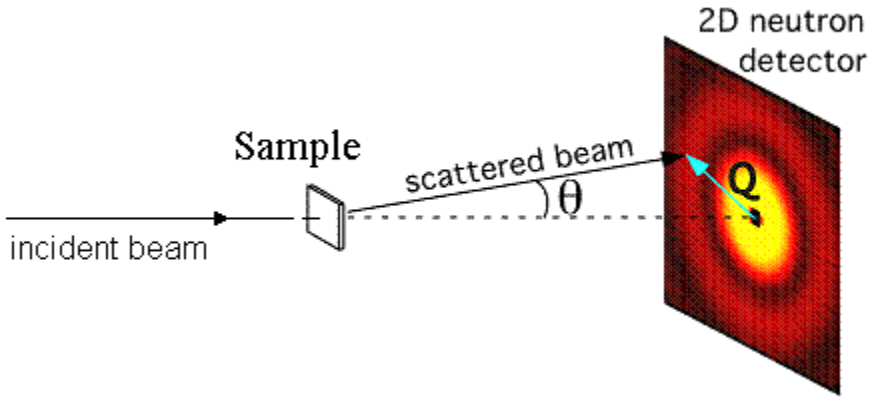

Figure 4.6: Scattering of neutrons by a sample. Picture courtesy of National Institute of Standards and Technology (NIST).

The magnitude of the scattering vector (Q) is given by:

$$Q = |Q| = |k_s - k_i| = \frac{4\pi n}{\lambda} \sin\left(\frac{\theta}{2}\right) \qquad \text{(Equation 4.1)}$$

where θ is the scattering angle, λ is the incident neutron wavelength and n is the neutron refractive index which is approximately 1. Q has dimensions of length^{-1} and is usually expressed as nm^{-1} or Å $^{-1}$.

Substituting equation 4.1 into Bragg's law of diffraction

$$\lambda = 2d \sin\left(\frac{\theta}{2}\right) \qquad \text{(Equation 4.2)}$$

yields a very useful expression

$$d = \frac{2\pi}{Q} \qquad \text{(Equation 4.3)}$$

where *d* is the molecular length scale obtainable over a particular Q range.

Equations 4.1 and 4.3 are critical to SANS experiments and help predict the accessible Q range of an instrument as well as the range of sample length scales it can probe.

4.5.2 Scattering length density and contrast matching

The neutron scattering length density (ρ_{SLD}) of a molecule comprising of i atoms can be calculated from the equation below:

$$\rho_{SLD} = \sum_i b_i \frac{DN_A}{Mw} \qquad \text{(Equation 4.4)}$$

where D is the bulk density of the scattering body, N_A is Avogadro's constant, M_w is molecular weight and b_i is bound coherent scattering length density of atom $_i$. ρ_{SLD} has dimensions of length^{-2} and can be negative.

The contrast term in any experiment is defined as the square of the difference between the scattering length density of the part of sample of interest (ρ_p) and the scattering length density of the surrounding medium (ρ_m). If $(\rho_p - \rho_m)^2$ is equal to zero, then the sample is said to be contrast matched. At the contrast match there is no scattering (King 1995).

Contrast matching is a powerful tool as it enables the study of multicomponent samples in detail. For example in scattering studies studying a layer of absorbed polymer on a particle, the particle can be contrast matched to the surrounding media rendering it effectively 'invisible', therefore scattering is obtained only from the region of interest, namely the adsorbed layer (Figure 4.7). A mixture of deuterated and protonated solvents are often used in contrast matching taking advantage of the different scattering length densities of H and D. Table 4.2 shows the scattering length densities of common hydrogenous and deuterated solvents.

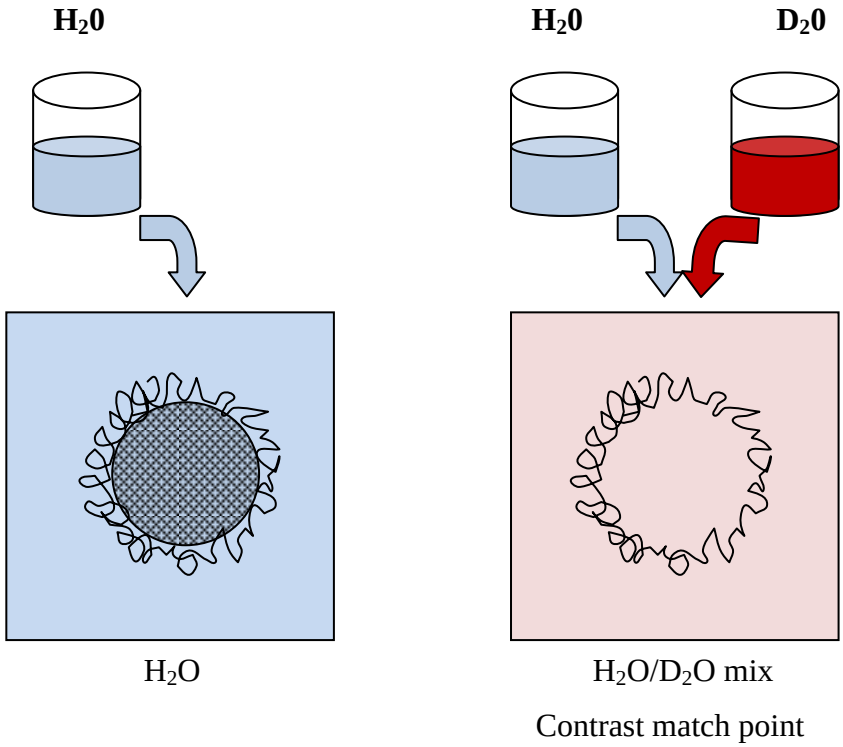

Figure 4.7: A schematic illustration of the contrast matching of a particle using a mixture of H_2O and D_2O to enable characterization of scattered layer

Table 4.2: Neutron scattering length densities of commonly used hydrogenous and deuterated solvents (King 1995)

Solvent	SLD h form (10^{10} cm^{-2})	SLD d form (10^{10} cm^{-2})
Water	- 0.56	+ 6.38
Octane	- 0.53	+ 6.43
Cyclohexane	- 0.28	+ 6.70
Toluene	+ 0.94	+ 5.66
Chloroform	+ 2.39	+ 3.16

4.5.3 SANS measurements

Experiment plan

A successful SANS experiment requires careful planning and consideration of desired Q range, sample size, environment (temperature, pressure, magnetic field), and sample counting time. The required Q range is determined by the length scales of interest, e.g. to probe large structures such as those of interest in the present study, a very low Q range is required. The instrument configuration is altered to achieve the desired Q range.

SANS can be used to examine liquid, solid or gel samples with the concentration of amount required being dependent upon the sample under study. Deuterated solvents are preferred as the sample medium since their incoherent scattering is significantly lower in comparison to hydrogenous solvents and therefore lower counting times are required to produce the necessary statistics. In a SANS experiment the coherent scattering contains important structural information while the incoherent scattering is the flat background and reduces the accessible Q range of the measurement (Choi 2000).

Data collection and handling

Raw SANS data consists of integer numbers with no statistical errors, which must be reduced to give anisotropic data (real data with calculated statistical errors) and finally isotropic data (one dimensional scattering information). The first step of data treatment involves scattering and transmission data from sample, scattering from empty sample holder, an incoherent calibration scatter e.g. water or vanadium, background as well as absolute scaling factors. From these data corrected anisotropic files are obtained. The second step, reduction of two-dimensional data into one dimension, is performed by radial averaging and requires input of the position of a beam centre (Keiderling 2002).

Apart from neutrons scattered by the sample, neutrons are also scattered by the empty sample cell, windows, collimation slits, or air. In addition stray neutrons, cosmic radiation or detector dark current can also reach the detector (Choi 2000). Therefore in addition to sample scattering measurements, transmission, background, empty beam, detector sensitivity and blocked beam measurements are needed for data correction.

$$I_{COR} = \left(I_{SAM} - I_{BKG}\right) - \left(\frac{T_{sample+cell}}{T_{cell}}\right) - \left(I_{EMP} - I_{BKG}\right) \qquad \text{(Equation 4.5)}$$

where I_{COR}, $I_{SAM,}$ I_{BKG} are the corrected scattering intensity, scattering intensity due to sample and background respectively, $T_{sample + cell}$, T_{sample} are the transmissions due to sample plus cell and cell respectively, and I_{EMP}, I_{BKG} intensity due to empty beam and blocked beam respectively.

The scattering is then calibrated with the normalized detector sensitivity.

$$I_{CAL} = \frac{(I_{COR})}{Normalized\,detector\ sensitivity} \qquad \text{(Equation 4.6)}$$

where I_{CAL} is the calibrated scattering intensity.

The absolute scaling yields a critical SANS parameter, namely the differential scattering cross section.

$$I(Q)_{CAL} = \phi A d T_{sample+cell} \left(\frac{d\sum(Q)}{d\Omega} \right)_{sample} \Delta\Omega \in t \qquad \text{(Equation 4.7)}$$

where $\left(\frac{d\sum(Q)}{d\Omega}\right)$ is the differential scattering cross section, I_{CAL} is the calibrated scattering intensity, ϕ is the incident neutron flux, A is the sample area, d is the sample thickness, $\Delta\Omega$ is the solid angle of each pixel, ε is the detector efficiency and t is the counting time.

Information concerning the size, shape and interaction between scattering centres in a sample is derived from the differential scattering cross section (Choi 2000).

4.6 SANS data interpretations

4.6.1 Models

SANS data from adsorbed layers is normally characterised at the zero contrast match point to give adsorption isotherms and volume fraction profiles. Away from the zero contrast match points, the measured scattering is due to both the adsorbed layer and the particle making it much more difficult to obtain any information (Cosgrove et al, 1987). Models used to interpret SANS data from adsorbed polymer/surfactant layers are outlined below.

Guinier approximation

This is the simplest model in which the size and shape of both bare and coated particle are determined. The thickness of the adsorbed layer is then simply obtained by subtraction. The drawback to this technique is that SANS is relatively insensitive to the few, well solvated, highly extended polymer tails at the periphery of adsorbed layer (King et al, 2000). The need for the measurement of the bare particles makes Guinier approximation unsuitable for the current study in which it is impossible to formulate drug nanoparticles without an adsorbed polymer/surfactant layer.

Core shell model

This approach models the particle and the adsorbed layer as two homologous concentric spheres (Figure 4.8). If the scattering length density of the particle is matched to that of the surrounding media, then the thickness of the spherical shell (i.e. the absorbed layer) can be deduced from the form factor. The drawback with this technique is that it assumes a uniform scattering length density throughout the adsorbed layer and thus a block profile volume fraction (King et al, 2000). The core shell model is therefore more useful in modelling the adsorption of short chain surfactants as opposed to that of polymers.

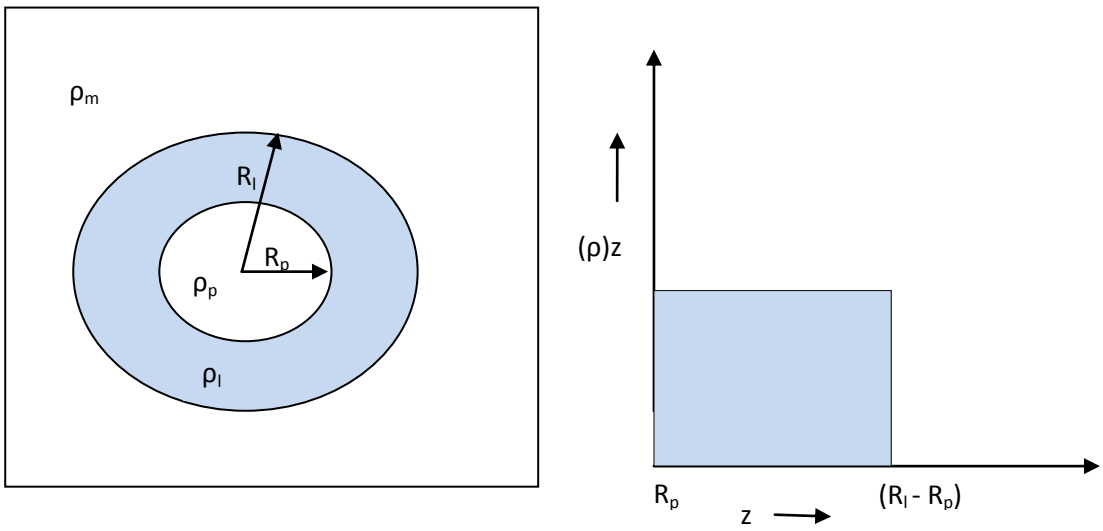

Figure 4.8 (a): Schematic representation of the 'core shell' model of an adsorbed layer onto a particle where ρ_m, ρ_l, ρ_p are the scattering length densities of media, adsorbed layer and particle respectively while R_p is the radius of the bare particle and R_l is the radius of the particle plus the adsorbed layer respectively. **(b)** The block volume fraction profile corresponding to the 'core shell' model of adsorbed layer onto a particle (King et al, 2000).

Inversion technique

This technique enables fitting parameters to be obtained without assuming a volume fraction (Φz). In fact this method can be used to determine the volume fraction of the absorbed layer (King et al, 2000). This model determines how the average density of the polymer chains vary with the distance (z) perpendicular to the interface, the layer thickness, the adsorbed amount (determined by integrating the area under the volume fraction profile curve), and the average fraction of the bound segments (determined from the portion of segments at z = 0) (Figure 4.9). The volume profiles obtained depend on the nature of the attachment of the polymer at the solid surface of the particle. For example, exponential profiles whereby the volume fraction decreases with distance from the interface are obtained with physically adsorbed polymers (Figure 4.9 (a)). Block copolymers with one block attached to the interface may display a parabolic volume fraction profile, while grafted polymers terminally attached to the interface may display a Gaussian volume fraction profile (Figures 4.9 (b-c)).

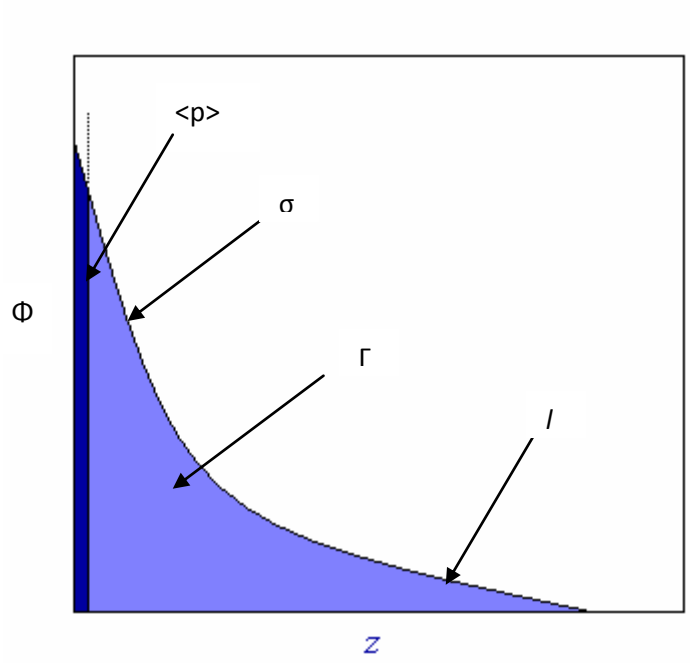

Figure 4.9 (a): Example of an exponential volume fraction profile of an adsorbed homopolymer, which shows how the polymer density (Φ) varies with distance from the interface (*z*). Labelled is the bound fraction (shaded dark blue),‹*p*›; the second moment of the thickness of the adsorbed layer, σ; the adsorbed amount (shaded blue), Γ; the span of the polymer layer, *l* (King et al, 2000).

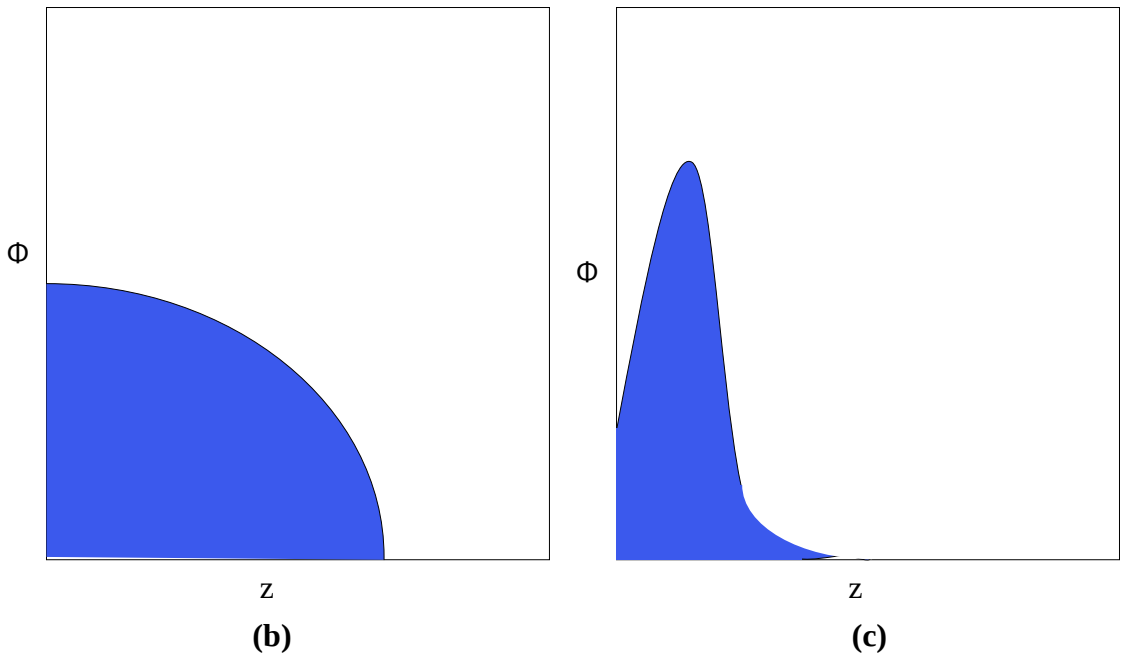

Figure 4.9 (b-c): Example of a parabolic volume fraction profile of a block copolymer (b) and Gaussian volume fraction profile of a terminally grafted polymer (c) adsorbed on a solid surface, showing how the polymer density (Φ) varies with distance from the interface (*z*) (King et al, 2000).

4.6.2 SANDrA program

SANS data in the present study was fitted to a surface Guinier model (King et al, 2000) using the program SANDrA which enables both the amount and thickness of the adsorbed layer to be determined without assuming a volume fraction profile.

The model fitting equations are outlined below;

$$\frac{\partial \sum}{\partial \Omega} Q = N_p P(Q) S(Q) + B \qquad \text{(Equation 4.8)}$$

where $\left(\frac{d\sum(Q)}{d\Omega}\right)$ is the differential scattering cross section, P(Q) is the form factor, S(Q) is the structure factor and B is the background.

The form factor is defined by

$$P(Q) = \left[\left(p_p - p_m\right)F_p(Q) + \left(p_l - p_m\right)F_l(Q)\right]^2 \qquad \text{(Equation 4.9)}$$

where $F_P Q$ is the intra particle form factor for the core particle, $F_l Q$ is the intra layer form factor for the adsorbed polymer.

The three major terms contributing to the form factor are the core particle, the adsorbed layer and the particle-surface interference. The contribution by the core particle and adsorbed layer can be ignored at the contrast match point (at which our experiments were carried out). If the particle radius is much greater than the adsorbed layer and ignoring the end fluctuations, the particle-surface interference can also be disregarded. Fortunately the drug particles in the current study are much larger (250-300 nm) than the thickness of the adsorbed surfactant/polymer layers and as a consequence therefore, the SANS data can be fitted with the limiting form of the layer scattering to partial form factor.

$$\frac{\partial \sum}{\partial \Omega} Q = \left(p_l - p_m\right)\left[\frac{6\pi\phi_p \Gamma^2}{Q^2\delta^2 R_p} \exp\left(-Q^2\sigma^2\right)\right] + B \qquad \text{(Equation 4.10)}$$

where Γ is the amount of polymer adsorbed, σ is the second moment of the mean of the adsorbed polymer layer which corresponding to the thickness of the adsorbed layer.

4.7 Methodology

4.7.1 Materials

Griseofulvin (97%) was purchased from Acros Organics (Geel, Belgium). Hydroxypropylmethylcellulose (HPMC) with a nominal molecular weight of 8K (Methocel E3LV (HPMC 8)) was obtained from Dow Company (Michigan, USA). All other chemicals were purchased from Sigma-Aldrich Co. Limited (Poole, UK). Chemicals were of the highest grade available and were used as received without further purification. Ultra pure water (UPW), obtained from a well seasoned, all glass still (D4000 Distinction, Sterling, UK) and D_2O (99.9%) from Sigma-Aldrich (Gillingham, UK) was used for all the SANS experiments.

4.7.2 Preparation of nanoparticles for SANS

The production of nanoparticles was carried out by wet bead milling of crude griseofulvin suspensions (2.2.2) using 0.44 mm YTZ beads as described in section 2.2.3. 10 g of griseofulvin was added to a 40 g suspension comprising of water and respective stabilisers giving a drug loading of 20% w/w. The resultant nanoparticles were then separated from the YTZ beads using a 60 mesh sieve.

About 2 mL of the resultant griseofulvin nanosuspension was centrifuged for 90 min in a Heraus centrifuge as described in section 3.2.1.The weights of supernatant and pellet were carefully recorded and supernatant replaced with an equivalent weight of D_2O/H_2O solvent mix. The volume fraction of the milled and re-suspended nanosuspensions was 14.7% v/v. This nanosuspension was then diluted to give a volume fraction of 3.5% using appropriate mixture of D_2O and H_2O. Selection of a 3.5% volume fraction for the SANS experiments was a balance of reducing to a minimum multiple scattering due to particle-particle interactions and obtaining sufficient scattering to be measured (Sepassi 2003; Goodwin 2006).

4.7.3 Determination of contrast match point

The scattering length density of griseofulvin and corresponding contrast solvent was calculated (section 4.5.2) using atom scattering length densities from the NIST

website giving a value of 2.38×10^{10} cm^2 and a 43.25: 56.75% v/v D_2O/H_2O contrast match solvent. The contrast match point was confirmed experimentally by determining the scattering intensity of nanoparticles prepared in a range of solvents containing different volume ratios of D_2O/H_2O (namely 30:70, 35:65. 40:60, 43:57, 45:55 and 50:50). The scattering intensity of the nanoparticles in the various solvents was then plotted against Q, with the solvent composition in which there was the minimum scatter being selected as the contrast match solvent, as at this composition scattering arises solely from the absorbed layer. Thereafter contrast match solvent was used to re-suspend all the nanoparticles for examination using SANS.

4.7.4 Sample selection

Samples studied at ILL were griseofulvin nanoparticles prepared using 0.25, 0.5, 1.0 and 1.5% w/w SDS/AOT, both in absence and presence of 1.88% w/w HPMC 8000. These experiments were designed to observe the effect of polymer, and of surfactant concentration, on the extent of polymer/surfactant adsorption. The volume fraction used in these experiments was 3.5% v/v, which had previously been determined as optimal for the present types of experiments (Sepassi 2003, Goodwin 2006).

The second set of samples studied at PSI comprised of griseofulvin nanoparticles prepared with 1.5% w/w SDS/AOT, both in absence and presence of 1.88% w/w HPMC 8000. The limited number of samples studied was due to the lower intensity flux of the beam line. In addition, a nanoparticle volume fraction of 14.7% v/v (as opposed to 3.5% v/v) was used to try and increase the sample scattering.

4.7.5 SANS measurements

SANS measurements were carried out at D11 at Institut Laue-Langevin (Grenoble, France) and SANS 2 at Paul Scherrer Institute (Villigen, Switzerland). While it would have been ideal to carry out both experiments using D11 at the ILL due to it being a more intense neutron source, the highly competitive nature of neutron experiments meant it was not possible. The main limitation of performing the experiments at two different facilities is the different intensities of the sources, although different instrument geometries also meant that differing Q ranges were accessible. For example the ILL experiments were carried out at a detector distances of 5 and 15 m using neutrons of a wavelength of 6 ± 0.6 Å accessing a Q range of 0.006 to 0.14 $Å^{-1}$ while the SANS 2 experiments were carried out at detector

distances of 2 and 6 m at a wavelengths of 5, 10 and 18 Å accessing a Q range of 0.04 to 1.4 $Å^{-1}$. Ideally the experiments should be performed at as low a Q range as possible due to the large size (in terms of SANS) of the nanoparticles

Transmission measurements were carried out at one detector distance (namely 6 m at SINQ, 15 m at ILL). Samples were placed in 1 mm quartz cells and measured for 2 and 120 min each for transmission and scattering runs respectively at ILL. Sample measurement times were ~ two times longer at SINQ. Measurements of direct beam, empty sample cell, water and dispersing solvent were all performed to enable subsequent data reduction. Experiments were performed at 25 ± 0.1ºC.

4.7.6 Data reduction

The principle of the SANS data reduction is identical at both faculties, although the specific programs used are dependent on the particular facility as each has its own preferred software package for use on its instruments. In principle, a mask file is created to remove data points at and around the beam stop and around the outermost perimeter of the detector as well as any damaged pixels on the detector. The data is then corrected with transmission files, radially averaged before being calibrated with the detector response.

D11 neutron data reduction was carried out using GRASP, a Matlab postscript application used for graphical analysis, inspection and reduction of SANS data from ILL instruments (Dewhurst 2003). SANS 2 neutron data was reduced by BERSANS, a similar software with graphical interface used for all SINQ instruments (Keiderling 2002). Another additional step in the data reduction involves merging of data from different detector distances to give a single curve. The merging of both ILL and SANS 2 data was carried out using OriginPro 8 software.

4.7.7 Data fitting

SANS data was fitted using the SANDrA program, a volume fraction independent surface Guiner model (King 2000). This program models the differential scattering cross section to obtain an estimate of the amount of polymer adsorbed (Γ) and the second moment of thickness (σ) of the adsorbed polymer layer. A detailed discussion of the equations used by the program is given in section 4.6. The parameters input in the SANDrA program in the present study are given in Table 4.3. The best model fit is attained at chi squares of between 0.82975 and 1.17025.

Table 4.3: Parameters input into SANDrA fitting program.

Nanoparticle formulation	Surfactant/ Polymer density (g/cm^3)	Scattering length density of adsorbed layer (cm^{-2})	Contrast point (cm^{-2}) ($\rho_l - \rho_m$)	Particle radius used in analysis (Å)
h-SDS + Gris	1.01	0.34×10^{10}	-2.04×10^{10}	1500
d-SDS + Gris	1.01	5.36×10^{10}	2.98×10^{10}	1500
AOT + Gris	1.1	0.62×10^{10}	-1.76×10^{10}	1500
h-SDS + HPMC + Gris	1.33	1.31×10^{10}	-1.07×10^{10}	1500
d-SDS + HPMC + Gris	1.33	1.31×10^{10}	-1.07×10^{10}	1500
AOT + HPMC + Gris	1.33	1.31×10^{10}	-1.07×10^{10}	1500

Additional parameters:
The volume fraction of the ILL samples was 0.035, while that of the SINQ samples was 0.147.
The scattering length density of griseofulvin (Gris) is $2.38 \times 10^{10}\ cm^2$

4.8 Results

4.8.1 Contrast matching

The contrast match solvent for griseofulvin obtained by scattering length density calculations was 43.25% v/v D_2O: 56.75% v/v H_2O. In order to confirm this theoretical calculation, experimentally griseofulvin nanoparticles (prepared in presence of 0.5% w/w SDS) were re-suspended in aqueous solvent containing varying amounts of D_2O. The neutron scattering intensities of these samples were measured and the variation in intensity with Q determined (Figure 4.10). From the data presented in Figure 4.10, the scattering intensity at a Q value of 0 was determined for each solvent composition and plotted against the % v/v D_2O in re-suspending solvent (Figure 4.11).

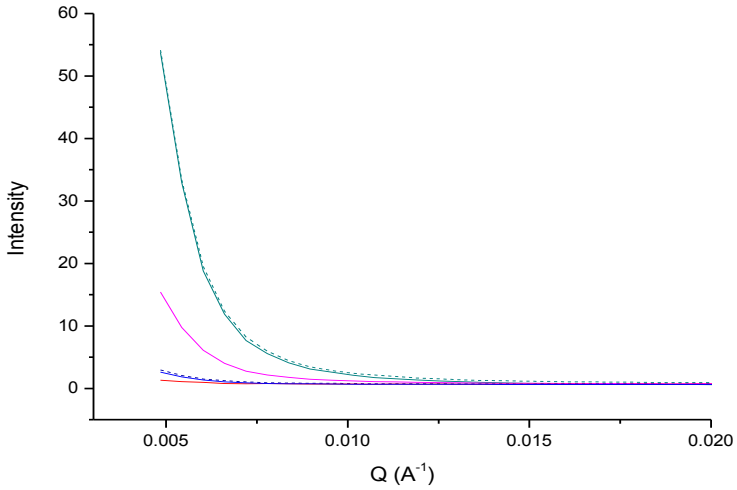

Figure 4.10: Variation in neutron scattering intensity as a function of Q for griseofulvin nanoparticles prepared in presence of 0.5% w/w SDS re-suspended in solvents of different D_2O/H_2O compositions namely: 30% v/v (—), 35% v/v (—), 40% v/v (····), 43% v/v (—), 45% v/v (—) and 50% v/v (····). Measurements carried out on D11 at 25 ± 0.1ºC.

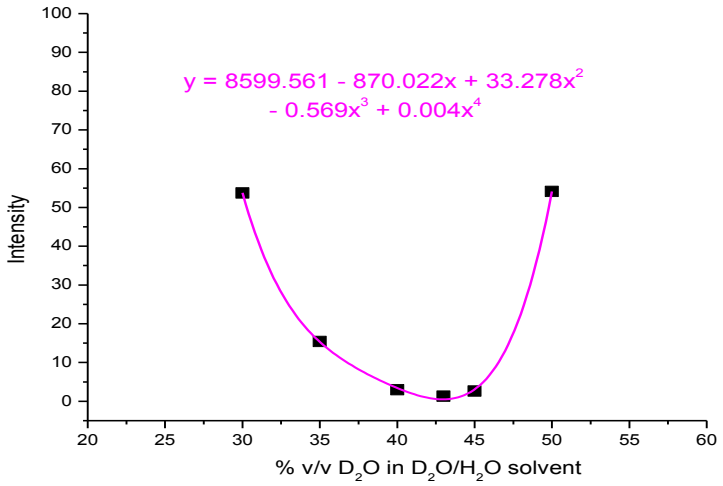

Figure 4.11: Variation of neutron scattering intensity at Q = 0 for griseofulvin nanoparticles, prepared in presence of 0.5% w/w SDS, with the % v/v D_2O present in the resuspending solvent. Measurements carried out on D11 at 25 ± 0.1ºC.

Reassuringly, the nanoparticles re-suspended in 43% v/v D_2O had the lowest experimentally measured scattering intensity (Figure 4.10-4.11) thereby confirming the theoretically calculated contrast match point for griseofulvin. At this solvent composition any scattering measured from the nanoparticle suspensions was solely due to the adsorbed surfactant layer. As a consequence, therefore solvent containing

43% v/v D_2O was used to re-suspend the nanoparticles for all other SANS experiments.

4.8.2 Data reduction

Data reduction was carried out using GRASP and BERSANS software for ILL and SANS 2 data, respectively. Merging of reduced SANS data at the different Q ranges was performed using OriginPro 8.0. Figure 4.12 shows an example of merged SANS data obtained at two detector distances from grisofulvin nanoparticles prepared in presence of 1.5% w/w SDS + 1.88% w/w/ HPMC 8000.

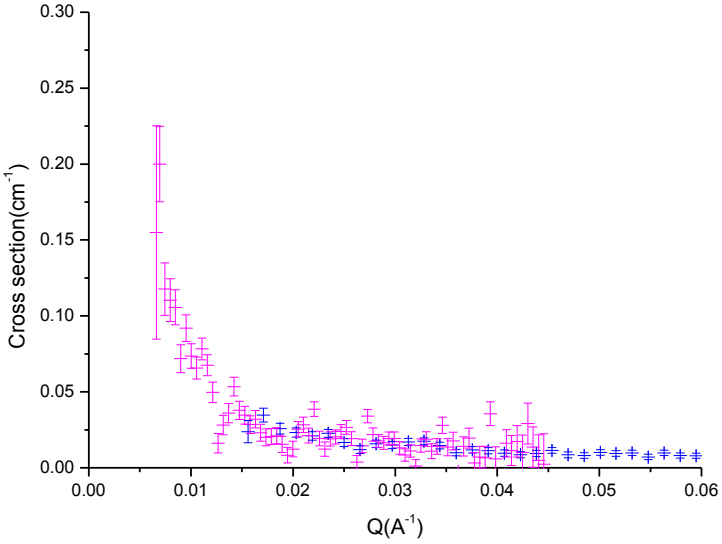

Figure 4.12: Merging of SANS data at 5 m (ɨ) and 15 m (ɨ) detector distances from griseofulvin nanoparticles prepared in presence of 1.5% w/w SDS + 1.88% w/w HPMC 8000. Measurements performed on D11 at 25 ± 0.1ºC.

4.8.3 Fitting of contrast matched data

4.8.3.1 Surfactant systems

ILL data

The surfactant samples comprised of griseofulvin nanoparticles prepared in the presence of 0.25% w/w SDS, 0.5% w/w SDS, 1.0% w/w SDS, 1.5% w/w SDS, 0.25% w/w AOT, 0.5% w/w AOT, 1.0% w/w AOT and 1.5% w/w AOT. The SANS data obtained for these surfactant stabilised samples was modelled using adsorption parameters obtained from spectroscopic measurements (Tables 4.4-4.5) and particle radius of 1500 Å to obtain expected fits shown in red (Figures 4.13-4.14(a-d)). The surfactant adsorption mechanisms proposed in section 3.3.3.1 were used to estimate

the thickness of the adsorbed layer, with a surfactant monolayer fixed at ~ 1.8 nm (Hubbard et al, 2005) and ~ 1.4 nm (Xu et al, 2004) for SDS and AOT, respectively. The data fits assuming a particle radius if 1500 Å were poor (chi squares of 4.532-98.7864). Interestingly however there was a better agreement between SANS data and expected fits when a higher particle radius of 6000 Å was used (fits shown in blue in Figures 4.13-4.14 (a-d)), suggesting that either PCS underestimated the size of the nanoparticles and/or that the nanoparticles were flocculated/aggregated. Indeed these surfactant stabilised nanoparticles were visibly cloudy on removal from the neutron sample chamber indicating physical instability. The data fits assuming a particle radius if 6000 Å gave chi squares of between 1.8763 and 5.8799.

Table 4.4: Surfactant adsorption parameters onto griseofulvin nanoparticles prepared in presence of SDS (% w/w) as obtained from the Stains All assay.

Formulation	Adsorbed amount (mg/m^2)	Thickness (nm)
0.25% SDS	0.627	0.5
0.5% SDS	0.986	1.8
1.0% SDS	1.628	2.4
1.5% SDS	2.085	3.6

Table 4.5: Surfactant adsorption parameters onto griseofulvin nanoparticles prepared in presence of AOT (% w/w) as obtained from the Stains All assay.

Formulation	Adsorbed amount (mg/m^2)	Thickness (nm)
0.25% AOT	0.692	0.5
0.5% AOT	0.874	1.4
1.0% AOT	1.345	2.1
1.5% AOT	1.847	2.8

All other formulations were fitted assuming a particle radius of 1500 Å inorder to enable comparison with adsorption data obtained from spectroscopy.

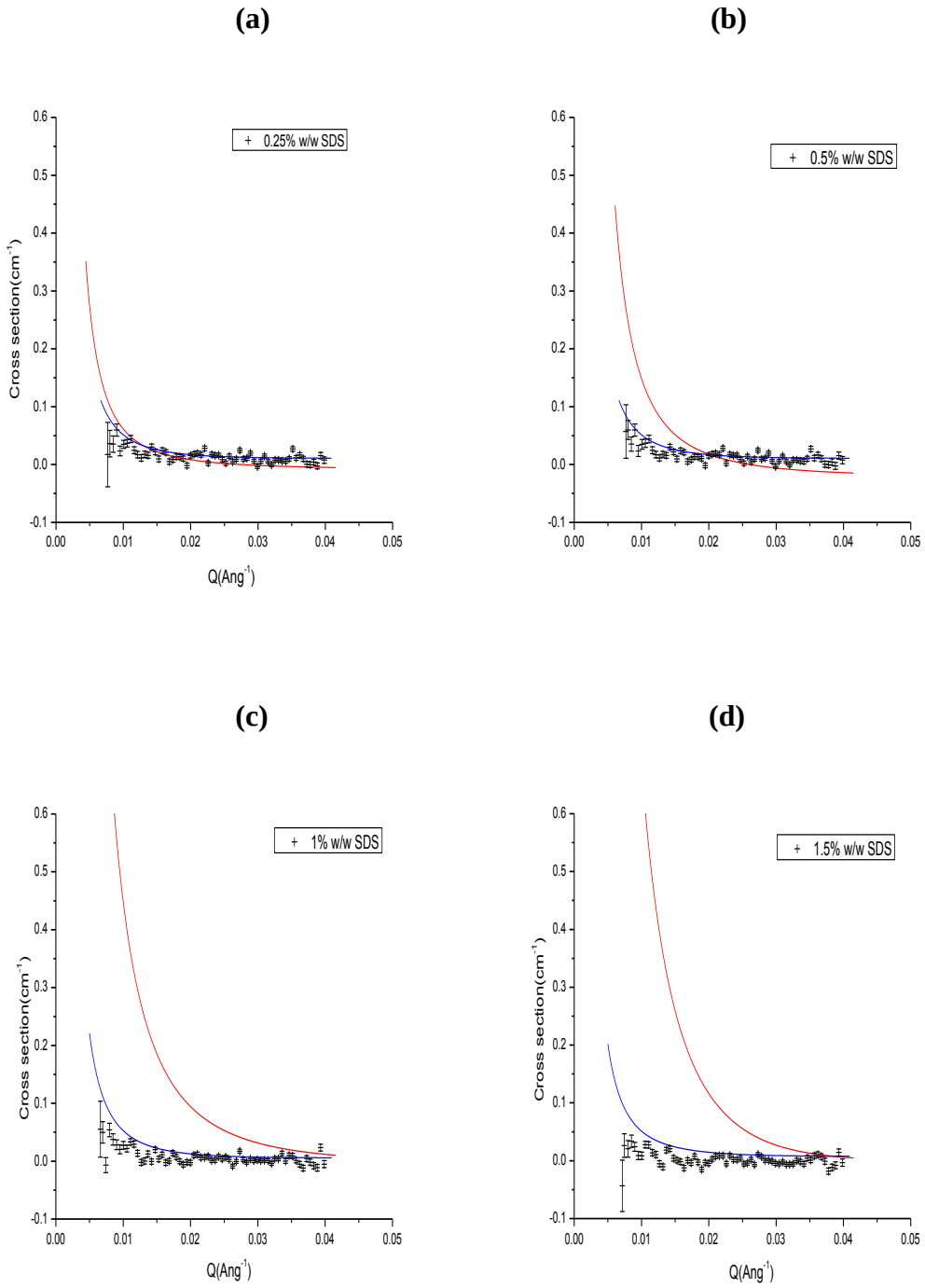

Figures 4.13 (a-d): SANS data of griseofulvin nanoparticles prepared in presence of 0.25% w/w SDS, 0.5% w/w SDS, 1.0% w/w SDS and 1.5% w/w SDS.

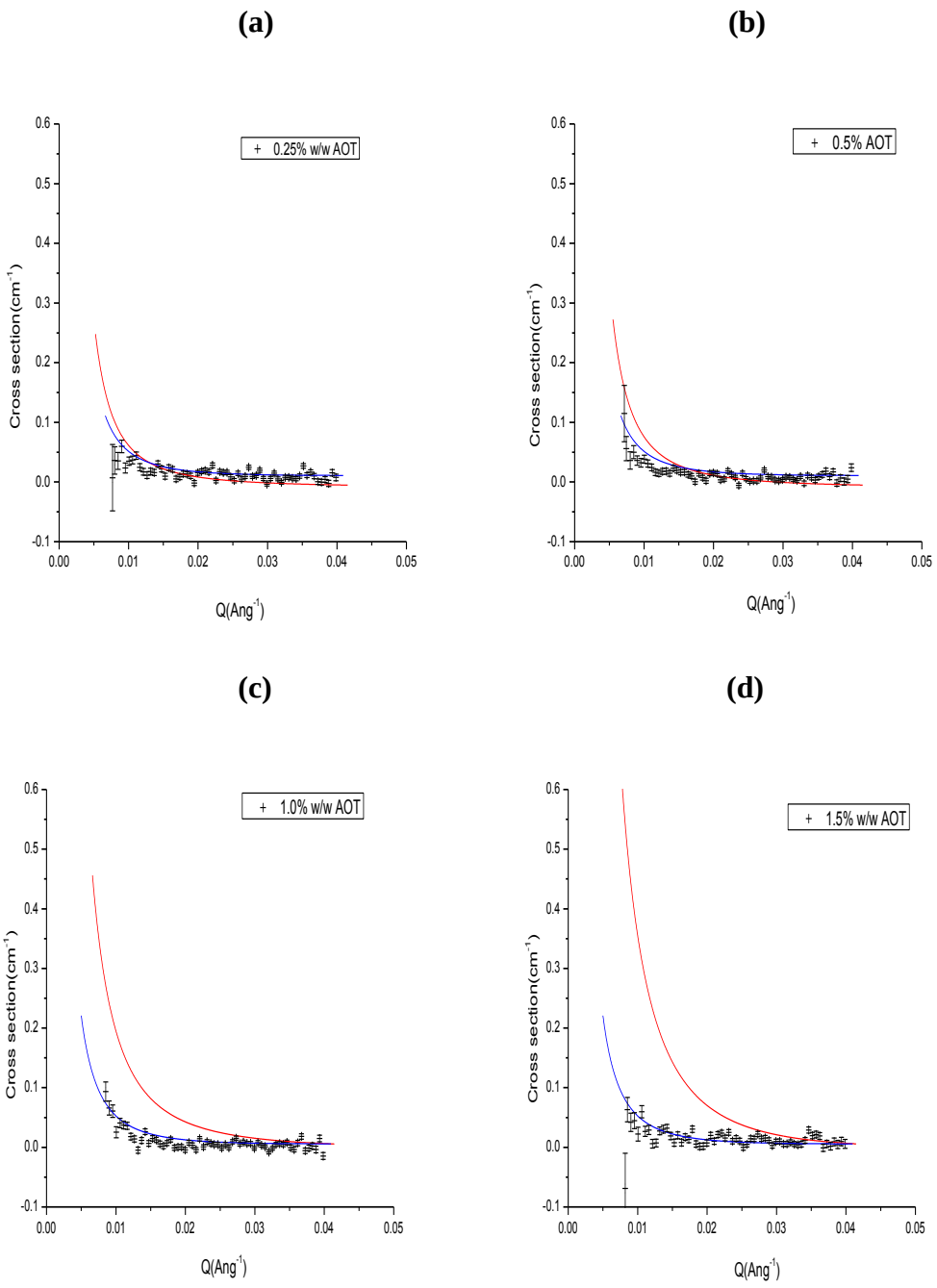

Figures 4.14 (a-d): SANS data of griseofulvin nanoparticles prepared in presence of 0.25% w/w AOT, 0.5% w/w AOT, 1.0% w/w AOT and 1.5% w/w AOT.

SANS 2 data

Griseofulvin nanoparticles prepared at one surfactant concentration namely 1.5% w/w h-SDS, d-SDS and AOT were analysed. These samples were studied at high volume fraction of 14.7% v/v. The surfactant stabilised nanoparticles were cloudy with visible aggregates and some sedimentation on removal from the neutron sample chamber indicating physical instability- particularly the 1.5% w/w AOT sample. SANS data obtained for these surfactant stabilised samples in Figures 4.15 (a-c) was modelled using adsorbed amount determined spectroscopically (Table 4.4-4.5) and particle size of 1500 Å to obtain expected fits shown in red (chi squares of 3.532-58.7864). The scattering from the SINQ surfactant only systems was minimal, which is in agreement with the data obtained from the samples analysed in ILL (Figures 4.13-4.14 (a-d)) and the fact that the data collected at SINQ did not go down to as low a Q value as that measured at the ILL. One interesting observation, seen only with SINQ data, was that the 1.5% w/w AOT sample seemed to have the notably stronger scatter than the 1.5% w/w SDS samples. It is worth commenting that the concentration of nanoparticles used for this study were much higher than those used on D11 at the ILL and as a consequence interparticulate interactions may have been present and influenced the data obtained.

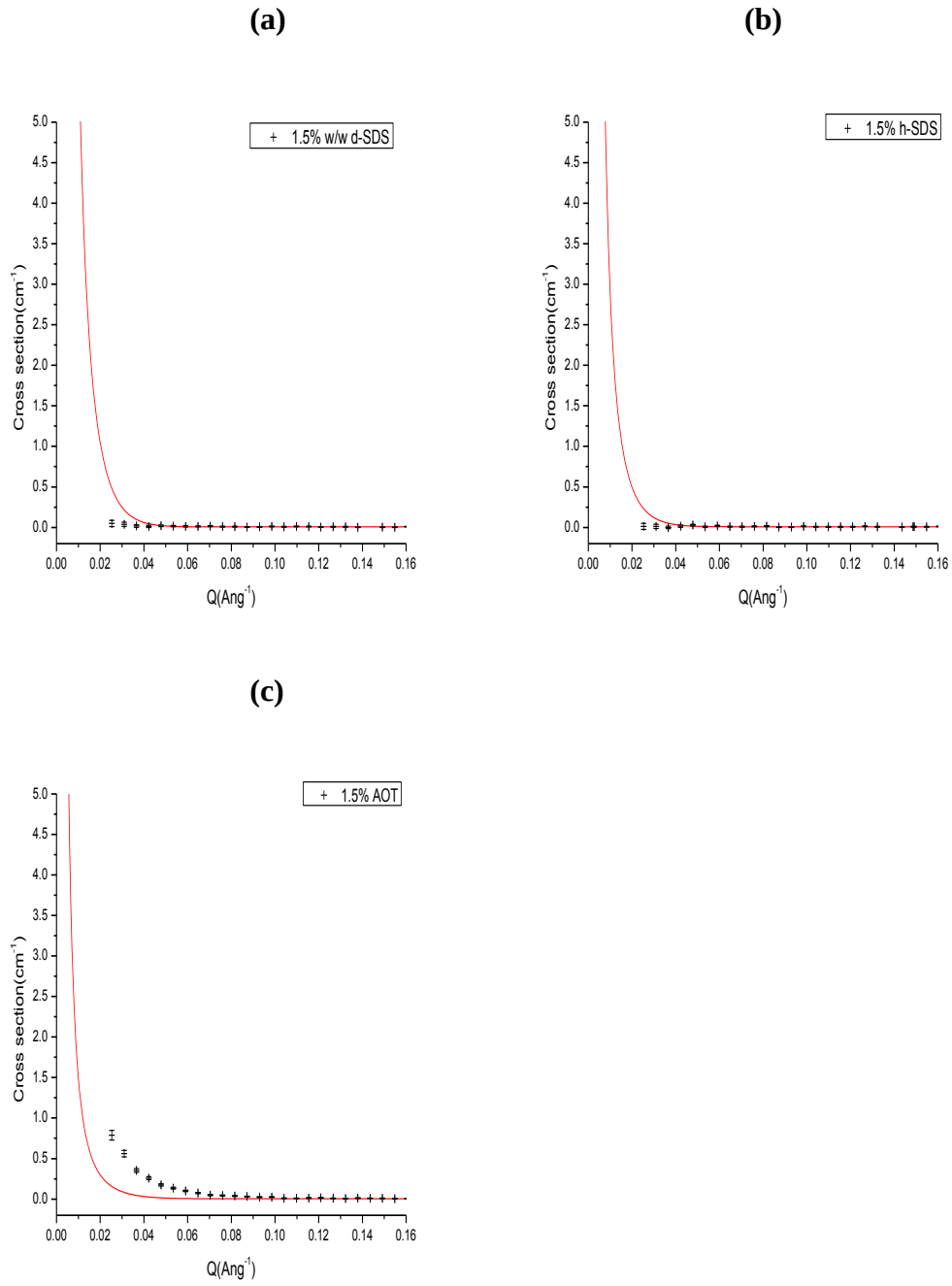

Figures 4.15 (a-c): SANS data of griseofulvin nanoparticles prepared in presence of 1.5% w/w d-SDS, 1.5% w/w h-SDS and 1.5% w/w AOT.

4.8.3.2 Polymer-surfactant systems

SANS data from nanoparticles prepared in presence of polymer and surfactant exhibited a markedly higher scatter compared to those prepared with surfactant only, supporting the hypothesis of co-adsorbed non-ionic polymer on the nanoparticle surfaces. As noted earlier, anionic surfactant was found to adsorb onto griseofulvin

nanoparticles while non-ionic polymer when used as sole stabiliser did not. However in the presence of HPMC, changes in anionic surfactant adsorption and nanoparticle stabilisation were seen, strongly suggestive of co-adsorption were observed (section 3.3.2). We postulate that a polymer-surfactant complex is formed at the nanoparticle surfaces, with anionic surfactant serving as an anchor for HPMC adsorption.

Previous members in our group (Sepassi 2003, Goodwin 2006) successfully fitted neutron data of polymer (HPMC, HPC or PVP) adsorbing on nabumetone and halofantrine nanoparticles using the SANDrA program. However, our griseofulvin systems present an added challenge in that they also contain adsorbed surfactant at the nanoparticle surfaces. The ORD assay (section 3.4) was unsuccessful therefore we have no prior determination of amount of polymer adsorbed, thus the results from the SANS experiments were used to provide an estimate of polymer adsorption onto the griseofulvin nanoparticles.

ILL data

The polymer data was fitted by the SANDrA guinier approximation. In order to do this some assumptions had to be made. Firstly, it was established by the depletion method that, even in the presence of HPMC, these nanoparticles adsorbed anionic surfactant on their surface. Therefore SANS data from the surfactant only formulations was subtracted from that of the corresponding polymer-surfactant formulations. The resultant SANS data was then fitted to determine amount of absorbed polymer. Scattering data was fitted to obtain the best visual fits to the data and lowest chi squares (1.6718-2.0194). The fits to the experimental data thus obtained are represented by the red lines in Figures 4.16-4.17 (a-d). In this way the SANS data was successfully fitted to quantify the amount of adsorbed polymer (Table 4.6-4.7). The results revealed that HPMC 8000 was adsorbing onto griseofulvin nanoparticles together with the anionic surfactant. The absorbed amounts of HPMC were in the region of 0.3-0.9 mg/m^2 – similar to values quoted in literature (Sawyer et al, 2001) but much lower than those obtained by Sepassi (2003) and Goodwin (2006) in our group, perhaps not surprisingly as HPMC was the sole stabiliser in their studies. Sepassi (2003) and Goodwin (2006) studied adsorption of HPMC 8000 onto nabumetone and halofantrine nanoparticles obtaining adsorption values of 4.6 mg/m^2 and 2.4 mg/m^2 respectively using a particle radius of 4000 Å.

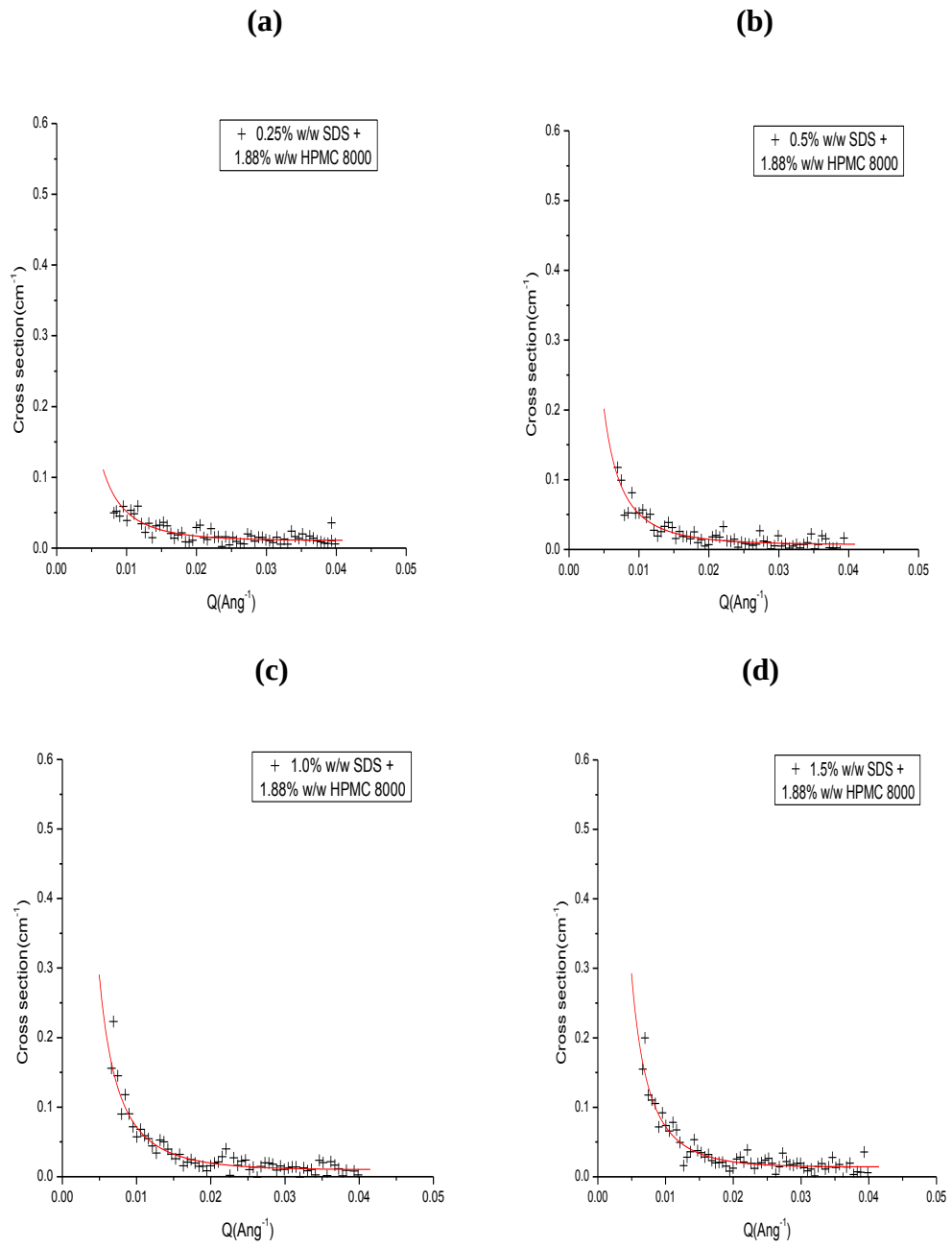

Figures 4.16 (a-d): SANS data of griseofulvin nanoparticles prepared in presence of 1.88% w/w HPMC 8000 + either 0.25% w/w SDS, 0.5% w/w SDS, 1.0% w/w SDS or 1.5% w/w SDS.

Table 4.6: Fitted parameters obtained from SANS data of griseofulvin nanoparticles prepared in presence of varying concentrations of SDS + 1.88% w/w HPMC 8000

Formulation	Adsorbed amount (mg/m^2)	Thickness (nm)
0.25% w/w SDS + 1.88% w/w HPMC 8000	0.57	3.98
0.5% w/w SDS + 1.88% w/w HPMC 8000	0.3	3.65
1.0% w/w SDS + 1.88% w/w HPMC 8000	0.68	4.01
1.5% w/w SDS + 1.88% w/w HPMC 8000	0.73	4.76

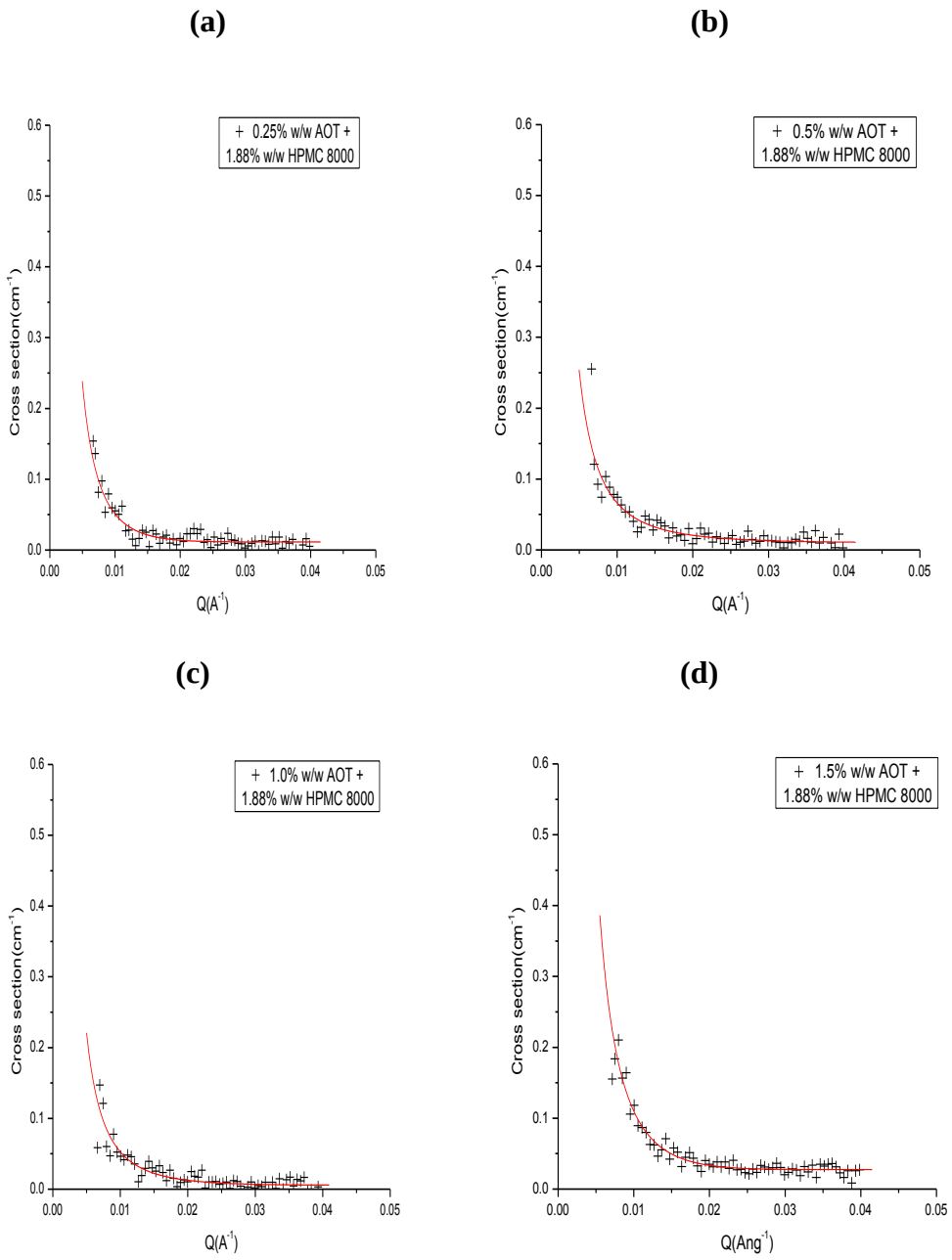

Figures 4.17 (a-d): SANS data of griseofulvin nanoparticles prepared in presence of 1.88% w/w HPMC 8000 + either 0.25% w/w AOT, 0.5% w/w AOT, 1.0% w/w AOT or 1.5% w/w AOT.

Table 4.7: Fitted parameters obtained from SANS data of griseofulvin nanoparticles prepared in presence of varying concentrations of AOT + 1.88% w/w HPMC 8000

Formulation	Adsorbed amount (mg/m^2)	Thickness (nm)
0.25% w/w AOT + 1.88% w/w HPMC 8000	0.7	6.80
0.5% w/w AOT + 1.88% w/w HPMC 8000	0.49	3.15
1.0% w/w AOT + 1.88% w/w HPMC 8000	0.33	4.21
1.5% w/w AOT + 1.88% w/w HPMC 8000	0.94	6.36

Figure 4.18 shows the variation in the amount of HPMC 8000 adsorbed (as determined by SANS) with starting surfactant concentration. Figure 4.19 shows the variation in the thickness of adsorbed HPMC 8000 layer with starting surfactant concentration. The average thickness of the adsorbed polymer layer was ~ 4 nm, while the thickness of a fully stretched HPMC 8000 layer, adsorbing with anchoring trains and outstretched tails, is 10.6 nm as determined by Sepassi (2003). These data suggest therefore that, in the present study, the polymer was lying flat on the surface of the griesofulvin nanoparticles. The thickness of the polymer layer obtained with the SDS-stabilised systems was more consistent that that obtained with the formulations containing AOT.

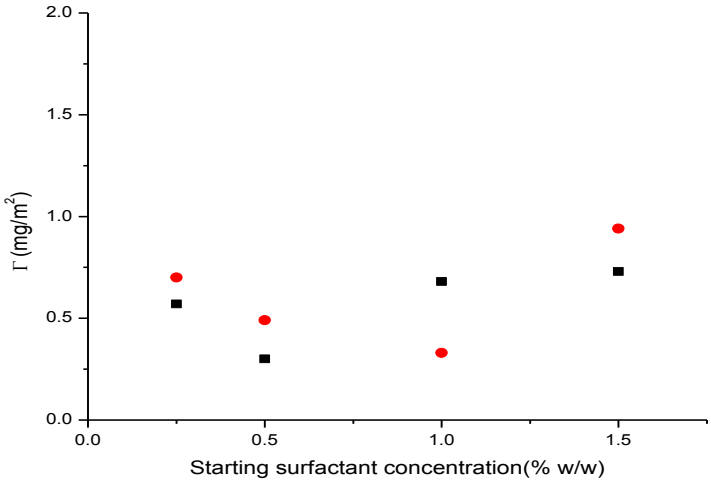

Figures 4.18: Amount of polymer adsorbed (Γ) onto griseofulvin nanoparticles prepared in presence of 1.88% w/w HPMC 8000 + either SDS (■) or AOT (●) on fitting SANS data with SANDrA.

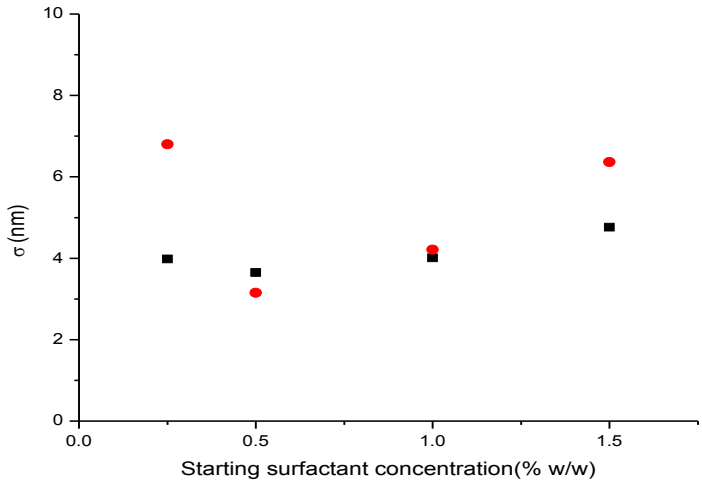

Figures 4.19: 2nd moment of thickness of adsorbed polymer layer (σ) on griseofulvin nanoparticles prepared in presence of 1.88% w/w HPMC 8000 + either SDS (■) or AOT (●) on fitting SANS data with SANDrA.

SANS 2 data

Samples at one surfactant concentration namely 1.5% w/w SDS, d-SDS and AOT in presence of 1.88% w/w HPMC 8000 were analysed. The SANS data was fitted (chi squares: 2.2518 - 3.6237) to obtain experimental fits shown in red (Figures 4.20 (a-c)) and presented in Table 4.8. The adsorption parameters indicated a very thin (~1 nm) but highly dense polymer layer which is unrealistic and suggests underestimation of volume fraction due to nanoparticle sedimentation. It must be noted, however, that the concentration of nanoparticles used for this study were much higher than those used on D11 at the ILL and as a consequence interparticulate interactions may have been present and account for the results obtained.

(a)

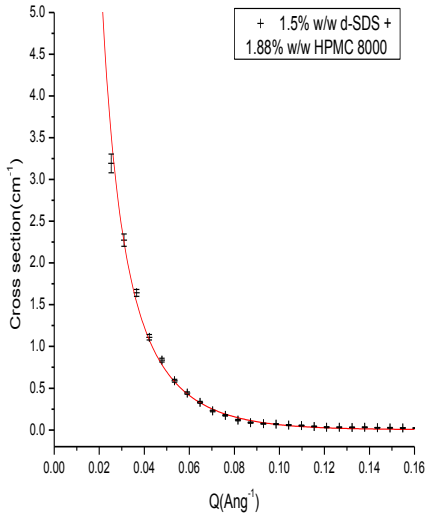

(b)

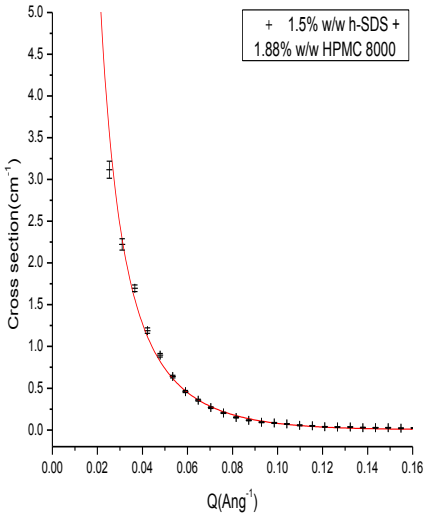

(c)

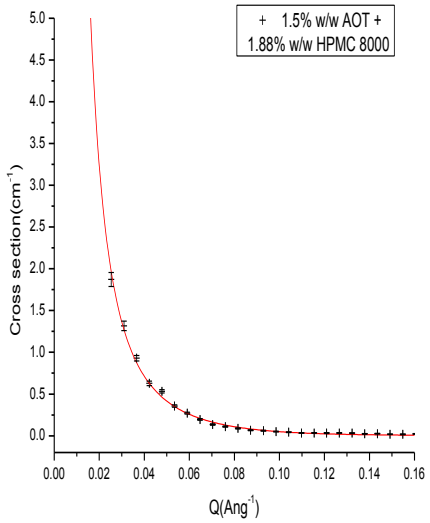

Figures 4.20 (a-c): SANS data of griseofulvin nanoparticles prepared in presence of 1.88% w/w HPMC 8000 + either 1.5% w/w d-SDS, 1.5% w/w h-SDS or 1.5% w/w AOT.

Table 4.8: Fitting parameters obtained from SANS data of griseofulvin nanoparticles prepared in presence of 1.88% w/w HPMC 8000 + either 1.5% w/w d-SDS, 1.5% w/w h-SDS or 1.5% w/w AOT.

Formulation	Adsorbed amount (mg/m^2)	Thickness (nm)
1.5% d-SDS + 1.88% HPMC 8000	11.21	1.19
1.5% h-SDS + 1.88% HPMC 8000	11.3	1.42
1.5% AOT + 1.88% HPMC 8000	8.92	1.76

4.9 Summary

Small angle neutron scattering (SANS) was used to investigate the adsorption of surfactant and/or polymer on the griseofulvin nanoparticles. Spectroscopic studies in Chapter 3 revealed the adsorption of anionic surfactant onto griseofulvin nanoparticles, but the amount of polymer adsorbed could not be determined due to interference by dissolved griseofulvin. Thus SANS was used to examine the polymer adsorption isotherms onto the griseofulvin nanoparticles. The SANS experiments were performed at ILL, France and SANS 2, Switzerland. SANS allows for detailed characterisation of adsorption providing information on the adsorbed amounts, thickness of adsorbed layer and the volume fraction profile. At the contrast match point, the particle and solvent neutron scattering lengths are matched thus only scattering from the adsorbed layer seen.

Both griseofulvin nanoparticles prepared in presence of anionic surfactant alone and in presence of anionic surfactant and non ionic polymer HPMC 8000 were studied. Notably the scatter from nanoparticles prepared in presence of 1.88% w/w HPMC 8000 polymer and anionic surfactant where consistently higher than the corresponding nanoparticles prepared in presence of anionic surfactant alone. The results from polymer-surfactant systems were corrected by subtraction of surfactant scatter then fitted to obtain the adsorbed polymer layer. Fitting of the resultant scattering revealed that HPMC 8000 was co-adsorbed onto griseofulvin nanoparticles together with anionic surfactant. The amounts of co-adsorbed polymer were 0.3-0.9 mg/m^2 with an average thickness of ~ 4 nm.

Chapter 5
Crystallographic studies

5.1 Introduction

5.1.1 Surface energy of pharmaceutical crystals

The surface energy of crystalline pharmaceutical solids influences manufacturing processes such as powder flow, granulation, compaction and the interaction with excipients (Wu et al, 2010). Of particular interest to the current work is the effect of surface energy of the milled drug crystals on the adsorption of stabilisers. No predictive model is currently available to aid in the selection of appropriate stabilisers for the production of drug nanoparticles by wet bead milling and the surface energetics of the drug crystals may provide useful insight.

Organic crystalline solids have been demonstrated to have anisotropic facet dependent surface chemistry. The surface chemistry of each crystal facet varies as the crystallographic planes dissect the unit cell at different angles and planar orientations exposing differing chemical groups and concentrations of those groups (Heng et al, 2006 a, b, c). During milling the crystal fractures to expose the weakest attachment face, with properties of this weakest attachment face dominating the milled state (York et al, 1998). The attachment energy is defined as the fraction of the total energy released upon the attachment of a lattice slice onto a growing surface. Previous authors have used a variety of techniques to characterise the surface energetics of particulate crystalline pharmaceuticals. For example York et al (1998) used inverse gas chromatography and computer modelling to characterise the surface energies of milled d,l-propanolol, while Heng et al (2006 a, b, c) used sessile contact angle measurements and X-ray photoelectron spectroscopy to elucidate the anisotropic surface chemistry of macroscopic aspirin, paracetamol and ibuprofen crystals. However, more recent studies by Shariare et al (2012) have shown that inter-planar d-spacings and the corrugation of lattice slip planes are superior to attachment energy calculations in prediction of the fracture of crystalline material.

5.1.2 Current work plan

The drug-stabiliser screen described in section 2.3.1 revealed that griseofulvin nanoparticles could only be produced in the presence of anionic stabilisers. Studies were performed to determine the surface energy of the griseofulvin crystal and its fracture plane. This work included growing macroscopic crystals of griseofulvin and characterising the individual crystal facets using contact angle measurements, X-ray photoelectron spectroscopy and single crystal X-ray diffraction.

In addition computer modelling was used to investigate the crystal surface energy at the (001), (010), (100), (-001), (-010) and (-100) planes of the griseofulvin crystals as well as the other drugs tested in section 2.3.1 namely albendazole, carbamazepine, frusemide, halofantrine, indomethacin, nabumetone and phenytoin.

5.2 Methodology

5.2.1 Macroscopic crystallisation of griseofulvin

Griseofulvin, as obtained from the manufacturer, was dissolved in acetone and stirred at ambient temperature for 24 h until the solubility limit of griseofulvin in

acetone was reached. Seed crystals of ~ 1-2 mm length were obtained by allowing the saturated solution to evaporate slowly over 2-3 days with stirring. The seed crystals were then suspended in a drug saturated acetone solution by means of a single aramid fibre (5 μm thickness) and macroscopic griseofulvin crystals (~ 1 cm) grown at ambient temperature by the slow solvent evaporation over a period of 3-4 months in the absence of stirring.

5.2.2 Contact angle measurements

Sessile contact angle measurements were made using a Krüss Drop Shape Analyser (DSA 10, Krüss GmbH, Hamburg, Germany). Deionized water, diiodomethane, ethylene glycol and formamide were used as probe liquids. The properties of the probe liquids are given in Table 5.1. Static contact angles were obtained using a drop volume of ~ 1.5 μL. A minimum of three droplets of each liquid on each of the eight crystal facets were used. The droplets were monitored with a CCD camera and analysed by the Drop Shape Analysis software supplied with the instrument. The droplet contour was fitted by the tangent method to obtain both the left and right contact angles of the drop. Measurements were performed at ambient temperature.

5.2.3 Surface energy calculations

The Owens Wendt approach (Owens et al, 1969) was used to calculate surface energies of the crystal facets (Equation 1.30). The dispersive and polar components of the probe liquids used for the surface energy calculations are given in Table 5.1.

Table 5.1: Properties of probe liquids used for contact angle measurements (Heng et al, 2006 c).

Liquids	Purity (%)	Density (kg/m^3)	γLV (mJ/m^2)	γL^d (mJ/m^2)	γL^p (mJ/m^2)
Diiodomethane	> 99	3325	50.8	50.8	0.0
Water	deionized	998	72.8	21.8	51.0
Ethylene glycol	> 99	1109	48.0	29.0	19.0
Formamide	> 99.5	1139	58.0	39.0	19.0

Where γLV is the liquid-vapour interfacial energy with both dispersive (γL^d) and polar components (γL^p).

5.2.4 Single crystal X-ray diffraction

Single crystal X-ray diffraction (XRD) experiments were kindly performed by Dr. Kenneth Shankland at the Chemical Analysis Facility, University of Reading. Data

were collected using an Oxford Gemini-Ultra diffractometer (Agilent technologies, UK).

5.2.5 X-ray photoelectron spectroscopy

X-ray photoelectron spectroscopy (XPS) experiments were kindly performed by Dr. Steve Hinder at the Surface Analysis Laboratory, University of Surrey. XPS data from individual facets of a macroscopic griseofulvin crystal were collected using a Theta Probe XPS instrument (Thermo Scientific, UK).

5.2.6 Computer modelling

The computer software MERCURY (Macrae et al, 2006) was used to generate drug crystals using the individual crystallographic information files (CIF) obtained from the Cambridge Structural Database. Crystal program database (PDB) files were then generated using the packing option after inputting the space group and the unit cell parameters from the Cambridge Structural Database. The freely available version of MERCURY, which was used for the modelling, did not include access to the Bravais-Friedel-Donnay-Harker model calculations for a (crude) prediction of crystal morphology. Therefore the crystals generated in the present study were all rectangular in shape, and may not necessarily represent the actual crystal morphology.

After MERCURY was used to generate the crystals, two in-house software programs namely ACCESS and EPOT (Barlow, 2011) were used to determine the charge per unit area and the electrostatic potential of the drug crystals at various crystal planes namely (001), (010), (100), (-001), (-010) and (-100). ACCESS reads the crystal PDB files together with partial atomic charge data and computes the charge per unit area for the individual crystal faces. EPOT reads the crystal PDB files together with the partial atomic charge data and then calculates the electrostatic potential across planes parallel with each of the crystal faces (3 angstroms beyond the centre of the furthermost atom on the test face).

The various drug crystal parameters used for modelling are given in Table 5.2. As phenytoin CIF was only available as a co-crystal with choline, and the halofantrine CIF contained disordered molecules, phenytoin and halofantrine were excluded from the computer modelling studies.

Table 5.2: Crystal parameters from the Cambridge Structural Database.

Drug	Crystal form	a	b	c	α	β	γ	Space group	CCDC code	Reference
Albendazole	Monoclinic	24.317	5.413	19.738	90	97.71	90	C2/c	BOGFUZ	Alhalawen et al, 2007
Carbamazepine	Monoclinic	7.529	11.148	15.47	90	92.91	90	$P2_1/c$	CBMZPNΦ1	Reboul et al, 1981
Frusemide	Triclinic	10.467	15.801	9.584	71.87	115.04	108.48	P1	FURSEMΦ1	Lamotte et al,1978
Griseofulvin	Tetragonal	8.969	8.969	19.951	90	90	90	$P4_1$	GRISFL03	Loew et al, 2004
Indomethacin	Triclinic	9.236	9.62	10.887	69.9	87.33	69.5	P1	INDMETΦI	Cox et al, 2003
Nabutemone	Monoclinic	22.054	5.327	22.483	90	110.83	90	$P2_1/c$	XOCXVI	Prabhakar et al, 1999

5.3 Results

5.3.1 Growth of macroscopic griseofulvin crystals

The macroscopic griseofulvin crystals obtained were bipyramidal with the vertical axis longer than the horizontal axis (Figures 5.1 a-b). Griseofulvin has previously been crystallised in acetone using supercritical CO_2 as an antisolvent (DeGioannis et al, 2004) where upon two morphologies were obtained depending on the speed of stirring; namely needle-like or bipyramidal crystals. Both the needle and bipyramidal crystals had similar XRD patterns, therefore excluding the presence of polymorphism.

The growth of the griseofulvin crystals was slow, taking several months. In addition the griseofulvin crystals could not be grown larger than ~ 1 cm, beyond this size secondary nucleation occurred. Interestingly, secondary nucleation occurred only on the tip of one pyramid's surface, suggesting that the two pyramids may possess different surface properties. As the Miller indices of the griseofulvin crystal are yet undetermined, the crystal facets were denoted facet 1-8 as shown in Figure 5.1 b.

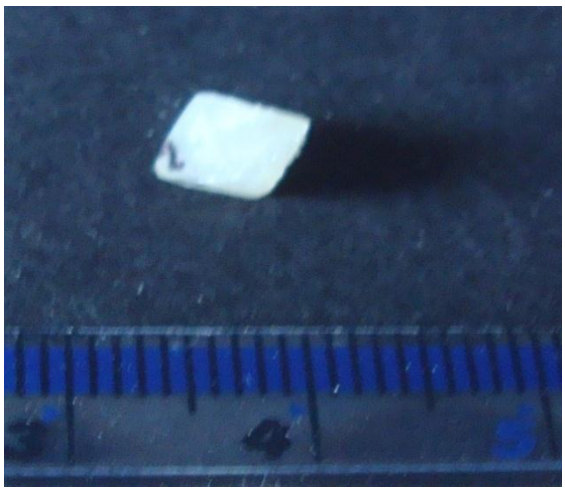

(a)

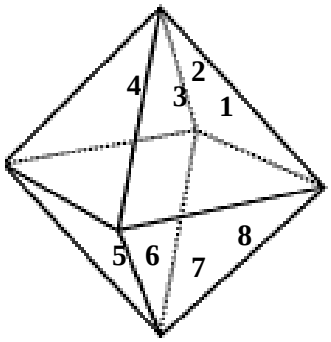

(b)

Top pyramid: Facet 1 2 3 4
Bottom pyramid: Facet 8 7 6 5

Figure 5.1: Picture of a griseofulvin macroscopic crystal grown in acetone solution (a) and the corresponding crystal morphology (b).

The macroscopic crystals were dried under ambient conditions prior to get rid of excess acetone before surface characterisation experiments.

5.3.2 Contact angle measurements on the griseofulvin crystal

Contact angle measurements revealed an anisotropic wetting behaviour of the griseofulvin bipyramidal crystal (Table 5.3). Although the four facets comprising each pyramid possessed very similar contact angles with the various probe liquids, the two pyramids exhibited very different contact angles. The contact angles of all polar liquids (water, formamide and ethylene glycol) were lower in the pyramid possessing facets 5-8. In contrast, the pyramid consisting of facets 1-4 was much more hydrophobic with a water contact angle approximately 35º higher than that obtained on facets 5-8.

Table 5.3: Results for static contact angles (°) on the griseofulvin crystal facets.

Facets	Water	Formamide	Ethylene glycol	Diiodomethane
1	79.6 ± 2.4	43.7 ± 2.3	44.7 ± 3.7	25.0 ± 2.5
2	79.1 ± 2.3	40.1 ± 3.1	46.6 ± 3.9	28.7 ± 3.1
3	78.6 ± 2.7	43.7 ± 2.4	43.5 ± 3.3	26.4 ± 2.6
4	79.3 ± 2.0	41.8 ± 2.6	41.4 ± 2.2	26.3 ± 2.7
5	43.6 ± 3.4	15.2 ± 2.5	24.5 ± 4.1	42.9 ± 3.1
6	45.2 ± 3.9	16.1 ± 3.1	21.3 ± 2.8	43.5 ± 2.8
7	44.8 ± 3.5	17.5 ± 2.9	21.6 ± 1.9	40.1 ± 4.0
8	45.0 ± 2.1	14.6 ± 2.7	19.5 ± 2.1	40.8 ± 3.6

The order of hydrophilicity of the facet – assessed using the contact angle of water;
{Facet 5 ≈ Facet 6 ≈ Facet 7 ≈ Facet 8} > {Facet 1 ≈ Facet 2 ≈ Facet 3 ≈ Facet 4}

Diiodomethane is a purely dispersive interacting liquid and is used to probe hydrogen binding potential. The pyramid containing facets 1-4 had a diiodomethane contact angle of approximately 15ºC lower than that obtained on facets 5-8.

The order of the Van der Waals type of interactions – assessed using the contact angle of diiodomethane;
{Facet 1 ≈ Facet 2 ≈ Facet 3 ≈ Facet 4} > {Facet 5 ≈ Facet 6 ≈ Facet 7 ≈ Facet 8}

The variation of the crystal facet contact angles as well as their deduced hydrophilicity and hydrogen binding potential, suggest that different chemical groups are exposed on the surface of the two pyramids. Interestingly the secondary nucleation seen during the griseofulvin crystal growth (section 5.3.1) was found to occur only on the tip of the hydrophilic crystal comprising facets 5-8.

5.3.3 Surface energy calculations of griseofulvin crystal

The contact angle data was analysed by the Owens-Wendt approach to obtain surface energies given in Table 5.4. As can be seen there was a facet dependent variation in the dispersive, polar and total surface energies.

Table 5.4: Surface energy of the griseofulvin crystal as calculated by Owens-Wendt approach.

Facet	γ_S^d (mJ/m^2)	γ_S^p (mJ/m^2)	γ (mJ/m^2)	γ_S^p/γ
1	46.2 ± 1.1	4.8 ± 0.8	51.0 ± 1.4	0.1
2	44.7 ± 1.3	5.9 ± 1.2	50.6 ± 1.6	0.1
3	45.6 ± 0.9	5.2 ± 0.9	50.8 ± 1.8	0.1
4	45.7 ± 1.2	4.0 ± 0.8	49.7 ± 1.5	0.1
5	38.1 ± 2	46.9 ± 2.4	85.0 ± 2.8	0.6
6	37.8 ± 1.7	41.6 ± 1.8	79.4 ± 2.5	0.5
7	39.6 ± 2.1	43.1 ± 1.5	82.7 ± 3.0	0.5
8	39.2 ± 1.8	41.7 ± 1.3	80.9 ± 2.6	0.5

Dispersive energies;

{Facet 1 ≈ Facet 2 ≈ Facet 3 ≈ Facet 4} > {Facet 5 ≈ Facet 6 ≈ Facet 7 ≈ Facet 8}

Polar energies;

{Facet 5 ≈ Facet 6 ≈ Facet 7 ≈ Facet 8} > {Facet 1 ≈ Facet 2 ≈ Facet 3 ≈ Facet 4}

Total surface energies;

{Facet 5 ≈ Facet 6 ≈ Facet 7 ≈ Facet 8} > {Facet 1 ≈ Facet 2 ≈ Facet 3 ≈ Facet 4}

The hydrophilic pyramid comprising facets 5-8 possessed higher polar and total surface energies in comparison with the hydrophobic pyramid comprising facets 1-4. In contrast, the hydrophobic pyramid had higher dispersive energies.

5.3.4 Single crystal X-ray diffraction of the griseofulvin crystal

The single crystal X-ray diffraction results revealed a tetragonal crystals with space parameters of a = b = 8.969 and c = 19.9, a result in agreement with values recorded in the Cambridge crystallographic database (Loew 2004) confirming that it was the griseofulvin form previously identified. The Miller indexing of the griseofulvin crystal had not been performed at the time of writing.

5.3.5 X-ray photoelectron spectroscopy of the griseofulvin crystal

XPS spectra was collected initially over a wide range of energies, then at a narrower range for the observed peaks (C1s, O1s e.t.c.) from both the top and bottom facets of the griseofulvin crystal (Appendix 6-9). A rough estimation of composition was then calculated giving a slightly higher O/C atomic compostition for the hydrophilic bottom pyramid surface.

The deconvolution and fitting of the peaks inorder to determine chemical functionalities exposed at each facet had not been performed at time of writing.

5.3.6 Computer modelling

5.3.6.1 Griseofulvin crystal

The percentage polar area and the electrostatic potential of the griseofulvin crystal across the (001), (010), (100), (-001), (-010) and (-100) planes are given in Table 5.5 (along with the corresponding results for the other drugs studied) and Figures 5.2 (a-f) respectively. A summary of the particle sizes obtained after milling griseofulvin with various stabilisers is given in Table 5.6 directly above Figures 5.2 (a-f).

The (001) plane of the griseofulvin crystal, which was the least polar of the studied griseofulvin crystal planes had a net positive electrostatic potential.

Table 5.5: The percentage polar area of the drug crystals across the (001), (010), (100), (-001), (-010) and (-100) planes.

Drug	(001)	(010)	(100)	(-001)	(-010)	(-100)
Albendazole	44.6	26.7	51.5	44.6	27.2	51.5
Carbamazepine	22.3	14.9	13.4	22.3	14.9	13.4
Frusemide	46.5	53.8	59.6	48.5	53.8	59.6
Griseofulvin	14.4	26.5	27.9	38.5	21.1	23.7
Indomethacin	24.2	49.9	47.2	24.2	49.9	47.2
Nabumetone	6.2	10.8	3	6.2	10.8	3

Table 5.6: Particle size (nm) obtained using photon correlation spectroscopy after 6 hours wet bead milling of griseofulvin in presence of a range of stabilisers (stabiliser concentration 1.5% w/w).

Drug	HPMC 8000	HPC 34000	HEC 33000	PVP 30	F127	Tween 80	SDS	DTAB
Griseofulvin	M	M	M	M	M	M	276.0	M

M: micron sized particles thus stabiliser not effective.

(a)

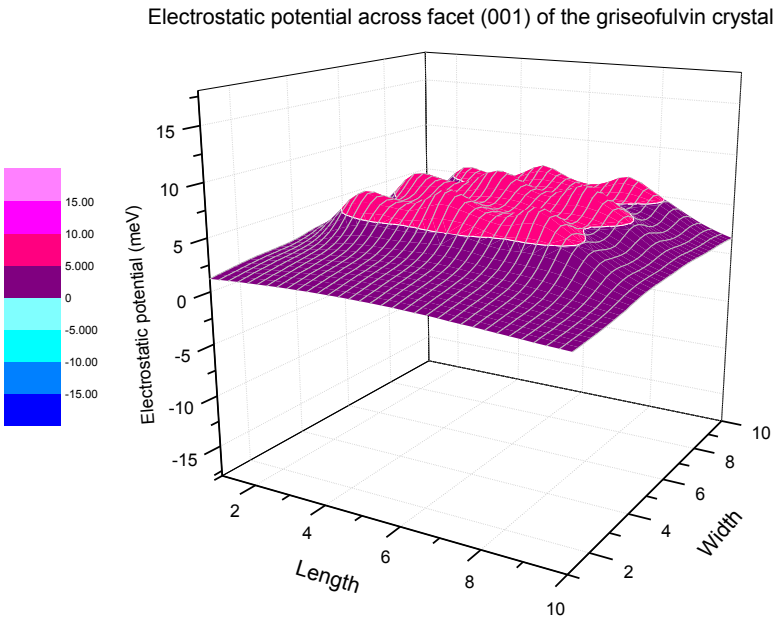

(b)

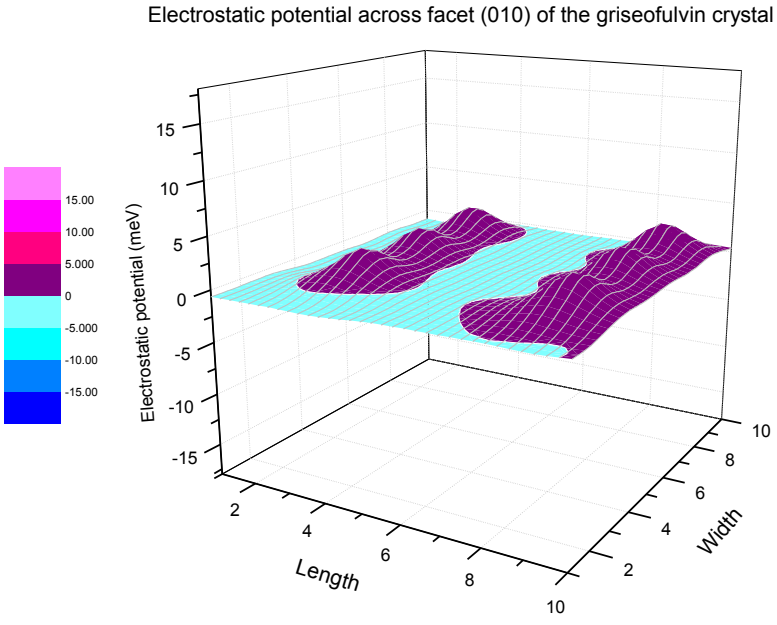

(c)

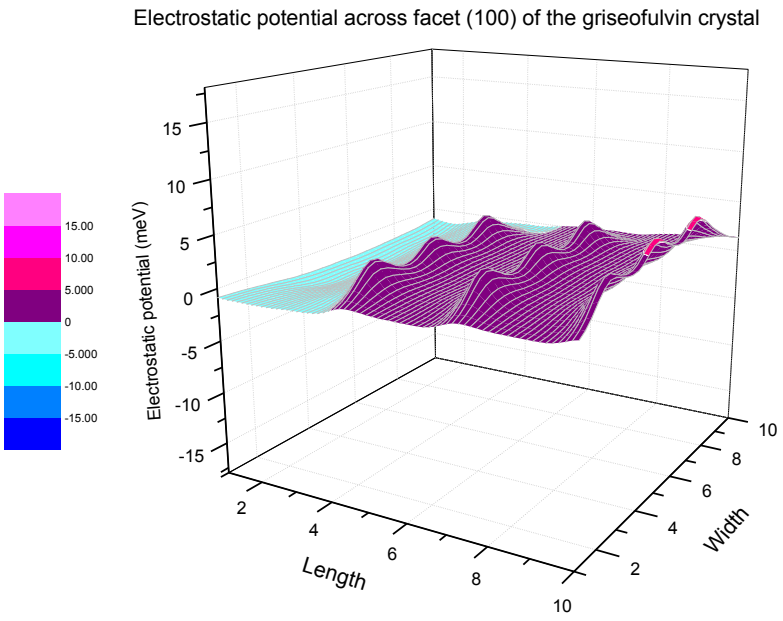
Electrostatic potential across facet (100) of the griseofulvin crystal
15.00
10.00
5.000
0
-5.000
-10.00
-15.00
Electrostatic potential (meV)
15
10
5
0
-5
-10
-15
2
4
6
8
10
Length
Width

(d)

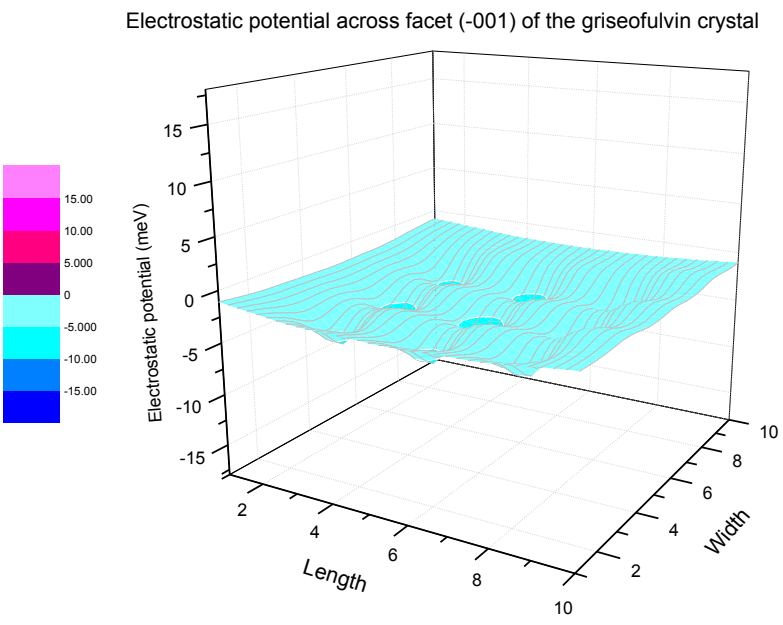
Electrostatic potential across facet (-001) of the griseofulvin crystal
15.00
10.00
5.000
0
-5.000
-10.00
-15.00
Electrostatic potential (meV)
15
10
5
0
-5
-10
-15
2
4
6
8
10
Length
Width

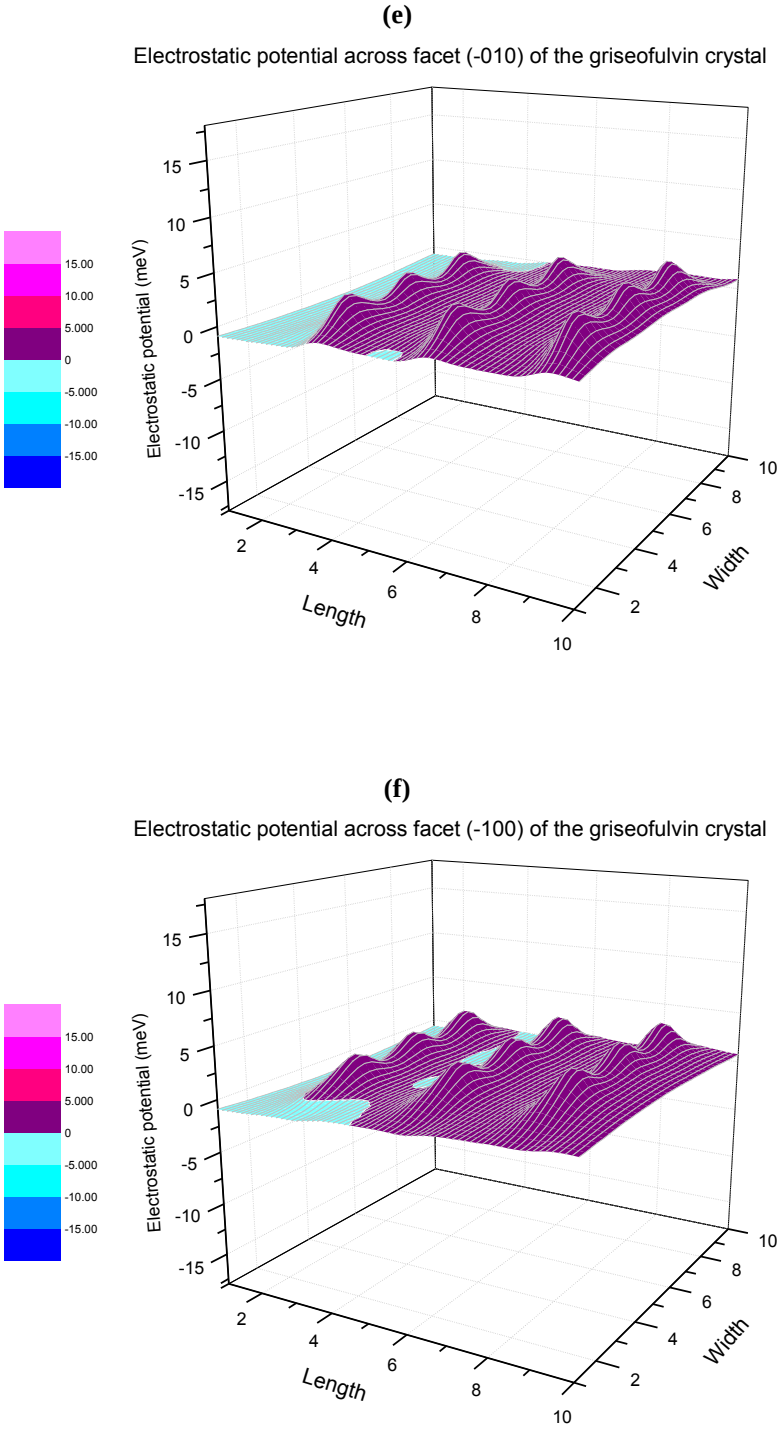

Figures 5.2 (a-f): Electrostatic potential (meV) of the griseofulvin crystal across facets (001), (010), (100), (-001), (-010) and (-100) respectively.

5.3.6.2 Other drug crystals

The percentage polar area and the electrostatic potential of the albendazole, carbamazepine, frusemide, indomethacin and nabumetone crystals across the (001), (010), (100), (-001), (-010) and (-100) planes are given in Table 5.5 and Figures 5.3-5.7 (a-f) respectively. A summary of the particle sizes obtained after milling the drugs with different stabilisers is given in the corresponding table (Tables 5.7-5.11) above each set of figures.

There was no clear pattern seen between the studied crystal facets and the properties of the stabilisers found to be effective during milling. In case of albendazole, carbamazepine, frusemide, indomethacin and nabumetone it is possibly that a different plane from the ones studied here is the crystal fracture plane.

Table 5.7: Particle size (nm) obtained using photon correlation spectroscopy after 6 hours wet bead milling of albendazole in presence of a range of stabilisers (stabiliser concentration 1.5% w/w).

Drug	HPMC 8000	HPC 34000	HEC 33000	PVP 30	F127	Tween 80	SDS	DTAB
Albendazole	513.4	316.2	406.8	440	M	M	309.4	463.5

M: micron sized particles thus stabiliser not effective.

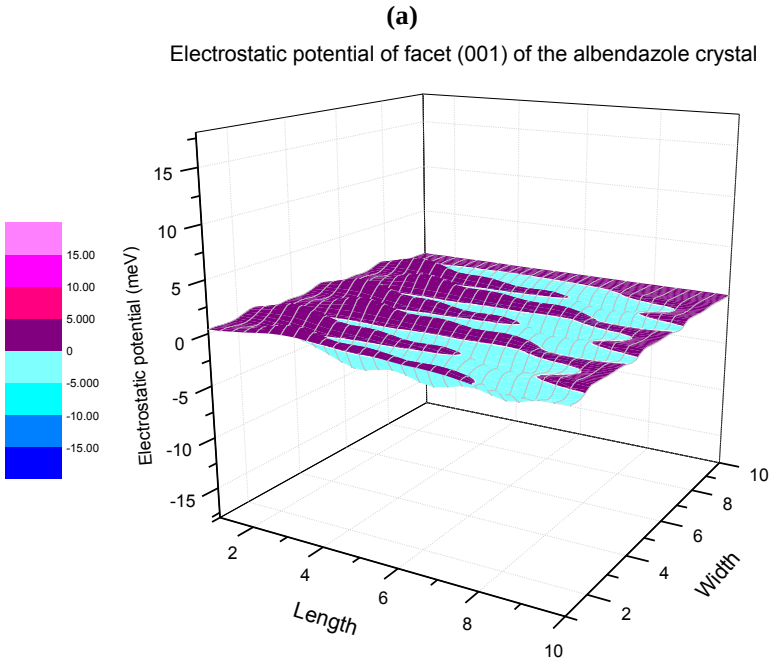

(b)

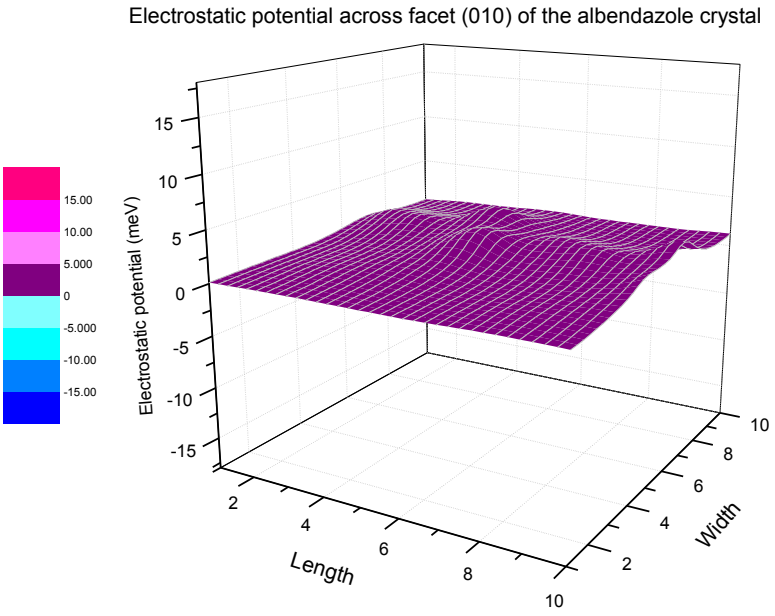
Electrostatic potential across facet (010) of the albendazole crystal
15.00
10.00
5.000
0
-5.000
-10.00
-15.00
Electrostatic potential (meV)
15
10
5
0
-5
-10
-15
2
4
6
8
10
Length
Width

(c)

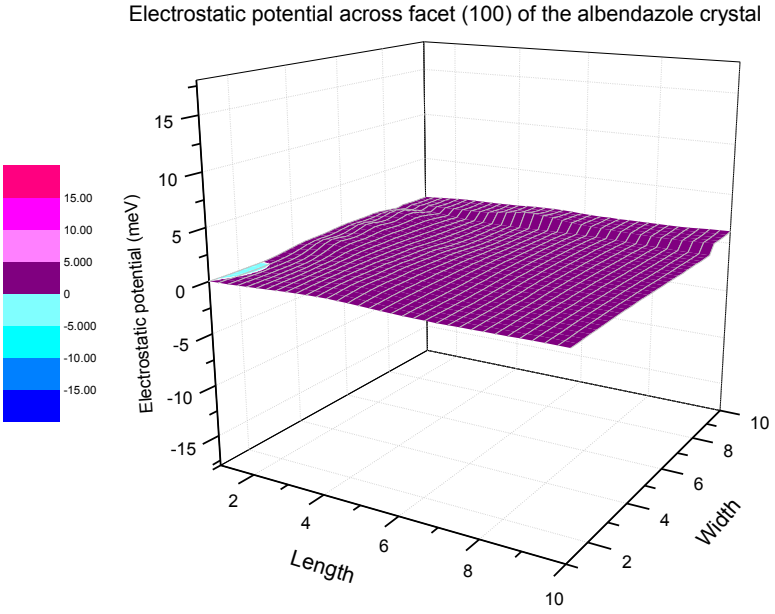
Electrostatic potential across facet (100) of the albendazole crystal
15.00
10.00
5.000
0
-5.000
-10.00
-15.00
Electrostatic potential (meV)
15
10
5
0
-5
-10
-15
2
4
6
8
10
Length
Width

(d)

Electrostatic potential across facet (-001) of the albendazole crystal

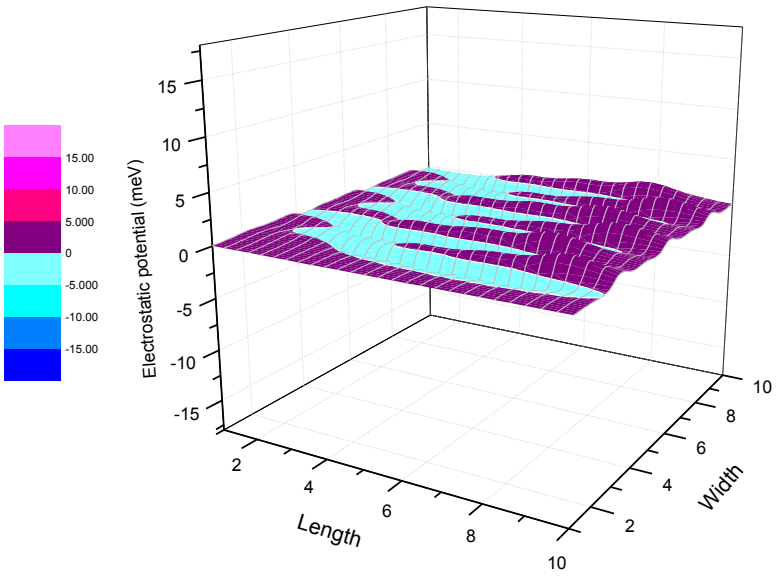

(e)

Electrostatic potential across facet (-010) of the albendazole crystal

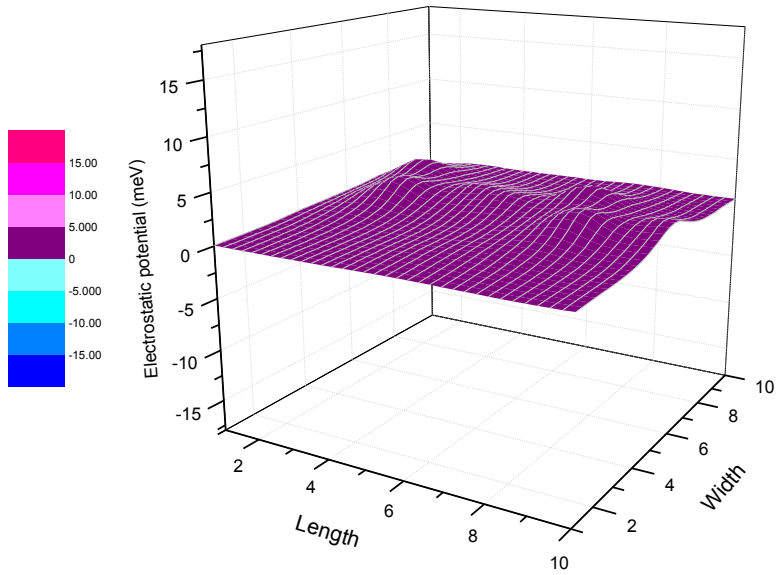

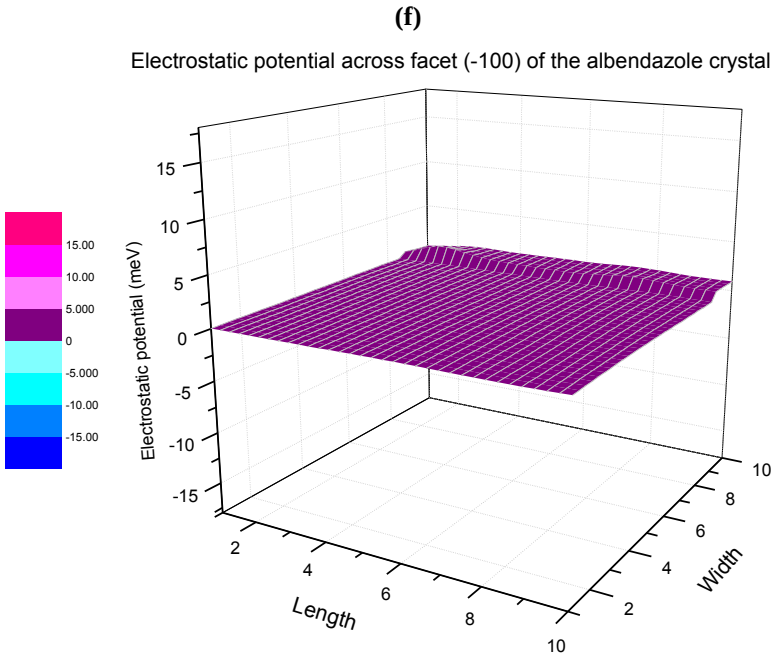

Figures 5.3 (a-f): Electrostatic potential (meV) of the albendazole crystal across facets (001), (010), (100), (-001), (-010) and (-100) respectively.

Table 5.8: Particle size (nm) obtained using photon correlation spectroscopy after 6 hours wet bead milling of carbamazepine in presence of a range of stabilisers (stabiliser concentration 1.5% w/w).

Drug	HPMC 8000	HPC 34000	HEC 33000	PVP 30	F127	Tween 80	SDS	DTAB
Carbamazepine	482.9	730.0	M	M	M	M	M	M

M: micron sized particles thus stabiliser not effective.

(a)

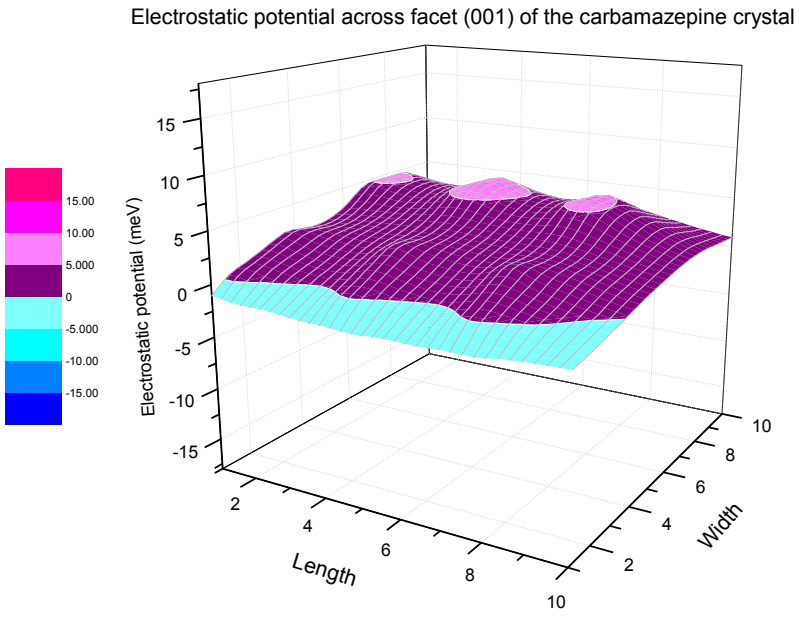

(b)

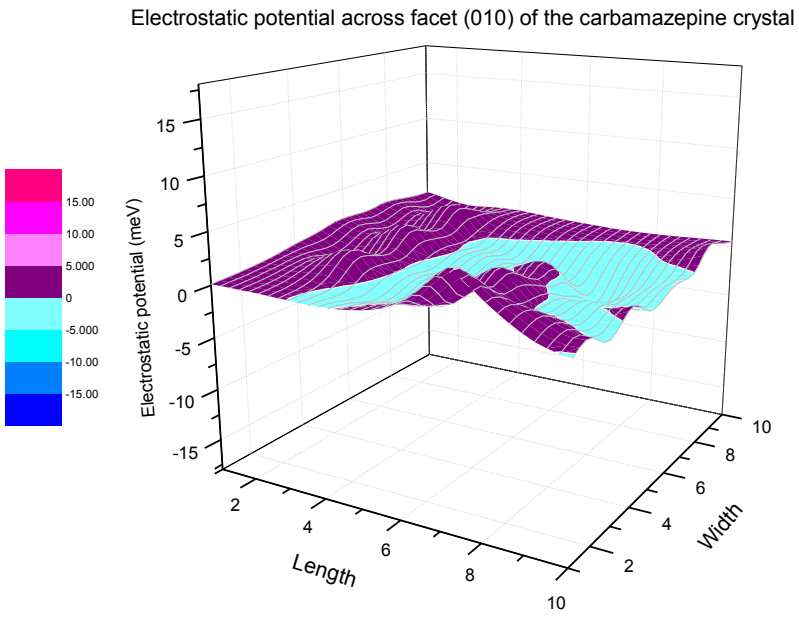

(c)

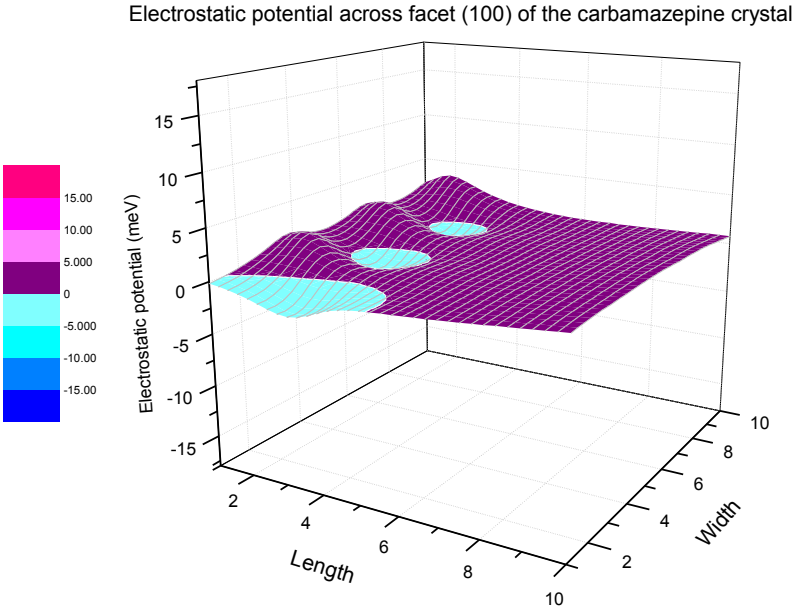
Electrostatic potential across facet (100) of the carbamazepine crystal
15.00
10.00
5.000
0
-5.000
-10.00
-15.00
Electrostatic potential (meV)
15
10
5
0
-5
-10
-15
2
4
6
8
10
Length
Width

(d)

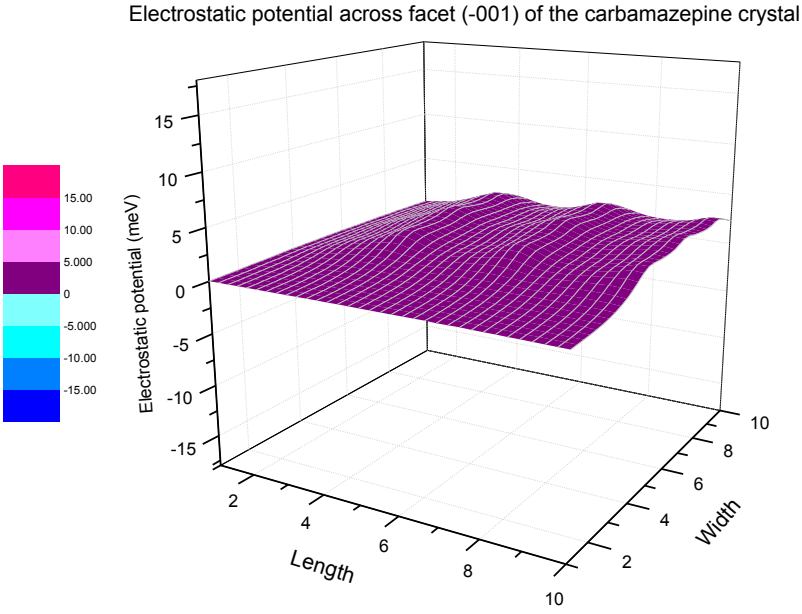
Electrostatic potential across facet (-001) of the carbamazepine crystal
15.00
10.00
5.000
0
-5.000
-10.00
-15.00
Electrostatic potential (meV)
15
10
5
0
-5
-10
-15
2
4
6
8
10
Length
Width

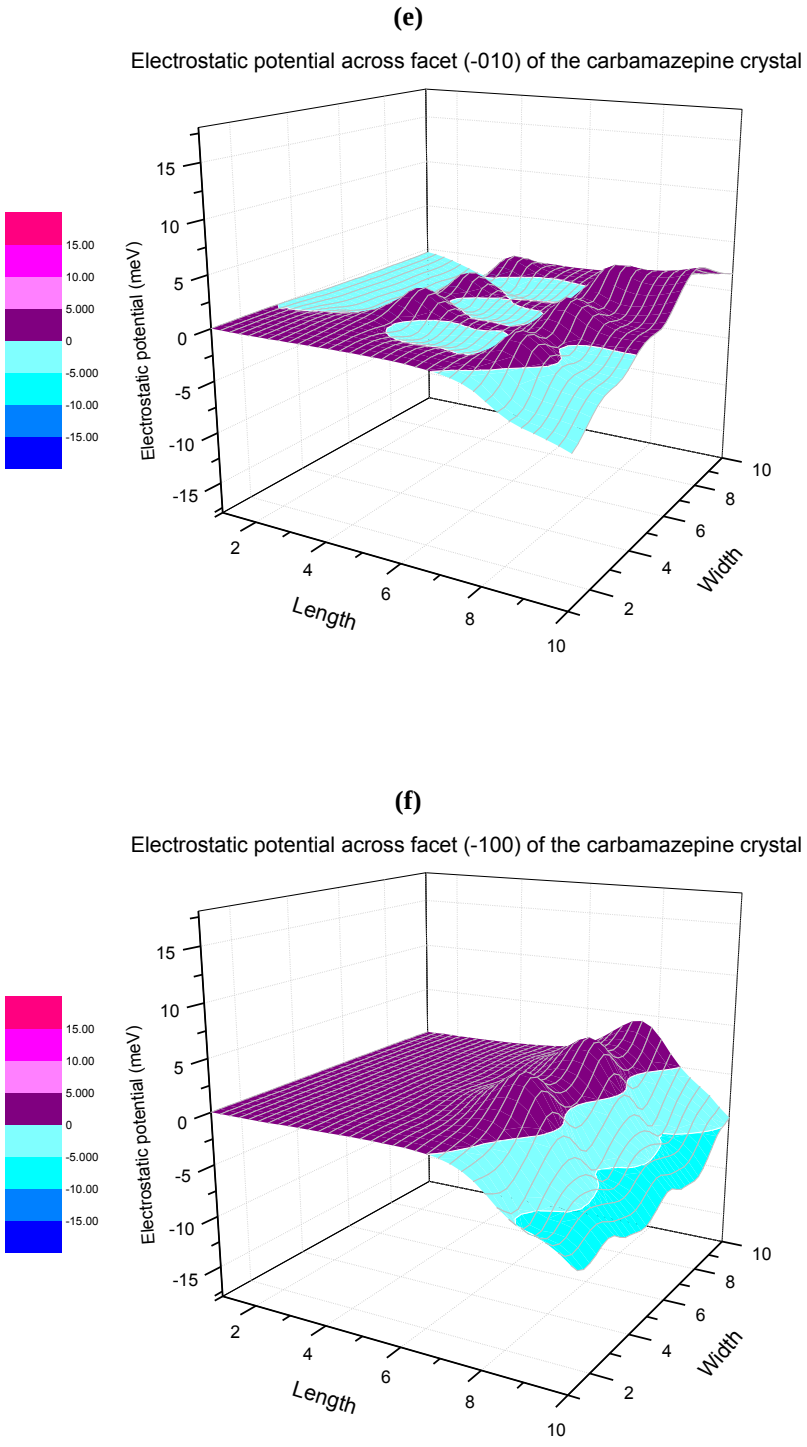

Figures 5.4 (a-f): Electrostatic potential (meV) of the carbamazepine crystal across facets (001), (010), (100), (-001), (-010) and (-100) respectively.

Table 5.9: Particle size (nm) obtained using photon correlation spectroscopy after 6 hours wet bead milling of frusemide in presence of a range of stabilisers (stabiliser concentration 1.5% w/w).

Drug	HPMC 8000	HPC 34000	HEC 33000	PVP 30	F127	Tween 80	SDS	DTAB
Frusemide	**246.4**	**199.6**	**380**	**234.9**	**347.8**	**417.3**	**M**	**M**

M: micron sized particles thus stabiliser not effective.

(a)

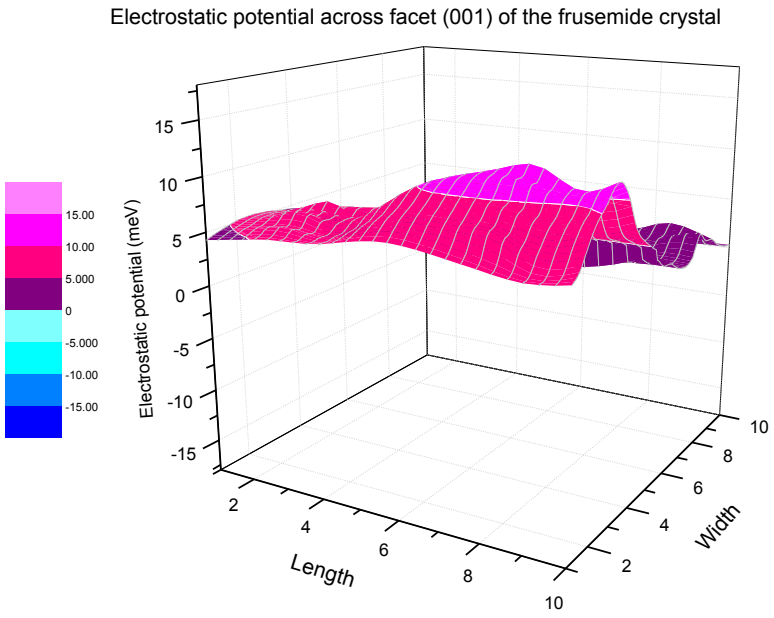

(b)

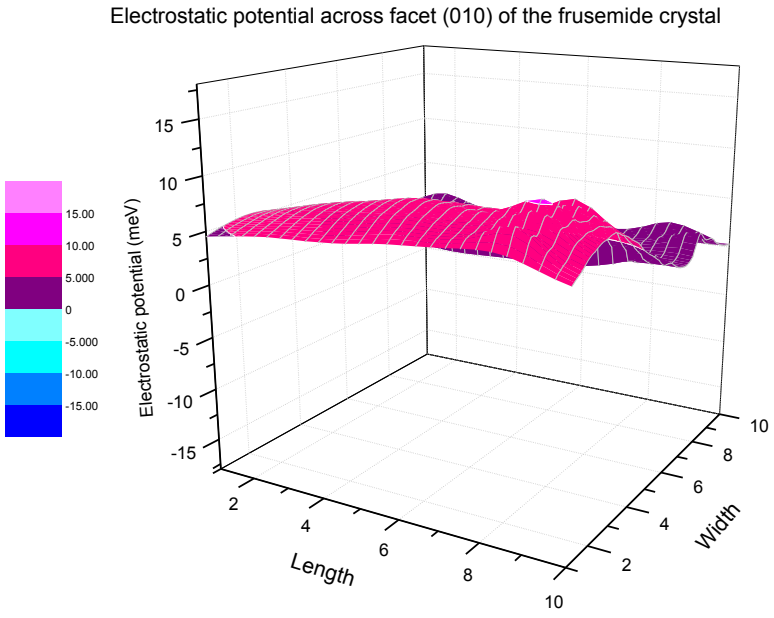

(c)

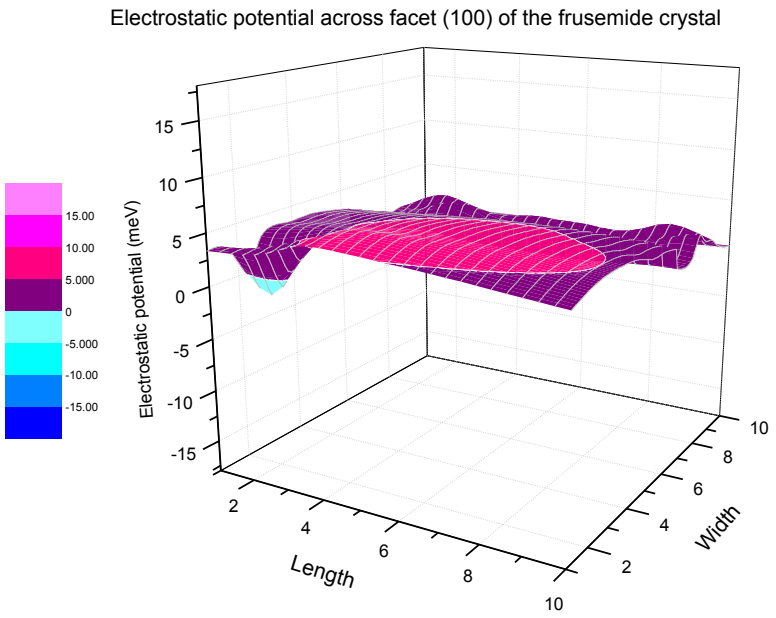
Electrostatic potential across facet (100) of the frusemide crystal
15.00
10.00
5.000
0
-5.000
-10.00
-15.00
Electrostatic potential (meV)
15
10
5
0
-5
-10
-15
2
4
6
8
10
Length
2
4
6
8
10
Width

(d)

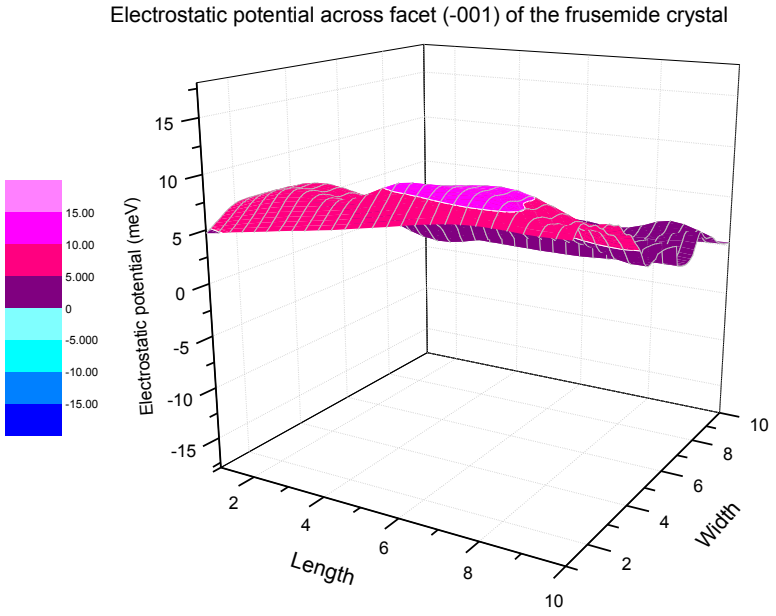
Electrostatic potential across facet (-001) of the frusemide crystal
15.00
10.00
5.000
0
-5.000
-10.00
-15.00
Electrostatic potential (meV)
15
10
5
0
-5
-10
-15
2
4
6
8
10
Length
2
4
6
8
10
Width

(e)

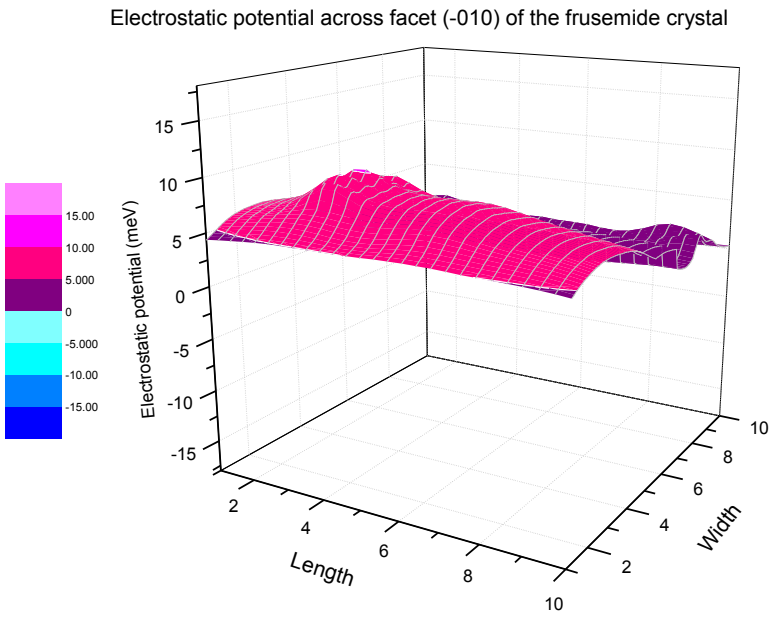

(f)

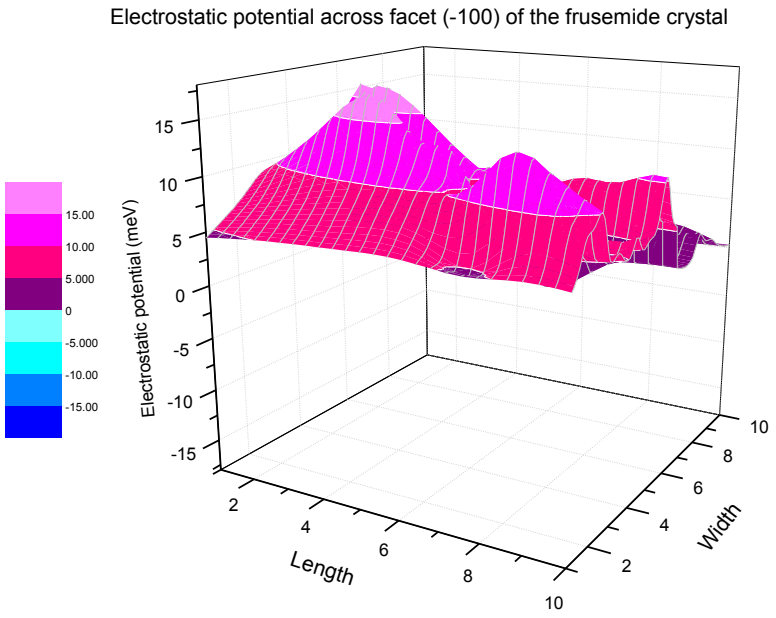

Figures 5.5 (a-f): Electrostatic potential (meV) of the frusemide crystal across facets (001), (010), (100), (-001), (-010) and (-100) respectively.

Table 5.10: Particle size (nm) obtained using photon correlation spectroscopy after 6 hours wet bead milling of indomethacin in presence of a range of stabilisers (stabiliser concentration 1.5% w/w).

Drug	HPMC 8000	HPC 34000	HEC 33000	PVP 30	F127	Tween 80	SDS	DTAB
Indomethacin	**237**	**210**	**320**	**260**	**640**	**308.9**	**M**	**M**

M: micron sized particles thus stabiliser not effective.

(a)

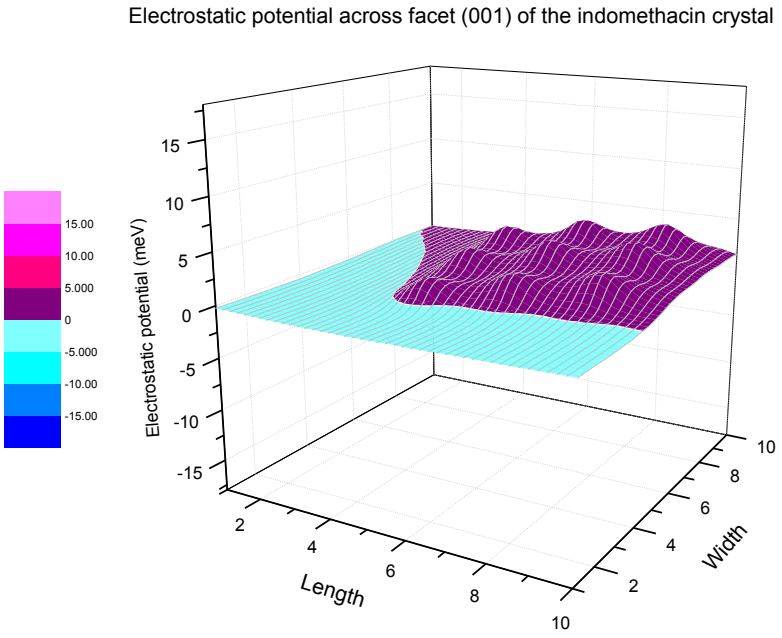

(b)

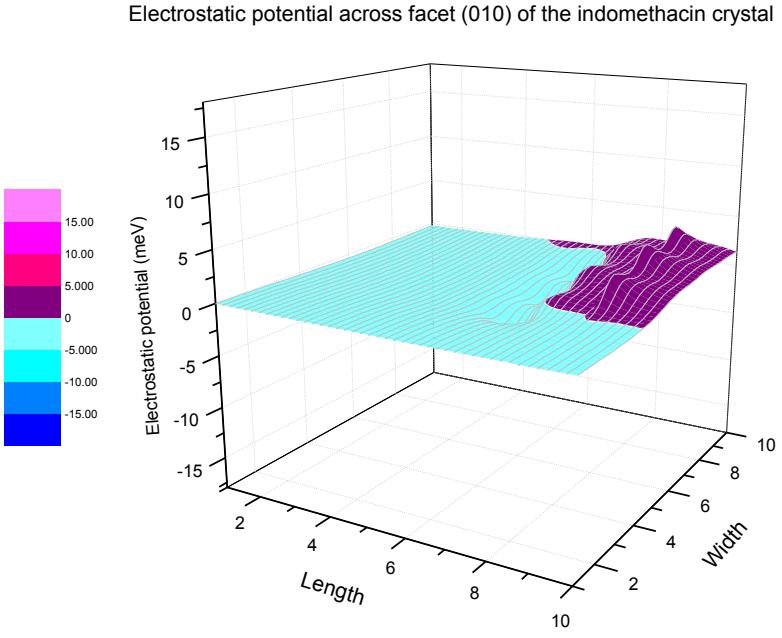

(c)

Electrostatic potential across facet (100) of the indomethacin crystal

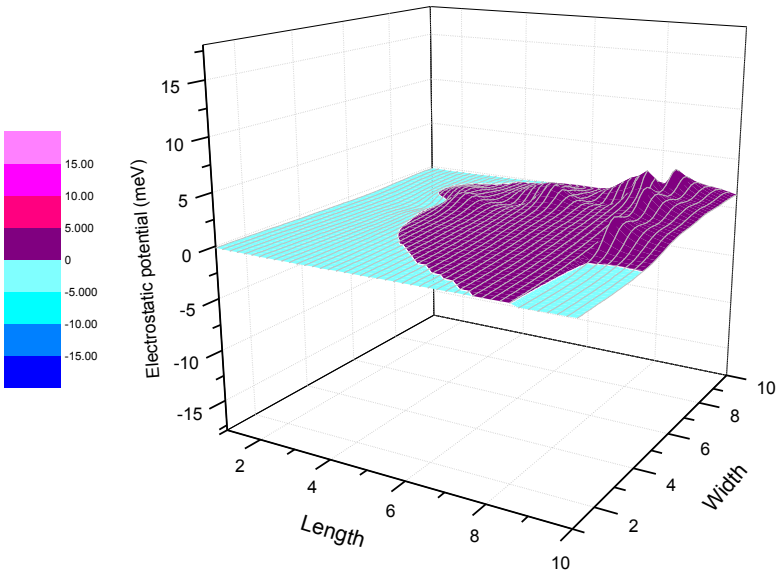

(d)

Electrostatic potential across facet (-001) of the indomethacin crystal

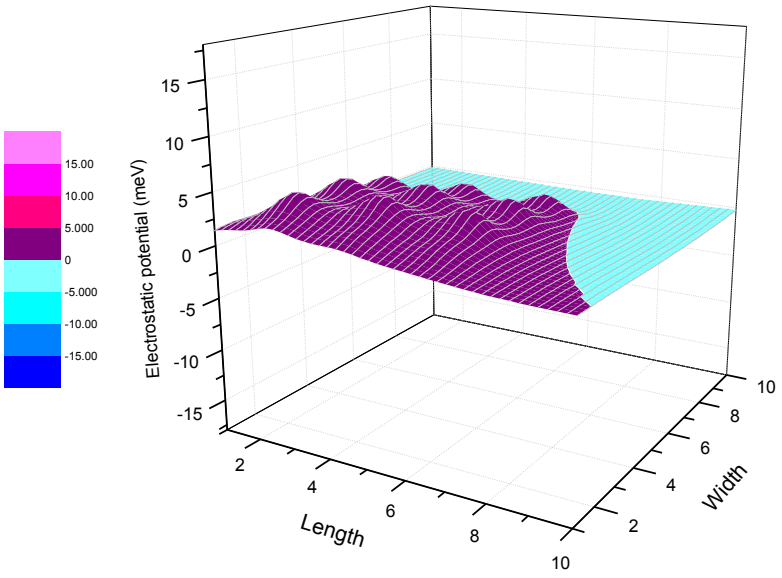

(e)

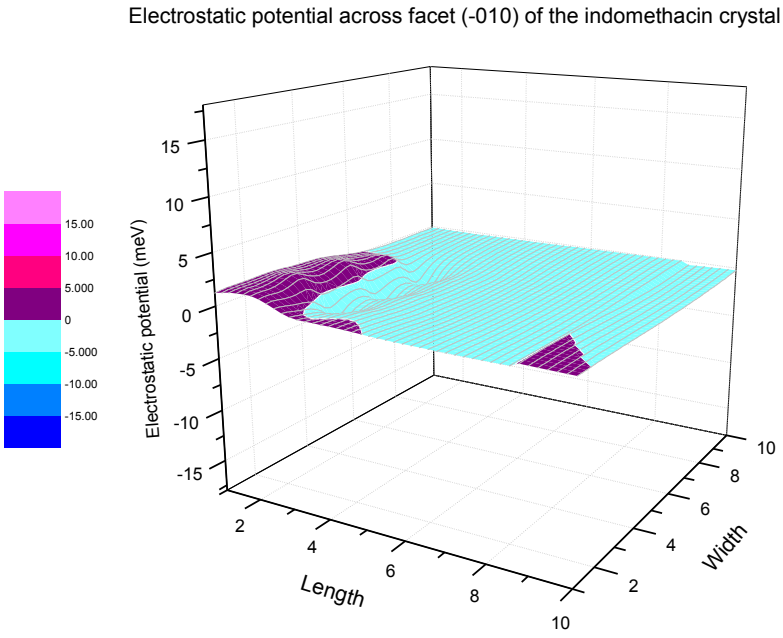

(f)

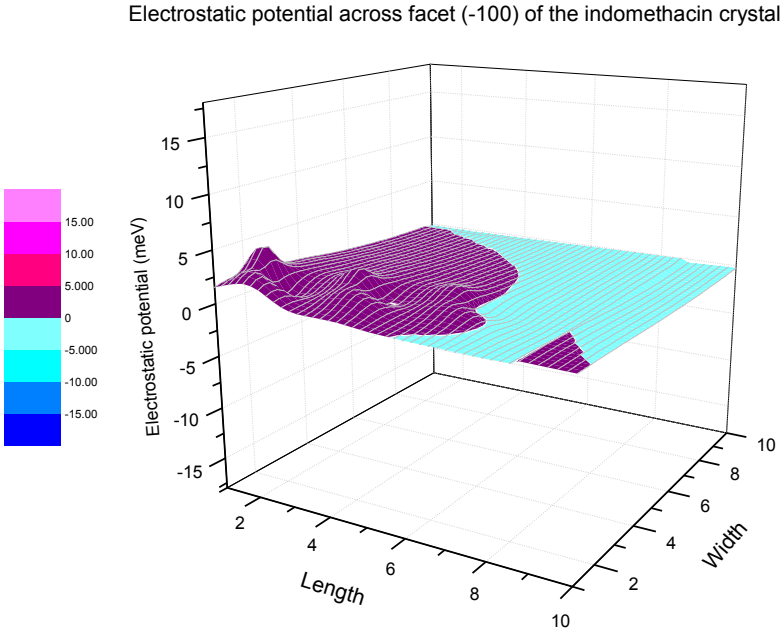

Figures 5.6 (a-f): Electrostatic potential (meV) of the indomethacin crystal across facets (001), (010), (100), (-001), (-010) and (-100) respectively.

Table 5.11: Particle size (nm) obtained using photon correlation spectroscopy after 6 hours wet bead milling of nabumetone in presence of a range of stabilisers (stabiliser concentration 1.5% w/w).

Drug	HPMC 8000	HPC 34000	HEC 33000	PVP 30	F127	Tween 80	SDS	DTAB
Nabumetone	**388.3**	**359.1**	**M**	**M**	**M**	**M**	**M**	**M**

M: micron sized particles thus stabiliser not effective.

(a)

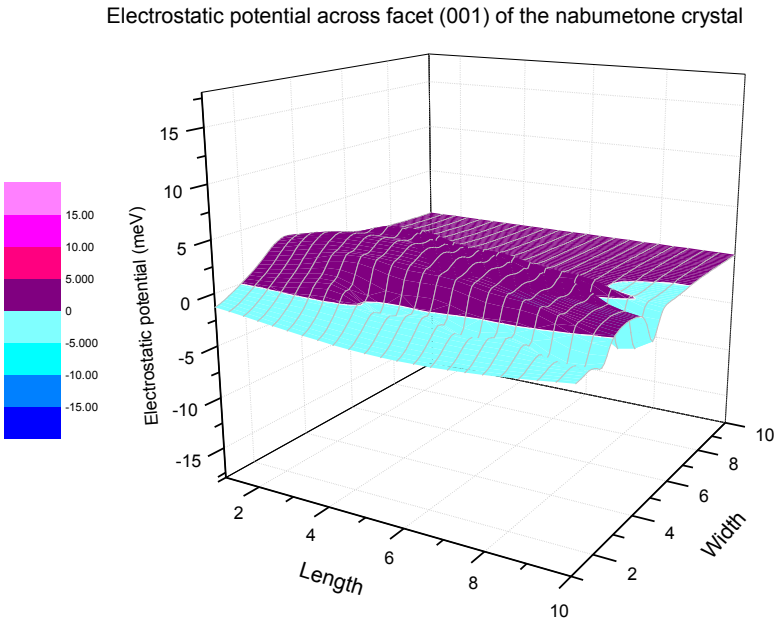

(b)

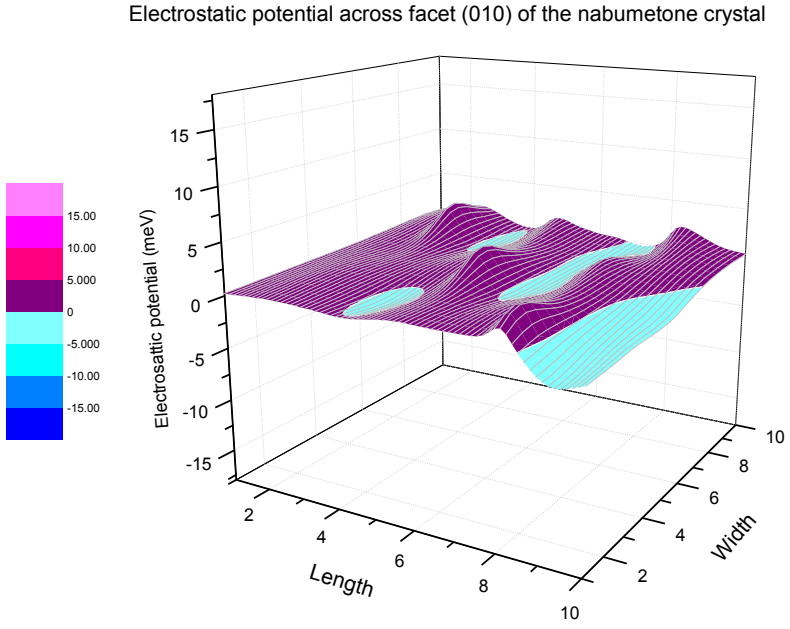

(c)

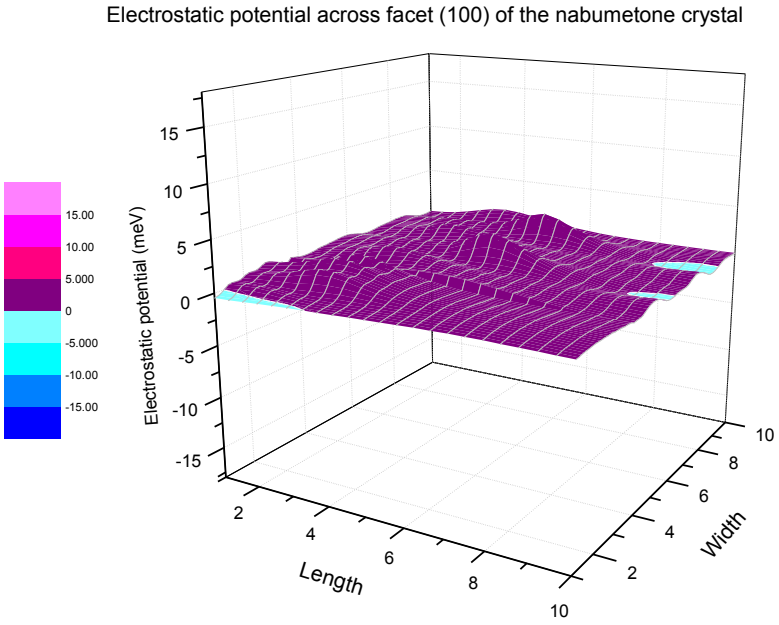
Electrostatic potential across facet (100) of the nabumetone crystal
15.00
10.00
5.000
0
-5.000
-10.00
-15.00
Electrostatic potential (meV)
15
10
5
0
-5
-10
-15
2
4
6
8
10
Length
2
4
6
8
10
Width

(d)

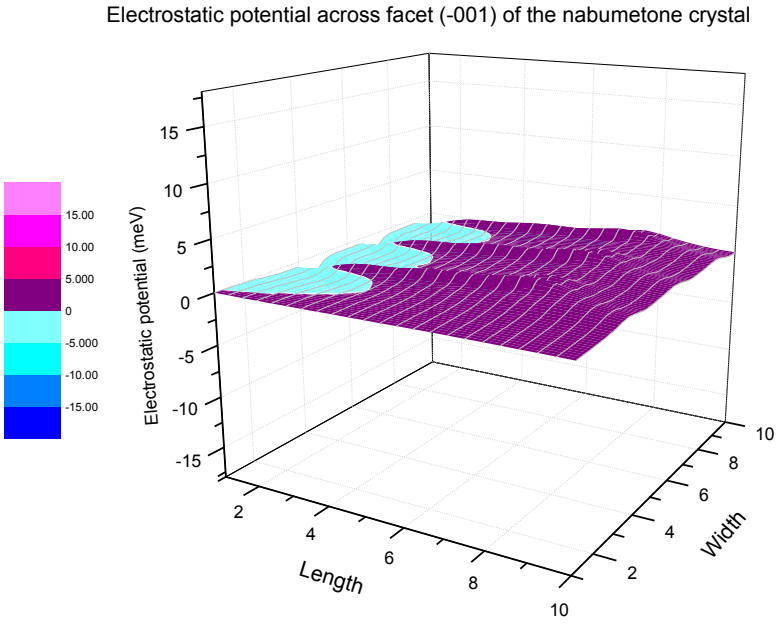
Electrostatic potential across facet (-001) of the nabumetone crystal
15.00
10.00
5.000
0
-5.000
-10.00
-15.00
Electrostatic potential (meV)
15
10
5
0
-5
-10
-15
2
4
6
8
10
Length
2
4
6
8
10
Width

(e)

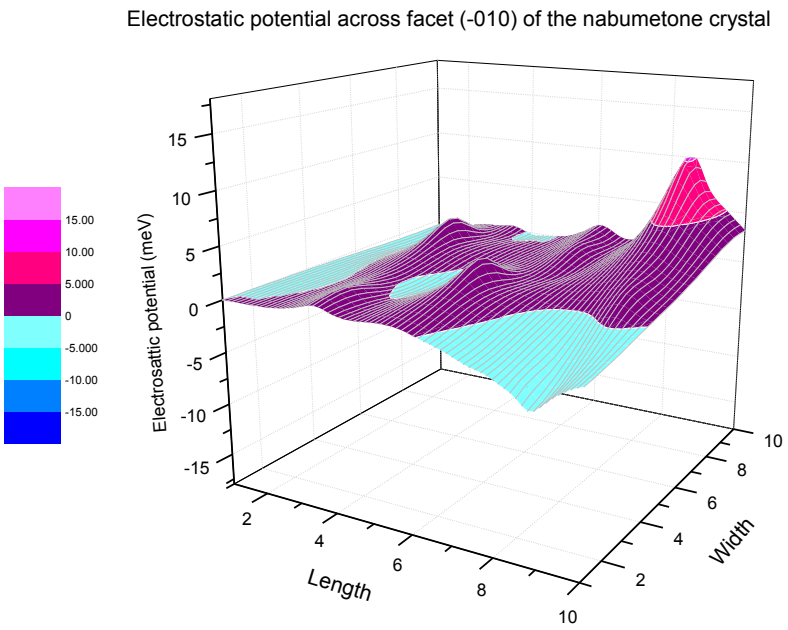

(f)

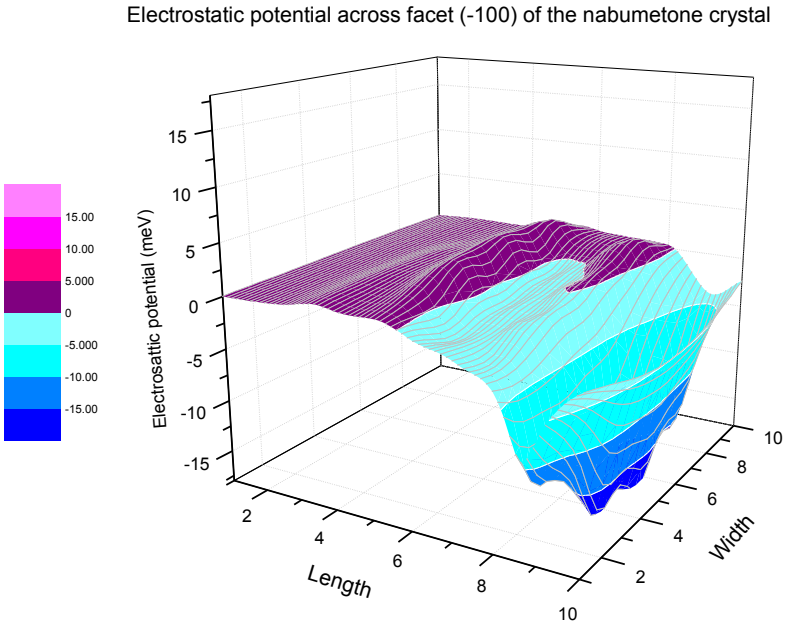

Figures 5.7 (a-f): Electrostatic potential (meV) of the nabumetone crystal across facets (001), (010), (100), (-001), (-010) and (-100) respectively.

5.4 Summary

Crystallographic studies were performed in order to establish the effect of the drug crystal surface energy on the drug-stabiliser interaction during milling. Crystals generally fracture along a particular face, whose properties dominate the milled state (York et al, 1998). Indeed it was hoped that prior knowledge of the fracture plane properties may enable prediction of suitable stabilisers for production of crystalline drug nanoparticles by wet bead milling.

Macroscopic griseofulvin crystals were grown in acetone yielding bipyramidal crystals of ~ 1 cm. Contact angle measurements were performed on each of the eight crystal faces using four probe liquids namely water, ethylene glycol, formamide and diiodomethane revealing anisotropic wetting behaviour of the two pyramids. Each of the four facets forming individual pyramids had very similar wetting properties. One pyramid was hydrophilic exhibiting lower contact angles for water, formamide and ethylene glycol, while the other pyramid was hydrophobic with a measured contact angle for water of more than 35º greater than that obtained for the hydrophilic pyramid. The measured contact angle of diiodomethane was greater for the hydrophilic pyramid indicating a lower dispersive energy. Surface energy calculations performed using the Owens-Wendt approach, determined that the hydrophobic pyramid possessed higher dispersive energies and lower polar energies than the hydrophilic pyramid.

Computer modelling was performed to elucidate the percentage polar area and electrostatic potential of the (001), (010), (100), (-001), (-010) and (-100) planes of the griseofulvin crystal. The (001) plane which was found to be the least polar was postulated to be the fracture plane of the griseofulvin crystal. The (001) plane also had a net positive electrostatic potential. This result is quite interesting as it would explain why griseofulvin could only be stabilised by anionic stabilisers during milling. Computer modelling of the (001), (010), (100), (-001), (-010) and (-100) planes of albendazole, carbamazepine, frusemide, indomethacin and nabumetone crystals was also performed. The properties of the assumed planes of these drug crystals were not predictive of stabiliser efficiency during drug milling indicating that the plane of fracture may be a plane not investigated in the present study.

Chapter 6
General discussion

The majority of drugs are administered orally, with their bioavailability being dependent on their dissolution within the gut and absorption across the gastrointestinal membranes. ~ 40% of newly discovered drugs being poorly water soluble (Lipinski 2002) pose a significant formulation challenge to the pharmaceutical industry. Poor water drug solubility is associated with poor dissolution and bioavailability, high fed to fasted ratio and high inter patient variability. Micronisation, salt formation, solubilisation, pH adjustment, complexation with cyclodextrins, polymorphism, the use of prodrugs, have been

used as formulation strategies to increase drug aqueous solubility. Recently formulation of poorly soluble drugs as drug nanoparticles, defined as drug particles below 1000 nm in size, using both 'top down' and 'bottom up' approaches has been the centre of focus. Top down approaches include media milling and high pressure homogenisation whereby the large drug particles are broken down into nano-sized particles; while bottom up approaches include crystallisation, precipitation whereby nano-sized drug is grown from drug in solution. Nanoparticles are produced in presence of stabilisers mainly polymers and/or surfactant which coat that nanoparticles on production, thereby providing a barrier against aggregation due to high Van der Waal forces. Wet bead milling has had the most success with five drugs namely Rapamune®, Emend®, Tricor®, Megace ES® and Sustenna® reaching the market. Despite success of this technique, the mastery behind the stabilisation mechanisms of drug nanoparticles is still lacking. The selection of stabilisers is carried out on an empirical basis by trial and error. Furthermore the effective stabilisers vary with drug and with technique used to produce the drug nanoparticles.

The overarching aim of the thesis is to gain a better understanding of nanoparticle stabilisation mechanisms by studying effect of different polymers and/or surfactant on nanoparticle production, determining polymer/surfactant adsorption isotherms on the nanoparticle surfaces and establishing the drug surface energetics. Wet bead milling was carried out using Retsch MM 200 mixer mills and yttrium zirconia beads (0.44 mm diameter) at a frequency setting of 30Hz for 6 hours with the resultant particle size determined by photon correlation spectroscopy. A drug-stabiliser screen was carried out using eight poorly water soluble structurally different drugs namely albendazole, carbamazepine, frusemide, halofantrine, griseofulvin, indomethacin, nabumetone and phenytoin and thirteen pharmaceutically acceptable stabilisers including cellulosic polymers, polyvinylpyrrolidone, Pluronic F127, surfactants; Tween 80, sodium dodecyl sulphate, aerosol-OT and dodecyltrimethyammonium bromide. The ease of stabiliser selection for nanoparticle production was found to increase with drug molecular weight and number of functional groups. The number of effective stabilisers was also found to be higher for the least water soluble drugs. The drug-stabiliser screen revealed no obvious pattern and each of the drugs studied displayed a unique stabilisation profile that could not be predicted from its physical or chemical properties.

Subsequent work was carried out using the non-ionic drug griseofulvin. Griseofulvin nanoparticles could only be produced in presence of anionic stabilisers namely sodium dodecyl sulphate, aerosol-OT and hydroxypropylmethylcellulose acetate succinate. The production of griseofulvin nanoparticles was effective at drug: anionic stabiliser weight ratios of between 2.5:1 and 125:1. Ionic stabilisers are not favoured for oral delivery due to their incompatibility with acid, salts and other ionic excipients. The use of electrosteric stabilisation using non-ionic polymer hydroxypropylmethylcellulose (HPMC) was investigated. Synergistic effects between non-ionic polymers and ionic surfactants have been utilised in fields such as paint, mineral and cosmetic industries. Inclusion of the non-ionic polymer in the milling slurry was aimed at reducing the amount of ionic surfactant required for nanoparticle production. Surface tension studies showed the interaction of the non–ionic polymer HPMC and anionic surfactants (SDS & AOT) at the air-water interface. Polymer-surfactant interaction at the solid-drug interface could be envisaged with co-adsorption of HPMC and ionic surfactant onto the griseofulvin nanoparticles.

Inclusion of a constant amount (1.88% w/w) of HPMC 8000 in the milling slurry lead to a reduction of the minimum concentration of anionic surfactant necessary for griseofulvin nanoparticle production. These observations were highly suggestive of non-ionic polymer and anionic surfactant co-stabilisation at the nanoparticle surfaces.

The effect of polymer molecular weight and concentration was investigated by milling griseofulvin in presence of varying concentrations of HPMC 8000, 15000, 86000 and constant amount (0.5% w/w) of SDS. Polymer concentration and molecular weight effects were observed. Nanoparticles could only be produced up to a maximum polymer concentration which decreased with increasing polymer molecular weight. For instance, nanoparticles could not be produced in presence of HPMC 86000 even at the lowest concentration of 0.1% w/w polymer. These observations were attributed to increase in slurry viscosity with polymer molecular weight and concentration as well as slower diffusion of the higher molecular polymer to cleaved drug surfaces.

Milling of pharmaceutical crystalline materials may introduce a degree of amorphicity due to exposure to mechanical stresses. Powder X-ray diffraction (XRD) was used to screen the griseofulvin samples for any milling induced disorder.

Similar XRD patterns in terms of peak presence and position were observed before and after milling indicating the crystallinity of griseofulvin was maintained. Scanning electron microscopy (SEM) of a selection of samples was used to visualise the griseofulvin nanoparticles after milling. The SEM particles sizes were in good agreement with those obtained by light scattering.

Polymer/surfactant adsorption was determined indirectly by measuring the depletion of respective entity from the supernatant obtained after centrifuging the drug nanoparticles. Spectroscopic techniques namely colorimetric stains all assay and optical rotatory dispersion (ORD) were used to establish adsorbed amounts of polymer and anionic surfactant respectively. Anionic surfactant adsorption onto griseofulvin nanoparticles was found to increase with starting surfactant concentration, reaching a plateau at about 2.2 mg/m^2. The adsorption isotherms of both surfactants namely SDS and AOT displayed no marked differences. The anionic surfactant head group is envisaged to be adsorbing via electrostatic interaction to a positively charged griseofulvin surface, with a surfactant bilayer forming at high surfactant concentrations. Anionic surfactant adsorption was found to be consistently lower (~ 0.6 mg/m^2) in the non-ionic polymer-anionic surfactant formulations compared with surfactant only formulations suggesting the presence of co-adsorbing HPMC at the drug surfaces. Polymer adsorption could not be quantified by optical rotation due to interference by dissolved griseofulvin which is optically active with a peak about the wavelength of interest. Attempts to extract griseofulvin from drug supernatants prior to ORD experiments were not successful due to the surface activity of the HPMC polymer.

Small angle neutron scattering (SANS) was used for direct visualisation of the polymer/surfactant adsorbed at the drug surfaces. Using D_2O:H_2O solvent contrast matching to the drug's neutron refractive index, the drug particles were made 'invisible'. Thus any scattering seen was due to the adsorbed polymer/surfactant layer. SANS experiments were carried out at the Institut Laue-Langevin (France) and Paul Scherrer Institut (Switzerland). A selection of griseofulvin nanoparicles prepared in presence of both surfactant and polymer-surfactant systems were selected for neutron studies. Neutron scattering obtained from the nanoparticles prepared using polymer-surfactant systems was markedly higher than that from nanoparticles prepared using surfactant only systems. The drug-surfactant data could not be fitted due to extremely low scatter. The drug-polymer-surfactant data were

successfully fitted confirming the earlier hypothesis of polymer-surfactant co-adsorption at the drug nanoparticle surfaces. The amount of HPMC adsorbing onto the drug nanoparticles was found to be 0.3-0.9 mg/m^2 in presence of either SDS or AOT. The thickness obtained for the polymer layer (~ 4 nm) was indicative of a polymer lying flat on the drug surfaces.

Association between a non-ionic polymer and an anionic surfactant is driven by hydrophobic interactions between surfactant hydrocarbon chains and hydrophobic parts of the polymer as well as by ion-dipole interactions between the ionic surfactant headgroups and the dipole of the hydrophilic parts of polymer (Goddard 1986). Figures 6.1-6.2 give schematic illustrations of the proposed interactions of the anionic surfactants and non-ionic polymer at the air-water and liquid-solid interfaces and in bulk liquid solution. In bulk solution SDS micelles are likely to interact with hydrophobic parts of polymer forming a 'pearl-necklace' model, while AOT which forms lamellar phase in bulk is likely interact with both hydrophobic and hydrophilic polymer parts.

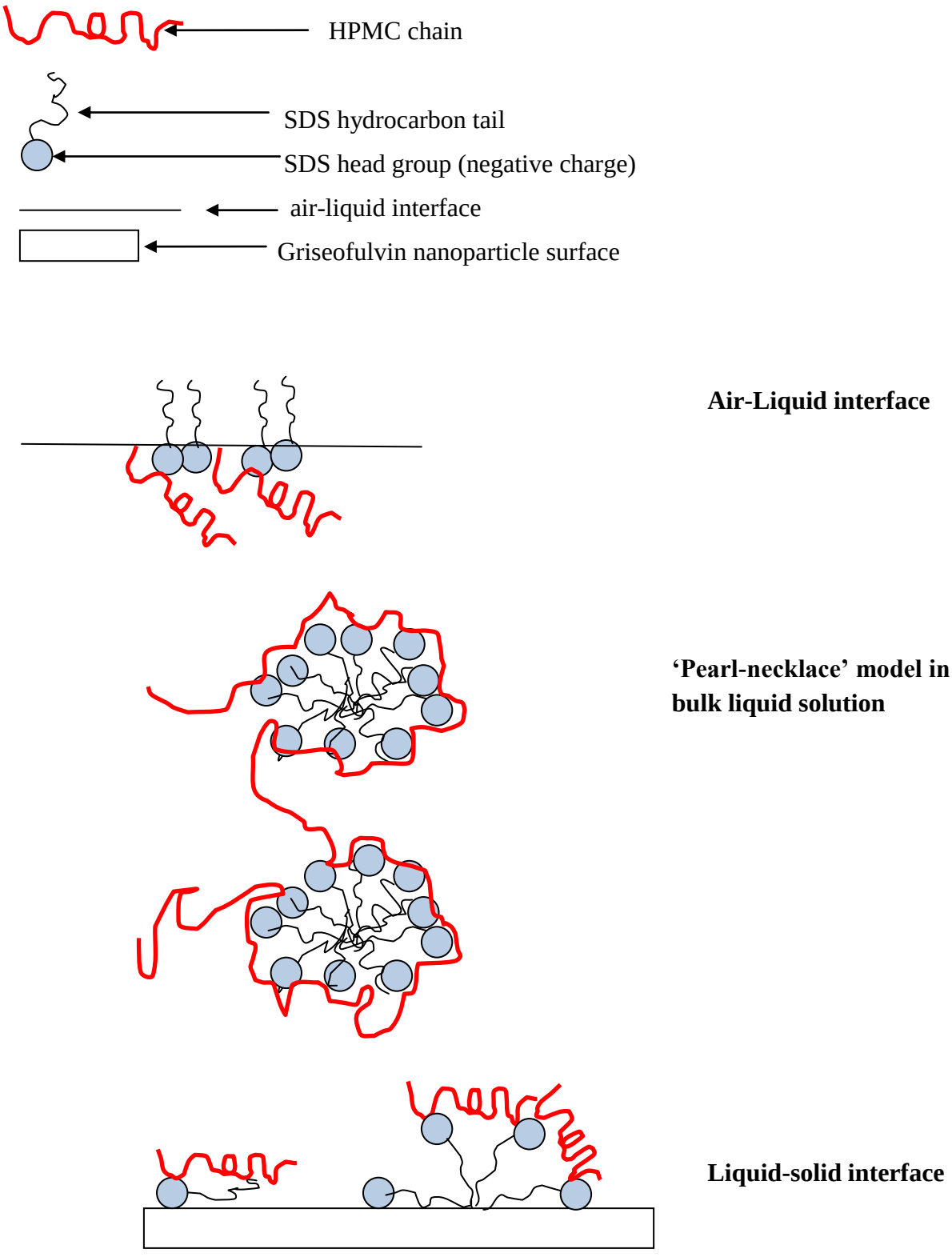

Figure 6.1: Schematic diagram illustrating the proposed interaction mechanism of HPMC and SDS at the air-liquid interface, in bulk solution and at the liquid-solid interface.

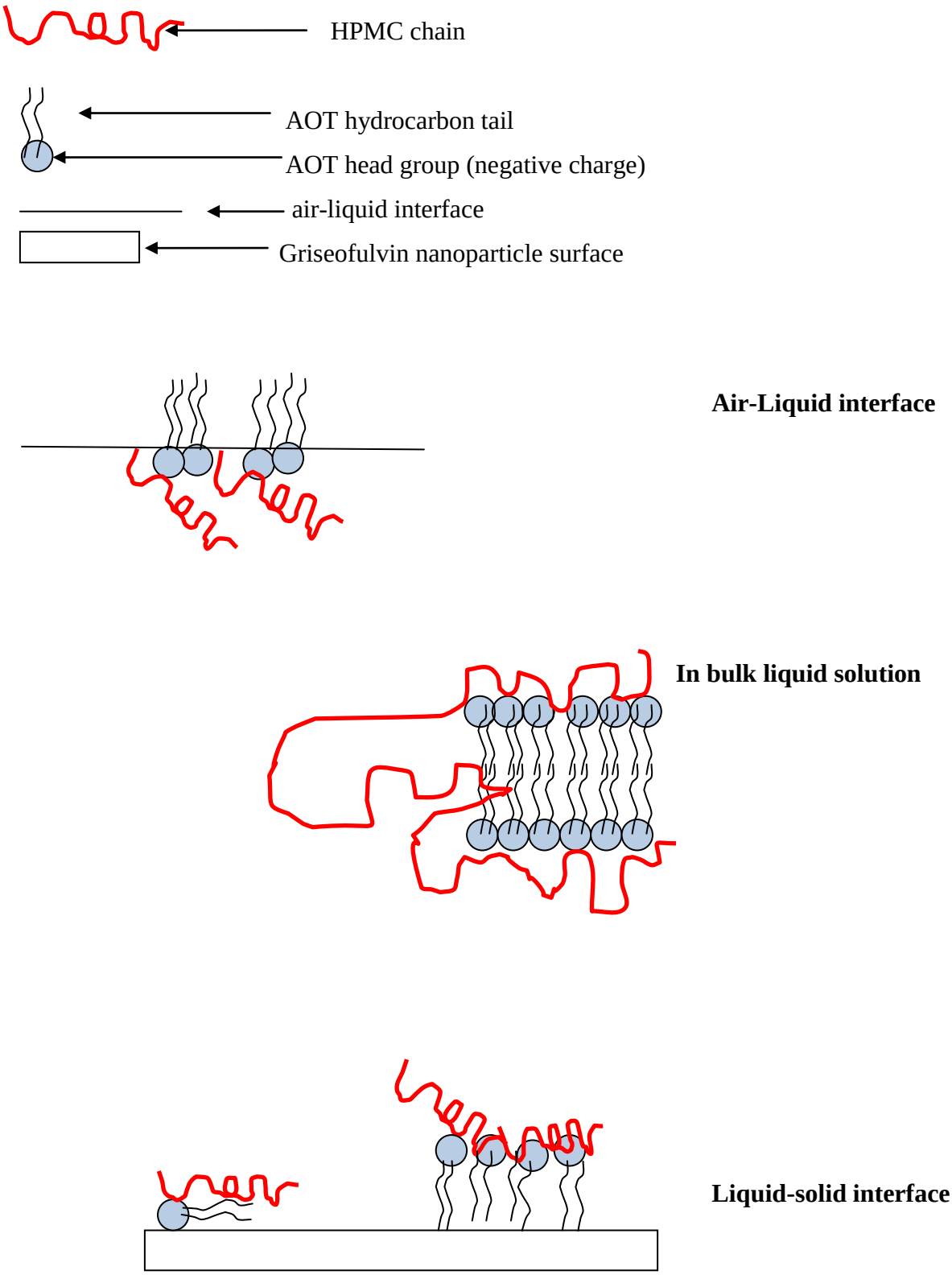

Figure 6.2: Schematic diagram illustrating the proposed interaction mechanism of HPMC and AOT at the air-liquid interface, in bulk solution and at the liquid-solid interface.

Griseofulvin nanoparticles were stored, as prepared in excess polymer/surfactant, for 1 year under ambient conditions and particle size monitored. Ostwald ripening was found to occur in all formulations due to the dissolution and reprecipitation of griseofulvin. The growth in particle size was more pronounced in the HPMC polymer-anionic surfactant formulations particularly at low anionic surfactant concentrations and high polymer concentration/molecular weight. It can be postulated that HPMC increased the solubilisation of griseofulvin leading to higher nanoparticle instability. Nanoparticles formulated in presence of anionic polymer HPMCAS were the least stable with most aggregating 1-3 months after storage. HPMCAS was the least suitable stabiliser for griseofulvin nanoparticles, which could partially explained by viscosity effects. The HPMCAS nanosuspensions were notably viscous on production. The Ostwald ripening seen with griseofulvin (64 μg/mL at 25ºC) may be explained by its high aqueous solubility, relative to nabumetone (4.7 μg/mL at 25ºC) and halofantrine (< 1.0 μg/mL at 25ºC) whose nanoparticles prepared and stored under similar conditions were stable for 1 year.

Simulation of the gastrointestinal stability of a nanoparticle formulation is important as the stomach microclimate favours aggregation, which may negate benefits conferred by particle size reduction (Zimmerman et al, 2001). pH stability of the nanoparticles was studied by monitoring particle size of griseofulvin nanoparticles resuspended in hydrochloric acid solutions of pH 1-6 and water - pH 7. The HPMCAS stabilised griseofulvin nanoparticles were the least stable, aggregating to form a visible cloudy precipitate on contact with a hydrochloric acid solution of pH in the range 1-4. HPMCAS was the least suitable stabiliser for griseofulvin nanoparticles intended for oral delivery. Some griseofulvin nanoparticles prepared in presence of anionic surfactant, aggregated on contact with a hydrochloric acid solution of pH in the range 1-2. Nanoparticles with the greatest amount of adsorbed surfactant and thus the higher zeta potential were least likely to aggregate at low pH. Electrosterically stabilised nanoparticles prepared in presence of anionic surfactant and non-ionic polymer HPMC were more stable at low surfactant concentrations, indicating non-ionic polymer conferred some protective effect.

Griseofulvin nanoparticles could only be produced in presence of anionic stabilisers, even though it is a neutral drug. The nature of surfaces exposed during milling depends on how the crystals fracture, with the properties of the weakest attachment face dominating (Heng et al, 2006 a,b,c). In a bid to characterise griseofulvin surface

energetics, sessile contact angle measurements were performed on macroscopic griseofulvin crystals (~ 1 cm) grown in acetone. Deionized water, formamide, ethylene glycol and diiodomethane were used as the liquid probes. The wetting results and surface energy calculations revealed anisotropic facet dependent surface chemistry of the griseofulvin crystal. Further work into determination of the chemical groups exposed at the various crystal surfaces and more so the drug's fracture plane would be instrumental in fully understanding the drug-stabiliser interaction mechanisms.

Chapter 7
Conclusion

Wet bead milling, in which a drug is milled in the presence of a solution of pharmaceutical acceptable stabilisers, is a promising technique for the formulation of poorly water-soluble drugs. The research investigated the use of non-ionic polymer-ionic surfactant systems for the production of drug nanoparticles by wet bead milling.

Interactions between the non-ionic polymer hydroxypropylmethylcellulose (HPMC) and anionic surfactants sodium dodecyl sulphate (SDS) and aerosol-OT (AOT) at the air-liquid interface, liquid-solid interface and in bulk solution were established. Surface tension measurements as a function of the anionic surfactant concentration were carried out both in absence and presence of 0.1% w/w HPMC 8000. In the

presence of polymer, a break point corresponding to the critical aggregation concentration (cac) was observed indicating the formation of HPMC-anionic surfactant complexes in the bulk solution. HPMC is surface active therefore we can envisage the adsorption of both the non-ionic polymer and the anionic surfactant at the air-liquid interface.

Polymer-surfactant interactions at the liquid-solid interface were investigated by milling griseofulvin whose nanoparticles could only be produced in presence of anionic surfactants in the presence of HPMC. The inclusion of HPMC in the drug milling slurry led to co-adsorption of HPMC and anionic surfactant on the griseofulvin nanoparticle surfaces. Notably HPMC on its own did not adsorb on griseofulvin particle surfaces. In addition there was a reduction in the amount of adsorbed anionic surfactant when polymer was co-adsorbing indicating synergistic effects at the liquid-solid interface. However, inclusion of high concentrations or higher molecular weight polymers in the milling slurry led to slower production of nanoparticles attributable to an increase in slurry viscosity thus cushioning of the drug particles from impact by the milling media.

References

Ahmad N., Ahmad B., (1990). Intrinsic-viscosity, Huggin constant and unperturbed chain dimension of polyvinylpyrrolidone. Journal of the Chemical Society of Pakistan **12**: 246-249.

Ahmed F., Alexandridis P., Neelamegham S., (2001). Synthesis and application of fluorescein-labeled pluronic block copolymers to the study of polymer-surface interactions. Langmuir. **17**: 537-546.

Alhalawen A., Benyong L., Bostrom D., Pvelagu S., (2007). Private communication to the Cambridge Crystallographic Data Centre. Department of Health Science, Lulea University of Technology, Lulea 5 971 87 Sweden.

Allen F.H., (2002). The Cambridge Structural Database: a quarter of a million crystal structures and rising. Acta Crystallographica **58**: 380–388.

Amidon G.L., Lennernas H., Shah V.P., Crison J.R., (1995). A theoretical basis for a biopharmaceutic drug classification: The correlation of *in vitro* drug product dissolution and *in vivo* bioavailability. Pharmaceutical Research **12**: 413-420.

Anton N., Vandamme T.F., (2011). Nano-emulsions and micro-emulsions: clarifications of the critical differences. Pharmaceutical Research **28**: 978-985.

Arnold C., Ulrich S., Stoll S., Marie P., Holl Y., (2011). Monte Carlo simulations of surfactant aggregation and adsorption on soft hydrophobic particles. Journal of Colloid and Interface Science. **353**: 188-195.

Atkinson R.M., Bedford C., Child K.J., Tomich E.G., (1962). Effect of particle size on blood griseofulvin-levels in man. Nature **193**: 588-589.

Attwood D., Florence A.T., (1983). 'Surfactant systems: their chemistry, pharmacy and biology.' 1st edition, Chapman and Hall.

Bahadur P., Dubin P., Rao Y.K., (1995). Complex formation between sodium dodecyl sulfate and poly(4-vinylpyridine N-oxide). Langmuir **11**: 1951-1955.

Barlow D.J., (2011). ACCESS: determination of the charge per unit area across crystal planes. King's College London.

Barlow D.J., (2011). EPOT: determination of the electrostatic potential across crystal planes. King's College London.

Bates S., Zografi G., Engers D., Morris K., Crowley K., Newman A., (2006). Analysis of amorphous and nanocrystalline solids from their X-ray diffraction patterns. Pharmaceutical Research. **23**: 2333-2349.

Bell C.G, Breward C.J.W., Howell P.D., Penfold J., Thomas R.K., (2010). A theoretical analysis of the surface tension profiles of strongly interacting polymer–surfactant systems. Journal of Colloid and Interface Science **350**: 486-493.

Bell C.G., Breward C.J.W., Howell P.D., Penfold J., Thomas R.K., (2007). Macroscopic modelling of the surface tension of polymer-surfactant systems. Langmuir **23**: 6042-6052.

Berge S.M., Bighley L.D., Monkhouse D.C., (1977). Pharmaceutical salts. Journal of Pharmaceutical Sciences **66**: 1-19.

Bilgili E., Hamey R., Scarlett B., (2004). Production of pigment nanoparticles using a wet stirred mill with polymeric media. China Particuology **2**: 93-100.

Birdi K.S., (2009). 'Handbook of Surface and Colloid Chemistry'. 3rd edition, CRC Press.

Boistelle R., Astier J.P., (1998). Crystallisation mechanisms in solution. Journal of Crystal Growth **90**: 14-30.

Breitenbach J., (2002). Melt extrusion: from process to drug delivery technology. European Journal of Pharmaceutics and Biopharmaceutics **54**: 107-117.

British Pharmacopeia Volume I & II (2010). Monographs: Medicinal and Pharmaceutical substances. Griseofulvin: Ph Eur monograph 0182.

Brown W., Henley D., Ohman, J., (1963). Studies on cellulose derivatives. Pt. II. The influence of solvent and temperature on the configuration and hydrodynamic behaviour of hydroxyethylcellulose in dilute solution. Makromoleculaire Chemie. **64**: 49-67.

Butler J.M., Dressman J.B., (2010). The Developability Classification System: application of biopharmaceutics concepts to formulation development. Journal of Pharmaceutical Sciences **99**: 4940–4954.

Byrappa K., Ohara S., Adshiri T., (2008). Nanoparticles synthesis using supercritical fluid technology – towards biomedical applications. Advanced Drug Delivery Reviews **60**: 299-327.

Byrn S.R., Pfeiffer R.R., Stowell J.G., (2000). Guidance for industry, Q6A Specifications: Test procedures and acceptance criteria for new drug substances and new drug products: Chemical substances, International conference on Harmonisation.

Chamarthy S.P., Pinal R., (2008). The nature of crystal disorder in milled pharmaceutical materials. Colloids and Surfaces A: Physicochemical and Engineering Aspects **331**: 68-75.

Chandar P., Somasundaran P., Turro N.J., (1986). Fluorescence probe studies on the adsorbed layer of dodecyl sulphate at the alumina-water interface. Journal of Colloid and Interface Science **117**: 31-46.

Chari K., Hossaint T., (1991). Adsorption at the air/water interface from an aqueous solution of poly(vinylpyrrolidone) and sodium dodecyl sulfate. Journal of Physical Chemistry **95**: 3302-3305.

Chatterjee A., Moulik S. P., Sanyal S. K., Mishra B. K., Puri P. M., (2001). Thermodynamics of micelle formation of ionic surfactants: A critical assessment for sodium dodecyl sulfate, cetyl pyridinium chloride and dioctyl sulfosuccinate (Na salt) by microcalorimetric, conductometric, and tensiometric measurements. Journal of Physical Chemistry B **105**: 12823-12831.

Chaubal M.V., (2004). Application of formulation technologies in lead candidate selection and optimization. Drug Discovery Today **9**: 603-609.

Chen H., Wan J., Wang Y., Mou D., Liu H., Xu H., Yang X., (2008). A facile nanoaggregation strategy for oral delivery of hydrophobic drugs by utilizing acid–base neutralization reactions. Nanotechnology **19**: 375104

Chen J.F., Zhou M.Y., Shao L., Wang Y.Y., Yun J., Chew N.Y.K., Chan H.K., (2004). Feasibility of preparing nanodrugs by high-gravity reactive precipitation. International Journal of Pharmaceutics **269**: 267-274.

Chikhalia V., Forbes R.T., Storey R.A., Ticehurst M., (2005). The effect of crystal morphology and mill type on milling induced disorder. European Journal of Pharmaceutics **27**: 19-26.

Chiou W.L., Riegelman S., (1971). Pharmaceutical applications of solid dispersion systems. Journal of Pharmaceutical Sciences **60**: 1281-1302.

Choi S.M., (2000). SANS experimental methods. Neutron small angle scattering and reflectometry from submicron structures [online]. Available http://www.ncnr.nist.gov/programs/sans/pdf/sans_methods.pdf [accessed 28Jun2011]

Claesson P.M., Bergström M., Dedinaite A., (2003). Surface force studies of polymer-surfactant complexes at the solid-liquid interface: relation to structure of bulk complexes. 3rd International Symposium on Food Rheology and Structure.

Cosgrove T., Heath T.G., Ryan K., Crowley T.L., (1987). Neutron scattering from adsorbed polymer layers. Macromolecules **20**: 2879-2882.

Cox P.J., Manson P.L., (2003). γ-Indomethacin at 120 K. Acta Crystallographica Section E, Structure reports online **59**: 0986-0988.

Custodio J.M., Wu C-Y., Benet L.Z., (2008). Predicting drug disposition, absorption/elimination/transporter interplay and the role of food on drug absorption. Advanced Drug Delivery Reviews **60**: 717–733.

Danielsson I., Lindman B., (1981). The definition of a microemulsion. Colloids and Surfaces **3**: 3391–3392.

DeGioannis B., Jestin P., Subra P., (2004). Morphology and growth control of griseofulvin recrystallized by compressed carbon dioxide as antisolvent. Journal of Crystal Growth **262**: 519-526.

Dejardin P., (1982). Volume effect of adsorption isotherms of macromolecules by depletion. Journal of Physical Chemistry. **86**: 2800-2801.

Derjaguin, B.V. and Landau, L.D. (1941). Theory of the stability of strongly charged lyophobicsols and of the adhesion of strongly charged particles in solutions of electrolytes. ActaPhysicochimica URSS. **14**: 633–662.

Dewhurst C., (2003). Graphical reduction and analysis SANS program for Matlab™ [online]. Available: www.ill.fr/lss/grasp [accessed 28Jun2011]

Dhirendra K., Lewis S., Udupa N., Atin K., (2009). Solid dispersions.Pakistan Journal of Pharmaceutical Sciences **22**: 234-246.

Dondos A., Papanagopoulos D., (1993). The intrinsic viscosity of polymers in the region of extremely dilute solutions: Detection of the conformational transitions of polymers. Die Macromolekular Chemie, Rapid Communications **14**: 7-11.

Dondos A., Tsitsilianis C., (1992). Viscometric study of extremely dilute macromolecular solutions: Critical concentration c and the intrinsic viscosity of the polystyrene through scaling laws. The values of the Huggins constant. Polymer International **28**: 151-156.

Dow Chemical Company., (1975). 'Handbook of Methocel Cellulose Ether Products' DOW Chemical Company.

Dressman J. B., Horter D., (2001). Influence of physiochemical properties on dissolution of drugs in the gastrointestinal tract. Advanced Drug Delivery Reviews **46**: 75 -87.

Duro R., Souto C., Gomez – Amoza J.L., Martinez – Pacheco R., Conchiero A., (1999). Interfacial adsorption of polymers and surfactants: Implications for the properties of disperse systems of pharmaceutical interest. Drug Development and Industrial Pharmacy **25**: 817 – 829.

Esumi K.,Iitaka M., Koide Y., (1998). Simultaneous adsorption of poly (ethylene oxide) and cationic surfactant at the silica/water interface. Journal of Colloid and Interface Science **208**: 178-182.

Ettmayer P., Amidon G. L., Clement B., Testa B., (2004). Lessons learned from marketed and investigational prodrugs. Journal of Medicinal Chemistry **47**: 2393–2404.

Evans D.F., Pye G., Bramley R., Clark A.G., Dyson T.G., Hardcastle J.D., (1988). Measurement of gastrointestinal pH profiles in normal ambulant human subjects. Gut **29**: 1035-1041.

Fadhel H. B., Frances C., (2001). Wet batch grinding of alumina hydrate stirred bead mill. Powder technology **119**: 257-268.

Fainerman V.B., Lylyk S.V., Aksenenko E.V., Makievski A.V., Petkov J.T., Yorke J., Miller R., (2009). Adsorption layer characteristics of triton surfactants: 1. Surface tension and adsorption isotherms. Colloids and Surfaces A: Physicochemical and Engineering Aspects. **334**: 1-7.

Feng T., Pinal R., Carvajal M.T., (2008). Process induced disorder in crystalline materials:differentiating defective crystals from the amorphous form of griseofulvin. Journal of Pharmaceutical Sciences **97**: 3207-3221.

Food and Drug Administration 2009: Approval of Invega Sustenna 39 mg, 78 mg, 117 mg, 156 mg, and 234 mg extended release suspension for treatment of schizophrenia. Approval date: 31st July 2009. Application number: 022264.

Ganong W.F., (2005). 'Review of medical physiology'. 21st edition, Appleton and Lange.

Gennaro A.R., (1995). 'Remington's Pharmaceutical Sciences'. 19th edition, Mack Publishing Company.

Goddard E.D., (1986). Polymer-surfactant interaction Part 1. Uncharged water-soluble polymers and charged surfactants. Colloids and Surfaces **19**: 255-300.

Goddard E.D., (2002). Polymer/Surfactant Interaction: Interfacial Aspects. Journal of Colloid and Interface Science **256**: 228–235.

Goodwin J, D., (2006). Polymer stabilised drug nanoparticles. PhD Thesis. University of London.

Govender S., Jacobs E.P., Bredenkamp M.W., Swart P., (2005). A robust approach to studying the adsorption of pluronic F108 on nonporous membranes. Journal of Colloid and Interface Science. **282**: 306-313.

Guidance for industry: Waiver of in vivo bioavailability and bioequivalence studies for immediate release solid oral dosage forms based on a Biopharmaceutics Classification System, (2000). U.S. Department of Health and Human, Food and Drug Administration (FDA), Centre for Drug Evaluation and Research (CDER).

Habich A., Qiao G.G., Ducker W., (2010). Enantioselective adsorption of surfactants monitored by ATR-FTIR. Langmuir. **26**: 13944-13953.

Hammouda B. (1995). A tutorial of small angle neutron scattering from polymers. National Institute of Standards and Technology [online]. Available: http://nanoparticles.org/pdf/NIST-SANS-Intro.pdf [accessed 28Jun2011]

Heng J.Y.Y., Bismarck A., Lee A.F., Wilson K., Williams D.R., (2006 a). Anisotropic surface chemistry of aspirin crystals. Journal of Pharmaceutical Sciences **96**: 2134-2144.

Heng J.Y.Y., Bismarck A., Williams D.R., (2006 b). Anisotropic surface chemistry of crystalline pharmaceutical solids. AAPS PharmSciTech **7**: E12-E20.

Heng J.Y.Y., Williams D.R., (2006 c). Wetting of paracetamol polymorphic forms I and II. Langmuir **22**: 6905-6909.

Higuchi W.I., Bernardo P.D., Mehta S. C., (1967). Polymorphism and drug availability II: Dissolution rate behaviour of the polymorphic forms of sulfathiazole and methylprednisdone. Journal of Pharmaceutical Sciences **56**: 200-207.

Hogben C.A.M, Dominick J. T., Bernard B. B., Lewis S. S., (1959). On the mechanism of intestinal absorption of drugs. Journal of Pharmacology and Experimental Therapeutics **125**: 275-282.

Hou Z., Li Z., Wang H., (1999). Interaction between poly(ethylene oxide) and sodium dodecyl sulfonate as studied by surface tension, conductivity, viscosity, electron spin resonance and nuclear magnetic resonance. Colloid & Polymer Science **277**: 1011-1018.

Huang L., Maltesh C., Somasundaran P., (1996). Adsorption behavior of cationic and nonionic surfactant mixtures at the alumina–water interface. Journal of Colloid and Interface Science. **177**: 222-228.

Hubbard F.P., Santonicola G.Jr., Kaler E.W., Abbott N.L., (2005). Small-angle neutron scattering from mixtures of sodium dodecyl sulphate and a cationic, bolaform surfactant containing azobenzene. Langmuir **21**: 6131-6136.

Iaccocca R.G., Burchom C.L., Hilden L.R., (2009). Particle Engineering: A strategy for establishing drug substance physical property specifications during small molecule development. Journal of Pharmaceutical Sciences **99**: 51-75.

Institut Laue-Langevin (ILL). (2011). D11 characteristics [online]. Available: http://www.ill.eu/instrument/d11/characteristics [accessed 28Jun2011]

Jacobs C., Muller R.H., (2002). Production and characterization of a budenoside nanosuspension for pulmonary administration. Pharmaceutical Research **19**: 189-194.

Jannick G., Cloizeaux J., (1990). Polymers in solution. Journal of Physics: Condensed Matter **2**: 1-24.

Kata M., Tuske B., (1988). Increasing the solubility characteristics of griseofulvin with γ-cyclodextrin. Pharmazie **43**: 52-53.

Keiderling U., (2002). The new 'BerSANS-PC' software for reduction and treatment of small angle neutron scattering data. Applied Physics A **74**: (Supplementary) S1455-S1457.

Kesisoglou F., Panmai S., Wu Y.H., (2007). Nanosizing - Oral formulation development and biopharmaceutical evaluation. Advanced Drug Delivery Reviews **59**: 631-644.

Khraisheha M., Holland C., Creany C., Harris P., Parolis L., (2005). Effect of molecular weight and concentration on the adsorption of CMC onto talc at different ionic strengths. International Journal of Mineral Processing. **75**: 197-206.

King S.M. (1995). Small angle neutron scattering. In: Pethrick R.A. and Dawkins J.V., editors. Modern Techniques for Neutron Scattering. John Wiley and Sons: New York: 171-225.

King S.M., Griffiths P., Hone J., Cosgrove T., (2000). SANS from adsorbed polymer layers. Macromolecular symposium **190**: 33-42.

Kipp J.E., (2004). The role of solid nanoparticle technology in parenteral delivery of poorly soluble drugs. International Journal of Pharmaceutics **284**: 109-122.

Kopeliovich D., (2011). Stabilization of colloids. SubsTech - substances and technologies [online]. Available http://www.substech.com/dokuwiki/doku.php?id=stabilization_of_colloids [accessed 28 November 2011].

Kronberg B., Kuortti J., Stenius P., (1986).Competitive and cooperative adsorption of polymers and surfactants on kaolinite surfaces. Colloids and Surfaces **18**: 411-425.

Kumar V., Wang L., Riebe M., Tung H.H., Prud'homme R.K, (2009). Formulation and stability of Itraconazole and Odanacatib nanoparticles: governing physical parameters. Molecular Pharmaceutics **6**: 1118-1124.

Kwade A., (1999). Wet comminution in stirred media mills - research and its practical application. Powder Technology **105**: 14-20.

Kwan K.C., (1997). Oral bioavailability and first-pass effects. Drug metabolism and disposition **25**: 1329-1336.

Kwok D.Y., Neumann A.W., (1999). Contact angle measurement and contact angle interpretation. Advances in Colloid and Interface Science **81**: 167-249.

Lamotte J., Campsteyn H., Dupont L.,Vermeire M., (1978). Molecular and crystal structure of furfurylamino acid-2-chloro-4-sulfamoyl benzoic acid 5, furosemide ($C_{12}H_{11}ClN_20_5S$). Acta Crystallographica Section B, Structural crystallography and crystal chemistry **34**: 1657-1661.

Law S.L., Kayes J.B., (1983). Adsorption of non-ionic water-soluble cellulose polymers at the solid water interface and their effect on suspension stability. International Journal of Pharmaceutics **15**: 251-260.

Lawrence M.J., Ress G.D., (2000). Microemulsion-based media novel drug delivery systems. Advanced Drug Delivery Reviews **45**: 89-121.

Lee Y., Choi J.Y., Park C.H., (2008). Characteristics of polymers enabling nanocommunition of water-insoluble drugs. International Journal of Pharmaceutics **355**: 328-336.

Lenneras H., Abrahamsson B., Persson E.M, Knutson L., (2007). Oral drug absorption and the biopharmaceutics classification system. Journal of Drug Delivery Science and Technology **17**: 237-244.

Li L.C., Tian Y., (2007). Zeta potential. Encyclopedia of Pharmaceutical Technology. 3rd edition, Informa Healthcare.

Lin S-Y., Dong C., Hsu T-J., Hsu C-T., (2002). Determination of adsorption of an ionic surfactant on latex from surface tension measurements. Colloids and Surfaces A: Physicochemical and Engineering Aspects. **196**: 189-198.

Lindenberg M., Kopp S., Dressman J.B., (2004). Classification of orally administered drugs on the World Health Organization model list of essential

medicines according to the Biopharmaceutics classification system. European Journal of Pharmaceutics and Biopharmaceutics **58**: 265-278.

Lipatov Y.S., Bliznyuk V.N., Todosiychuk T.T., Chornaya V.N, Katumenu R.K., Konovalyuk V.D., (2006). On the nanostructure of polymer layers formed by adsorption from binary and ternary solutions on a solid SiO_2: a combined adsorption and atomic force microscopy (AFM) study. Colloid and Polymer Science. **284**: 893-899.

Lipinski C., (2002). Poor aqueous solubility - an industry wide problem in drug discovery. American Pharmaceutical Review **5**: 82-85.

Liu C.L., Nikas Y.J., Blankschtein D., (1996). Novel bioseparations using two-phase aqueous micellar systems. Biotechnology and bioengineering **52**: 185-192.

Liu P., Rong X., Laru J., van Veen B., Kiesvaara J., Hirvonen J., Laaksonen T., Peltonen L., (2011). Nanosuspensions of poorly soluble drugs: Preparation and development by wet bead milling. International Journal of Pharmaceutics **411**: 215-222.

Lockman, P.R., Oyewumi M.O., Koziara J.M., Roder K.E., Mumper R.J., Allen D.D., (2003). Brain uptake of thiamine-coated nanoparticles. Journal of Controlled Release **93**: 271-282.

Loew E., Steglich W., Polborn K., (2004). Private communication to the Cambridge Crystallographic Data Centre. Department Chemie, Universitat Munchen, Butenand str, 5-13, 81377, Munchen, Germany.

Loftsson T., Jarho P., Másson M., Järvinen T., (2005). Cyclodextrins in drug delivery. Expert Opinions in Drug Delivery **2**: 335 -351.

Lown K.S., Mayo R.R., Leichtman A.B., Hsiao H., Turgeon D.K., Schmiedlin-Ren P., Brown M.B., Guo W., Rossi S.J., Benet L.Z., Watkins P.B., (1997). Role of intestinal P-glycoprotein (mdr1) in interpatient variation in the oral bioavailability of cyclosporine**.** Clinical Pharmacology and Therapeutics **62**: 248–260.

Macrae C.F., Edgington P.R., McCabe P., Pidcock E., Shields G.P., Taylor R., Towler M., Streek G.V.D., (2006). MERCURY: visualisation and analysis of crystal structures. Journal of Applied Crystallography **39**: 453-457.

Mahajan A.J., Kinvan D.J., (1993). Rapid precipitation of biochemicals. Journal of Physics D: Applied Physics **26**: B176-B180.

Maltesh C., Somasundaran P., (1992). Binding of sodium dodecyl sulfate to polyethylene oxide at the silica-water interface. Journal of Colloid and Interface Science. **153**: 298-301.

Martin N.A., (2005). 'Martin's physical pharmacy and pharmaceutical sciences'. 5th edition, Lippincott Williams & Wilkins.

McCrackin F.L., (1987). Relationship of intrinsic viscosity of polymer solutions to molecular weight. Polymer **28**: 1847-1850.

Mehnert W., Madre K., (2001). Solid lipid nanoparticle: Production, characterization and applications. Advanced drug delivery reviews **25**: 165-196.

Merisko-Liversidge E., Liversidge G.G., (2008). Drug nanoparticles: Formulating poorly soluble compounds. Toxicologic Pathology **36**: 43-48.

Merisko-Liversidge E., Liversidge G.G., Cooper E.R., (2003). Nanosizing: a formulation for approach for poorly water soluble compounds. European Journal of Pharmaceutical Sciences **18**: 113-120.

Mezdoura S., Cuveliera G., Cashb M.J., Michona C., (2007). Surface rheological properties of hydroxypropyl cellulose at air–water interface. Food Hydrocolloids **21**: 776-781.

Muller R.H., Bohm B.H.L., Grau M.J., (1999). Nanosuspensions – Formulations for poorly soluble drugs with poor bioavailability/1st communication: Production and properties. Industrial Pharmacy **61**: 74-78.

Murdande S.B., Pikal M.J., Shanker R.M., Bogner R.H., (2011). Solubility advantages of amorphous pharmaceuticals, part 3: Is maximum solubility

advantage experimentally attainable and sustainable? Journal of Pharmaceutical Sciences **100**: 4349-4356.

Nahringbauer I., (1995). Dynamic surface tension of aqueous polymer solutions, I: Ethyl(hydroxyethyl)cellulose (BERMOCOLL cst-103). Journal of Colloid and Interface Science **176**: 318-328.

Napper D.H, (1983). 'Polymeric Stabilization of Colloidal Dispersions'. Academic Press, London.

National Institute of Standards and Technology (NIST) centre for Neutron Research. Neutron scattering lengths and cross sections [online]. Available http://www.ncnr.nist.gov/resources/n-lengths/ [accessed 28Jun2011]

Netz R.R., Andelman D., (2003). Neutral and charged polymers at interfaces.Physics Reports **380**: 1-95.

Newbury D.E., Williams D.B., (2000). The electron microscope: The materials characterization tool of the millennium. Acta Materialia **48**: 323-346.

Nodehi, A., Moosavian, M., Haghighi, M., Sadr, A., (2007). A new method for determination of the adsorption isotherm of SDS on polystyrene latex particles using conductometric titrations. Chemical Engineering & Technology. **30**: 1732-1738.

Ofokansi, K. C., Chukwu, K. I., Ugwuanyi, S. I., (2009). The use of liquid self-microemulsifying drug delivery systems based on peanut oil/Tween 80 in the delivery of griseofulvin. Drug Development and Industrial Pharmacy **35**: 185-191.

Orme M., (1984). Drug absorption in the gut. British Journal of Anaesthesia **56**: 59-67.

Osmond D.W.J., Vincent B., Waite F.A., (1975). Steric stabilisation: A reappraisal of current theory. Colloid and Polymer Science **253**: 676-682.

Otsuka H., Esumi K., (1994). Simultaneous adsorption of poly(vinylpyrro1idone) and anionic hydrocarbon/fluorocarbon surfactant from their binary mixtures on alumina. Langmuir **10**: 45-50.

Owens D.K., Wendt R.C., (1969). Estimation of the surface free energy of polymers. Journal of Applied Polymer Science **13**: 1741-1747.

Ozturk S.S., Palsson B.O., Dressman J.B., (1988). Dissolution of ionisable drugs in buffered and unbuffered solutions. Pharmaceutical Research **5**: 272-282.

Parrott E.L, (1974). Milling of pharmaceutical solids. Journal of Pharmaceutical Sciences **63**: 813-829.

Patravale V.B., Date A.A., Kulkrani R.M., (2004). Nanosuspensions: a promising drug delivery strategy. Journal of Pharmacy and Pharmacology **56**: 827-840.

Paul Scherrer Institut (PSI). (2011). SANS 2 characteristics [online]. http://www.kur.web.psi.ch.sans2/ [accessed 28Jun2011]

Pe´reza O.E., Sa´nchezb C.C., Pilosofa A.M.R., Patinob J.M.R., (2008). Dynamics of adsorption of hydroxypropyl methylcellulose at the air–water interface. Hydrocolloids **22**: 387-402.

Penfold J., Staples E., Tucker I., Cummins P., (1996). Adsorption of non ionic surfactants on silica sol particles: The effects of sol type and concentration, surfactant type, concentration, and temperature. Journal of Physical Chemistry **100**: 18133-18137.

Pierri E., Avgoustakis K., (2005). Poly(lactide)-poly(ethylene glycol) micelles as a carrier for griseofulvin. Journal of Biomedical Materials Research A **75**: 639-647.

Prabhakar C., Reddy G.B., Reddy C.M., Nageshwar D., Devi A.S., Babu J.M., Vyas K., Sarma M.R., Reddy G.O., (1999). Process research and structural studies on nabumetone. Organic Process Research Development **3**: 121-125.

Qiu D., Cosgrove T., Revell P., Howell I., (2009). Poly(ethylene oxide) adsorption on polystyrene latex particles in the presence of poly(styrenesulfonate sodium). Macromolecules. **42**: 547-552.

Qiu D., Flood D., Cosgrove T., (2008). A small-angle neutron scattering study of adsorbed polymer structure in concentrated colloidal dispersions. Langmuir **24**: 2983-2986.

Rabinow E. B., (2004). Nanosuspensions in Drug Delivery. Nature Reviews Drug Discovery **3**: 786-795.

Rangel-Yagui C.O., Pessoa A.Jr., Tavares L.C., (2005). Micellar solubilization of drugs. Journal of Pharmacy and Pharmaceutical Sciences **8**: 147-163.

Rao A., Dhinojwala A., (2003). Two-photon fluorescence technique to study polymer adsorption at the toluene-water interface. Langmuir **19**: 8813-8817.

Rao V.M., Lin M., Larive C.K., Southard M.Z., (1997). A mechanistic study of griseofulvin dissolution into surfactant solutions under laminar flow conditions. Journal of Pharmaceutical Sciences **86**: 1132-1137.

Rautio J., Kumpulainen H., Heimbach T., Oliyai R.,Oh D., Järvinen T., Savolainen J., (2008). Prodrugs: design and clinical applications. Nature Reviews Drug Discovery **7**: 255-270.

Rawle A., (2002). The importance of particle sizing in the coating industry. Part 1: Particle size measurement. Advances in Colour Science and Technology **5**: 1-12.

Reboul J.P., Cristau B., Soyfer J.C., Astier J.P., (1981). 5*H*-Dibenz[*b,f*]azepinecarboxamide-5 (carbamazepine). Acta Crystallographica Section B, Structural crystallography and crystal chemistry **37**: 1844-1848.

Reverchon E., (2003). Process for the production of micro and/or nano particles. European Patent WO/2003/004142.

Reverchon E., Adamia R., (2006). Nanomaterials and supercritical fluids. Journal of Supercritical Fluids **37**: 1-22.

Roger E., Lagarce F., Benoit J.P., (2009). The gastrointestinal stability of lipid nanocapsules. International Journal of Pharmaceutics **372**: 260-275.

Rosen M.J., (2004). 'Surfactants and interfacial phenomena'. John Wiley & Sons Inc., 3rd edition.

Rubinstein M.H., Wells J.I., (1977). Generated surface area measurement of disintegrating tablets. Journal of Pharmacy and Pharmacology **29**: 363-366.

Ruddy S.B., Roberts M.E., (1998). Nanoparticles containing R (-) enantiomer of ibuprofen. US Patent No. 5718919.

Rusconi F., Valton E., Nguyen R., Dufourc E., (2001). Quantification of sodium dodecyl sulfate in microliter-volume biochemical samples by visible light spectroscopy. Analytical Biochemistry. **295**: 31-37.

Sakagami K., Esumi K., Yoshimura T., (2002). Simultaneous adsorption of poly(1-vinylpyrrolidone-co-acrylic acid) and sodium dodecyl sulphate at the alumina/water interface. Langmuir. **18**: 6049-6053.

Santhiya D., Nandini G., Subramanian S., Natarajan K.A., Malghan S.G., (1998). Effect of polymer molecular weight on the absorption of polyacrylic acid at the alumina-water interface. Colloids and Surfaces A: Physicochemical and Engineering Aspects. **133**: 157-163.

Sawyer C.B., Reed J.S., (2001). Adsorption of hydroxyl methyl cellulose in an aqueous system containing multi component oxide particles. Journal of American Ceramic Society **24**: 1241-1249.

Scatchard G., (1962). The Gibbs adsorption isotherm. Journal of Physical Chemistry **66**: 618-620.

Schreier P., Bernreuther A., Huffer M., (1995). Analysis of chiral organic molecules: methodology and applications. Walter de Gruyter and Co.

Sepassi S., Goodwin D.J., Drake A.F., Holland S., Leonard G., Martini L., Lawrence M.J., (2007). Effect of polymer molecular weight on the production of drug nanoparticles. Journal of Pharmaceutical Sciences **96**: 2655-2666.

Sepassi-Ashtiani, S. (2003). Polymer stabilised drug nanoparticles. PhD Thesis, University of London.

Serajuddin A.T.M., (2007). Salt formation to improve drug solubility. Advanced Drug Delivery Reviews **59**: 603-616.

Sesta B., D'Aprano A., Segre A.L., Proietti N., (1997). Influence of the polymer molecular weight on the surfactant-polymer interactions: LiPFN-PVP and SDS-PVP systems. Langmuir **13**: 6612-6617.

Shah B., Kakumanu V.K., Bansal A.K., (2006). Analytical techniques for quantification of amorphous/crystalline phases in pharmaceutical solids. Journal of Pharmaceutical Sciences **95**: 1641-1665.

Shariare M.H., Leusen F.J., de Matas M., York P, Anwar J., (2012). Prediction of the mechanical behaviour of crystalline solids. Pharmaceutical Research **29**: 319-331.

Shea S.S., Murray P.E., Mehta B.V., Hachae L.S., (1994). Assay of hydroxypropylmethylcellulose in an ophthalmic formulation by size exclusion chromatography. International GPC conference proceedings.

Shekunov B.Y., Chattopadhyay P., Tong H.Y., Chow H.L., (2006). Particle size analysis in pharmaceutics: principles, methods and applications. Pharmaceutical Research **24**: 203-227.

Shi J., (2002). Steric stabilization. Centre for Industrial Sensors and Measurements, Department Material Science and Engineering Group Inorganic Materials Science. Literature Review.

Shimabayashi S., Nishine S., Uno T., Hino T., (2002). Adsorption of hydroxypropylcellulose on hydroxyapatite via formation of surface complex with sodium dodecyl sulfate. Water Soluble Polymers.

Shin-Etsu AQOAT Hypromellose Acetate Succinate Enteric coating agent handbook, Shin Etsu Chemical Company Ltd (2005).

Singh P., Desai S.J., Simonelli A.P., Higuchi W.I., (1968). Role of wetting on the rate of drug release from inert matrices. Journal of Pharmaceutical Sciences **57**: 217-226.

Sinha, S.K. (2006). Introduction of X-rays and neutrons with matter (presentation)[online]. Available: http://www.dep.anl.gov/nx/lecturenotes.pdf [accessed 28Jun2011]

Somasundaran P., Fuerstenau D.W., (1966). Mechanisms of alkyl sulfonate adsorption at the alumina-water interface. Journal of Physical Chemistry **70**: 90-96.

Somasundaran P., Krishnakumar S., (1997). Adsorption of surfactants and polymers at the solid-liquid interface. Colloids and Surfaces A: Physicochemical and Engineering Aspects **123-124**: 491-513.

Somasundarun P., Shrolri S., Huung L., (1998). Thermodynamics of adsorption of surfactants at solid-liquid interface. Pure and Applied Chemistry **70**: 621-626.

Stachurek I., Pielichowski K., (2009). Preparation and thermal characterization of poly(ethylene oxide)/griseofulvin solid dispersions for biomedical applications. Journal of Applied Polymer Science **111**: 1690-1696.

Stanjek H., Hausler W., (2004). Basics of X-Ray diffraction. Hyperfine Interactions **154**: 107-119.

Staples E., Tucker I.,Penfold J.,Warren N.,Thomas R.K.,Taylor D.J.F., (2002). Organization of polymer-surfactant mixtures at the air-water interface: Sodium dodecyl sulfate and poly(dimethyldiallylammonium chloride). Langmuir **18**: 5147-5153.

Taylor D.J.F., Thomas R.K., Hines J.D., Humphreys K., Penfold J., (2002). The Adsorption of oppositely charged polyelectrolyte/surfactant mixtures at the air/water interface: Neutron reflection from dodecyl trimethylammonium bromide/sodium poly(styrene sulfonate) and sodium dodecyl sulfate/poly(vinyl pyridinium chloride). Langmuir **18**: 9783-9791.

Taylor D.J.F., Thomas R.K., Penfold J., (2007). Polymer/surfactant interactions at the air/water interface. Advances in Colloid and Interface Science **132**: 69-110.

Thakur R., Gupta R.B., (2005). Rapid expansion of supercritical solution with solid cosolvent (RESS - SC) process: Formation of griseofulvin nanoparticles. Industrial and Engineering Chemistry Research **44**: 7380-7387.

Tougaard S., (2005). Surface analysis/X-ray photoelectron spectroscopy. Encyclopedia of Analytical Science. 2nd edition, Elsevier Ltd.

Touhami Y., Rana D., Neale G.H., Hornof V., (2001). Study of polymer-surfactant interactions via surface tension measurements. Colloid and Polymer Science **279**: 297-300.

Tscharnuter W., (2000). Photon correlation spectroscopy in particle sizing. Encyclopedia of Analytical Chemistry. 1st edition, John Wiley & Sons Ltd.

Um S.U., Poptoshev E., Pugh R.J., (1997). Aqueous solutions of ethyl(hydroxyethyl)cellulose and hydrophobic modified ethyl(hydroxyethyl)cellulose polymer: dynamic surface tension measurements. Journal of Colloid and Interface Science **193**: 41-49.

United States Pharmacopeia, USP 26, NF 21, 2003.

van de Waterbreemd H., Gifford E., (2003). ADMET *in silico* modelling: towards prediction paradise? Nature Reviews Drug Discovery **2**: 192-204.

van Eerdenbrugh B., Van den Mooter G., Augustijns P., (2008). Top-down production of drug nanocrystals: Nanosuspension stabilization, miniaturization and transformation into solid products. International Journal of Pharmaceutics **364**: 64-75.

van Eerdenbrugh B., Vermant G., Martens J.A., Froyen L., Van Humbeeck J., Augustijns P., Van den Mooter G., (2009). A screening study of surface stabilization during production of drug nanocrystals. Journal of Pharmaceutical Sciences **98**: 2091-2103.

Verma S., Gokhale R., Burgess D.J., (2009).A comparative study of top-down and bottom-up approaches for the preparation of micro/nanosuspensions. International Journal of Pharmaceutics **308**: 216-222.

Verwey, E.J.W. and J.T.G. Overbeek. (1948). Theory of Stability of Lyophobic Colloids. Elsevier: Amsterdam

Violante M.R., Fischer, H.W., (1991). Method for making uniformly-sized particles from insoluble compounds.United States Patent 4997454.

Waard H., Hinrichs W.L.J., Frijlink H.W., (2008). A novel bottom–up process to produce drug nanocrystals: Controlled crystallization during freeze-drying. Journal of Controlled Release **128**: 179-183.

Winnik F.M., (1989). Association of hydrophobic polymers in water: fluorescence studies with labeled (hydroxypropyl)celluloses. Macromolecules. **22**: 734-742.

Winnik F.M., Winnik M.A., Tazuke S., Ober C.K., (1987). Synthesis and characterization of pyrene-labeled hydroxypropylcellulose and its fluorescence in solution. Macromolecules **20**: 38-44.

Wollenweber C., Makievski A. V., Miller R., Daniels R., (2000). Adsorption of hydroxypropylmethylcellulose at the liquid/liquid interface and the effect on emulsion stability. Colloids and Surfaces A: Physicochemical and Engineering Aspects. **172**: 91-101.

Wong S. C., Ramkissoon Y. D., Lopez M., Page K., Parkin I. P., Sullivan P. M., (2009). Use of hydroxypropylmethylcellulose 2% for removing adherent silicone oil from silicone intraocular lenses. British Journal of Ophthalmology **93**: 1085-1088.

World Health Organization Technical Report Series (2006). No. 937, Annex 8: Proposal to waive *in vivo* bioequivalence requirements for WHO model list of essential medicines immediate-release, solid oral dosage forms.

Wu X., Li X., Mansour H.M., (2010). Surface analytical techniques in solid-state particle characterization for predicting performance in dry powder inhalers. KONA Powder and Particle Journal **28**: 3-19.

Xu W., Akins D.L., (2004). Reverse micellar synthesis of CdS nanoparticles and self assembly into a superlattice. Materials **58**: 2623-2626.

Yan P., Xiao J.X., (2004). Polymer–surfactant interaction: Differences between alkyl sulfate and alkyl sulfonate**.** Colloids and Surfaces A: Physicochemical and Engineering Aspects **244**: 39-44.

Yanga W., Tamb J., Millera D.A., Zhouc J., McConville J.T., Johnstonb K.P., Williams R.O., (2008). High bioavailability from nebulized itraconazole nanoparticle dispersions with biocompatible stabilizers. International Journal of Pharmaceutics **361**: 177-188.

Yao J.H., Elder K.R., Guo H., Grant M., (1993). Theory and simulation of Ostwald ripening. Physical Review B **47**: 14110-14125.

Yokoyama T., Tamura K., Usui H., Jimbo G., (1996). Simulation of ball behavior in a vibration mill in relation with its grinding rate: Effects of fractional ball filling and liquid viscosity. International Journal of Mineral Processing **44**: 413-424.

York P., Ticehurst M.D., Osborn J.C., Roberts R.J., Rowe R.C., (1998). Characterisation of the surface energetics of milled dl-propanol hydrochloride using inverse gas chromatography and molecular modelling. International Journal of Pharmaceutics **174**: 179-186.

Yu L.X., Amidon G.L., Polli J.E., Zhao H., Mehta M.U., Conner D.P., Shah V.P., Lesko L.J., Chen M.L., Lee V.H., Hussain A.S., (2002). Biopharmaceutics Classification System: the scientific basis for biowaiver extensions. Pharmaceutical Research **19**: 921-925.

Yunhui Wu, Fillippos K., Santipharp P., (2007). Nanosizing - oral formulation development and biopharmaceutical evaluation. Advanced Drug Delivery Reviews **59**: 631-644.

Zajac J., Chorro C., Lindheimer M., Partyka S., (1997). Thermodynamics of micellization and adsorption of zwitterionic surfactants in aqueous media. Langmuir **13**: 1486-1495.

Zhao J., Brown W., (1995). Dynamic light scattering study of sodium dodecyl sulfate adsorption on polystyrene latex particles modified with aromatic amino groups. Journal of Physical Chemistry. **99**: 15215-15221.

Zimmerman E., Muller R.H., (2001). Electrolyte and pH-stabilities of aqueous solid lipid nanoparticles (SLN^{TM}) dispersions in artificial gastrointestinal media. European Journal of Pharmaceutics and Biopharmaceutics **52**: 203-210.

Appendices

Appendix 1: Calculation of the surface area of nanoparticles

The volume of each nanoparticle was calculated assuming sphericity of particles.

$$V = \frac{4}{3}\pi r^3$$

where V is volume of particle and r is radius

For example a nanoparticle with a mean diameter 251.3 nm, has a volume of 8.309×10^6 nm^3.

The total volume of the grioseofulvin nanoparticles was determined using the known suspension mass of 10 g and a griseofulvin density of 1.455 g/cm^3.

The total volume of griseofulvin in each suspension was found to be 6.8729×10^{21} nm^3.

The number of particles in each respective formulation could be calculated by the following equation;

$$Number\ of\ particles\ in\ suspension = \frac{Total\ volume\ of\ particles\ in\ suspension}{Volume\ of\ one\ drug\ particle}$$

The number of particles in this formulation is 8.2716×10^{14}.

Surface area of one drug particle could be determined and then multiplied by total number of nanoparticles in formulation to give the total surface area of nanoparticles.

$$SA = 4\pi r^2$$

where SA is surface area of particle and r is radius

The surface area of each nanoparticle is 1.9840×10^5 nm^2, multiplied by total number of particles in formulation giving a total surface area of 1.6378×10^{20} nm^2 /163.78 m^2.

Appendix 2: ^{1}H-NMR of HPMC 8000

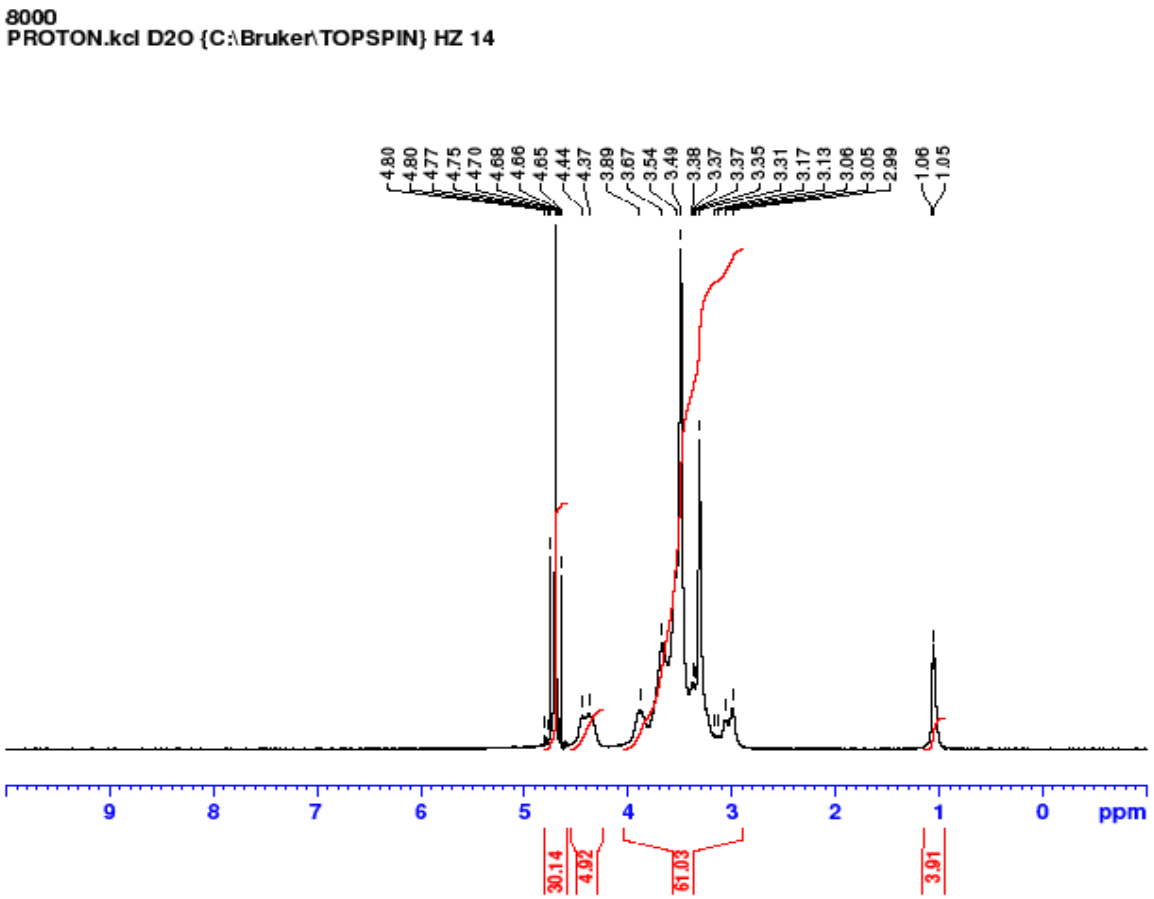

BRUKER

```
Current Data Parameters
NAME      HZ_20110826_JGA9100
EXPNO                      10
PROCNO                      1

F2 - Acquisition Parameters
Date_               20110826
Time                   15.46
INSTRUM                DRX400
PROBHD   5 mm QNP 1H/13
PULPROG                zg30
TD                    65536
SOLVENT                 D2O
NS                         16
DS                          0
SWH                 8250.825 Hz
FIDRES              0.125898 Hz
AQ                  3.9715922 sec
RG                        256
DW                     60.600 usec
DE                      6.00 usec
TE                     296.8 K
D1                1.00000000 sec
TD0                         1

======== CHANNEL f1 ========
NUC1                       1H
P1                     10.75 usec
PL1                    -3.00 dB
SFO1           400.1324710 MHz

F2 - Processing parameters
SI                         65536
SF              400.1300000 MHz
WDW                           EM
SSB                            0
LB                          0.30 Hz
GB                             0
PC                          1.00
```

Appendix 3: ^{1}H-NMR of HPMC 11000

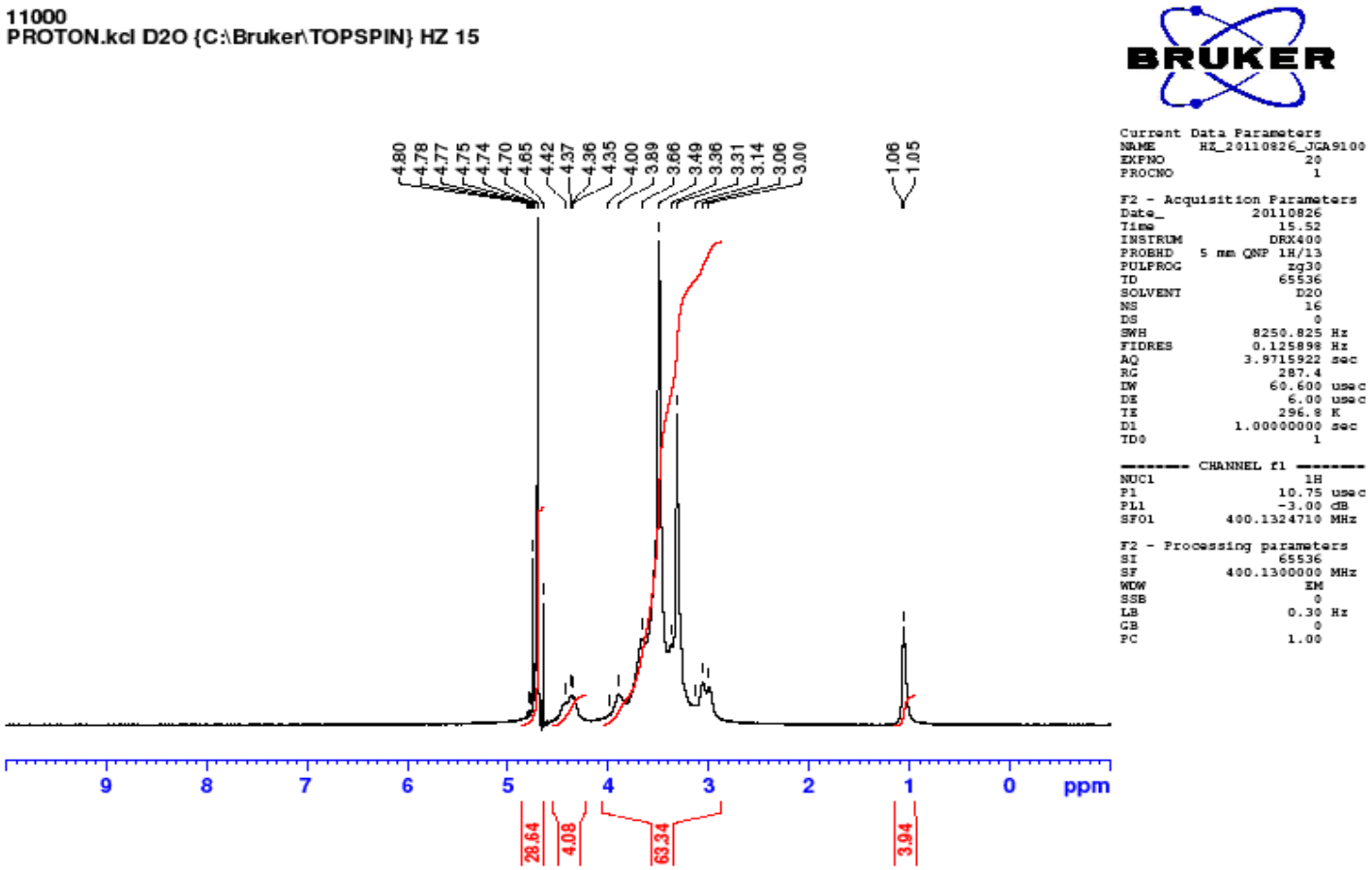

Appendix 4: ^{1}H-NMR of HPMC 15000

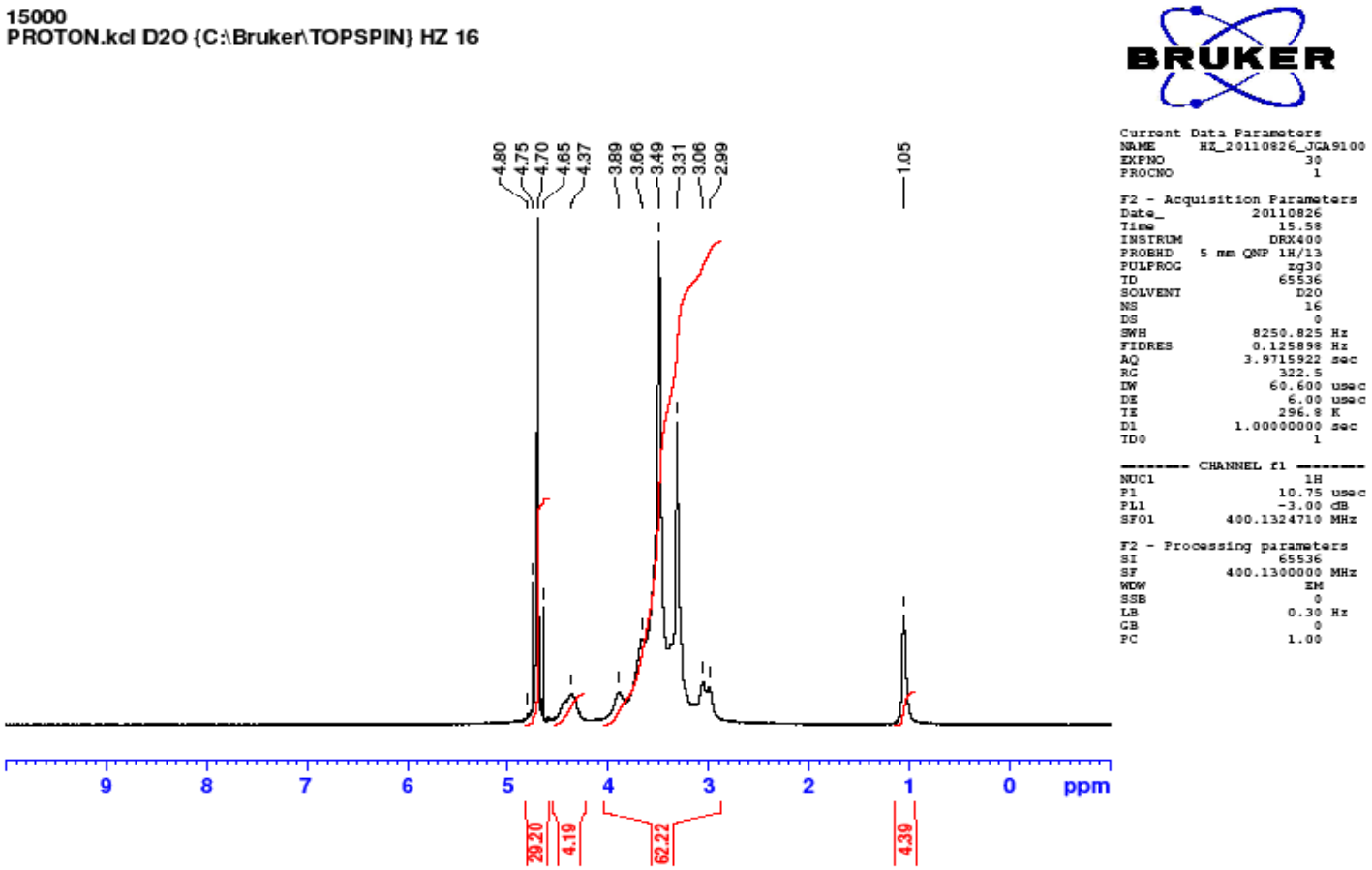

Appendix 5: Calculation of the surfactant area per molecule

The amount of adsorbate mg/m^2 was calculated by the equation:

$$Amount\,of\,adsorbate\,(mg/m^2) = \frac{Amount\,of\,adsorbate(mg/g) \times Total\,mass\,of\,suspension}{Total\,surface\,area\,of\,drug\,particles\,in\,suspension}$$

where amount of adsorbate is the amount of polymer/surfactant adsorbed, total mass of suspension is 50 g and total surface area of drug particles is calculated as shown in Appendix 1.

The area per surfactant molecule (Å) is calculated by

$$Area\,per\,surf\,molecule = \frac{Molecular\,weight\,of\,surf \times 10^{20}}{Amount\,of\,adsorbate(mg/g) \times N_A}$$

where amount of adsorbate is the amount of polymer/surfactant adsorbed, surf is surfactant and N_A is Avogadro's constant (6.023×10^{23}).

Appendix 6: Survey X-ray photoelectron spectra of griseofulvin pyramid comprising facets 1-4

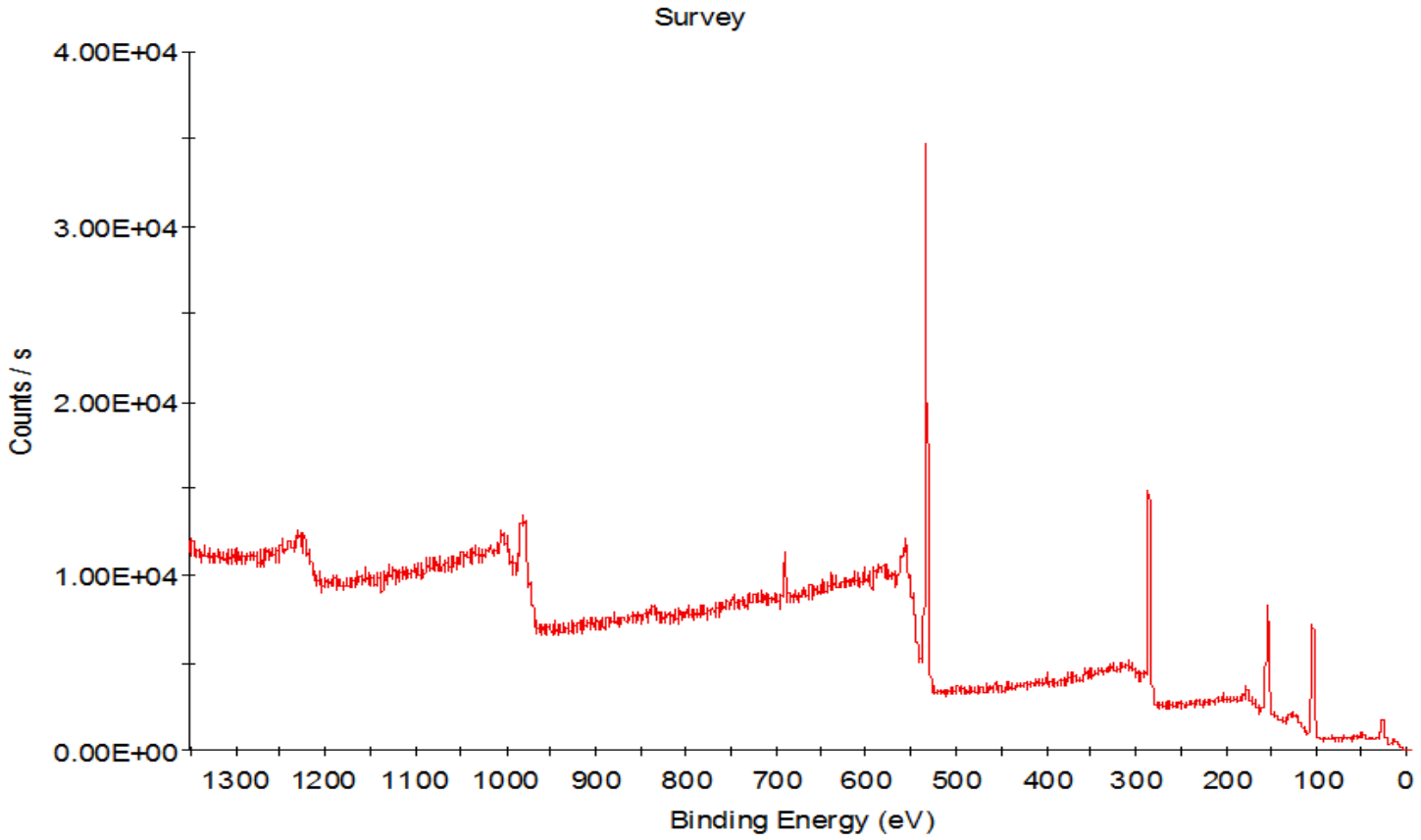

Appendix 7: High resolution X-ray photoelectron spectra of griseofulvin pyramid comprising facets 1-4

Peaks

Name	Start BE	Peak BE	End BE	Height CPS	FWHM eV	Area (P) CPS.eV	Area (N)	At. %	F	Q	SF	TXFN	PP Height	File Name
C1s	289.90	284.82	281.50	1848.21	2.12	4296.16	93.156585	35.18		Y	0.250	2.59	1948.64	C:\DOCUME~1\DATAUS~1\LOCALS~1\Temp\VGD3B.tmp
F1s	694.30	689.86	686.50	336.15	2.12	916.90	5.844437	2.21		Y	1.000	3.00	408.51	C:\DOCUME~1\DATAUS~1\LOCALS~1\Temp\VGD3C.tmp
N1s	402.90	400.14	397.80	92.32	1.28	255.62	1.348690	0.51		Y	0.420	6.84	121.74	C:\DOCUME~1\DATAUS~1\LOCALS~1\Temp\VGD3D.tmp
O1s	537.90	532.97	528.70	5304.65	2.28	13094.30	117.867545	44.52		Y	0.660	2.82	5474.21	C:\DOCUME~1\DATAUS~1\LOCALS~1\Temp\VGD3E.tmp
Si2p	107.50	103.37	98.70	902.04	2.57	2453.43	46.556618	17.58		Y	0.270	2.45	884.79	C:\DOCUME~1\DATAUS~1\LOCALS~1\Temp\VGD3F.tmp

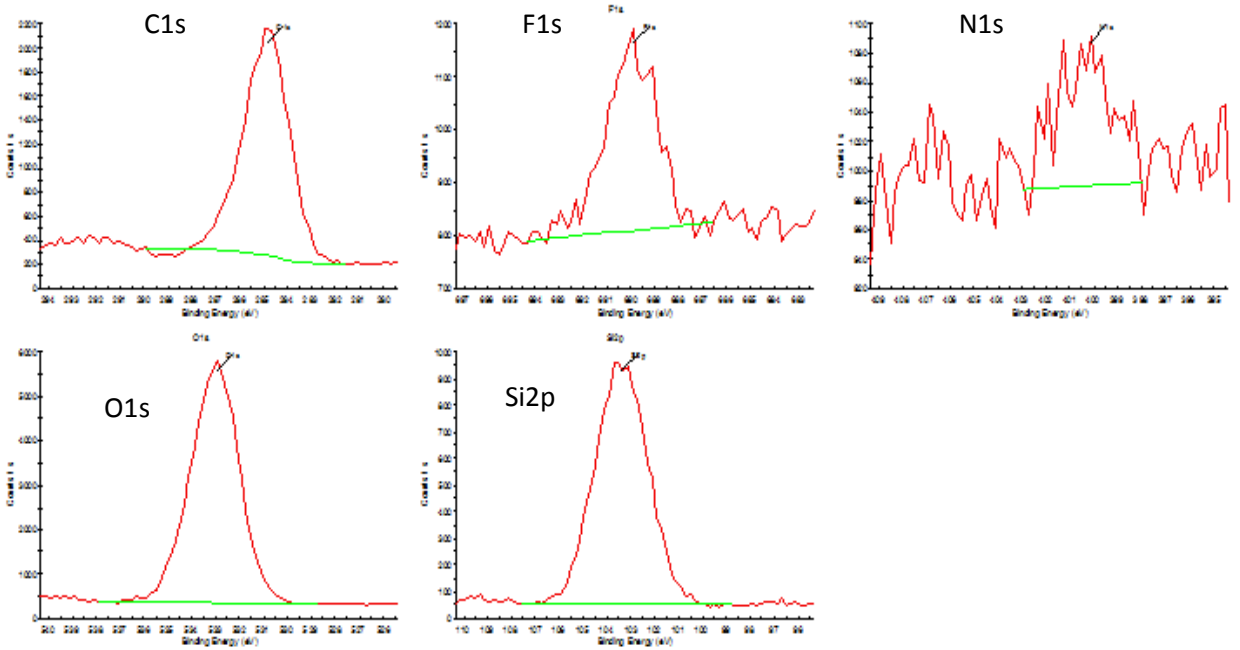

Appendix 8: Survey X-ray photoelectron spectra of griseofulvin pyramid comprising facets 5-8

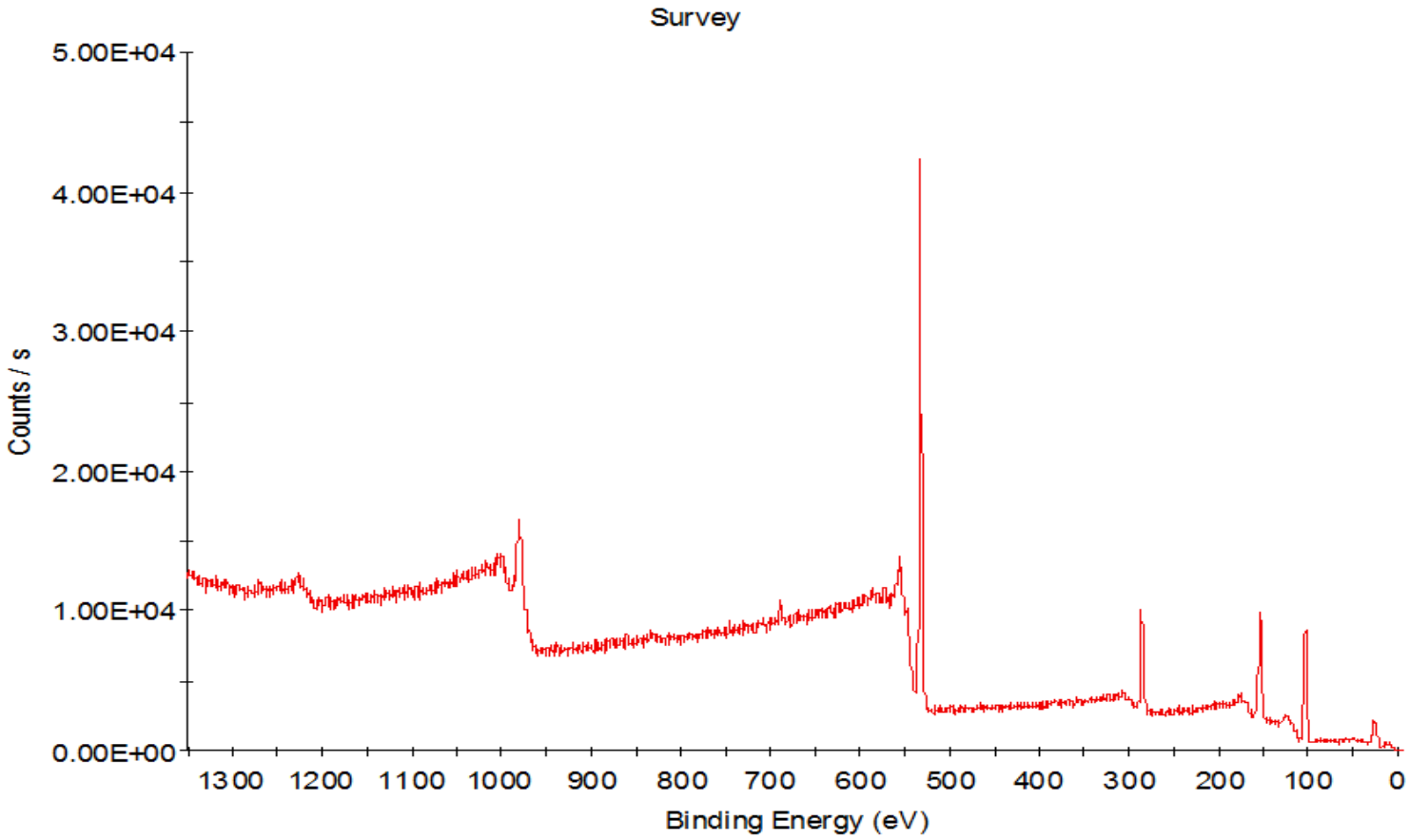

Appendix 9: High resolution X-ray photoelectron spectra of griseofulvin pyramid comprising facets 5-8

Peaks														
Name	Start BE	Peak BE	End BE	Height CPS	FWHM eV	Area (P) CPS.eV	Area (N)	At. %	F	Q	SF	TXFN	PP Height	File Name
C1s	290.50	284.81	280.70	1027.75	2.46	2839.32	61.566793	22.20		Y	0.250	2.59	1078.76	C:\DOCUME~1\DATAUS~1\LOCALS~1\Temp\VGD7F.tmp
F1s	693.50	689.48	685.30	653.45	2.08	1802.44	4.580688	1.65		Y	1.000	7.53	701.37	C:\DOCUME~1\DATAUS~1\LOCALS~1\Temp\VGD80.tmp
O1s	537.10	532.90	528.70	6683.91	2.34	17087.35	153.806232	55.46		Y	0.660	2.82	6807.69	C:\DOCUME~1\DATAUS~1\LOCALS~1\Temp\VGD81.tmp
Si2p	107.90	103.29	98.70	1124.27	2.49	3023.85	57.379603	20.69		Y	0.270	2.45	1117.49	C:\DOCUME~1\DATAUS~1\LOCALS~1\Temp\VGD82.tmp